## AD NUMBER

AD809831

## NEW LIMITATION CHANGE

TO

Approved for public release, distribution
unlimited

FROM

Distribution authorized to U.S. Gov't.
agencies and their contractors;
Administrative/Operational Use; Jan 1967.
Other requests shall be referred to Air
Force Materials Laboratory, Attn: MAAM,
Wright-Patterson AFB, OH 45433.

## AUTHORITY

USAFML ltr, 29 Mar 1972

AD-809831

NICKEL-BASE SUPERALLOY OXIDATION
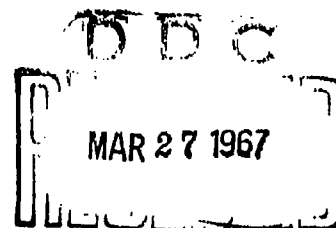
G. E. Wasielewski
General Electric Company

Technical Report AFML-TR-67-30

January 1967

This document is subject to special export controls and each transmittal
to foreign governments or foreign nationals may be made only with prior
approval of the Metals and Ceramics Division (MAAM) Air Force Materials
Laboratory, Wright-Patterson AFB, Ohio 45433.

Air Force Materials Laboratory
Research and Technology Division
Air Force Systems Command
Wright-Patterson Air Force Base, Ohio

50th Anniversary
1917   1967
Materials Research in the Air Force
AIR FORCE MATERIALS LABORATORY

DDC
MAR 27 1967

209

## NOTICES

When Government drawings, specifications, or other data are used for any purpose other than in connection with a definitely related Government procurement operation, the United States Government thereby incurs no responsibility nor any obligation whatsoever; and the fact that the Government may have formulated, furnished, or in any way supplied the said drawings, specifications, or other data, is not to be regarded by implication or otherwise as in any manner licensing the holder or any other person or corporation, or conveying any rights or permission to manufacture, use, or sell any patented invention that may in any way be related thereto.
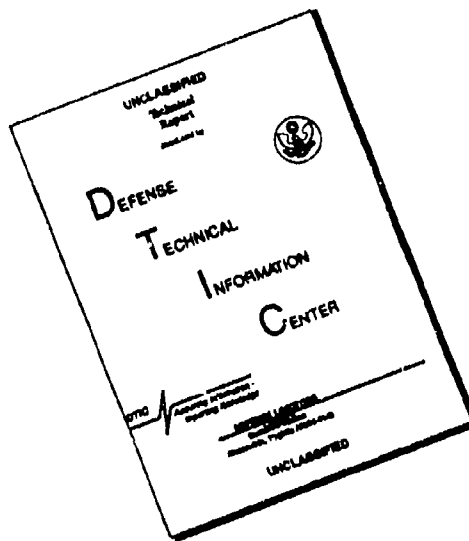
DDC Release to CFSTI Not Authorized.

Copies of this report should not be returned to the Research and Technology Division unless return is required by security considerations, contractual obligations, or notice on a specific document.

# DISCLAIMER NOTICE

THIS DOCUMENT IS BEST QUALITY AVAILABLE. THE COPY FURNISHED TO DTIC CONTAINED A SIGNIFICANT NUMBER OF PAGES WHICH DO NOT REPRODUCE LEGIBLY.

DDC REPORT BIBLIOGRAPHY    SEARCH CONTROL NO. /FAYE3

AD-809 831        11/6
   GENERAL ELECTRIC CO CINCINNATI OHIO MATERIALS DEVELOPMENT
   LAB OPERATION

   NICKEL-BASE SUPERALLOY OXIDATION.                    (U)

DESCRIPTIVE NOTE:  TECHNICAL REPT. 1 JUL 65-15 DEC 66.
     JAN  67   191P     WASIELEWSKI,GERALD E. :
CONTRACT:  AF 33(615)-2861
PROJ:  AF-7312
TASK:  731202
MONITOR:  AFML    TR-67-30

         UNCLASSIFIED REPORT
   DISTRIBUTION: NO FOREIGN WITHOUT APPROVAL OF AIR
   FORCE MATERIALS LAB., ATTN: MAAM. WRIGHT-
   PATTERSON AFB, OHIO 45433.

DESCRIPTORS:   (*NICKEL ALLOYS, *OXIDATION),
   FILMS, WEIGHT, TEST METHODS, REACTION KINETICS,
   SURFACE PROPERTIES, METALLOGRAPHY, X-RAY
   DIFFRACTION ANALYSIS, ELECTRON MICROSCOPY,
   MICROSTRUCTURE, DATA, TABLES                    (U)

   A PROGRAM TO DETERMINE THE PHENOMENOLOGICAL
   OXIDATION BEHAVIOR OF FIVE COMMERCIAL NICKEL-BASE
   ALLOYS (IN-100, SM-200, INCO 713C, RENE 41,
   AND U-700) AND ONE EXPERIMENTAL ALLOY (RENE
   Y) IS DESCRIBED TO ASSURE THE INTELLIGENT
   APPLICATION OF THESE ALLOYS AND AID IN THE
   DEVELOPMENT OF ALLOYS WITH IMPROVED SURFACE
   STABILITY. THE OXIDATION CHARACTERISTICS WERE
   ESTABLISHED AS A FUNCTION OF ALLOY COMPOSITION,
   SURFACE PREPARATION, AND ENVIRONMENTAL VARIABLES SUCH
   AS TIME (5 MIN TO 1000 HRS), TEMPERATURE (1400
   TO 2100 F), AND AIR FLOW RATE (TO 75 FT/SEC).
   THE EXTENT OF SCALE AND SUBSCALE REACTIONS WERE
   MEASURED, THE REACTION PRODUCTS IDENTIFIED AND
   CORRELATED WITH MORPHOLOGY, AND THE ACCOMPANYING
   KINETICS OF THEIR FORMATION STUDIED. THE OXIDATION
   BEHAVIOR OF THESE ALLOYS IS COMPLEX DUE TO THE
   INTERPLAY BETWEEN HETEROGENEOUS OXIDE GROWTH, OXIDE
   INTERACTION, OXIDE VOLATILIZATION, AND SPALLING.
   HOWEVER, THE GENERAL OXIDATION BEHAVIOR IS
   CONTROLLED BY THE COMPETITION BETWEEN BETWEEN SCALING
   AND INTERNAL OXIDATION REACTIONS WHICH COULD BE
   ESTIMATED BY THERMODYNAMICS. INCREASED AIR FLOW,
   THERMAL CYCLING, AND SURFACE DEFORMATION GENERALLY
   DECREASED THE OXIDATION RESISTANCE OF THE ALLOYS.
   ALL THE COMMERCIAL ALLOYS WOULD BE LIMITED TO
   SERVICE TEMPERATURES BELOW 1800 F DUE TO EXCESSIVE
   SPALLING, OXIDE VAPORIZATION, OR INTERGRANULAR        (U)

⑨ Technical rept. 1 Jul 65-15 Dec 66,

⑥ NICKEL-BASE SUPERALLOY OXIDATION.

⑩ Gerald
G. E. Wasielewski

⑪ Jan 67
⑫ 191p.
⑮ AF 33(615)-2861
⑯ AF-7312
⑰ 7312023.

(401573)

## FOREWORD

This technical report has been reviewed and is approved.

I. Perlmutter, Chief
Metals Branch
Metals and Ceramics Division
Air Force Materials Laboratory

11

# ABSTRACT

A program to determine the phenomenological oxidation behavior of five commercial nickel-base alloys (IN-100, SM-200, Inco 713C, René 41, and U-700) and one experimental alloy (René Y) is described to assure the intelligent application of these alloys and aid in the development of alloys with improved surface stability.

The oxidation characteristics were established as a function of alloy composition, surface preparation, and environmental variables such as time (5 min to 1000 hrs), temperature (1400 to 2100°F), and air flow rate (to 75 ft/sec). The extent of scale and subscale reactions were measured, the reaction products identified and correlated with morphology, and the accompanying kinetics of their formation studied.

The oxidation behavior of these alloys is complex due to the interplay between heterogeneous oxide growth, oxide interaction, oxide volatilization, and spalling. However, the general oxidation behavior is controlled by the competition between scaling and internal oxidation reactions which could be estimated by thermodynamics. Increased air flow, thermal cycling, and surface deformation generally decreased the oxidation resistance of the alloys. All the commercial alloys would be limited to service temperatures below 1800°F due to excessive spalling, oxide vaporization, or intergranular oxidation. René Y displayed potential application at temperatures in excess of 2000°F due to the lanthanum induced formation of a protective $MnCr_2O_4$ spinel oxide.

Higher Al/Cr ratios (lower Cr) and minor additions of "rare earths" and Mn were suggested and demonstrated as an effective means of improving the surface stability of nickel-base alloys.

# TABLE OF CONTENTS

## LIST OF ILLUSTRATIONS

vi

# LIST OF ILLUSTRATIONS
## (Continued)

# LIST OF ILLUSTRATIONS

## (Continued)

# LIST OF ILLUSTRATIONS

## (Continued)

## LIST OF ILLUSTRATIONS
### (Continued)

# LIST OF ILLUSTRATIONS

## (Continued)

# LIST OF TABLES

## LIST OF TABLES

### (Continued)

# LIST OF TABLES

## (Continued)

# LIST OF TABLES IN APPENDIX

# I INTRODUCTION

The oxidation behavior of a metal or alloy is dependent not only on the composition of the reactants, but can also be affected by the internal and surface structure, the state of stress, and even the geometry. The oxidation process is, in addition, sensitive to the velocity, density, composition, and flow pattern of the oxidizing environment. Oxidation of even the simplest system is therefore a complex process which has to be understood before solutions to practical environmental problems can be successful. In this respect, materials used in the combustion, turbine, and tailpipe sections of aircraft gas turbine engines are exposed to severe environments in which most such components must withstand the combined effects of stress, high temperature, high velocity combustion products, and erosion from foreign particles. Gas turbines may also ingest sea water which can cause hot corrosion (sulfidation) of nickel and cobalt-base alloy components at temperatures above 1400°F.

The work described here attacks one aspect of the high-temperature corrosion problem: the oxidation behavior of nickel-base alloys of the type commonly used in aircraft gas turbine engines. Consideration is also given to the effects of air velocity and surface preparation on the oxidation behavior. The erosion and hot corrosion problems, although interrelated with oxidation, are subjects requiring separate investigation.

In the past, nickel-base alloy development efforts have been directed toward improving high-temperature strength and primary or secondary working characteristics with relatively minor concern for oxidation behavior. Previous studies at this laboratory[1-3] and elsewhere[4-6] have provided a good basis for understanding some of the oxidation behavior of commercial nickel-base alloys. The present program was planned to investigate additional facets of the high-temperature oxidation problem with the greatest emphasis placed on gaining a deeper understanding of the oxidation mechanisms governing the behavior of the complex nickel-base alloys used in gas turbines. It was felt that a detailed understanding of the oxidation behavior of the best commercial superalloys could be obtained from such a study by correlating the scaling and subscaling processes with the composition, oxidation kinetics, and morphology of the resultant oxides. The resultant knowledge will permit better use of these alloys and provide a useful guide for the design of improved alloys in the future.

With the exception of the studies by Preece and Lucas[7], relatively few data exist in open literature regarding the behavior of superalloys in high velocity combustion products. Most alloys exhibit different behavior in high velocity versus relatively static environments. Although these differences in behavior have been qualitatively observed and considered in the selection of alloys for

1

jet-engine application, the mechanisms through which such differences occur has not been rigorously studied to date in the gamma prime strengthened alloys. Such studies formed an important part of the present work.

It has long been realized that surface preparation can influence oxidation behavior. However, this effect has been considered to be primarily of academic interest with no practical implications. Contrary to this view, studies[2,8-10] have indicated significant influence of surface preparation on the oxidation of Ni-Cr-Al-Ti-Mo-type alloys. Therefore, a third objective of this work was to clarify the surface preparation effect.

In summary, the prime objectives of this program were:

(1) Establish the oxidation mechanisms for selected commercial Ni-base alloys so that the resultant understanding can be used to design improved compositions and assure the intelligent application of these and similar alloys.

(2) Establish the effects of high velocity natural gas combustion products and surface preparation on the oxidation behavior of the subject alloys.

## II  CONCLUSIONS & RECOMMENDATIONS

During this study, five of the most promising commercial nickel-base alloys
(IN-100, SM-200, Inco 713C, René 41, and Udimet 700) and one development
alloy (René Y) were extensively evaluated to determine the characteristics
of their oxidation behavior.  The intent of the study was to apply the
resultant understanding ultimately to the application of these alloys and
to the design of alloys with superior surface stability.

The surface and subscale reactions for these alloys were studied in both
static and dynamic atmospheres over the temperature range 1400 to 2100°F
for times of five minutes to 1000 hours.  The extent of the subscale
reaction processes; internal oxidation and nitrification, $\gamma'$ depletion,
degenerate $\gamma'$ formation, and metal loss, were measured, the scale and
subscale reaction products identified, and their kinetics of formation
studied.  The results of the study were derived primarily from the cor-
relation of microstructural features with reaction products, since the
oxidation mechanism proved too complex for a true kinetic evaluation.

Supplementary oxidation studies to determine the effects of cyclic conditions
and various surface finishes were also conducted.

### 2.1  Conclusions

The following major conclusions are cited on the basis of the results of
this investigation:

(1)  The oxidation processes in commercial nickel-base alloys, particularly
     those in cast form, are too complex for a kinetic analysis to determine
     meaningful activation energies.  This complexity is a result of
     heterogeneous oxide growth, oxide interactions, oxide vaporization,
     and spalling.

(2)  The weight-gain rates are not indicative of the extent or type of
     internal oxidation.  However, the converse is true in that the nature
     of the internal oxidation process can alter the scaling behavior and
     the resultant weight-gain kinetics.

(3)  All commercial alloys except René Y would be limited to service
     temperatures below 1800°F due to excessive spalling, intergranular
     oxidation and oxide volatilization at the higher temperatures.  In
     comparison, René Y shows potential for application at temperatures
     in excess of 2000°F.

3

(4) The general oxidation behavior for these alloys is controlled by the competition between scaling and internal oxidation reactions. If there is selective oxidation of the least noble constituents into the surface scale, a relatively stable layer will result to prevent or minimize internal oxidation. If, the least noble constituent does not form first, internal oxidation of these elements will occur by reduction of the more noble surface scale at the oxide/metal interface.

(5) The interplay between the scaling and subscaling processes is controlled by thermodynamics and to some extent can be predicted. For the alloys studied, the oxidation behavior was primarily a function of the Cr, Al, and Ti concentrations. Based on their affinities for oxygen and the activities of the constituents in the alloy, higher Al/Cr ratios are believed to promote surface stability.

(6) The mode of oxidation can vary significantly as a function of temperature which controls the rate of $\gamma'$ dissolution and the Al activity. However, length of exposure at any specific temperature has no apparent effect on the oxidation mode.

(7) Due to the relatively low activities of the least noble constituents in René Y (Si) and René 41 (Al), these were the only alloys which suffered internal oxidation over the entire range of time and temperature studied. This internal oxide growth was controlled by $O^=$ diffusion for René Y and $Al^{+++}$ diffusion for René 41. The growth of the internal oxide front in these alloys displayed parabolic kinetics as expressed by:

$$\xi^2 \text{ (René 41)} = \left[8.91 \times 10^6 \exp\left(-\frac{47,000}{RT}\right)\right]t + 0.30$$

$$\xi^2 \text{ (René Y)} = \left[8.32 \exp\left(-\frac{28,000}{RT}\right)\right]t + 0.20$$

(8) Oxidation in high velocity combustion products was more severe than in static air. This is attributed to oxidation of $Cr_2O_3$ present in the scale to the volatile $CrO_3$, yielding a less protective oxide (NiO), a higher oxidation rate, and a resultant increase in metal consumption. However, the resistance to dynamic oxidation environments was not solely dependent upon the Cr content of the alloy but rather the Al/Cr activity ratio.

(9) Additions of minor amounts of La and Mn to Hastelloy X (René Y) markedly improves the oxide scale adherence and resistance to dynamic environments. The La addition increases the activity of Mn and Cr to form a stable $MnCr_2O_4$ spinel which minimizes scale volatilization. By concentrating in the grain boundary cusps adjacent to the oxide/metal interface, La

4

appears to promote scale adherency interface, through a mechanical keying effect which minimizes the scale/metal interfacial shear stress.

(10) The effects of surface preparation were shown to be complex and not always predictable. In general, however, surface preparation induced cold work tends to alter scale/subscale processes, thereby producing greater internal oxidation.

## 2.2 Recommendations

To improve the surface stability of nickel-base alloys and obtain a better understanding of the reactions involved, the following recommendations can be made, based on the findings of this investigation:

(1) Emphasize the development of nickel-base alloys with a higher Al/Cr ratio, consistent however, with hot corrosion and ductility requirements.

(2) Develop an understanding of the effects of minor addition elements* on the environmental resistance of high-strength, nickel-base alloys.

(3) Continue efforts to establish the influence of surface deformation on the oxidation of nickel-base alloys and determine the practical significance of these effects.

(4) Make more use of the cyclic and hot corrosion tests to more fully simulate the surface stability in a gas turbine environment.

---

*Refers to Group IIB metals, the rare earth metals, thorium and manganese.

5

# SECTION III

## EXPERIMENTAL

A literature review of the oxidation behavior of metals or alloys generally
expose numerous conflicting results. In such a complex phenomenon as oxi-
dation, many of these conflicts can be attributed to differences in
experimental procedure. In those instances where experimental techniques
are thoroughly reported, the cause of the discrepancy is usually apparent,
and in fact, results in a better understanding. However, where experimental
techniques are not reported or are obscure, the discrepancies may never be
resolved. It is therefore considered essential that all experimental pro-
cedures and techniques used in this investigation be fully described. This
is intended not only to permit confirmation of any portion of these studies,
but also to expose other factors which may influence the oxidation of these
alloys.

## 3.1 Materials

### 3.1.1 Alloy Selection

Nickel-base alloys were selected for this study which are not only leading
candidates for jet-engine combustion and turbine section applications based
upon their strength and oxidation resistance, but which also offer variability
in their manner of fabrication, strengthening mechanism, and chemical
composition.

The commercial alloys selected for this program along with a summary of
factors influential in their selection are presented in Table I. The selection
has been made to include a forging alloy, casting alloys, a high-strength
sheet alloy, and a lower strength sheet alloy possessing high oxidation
resistance. The following presents a brief description of each alloy, its
common usage, and the principal factors in its selection.

Udimet 700 (U-700) represents the highest strength nickel-base forging
alloy currently available and is generally used for wrought turbine blades
and other components requiring superior elevated temperature strength. This
alloy is of the age-hardened type. The predominant strengthening phase is
gamma prime $[Ni_3(Al,Ti)]$, but strengthening contributions from solution
strengthening and carbide phases are also important. Constitutionally, the
alloy contains a moderate Cr content, a relatively low Al/Ti ratio, moderate
molybdenum, and the highest cobalt content of the alloys selected.

6

TABLE I

FACTORS INFLUENCING ALLOY SELECTION

| Alloy | Common Form | Strengthening* Mechanism | Unique Alloying Features |
|---|---|---|---|
| U-700 | Bar & Forgings | PPT - ($\gamma'$) | Mod. Cr, Highest Co, Mo |
| IN-100 | Casting | PPT - ($\gamma'$) | Low Cr. Highest Co, Mo, Highest Ti |
| SM-200 | Casting | PPT - ($\gamma'$) | Lowest Cr, High Co & W, No Mo, and Cb |
| Inco 713C | Casting | PPT - ($\gamma'$) | Mod. Cr, No Co, Highest Cb & Al, Highest Al/Ti |
| René 41 | Sheet | PPT - ($\gamma'$) | High Cr, High Co, High Mo, Lowest Al/Ti |
| René Y | Sheet | SS** | Highest Cr, High Mo and Fe, Mn, Si, and La |

*PPT - ($\gamma'$) refers to $Ni_3$(Al,Ti) ppt hardened with secondary strengthening effects from MC.

**SS refers to solid solution plus carbide strengthened.

IN-100, SM-200, and Inco 713C represent high strength cast alloys for turbine blade applications. These alloys are also basically gamma prime ($\gamma'$) strengthened but differ with respect to solid solution strengthening elements and carbide formers. Inco 713C has a moderate chromium content, whereas IN-100 and SM-200 have the lowest chromium contents of the alloys selected. The major ternary constituent in each alloy also differs, being Co for IN-100, W and Co for SM-200, and Mo and Cb for Inco 713C. Inco 713C has an Al/Ti ratio of approximately eight, which is the highest of the selected alloys. Other subtle compositional features of these alloys include small Zr and B additions. The variety in chemistry offered by these alloys should provide an excellent basis for designing oxidation resistant cast alloys for future applications.

René 41 represents the highest strength sheet alloy available for sheet metal structural component applications in the temperature range of 1200-1800°F. This alloy is also $\gamma'$ and carbide ($MC$ and $M_{23}C_6$) strengthened and is unique with respect to the combination of high Cr, Co, and Mo concentrations and a relatively low Al/Ti ratio.

René Y is a General Electric development alloy strengthened by solid solution and carbides which possesses excellent oxidation resistance at temperatures to 2200°F. This alloy is a modification of Hastelloy X and has relatively low high-temperature strength. It was primarily developed for combustion liners and afterburner components which do not require high strength. The unique compositional features of this alloy include the highest Cr and Fe contents of the alloys tested, a moderate Mo content, relatively high concentrations of Mn and Si, and the addition of lanthanum for improved oxidation resistance and scale adherence.

### 3.1.2 Alloy Procurement and Characterization

All alloys were procured from commercial sources. For those alloys to be evaluated extensively, two heats were obtained to determine the heat-to-heat variations. This factor is particularly important in cast materials where variations in melting and pouring practices can produce both structural and compositional differences which may subsequently influence the oxidation performance. The alloys, their heat numbers, and the form in which they were procured are given in Table II. The master heat analysis as provided by the vendor and an independent analysis to check if compositional changes occurred during the processing of the materials are presented in Table III. The greatest differences between these two analyses is observed for Al and Ti. All other elements check well.

## TABLE II

### MATERIALS PROCUREMENT

| Alloy | Vendor Heat No. | Our Heat Designation | Vendor | Form Ordered |
|---|---|---|---|---|
| U-700 | 64084 | Heat #1 | Special Metals | 5/8" diameter extruded bar |
| IN-100 | 67V3261 | Heat #1 | Austenal | 3/4" x 1-3/4" X 6" precision cast pieces |
| IN-100 | VD-582/583* | Heat #2 | GE Foundry | 3/4" X 1-3/4" X 3-4" precision cast pieces |
| SM-200 | 34V2804 | Heat #1 | Austenal | 3/4" X 1-3/4" X 6" precision cast pieces |
| SM-200 | 34V2865 | Heat #2 | Austenal | 3/4" X 1-3/4" X 6" precision cast pieces |
| Inco 713C | 601 | Heat #1 | LTV Aero | 1/8" TK as-cast sheet |
| Inco 713C | 602 | Heat #2 | LTV Aero | 1/8" TK as-cast sheet |
| René Y | 64-711 | Heat #1 | Haynes Stellite | 0.060" sheet (50# Heat) |
| René Y | 65-590 | Heat #2 | Haynes Stellite | 0.25" hot rolled plate** (50# Heat) |
| René 41 | TV-394 | Heat #1 | Haynes Stellite | 0.070" sheet |

*50% of heat VD-582 and 50% of Heat VD-583

**Rolled to 0.060" sheet at GE-MDLO

9

TABLE III

MATERIAL ANALYSIS

| Alloy | Heat | Ni | Cr | Co | Mo | Fe | Al | Ti | W | Mn | Cb | V | Zr | C | Si | S | B | La |
|---|---|---|---|---|---|---|---|---|---|---|---|---|---|---|---|---|---|---|
| René Y | #1 (64-711) (a) | Bal | 21.93 | 2.08 | 9.18 | 18.60 | - | - | 0.64 | 1.00 | - | - | - | - | 0.76 | - | - | 0.12 |
| | (b) | Bal | 21.78 | 1.91 | 9.16 | 18.50 | - | - | 0.64 | 1.00 | - | - | 0.09 | - | 0.79 | 0.006 | - | 0.17 |
| René Y | #2 (65-530) (a) | Bal | 22.25 | 2.06 | 9.19 | 18.74 | - | - | 0.47 | 1.02 | - | - | - | - | 0.76 | - | - | 0.11 |
| | (b) | Bal | 22.21 | 1.75 | 8.03 | 19.00 | - | - | 0.60 | 0.94 | - | - | 0.06 | - | 0.80 | - | - | 0.16 |
| IN-100 | #1 (67V32611) (a) | Bal | 9.92 | 14.80 | 2.83 | <0.20 | 5.85 | 4.43 | - | <0.02 | - | 0.94 | 0.08 | - | 0.06 | 0.001 | 0.0095 | - |
| | (b) | Bal | 10.24 | 15.65 | 3.06 | 0.14 | 5.25 | 4.30 | - | <0.05 | - | 0.93 | 0.05 | 0.18 | <0.10 | 0.002 | 0.014 | - |
| IN-100 | #2 (VD-582/3) (a) | Bal | 10.08 | 14.56 | 2.87 | 0.92 | 5.88 | 4.77 | - | <0.02 | - | 0.92 | 0.21 | 0.17 | 0.09 | 0.010 | 0.0145 | - |
| | (b) | Bal | 9.32 | 14.98 | 3.06 | 0.44 | 5.63 | 4.44 | - | 0.03 | - | 0.92 | 0.08 | - | 0.05 | 0.034 | 0.012 | - |
| SM-200 | #1 (34V2894) (a) | Bal | 9.36 | 10.10 | - | 0.93 | 4.45 | 2.08 | 11.14 | 0.006 | 1.25 | - | 0.03 | - | 0.13 | - | - | - |
| | (b) | Bal | 9.06 | 9.90 | - | 0.95 | 5.00 | 2.07 | 12.23 | <0.01 | 0.94 | - | 0.05 | 0.15 | 0.003 | - | 0.015 | - |
| SM-200 | #2 (34V2865) (a) | Bal | 9.37 | 10.12 | - | 0.95 | 4.47 | 2.07 | 11.14 | 0.006 | 1.16 | - | 0.04 | - | 0.10 | - | - | - |
| | (b) | Bal | 9.09 | 9.86 | - | 0.94 | 5.10 | 2.05 | 11.95 | <0.01 | 0.92 | - | 0.05 | 0.15 | 0.004 | - | 0.017 | - |
| Inco 713C | #1 (601) (a) | Bal | 13.60 | 0.65 | 5.53 | 0.64 | 5.79 | 1.11 | - | 0.03 | 2.69 | - | 0.04 | - | 0.08 | - | 0.0077 | - |
| | (c) | Bal | 13.50 | - | 5.40 | - | 6.30 | 0.80 | - | - | 2.30 | - | - | 0.14 | 0.10 | - | - | - |
| Inco 713C | #2 (602) (a) | Bal | 13.57 | 0.65 | 5.53 | 0.63 | 5.63 | 1.18 | - | 0.03 | 2.69 | - | 0.04 | - | 0.09 | - | 0.0071 | - |
| | (c) | Bal | 13.50 | - | 5.40 | - | 6.30 | 0.80 | - | - | 2.30 | - | - | 0.14 | 0.10 | - | - | - |
| René 41 | (TV-394) (a) | Bal | 19.67 | 10.52 | 9.51 | 0.20 | 1.43 | 3.05 | - | 0.06 | - | - | - | - | 0.07 | 0.002 | 0.0022 | - |
| | (b) | Bal | 19.35 | 11.03 | 9.94 | 3.80 | 1.47 | 3.10 | - | 0.01 | - | - | - | 0.11 | 0.07 | - | 0.006 | - |
| U-700 | (64084) (a) | Bal | 14.90 | 14.75 | 4.09 | <0.20 | 4.06 | 3.60 | - | <0.02 | - | - | - | - | 0.05 | 0.001 | 0.015 | - |
| | (b) | Bal | 14.80 | 15.10 | 4.15 | 0.10 | 4.27 | 3.41 | - | <0.01 | - | - | <0.04 | 0.12 | <0.10 | 0.002 | 0.015 | - |

(a) Analysis performed at LJED and MDLO laboratories.

(b) Vendor's analysis of master heat.

(c) No actual analysis available, the analysis given is an average of four similar type heats.

Additional characterization of the alloys is afforded by their mechanical properties given in Table IV and their microstructures depicted in Figures 1, 2, and 3. Variations in the microstructures are seen to exist between heats of the same alloy. However, for these studies, the differences in structure are considered insignificant and reflect the slight variations normally expected in processing and/or composition.

The cast alloys are characterized by a large grain size (1/32"-1/8") and the presence of shrinkage voids. The grain size was found to vary from alloy to alloy, heat to heat, and in some cases between specimens cut from the same cast piece. Although shrinkage voids were present in all cast alloys, they were most pronounced in IN-100 (Heat 2) and both heats of Inco 713C.

The effects of heat treatment on the oxidation behavior of the alloy is not being emphasized in this program. Therefore, unless otherwise specified, all alloys were evaluated in the normal heat-treatment condition used in service, (See Table IV).

## 3.2  Specimen Preparation

All specimens used in these studies were machined from the starting materials into the form of thin rectangular coupons. The coupons were 50 to 60 mils thick with the exception of those from Inco 713C which were approximately 120 mils thick. The size of the coupons varied dependent upon the type of oxidation test to be performed. Continuous weight-gain specimens were 1-1/2 in. X 1/2 in. (area $\cong$ 10 sq. cm.), those to be used for static oxidation tests, thin film studies, and surface preparation effects were 3/4 in. X 1/2 in. (area $\cong$ 5 sq. cm.), and the dynamic oxidation specimens were 2 in. X 1/2 in. (area $\cong$ 13 sq. cm.). After machining, all specimens were reconditioned to remove tool marks and other imperfections. The specimens were wet abraded by hand through 600 grit silicon carbide paper. To minimize the tendency toward oxide spalling at the sharp corners of the specimens, they were rounded during hand grinding. In all instances, the dimensions of any one specimen were held to a tolerance of ± 1 mil.

To compute the surface area of the specimens, only width and length measurements as determined by flat anvil micrometers were used. The surface area contribution from the sides of the coupons were neglected since at most they constituted 15% of the total surface area which was further reduced by rounding the corners of the specimens. Further, the fact that the specimens were approximately the same thickness permitted a comparative evaluation of

11

TABLE IV

## MECHANICAL PROPERTIES OF STARTING MATERIALS

| Alloy | Heat | Tensile Properties At Various Temperatures | | | | | | Stress Rupture at 1800°F | | | |
|---|---|---|---|---|---|---|---|---|---|---|---|
| | | Temp °F | Ultimate psi | 0.2% YS psi | Elong % | % RA | R_c | Stress psi | Life hrs | % RA | Elong % |
| René Y(a) | 64-711 | RT | 98,500 | 38,500 | 51.2 | - | - | | | | |
| | | 1200 | 65,500 | 22,000 | 53.8 | - | - | | | | |
| | | 1600 | 30,900 | 20,200 | 8.3 | - | - | | | | |
| | | 1800 | 20,900 | 19,900 | 14.3 | - | - | | | | |
| René Y(a) | 65-590 | RT | 109,100 | 45,850 | 46.1 | - | - | | | | |
| | | 1600 | 29,175 | 21,950 | 48.8 | - | - | | | | |
| IN-100(b) | 67V3261 | 1300 | 145,000 | 108,700 | 10.7 | 15.7 | - | 27,500 | 47.2 | 14.7 | 12.3 |
| IN-100(b) | VD-582/583 | 1300 | 146,000 | 125,000 | - | - | - | 27,500 | 41.3 | 6.6 | - |
| SM-200(b) | 34V2804 | RT | 140,000 | 127,000 | 5.0 | - | 41 | 29,000 | 65.1 | - | 9.0 |
| SM-200(b) | 34V2865 | RT | 120,000 | 100,000 | 5.0 | - | 39 | 29,000 | 75.5 | - | 10.0 |
| René 41(c) | TV-394 | RT | 143,000 | 75,000 | 44.0 | - | 22 | | | | |
| | | 1400 | 168,000 | 126,000 | 11.0 | - | - | | | | |
| U-700(d) | 64084 | 1300 | 168,000 | 123,000 | 34.6 | 32.8 | 37 | 18,000 | 81.3 | - | - |

(a) Solution annealed 30 min. @ 2150°F AC - Test conducted at GE - MDLO

(b) As Cast

(c) Heat Treatment - Solution annealed 30 min. @ 1975°F AC, aged 16 hrs. @ 1400°F AC

(d) Heat Treatment - 4 hrs. @ 2135°F AC, 4 hrs. @ 1975°F AC, 24 hrs. @ 1550°F AC, 16 hrs. @ 1400°F AC
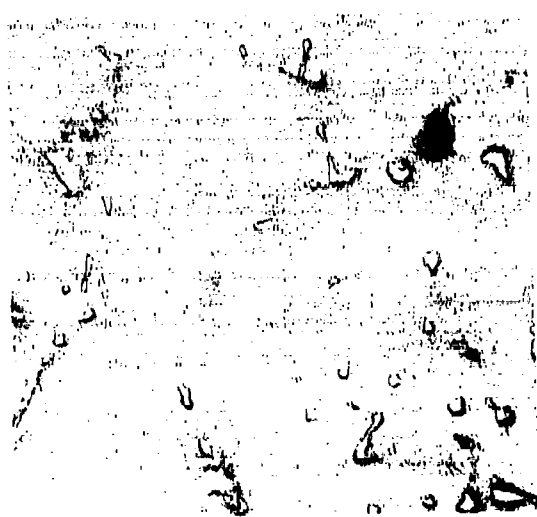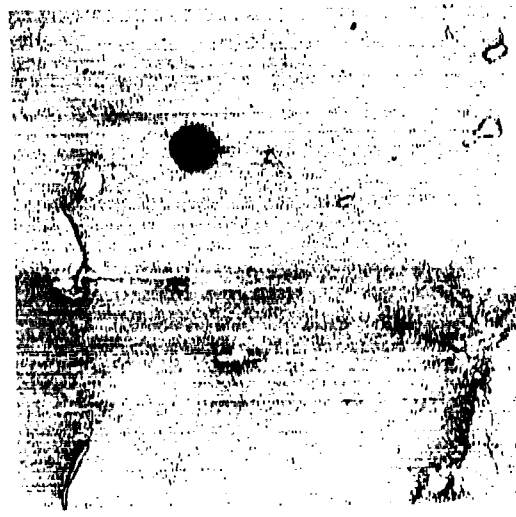
(a)  Heat  #1      L5176                    (b)  Heat  #2      L5177

SM-200
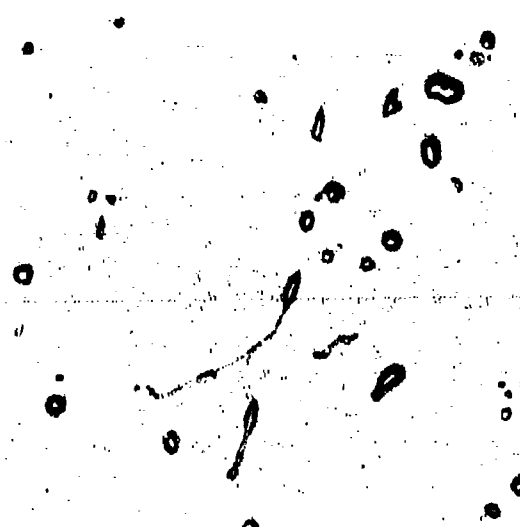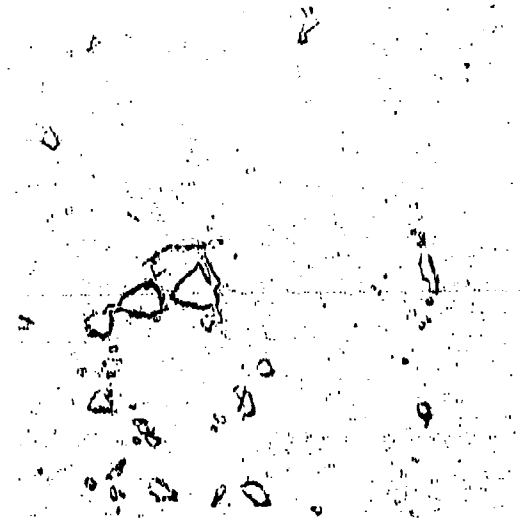
(c)  Heat  #1      L5174                    (d)  Heat  #2      L5175

IN-100

Figure 1.  Representative As Cast Microstructures Of SM-200 And IN-100.
           Etched Electrolytically In 3% HCl - $H_2O_2$.  250X
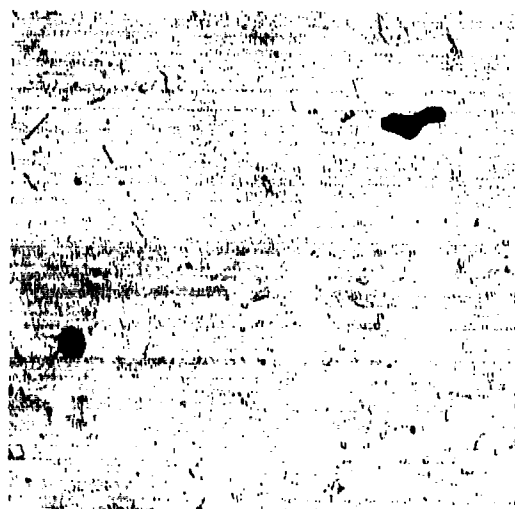
L5172

L5173
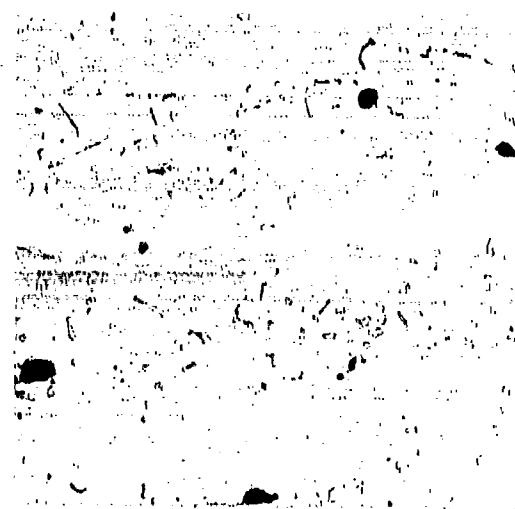
INCO 713C
(250X)
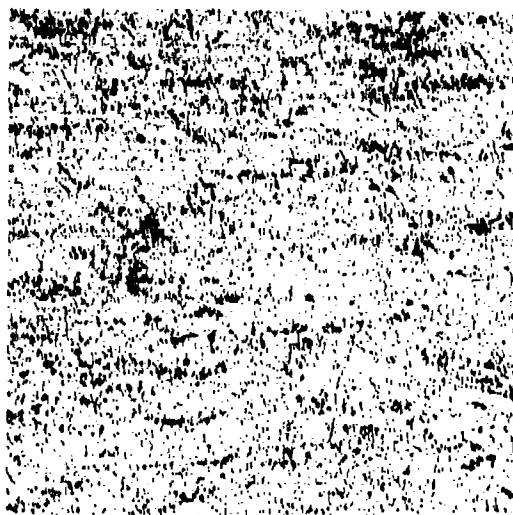
(a) Heat #1

(b) Heat #2

Rene Y
(100X)

L5117

(c) Heat #1
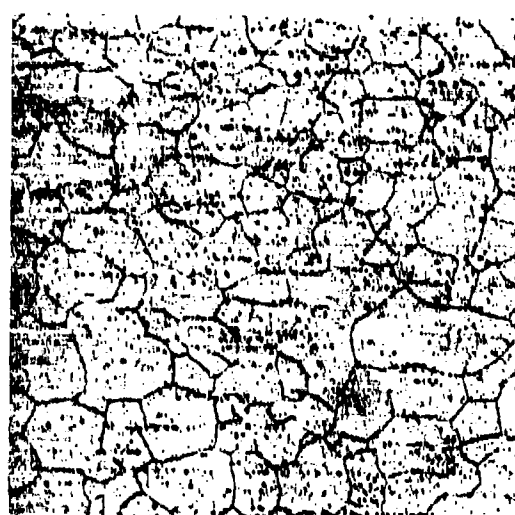
(d) Heat #2

FIGURE 2    Representative Microstructures of INCO 713C and René Y.    Etched
electrolytically in 3% HCl - $H_2O_2$.

(b) Microstructure Of
René 41 As Mill Annealed    100X

(a) Longitudinal Microstructure
Of U-700 Bar As Stress
Relieved          250X

Figure 3.   Representative As Received Microstructures Of U-700 And René 41.   Electrolytically Etched
In 3% HCl - $H_2O_2$

15

oxidation weight gain without considering the area contribution from the sides. In computing the area for weight-gain measurements of continuous weight-gain specimens, the surface area change produced by drilling the specimen hanger hole was also neglected. Surface area calculations demonstrated that the apparent surface area reduction produced by removing surface metal during drilling is more than compensated for by considering the area contribution from the hole circumference.

### 3.2.1 Continuous Weight-Gain Specimens

Following the hand polishing process, the continuous weight-gain specimens were electropolished to (1) produce a surface which was both uniform and reproducible; and (2) remove the stressed or flowed metal (Beilby layer) which could affect initial oxidation kinetics. Some difficulty was encountered in establishing an electropolishing procedure suitable for all the superalloys to be tested in this program. This was apparently the result of composition and structural differences among the alloys. Of all the electropolishing variables tried, which included type of electrolyte, temperature of electrolyte, current density, and time of polishing, an electrolyte of 150 $H_2O$, 500 cc $H_3PO_4$ (85% conc.), and 3 gm $Cr_3O_3$ at a temperature of 70°F and the parameters tabulated below was found to yield the best results.

| Alloy | Current Density (amp/cm$^2$) | Time (Sec) |
|---|---|---|
| IN-100 | 0.4 | 10 |
| Inco 713C | 0.3 | 6 |
| SM-200 | 0.3 | 5 |
| René Y | 0.5 | 10 |

Subsequent to electropolishing, the specimens were depassivated in a solution of 10% HCl in ethanol, washed in water, final rinsed in ethanol, and dried.

### 3.2.2 Other Type Specimens

Specimens to be used for static oxidation tests and dynamic oxidation studies were thoroughly rinsed in ethanol and dried subsequent to the 600 grit polish. Specimens for thin film studies were prepared as per the continuous weight-gain specimens.

Specimens to be used to determine surface preparation effects were given three different finishes resulting in different degrees of roughness. They were electropolished, dry grit blasted, and coarse wet ground. The roughness of the resulting surface was measured employing a Profilometer and the nominal surface roughnesses obtained are listed below along with the variation observed:

| | | |
|---|---|---|
| Electropolished | | $3\mu \pm 1$ RMS |
| *Wet Ground | (600 grit $SiO_2$) | $5\mu \pm 2$ RMS |
| Grit Blasted | (150 grit $Al_2O_3$) | $55\mu \pm 10$ RMS |
| Wet Ground | (50 grit $SiO_2$) | $130\mu \pm 20$ RMS |

*Preparation used for static oxidation tests.

The tolerance in the measured roughness not only reflects actual variations within the same alloy, but primarily denotes variations in the abrasion resistance (or hardness) of the various alloys used.

3.3   Test Apparatus and Procedures

3.3.1   Continuous Weight-Gain Testing

Continuous weight-gain testing was performed using two Mauer automatic recording balances positioned above platinum-wound Marshall furnaces.  Each of the units, along with the automatic recording equipment and associated accessories, is mounted in a support frame as illustrated in  Figure 4. The two units, which are identical in design, are capable of operating for extended periods at 2300°F  Temperature control was achieved through the use of saturable core reactors which were found to yield a temperature variation of ± 3°F over a 4-in. hot zone at 2100°F.  The length of this zone was further extended at lower temperatures.  Temperatures were monitored using Pt/Pt-13% Rh thermocouples sheathed in alumina and positioned in the reaction chamber adjacent to the test specimen.

The Mauer weight recording system consists of an analytical balance with an alnico magnet suspended from one arm into the magnetic field of a solenoid. The sample, whose rate of weight change is to be recorded, is suspended from the other arm of the balance into the furnace.  The basic principle of operation involves counterbalancing the weight changes of the specimen by altering the current through the solenoid which applies a force to the magnet.  The balance operates, therefore, in the null position.  Any deviation

17
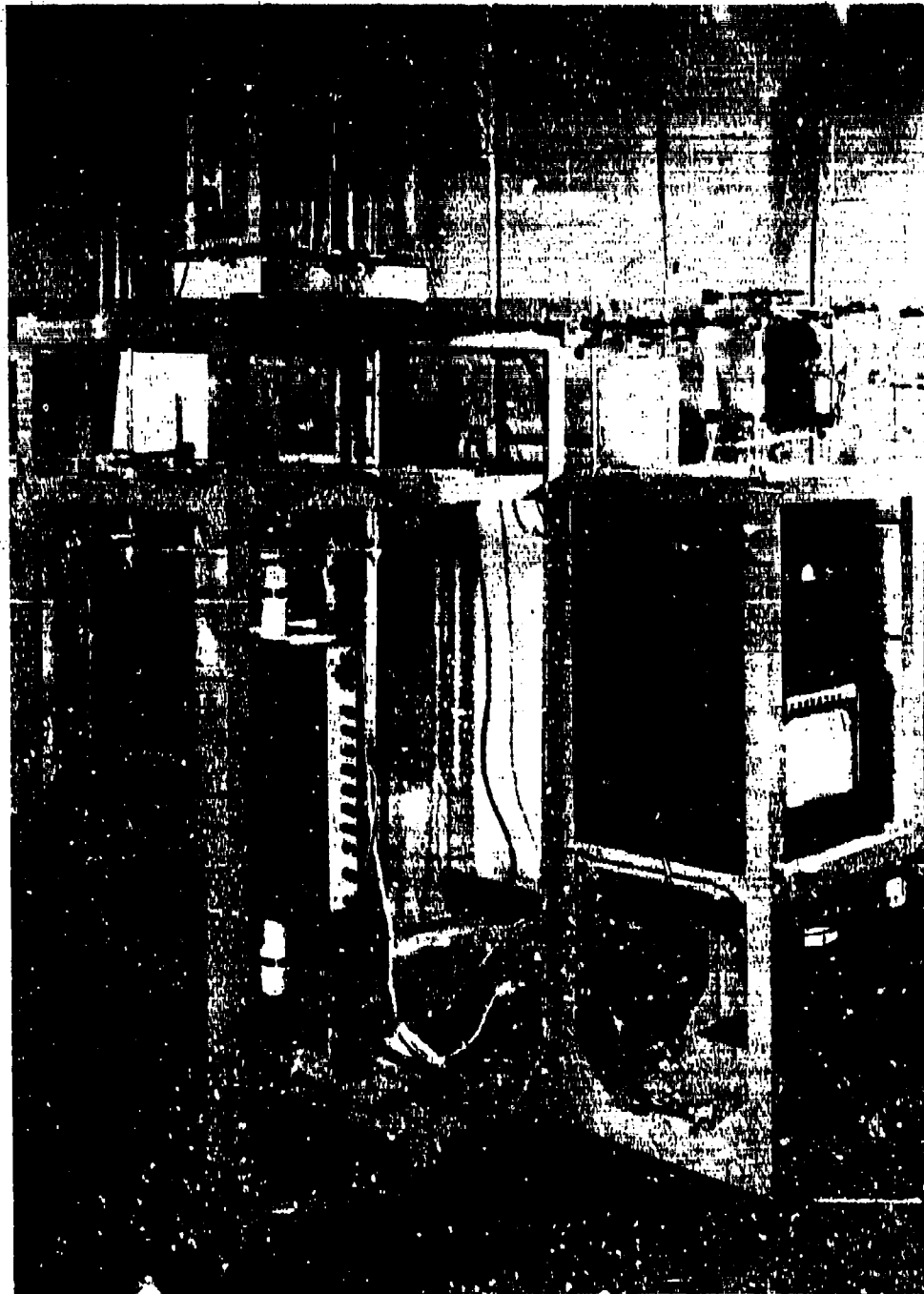
C1092218

FIGURE 4  One of the two continuous weight-gain oxidation test stations
used in this investigation.

18

in the balance beam from the horizonal is sensed by a carefully adjusted photo tube and electric circuit. Thus deviations in the weight of the specimen are compensated for by the automatic adjustment of the solenoid current acting on the alnico magnet, which restores the magnet to its null position. The actual record of weight change is obtained by calibrating and recording the solenoid current on an X-Y recorder. The recording system is so instrumented that three scales of sensitivity and range can be selected. Full-scale ranges for one chart traverse of 10, 50, and 100 mg are available. The practical accuracy of each of the above ranges is 1% of full scale or an accuracy capability of ± 0.1 mg for the most sensitive scale. Since the recording system is self-zeroing once full scale deflection is attained, a bank of 11 zero-counters allows the automatic recording of eleven times full scale weight gain or weight loss. The relative oxidation resistance of the alloys studied in this program required the use of the most sensitive scale range; hence, no weight gain was greater than 110 mg and the accuracy of the results were ± 0.1 mg.

The specimens to be tested were suspended from the balance into the furnace by means of a chain. That portion of the chain between the balance and the top of the furnace was gold plated and connected to a platinum chain for actual suspension into the furnace. The reaction chamber consisted of a two-inch diameter mullite tube capped on top with a water-cooled copper plate which had two holes drilled to allow passage of the suspension system and the monitoring thermocouple. This water-cooled plate, as well as the suspension chain, served as a condenser for the recovery of volatile reaction products. Thus, it was possible to estimate the extent of volatilization by the discoloration produced on the chain and condenser plate. The bottom of the mullite tube was ground to a male 55/50 taper and sealed by a female pyrex ground glass joint equipped with a viewing port and a side arm for introducing the oxidizing atmosphere. This arrangement allowed the observation of the specimen during oxidation and any subsequent spalling which may have occurred during the test or while cooling. It also provided a means of collecting spalled or exfoliated reaction products.

The specimens were oxidized in slow flowing air closely controlled to a flow rate of 1000 ml/min. Prior to the introduction into the reaction chamber the gross impurities in the air were removed by passing over angel hair. The air was then dried to a dew point of -70°F by passage through drying columns arranged in parallel to insure dry air for the duration of the test. The buoyancy effect produced by the flowing air coupled with the sensitivity of the balance necessitated close control of the flow rate to insure reproducibility between tests.

19

During a test, the following calibration and loading procedure was rigorously employed. With the furnace at the desired temperature and the air flowing, the specimen was hung from the chain above the reaction chamber. The balance and recorder were zeroed, employing the most sensitive scale (10 mg full scale), and a 5 mg weight was added to the pan from which the specimen hung. This produced a mechanical unbalance which placed the recording pointer at mid-scale and enabled the detection of specimen weight losses as well as weight gains during the initial stages of oxidation. The recorder was turned off, the balance placed on arrest, and the specimen lowered into the center of the reaction chamber hot zone. Care was taken to prevent the specimen from striking the chamber walls or the thermocouple, which was already in place. Any sway present in the chain was stopped and a plastic shroud placed around the exposed portion of the suspension chain between the the top of the reaction chamber and the bottom of the balance to minimize the anomolous effects produced by air currents. The balance was then taken off arrest and the recorder turned on. Although the specimen had been in the furnace two to three minutes while all the final adjustments were being made, the position of the recorder pointer, when it was first turned on, was considered the "zero". This "zero" point proved to be a critical measurement since, as will be shown in the results, the initial rate of oxidation was relatively high, particularly at temperatures above 1800°F. The two to three-minute delay in recording the oxidation rate was also considered necessary to ensure that the specimen was at the specified temperature. Therefore, although the necessary delay may have produced a theoretical shift in the position of the resultant weight gain versus time curves, the actual time lost was a very small fraction of the total 100-hour run and can be considered the same for all runs.

The two continuous weight-gain test stations operated continuously during this investigation without any serious malfunctions. However, during the initial tests the high sensitivity of the equipment and associated line power fluctuations produced some erratic results, making it necessary to install constant voltage transformers. They have proved effective in yielding specimen weight-gain data which is more amenable to evaluation. Occasionally, however, anomalies occur during the chart recording of oxidation weight changes. These fluctuations are generally small and insignificant unless the weight change of the specimen approaches the accuracy of the balance (± 0.1 mg) as observed during some of the low-temperature tests (1400°F). The variations observed are believed to be the result of fluctuation in air currents and general vibration.

### 3.3.2 Isothermal (Static) and Cyclic Oxidation Testing

All static and cyclic oxidation tests were conducted by placing specimens in zircon cup-type crucibles and oxidizing them in the static atmosphere of electric box furnaces. The furnaces, which were equipped with saturable core reactors and proportioning controllers to insure stability for long-time operation, possessed excellent temperature uniformity within their hot zones. For the two furnaces used, a temperature variation of ± 5°F existed at 1800°F within the usable 7" × 10" hot zone. At 1600°F the temperature variation in the same zone was reduced to ± 2°F. This large, uniform temperature zone permitted up to 40 specimens to be tested at any one time.

Where possible, the specimens were positioned such that the long-time test specimens were placed to the rear of the hot zone permitting rotation of shorter time test specimens near the front of the furnace. Upon completion of any test, or test cycle, the crucible was removed from the furnace and immediately covered. This prevented the loss of reaction products from the specimens, which in some instances spalled quite vigorously during cooling. After cooling to room temperature, the specimen, crucible, and specimen plus crucible weights were recorded.

### 3.3.3 Flame Tunnel Testing

The dynamic oxidation tests were performed in a natural gas fired flame tunnel of special design, illustrated in Figure 5. These flame tunnels are six inches in diameter, insulated to four and one-half inches inside diameter, and water cooled by external copper coils. Heating is provided by the combustion of a natural gas/air mixture through a ring of eight solas burners. The normal mass flow rate through the tunnel is approximately 100 lbs/in$^2$/hr., and secondary air is drawn in the center of the gas manifold. The resultant gas velocity is 50 - 75 ft/sec. The composition of combustion products and gases vary somewhat along the length of the tunnel. A typical chromatographic gas analysis made at various positions relative to the specimens at 1650 and 2000°F are tabulated below:

#### 1650°F

| Position* | Percent Gas Composition | | | |
| --- | --- | --- | --- | --- |
| | $O_2$ | $N_2$ | $H_2$ | $CO_2$ |
| 1" in front | 18.89 | 79.30 | 0.0006 | 1.14 |
| 1" in front | 18.85 | 79.43 | 0.0006 | 1.19 |
| 4" in back | 14.24 | 81.33 | 0.0007 | 3.77 |
| 4" in back | 12.78 | 81.82 | 0.0009 | 4.56 |

#### 2000°F

| 1" to right | 9.49 | 83.04 | 0.0001 | 6.36 |
| 1" to left | 9.44 | 83.18 | 0.0001 | 6.40 |
| middle/above | 9.95 | 83.11 | 0.0001 | 6.12 |

*Relative to specimens

21
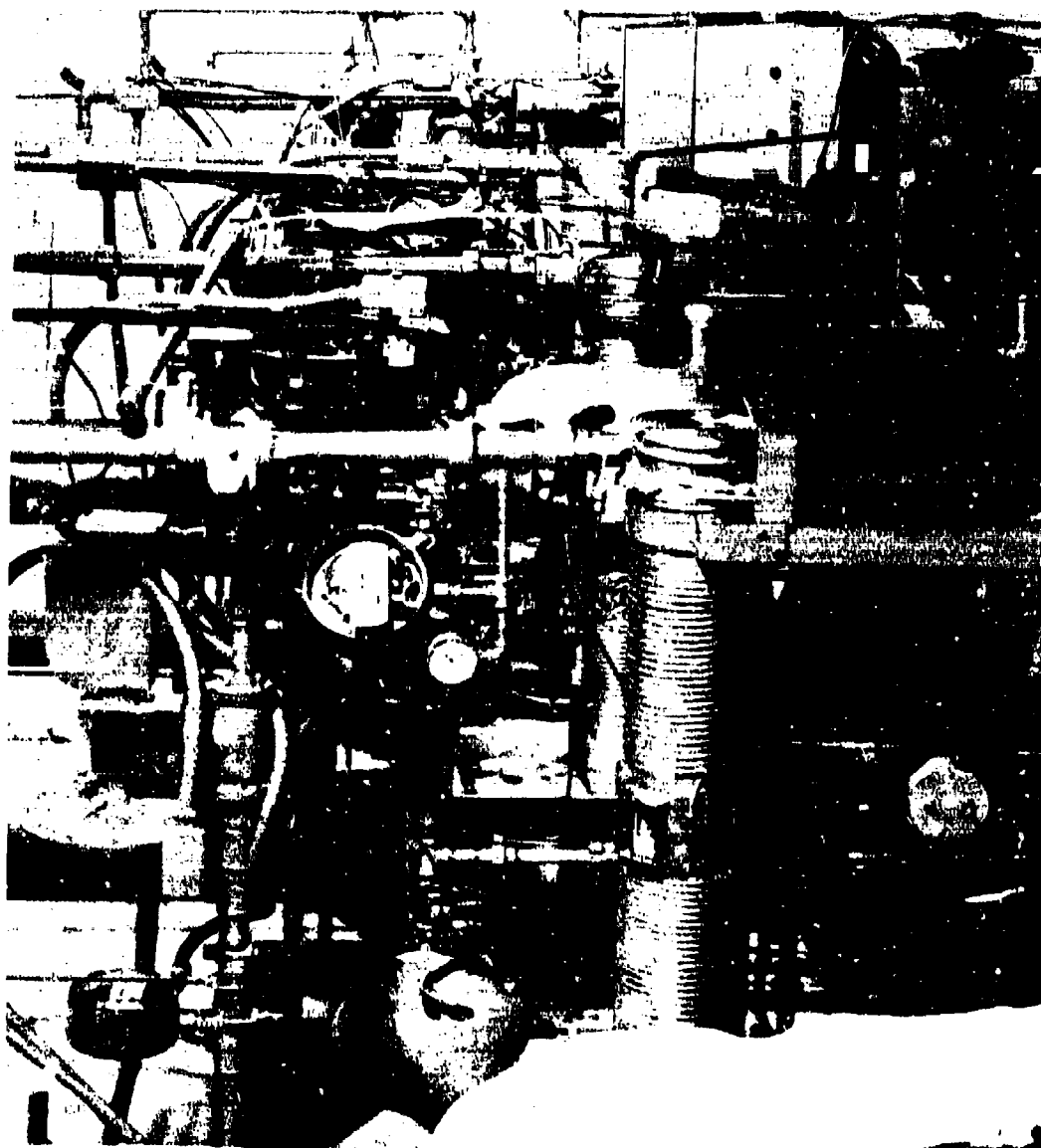
FIGURE 5    Dynamic Oxidation Flame Tunnel Facilities

(CDC-7126)

The test specimens were mounted in a K-30 fire brick, as illustrated in Figure 6, and placed in a motor driven rotating metal holder. The holder, which is air cooled, is positioned such that the specimens rotate within the hot zone of the flame tunnel perpendicular to the gas flow. This specimen holder, with a capacity of 14 specimens, rotates at 10 rpm and provided the following advantages:

(1) All alloys to be tested (six), including duplicates, could be tested at the same time while exposed to identical environmental conditions.

(2) A more quantitative and comparative evaluation of metal loss and internal oxidation was permitted due to the symmetrical arrangement of the specimens in the holder.

The temperature of the specimens was measured and controlled by means of a Pt/Pt-13% Rh thermocouple attached to a dummy specimen located just above the test specimens and was checked periodically by an optical pyrometer. At 2000°F the temperature variation of any one specimen was found to be no greater than 20°F.

During these tests the specimens were also cycled every thirty minutes from the test temperature to 1000°F at a cooling rate of approximately 3000°F/min. This was accomplished by a blast of cold air which automatically cut off at 1000°F.

### 3.3.4 Thin Film Oxidation

These tests were conducted similar to the static oxidation tests, the only difference being the time of oxidation. For the short-time, thin-film tests (five minutes to four hours), there was no means of determining the absolute time at temperature due to heat-up considerations. Therefore, the test specimens were inserted simultaneously into the furnace and arbitrarily allowed five minutes to attain the desired temperature. Since these tests were intended only to produce thin films for structural evaluation, absolute times of exposure were not considered critical.

### 3.4 Measurement of Subscale Reactions

Subsequent to the static oxidation tests the type and extent of subscale reaction was determined for both heats of all alloys. Each specimen was prepared for metallographic observation by sectioning it, placing it on a wedge* and then vacuum mounting in a cold setting plastic reinforced with

---

*∠ = 11°32' (5:1) or 14°31' (4:1)

23

1"
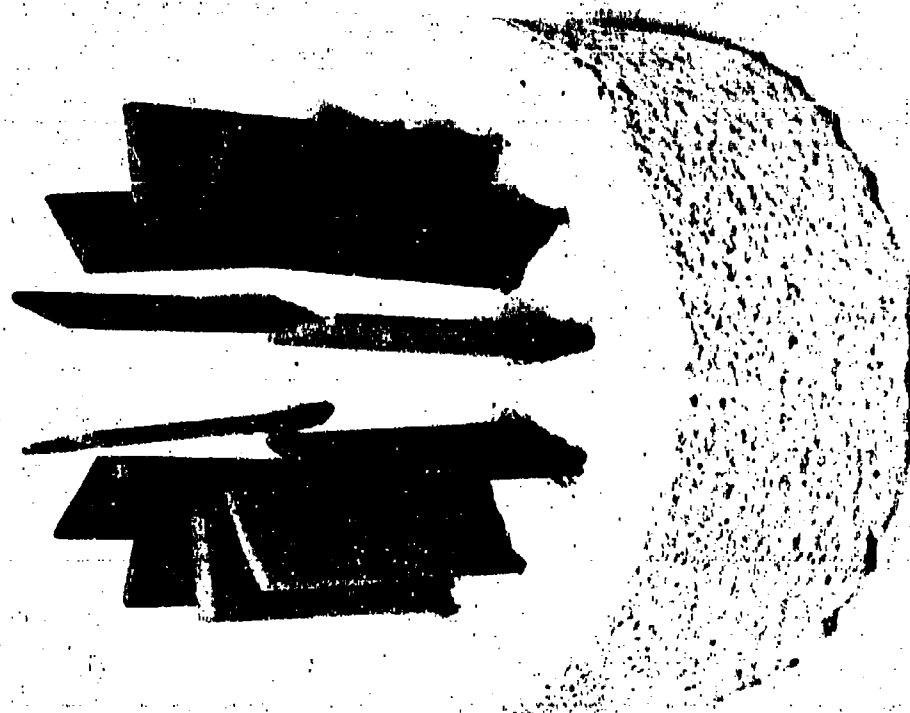
C651110804

FIGURE 6   Flame Tunnel Rotating Specimen Holder Illustrating the Positioning of Specimens

$Al_2O_3$[11]. Standard metallographic polishing procedures were employed until the plane of polish intersected the oxidized surface of the specimen. This produced a tapered section through the oxidized surface with a vertical distortion or magnification of either 4 or 5:1. Thus an oxidized surface when mounted on a 5:1 taper and viewed at 100X was in reality at 500X in a direction perpendicular to the oxide scale. This mounting technique yielded a measurement accuracy for determining the depth of subscale features of ±0.25 mils. In conjunction with the special mounting material, which proved very effective in preserving the oxidized edge, excellent metallographic results were obtained.

After the normal metallographic polish the specimens were etched to more clearly reveal the extent of the subscale reaction, i.e., $\gamma'$ dissolution and $\gamma'$ agglomeration. The most successful etching technique found suitable for all alloys consisted of electrolytically etching in a solution of 2% chromic acid + 5-10% $H_2SO_4$ in water at 3-6 volts. Although some materials readily stained employing this etch, the stain could be easily removed by a 10% HCl methanol solution. An alternate etch used with moderate success contained equal parts HCl and Schantz reagent* , applied with a cotton swab.

Measurements to determine the extent of scale and subscale reactions were performed on these alloys not only to assist in developing an understanding of the oxidation mechanism, but also to provide data useful for application of these alloys as structural components. It is therefore important that each type of measurement be thoroughly defined. A definition of the measurements employed to depict the resultant scale and subscale morphology is presented below and typically illustrated in Figure 7.

(a) Scale thickness - The thickness in mils of the outermost continuous and relatively dense surface layer formed during the reaction. Usually made up of oxide phases but occasionally contains matrix metal inclusions.

(b) Internal oxidation (I.O.) - The depth below the scale/metal interface in mils where selective oxidation of reactive alloying elements occurs through the dissociation of oxide(s) at the scale/metal interface or anion diffusion through the surface scale.

Due to the variety of alloys studied and differences in the type of I.O. observed, this definition had to be further subdivided into I.O. and I.G.O. (intergranular oxidation). Hence, the broad term I.O. refers to both the classical type salt and pepper suboxide formation and/or intergranular oxidation. Since the latter type usually extends deepest into the material, it is also referred to here as the maximum I.O. (see Figure 7). Internal nitrides are also included in this measurement since they generally fall within the I.O. region.

---

* 150 ml $H_2O$, 30 ml $H_2SO_4$, 360 ml HCl, 100 ml $HNO_3$, 150 ml acetic acid and $FeCl_3$
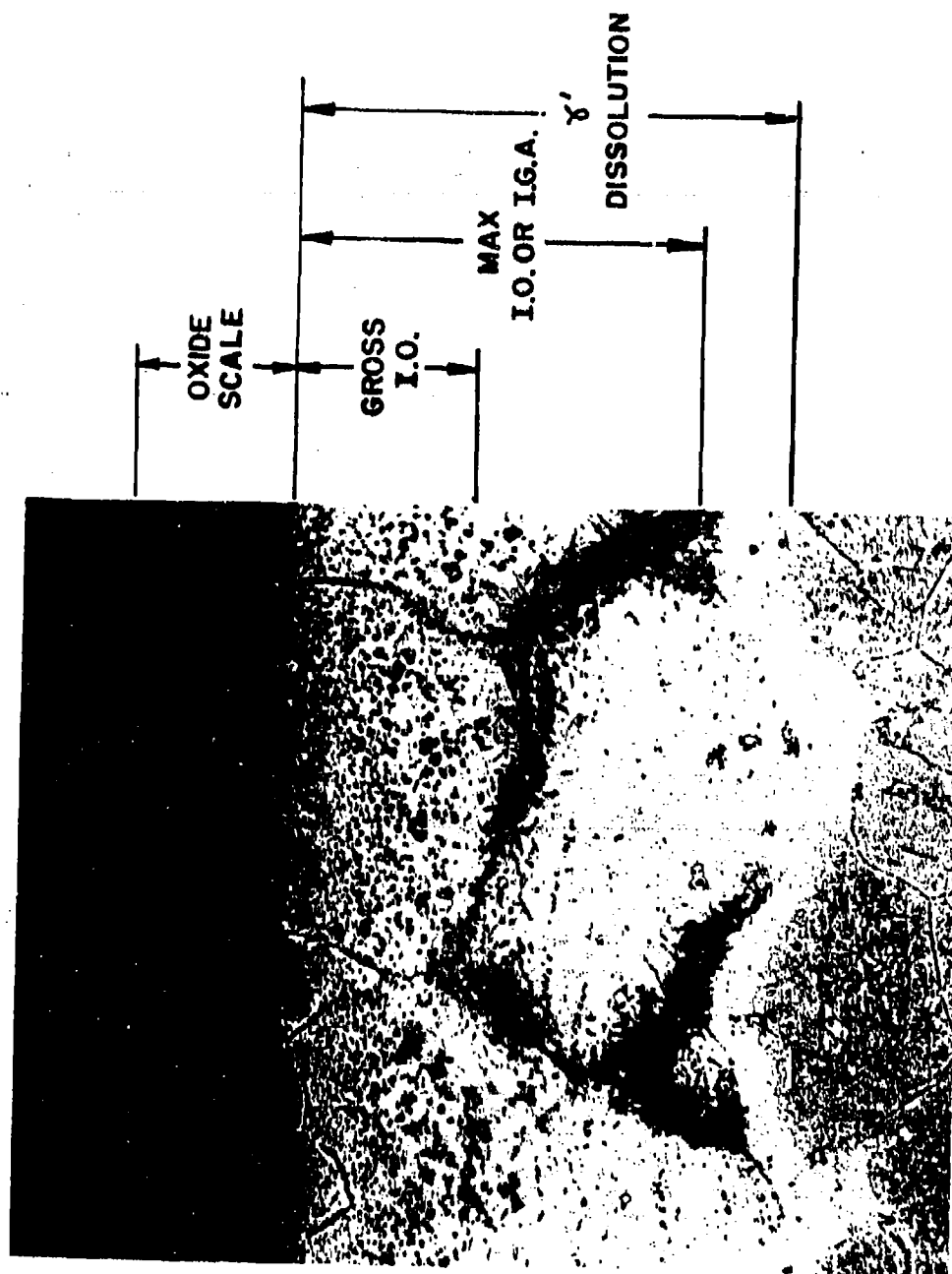
FIGURE 7    Identification of Measurements Used to Characterize Metallographic Scale and Subscale Morphology.

26

(c)  γ' dissolution - The depth below the scale/metal interface
     at which significant structural changes occur because of
     the preferential depletion or enrichment of alloying
     elements. This effect is primarily evident after etching
     due to the dissolution of γ' and for this reason is so
     classified. The dissolution of other intermetallics such
     as carbides and borides are also observed resulting in a
     zone consisting of essentially γ phase (F.C.C. solid
     solution). This measurement is the same as that sometimes
     referred to as alloy depletion (A.D.). However, since the
     concentration of some elements actually increase in this
     region, as will be illustrated by the EMX results, the
     term A.D. is considered misleading.

(d)  Metal loss - The physical reduction in material thickness
     brought about by the conversion of metal to oxide scale.
     The measurement is obtained by comparing the metal thickness
     (including I.O.) before and after the oxidation test. The
     expected accuracy for this measurement is ±0.5 mil, since
     vertical sections are employed. In many instances this
     measurement was not reported for static oxidation specimens
     since the measurement was within the cited accuracy.

As illustrated in Figure 7, the original oxide metal interface is taken as the
base-line for all measurements and as such is assumed not to vary during
oxidation. This assumption might be reasonable in a simple alloy system con-
trolled by cation diffusion. However, in the complex alloys studied here
this assumption is questionable at high temperatures and long times where
oxide spalling occurs, scale interfaces are irregular, and internal oxidation
may be replaced by a more favored sub-oxide formation. Hence, for some
alloys the above scale and subscale measurement identification may not be
valid over the entire time/temperature range investigated due to either
movement or loss of identity of the original oxide/metal interface.


3.5  Reaction Product Identification Procedures

To characterize the reaction products formed during the various types of tests
performed in this investigation, a number of quantitative and/or semi-
quantitative evaluation techniques had to be employed. X-ray diffraction
together with electron microprobe X-ray (EMX) analysis and light microscopy
evaluations served as the major means of identifying the reaction products
formed. In addition, however, electron diffraction and electron microscopy
were used to establish the morphology of thin films, while X-ray florescence

27

and chemical analysis were employed when necessary for further substantiation. It has been emphasized throughout this investigation that at least two independent techniques be employed for all critical structural identifications and where possible duplicate specimens be analyzed.

### 3.5.1  X-Ray Diffraction

X-ray diffraction spectrometer traces and Debye Scherer type photograms were obtained using filtered chromium or copper radiation. The X-ray diffraction studies were conducted on electrolytically stripped oxide films, scraped oxides, oxide scales in situ, spalled reaction products, and any other features of the oxide such as protrusions which might lead to a better understanding of the oxide morphology. Information regarding suboxides and the general oxide arrangement was obtained by comparing the oxides identified from the different type X-ray specimens (i.e., oxide in situ versus electrolytically stripped). Lattice parameter determinations were performed in those instances where the information was required to identify the oxide, as in the case of spinel-type structures or where oxide solubilities were expected. In general, these parameters were determined employing the Strammanis technique where only the high single reflections are used for the computation. Where possible, the standard ASTM Powder Diffraction Index was used for identification purposes. There were instances, however, where the identity of certain lines could not be made due to nonavailability of ASTM Index patterns. This necessitated the synthesis of compounds such as $NiTiO_3$ for firm identification and clarification of the various alloy matrix reflections.

### 3.5.2  Electron Microprobe X-Ray Analysis

For the majority of the EMX analysis concentration versus distance traces were taken on cross sections of the oxidized specimens mounted on 5:1 tapers identical to those employed for metallographic evaluation. These traces clearly denoted the concentration variation of any element as affected by the oxidation process since the oxidized region was effectively expanded. Occasionally counting techniques were employed to more quantitatively determine the concentration of specific features. Calibration of the element concentration was established using pure standards, since correction factors for interaction effects between elements were not considered significant enough in this study to warrant their inclusion.

Aside from determining the major alloying element distribution and the concentration variation in the oxide scale for correlation with X-ray results, the EMX proved to be a useful tool in identifying constituents present as internal reaction products. By simultaneously following the concentration plot and observing the traversing electron beam ($\sim$ 0.5 micron) through a microscope concentration peaks could be related to particles in the subscale. The fact

that oxide particles fluoresce when bombarded by the electron beam served to distinguish them from intermetallics and carbides and to identify their relative position in the metal matrix (i.e., transgranular or intergranular). It was this very technique which permitted the identification of TiN. Wavelength scans were also employed to qualitatively identify constituents contained in various intermetallic phases.

### 3.5.3 Light Microscopy

Light microscopy was used to complement the phase identification of the above two techniques. The reaction zones of the metallographic specimens were magnified by the taper mounting technique employed. This permitted an evaluation of the number of surface oxide phases present and the general morphology of internal reaction products which were correlated with the other features. Occasionally polarized light was incorporated to distinguish between isotropic and anisotropic constituents.

### 3.5.4 Electron Microscopy

Electron microscopy was used to follow the differences in oxide topography between the alloys during oxidation. Some studies were also made of the oxide/metal interface morphology.

The morphology of the oxidized surfaces were determined by direct replication in collodion, and preshadowing with germanium at approximately 65°. The replicas were then shadowed with carbon and the original collodion replica dissolved. The resultant replicas were examined in a Philips Model 100B electron microscope.

### 3.5.5 Electron Diffraction

The surface oxides or thin films produced in the early stages of oxidation were identified employing electron diffraction reflection techniques. In this method electrons are diffracted from the bulk surface of the oxidized specimens at a low angle and the resultant Debye rings analyzed as in the case of X-ray diffraction.

## 4.1 Oxidation Kinetics

Since the measure of the intensity of an oxidation process is its rate, a means must be established for defining this rate process. In this investigation the thermogravimetric (continuous-weight gain) method was employed where the rate of oxidation can be derived from the change in weight of the sample as a function of time at the selected temperature. Ideally these experimental results should be evaluated by empirically "fitting" the data to the normal oxidation rate laws. The form of the rate law which is most generally applicable can be expressed as:

$$\left(\frac{\Delta W}{A}\right)^n = K \cdot t + C \qquad\qquad \text{Equation 1}$$

where $\frac{\Delta W}{A}$ = change in weight/unit area ($mg/cm^2$)

      $n$ = the reaction index expressed as a whole integer and being 1 for a linear rate, 2 for a parabolic rate, 3 for a cubic rate, etc.

      $t$ = time in minutes

      $K$ = the rate constant for the process, the order of which depends upon "n"

      $C$ = an integration constant

If the integration constant "C" is assumed to be zero, which would be the case if no oxide film were present on the metal surface at t = 0, the reaction index "n" can be estimated from the slope of log (W/A) versus log t plots by considering the general rate equation in the following form:

$$\frac{\Delta W}{A} \approx K t^{\frac{1}{n}}$$

$$\text{or } \log \frac{\Delta W}{A} = \log K + \frac{1}{n} \log t \qquad\qquad \text{Equation 2}$$

Where the slope of the straight line portion of the resultant curves is equal to the reciprocal of the exponent for the rate law that is controlling the reaction. However, since "C" can usually only be assumed zero for the initial oxidation rate process (< 10 min) log-log plots serve only to approximate the order of the reaction (n) and do not permit a determination of the actual rate

constant (K). The rate constant must be determined from either the slope of
the straight line formed by plots of $(\Delta W/A)^n$ versus t or by computations.
Having established the rate of reaction (K) and providing the order of the
reaction (n) is constant the temperature dependence of the oxidation process
can be determined from the following equation:

$$K_n = A \cdot exp^{(-Q/RT)} \qquad \text{Equation 3}$$

where $K_n$ = rate constant $(mg/cm^2)^n/sec$

$A$ = constant

$Q$ = activation energy (cal/mole)

$R$ = gas constant (cal/mole/°K)

$T$ = absolute temperature (°K)

If from Equation 3 a plot of log K versus 1/T produces a straight line, the
slope is representative of the activation energy of the oxidation process.
The activation energy may in turn provide information regarding the mechanism
of the reaction.

Although the kinetic analysis presented above is valid in theory, and in fact
applicable for some pure metals or simple alloy systems, the complex and
heterogeneous oxidation processes displayed by the alloys studied in this
investigation would appear to preclude a rigorous analysis of this type.
However, all the alloys studied displayed some indications of para-linear type
oxidation either at the lower temperatures or during initial times at the
higher temperatures. It was only after long time or high temperature exposures
that considerable deviation from parabolic rates were observed. Therefore, to
provide some quantitative means of comparing the oxidation rates of these
alloys a kinetic evaluation was conducted employing linear and parabolic rate
constants determined by "curve fitting" to Equations 1 and 3.

The continuous weight gain test data for both heats of René Y, IN-100, SM-200,
and Inco 713C as obtained from the actual continuous chart recordings are
tabulated in Tables IA, IIA, IIIA and IVA respectively. Some of these data
are plotted on a logarithmic basis to:

(a)  Present the typical oxidation behavior of each alloy as a
function of time and temperature

(b)  Illustrate the heat-to-heat variation which exists

(c)  Approximate the order of the reaction and the time interval
which it applies

31

Some variation is noted to exist in the oxidation behavior between the two heats of these alloys. However, this heat-to-heat variation is observed to be no worse than that which exists between identical test specimens of the same heat. The variability can then be ascribed to differences in the individual specimens (i.e., surface porosity, microstructure, and varying degrees of electropolishing) or inherent errors in the experimental technique.

### 4.1.1  René Y

Of the alloys evaluated, René Y conformed most readily to a kinetic analysis. From the curves illustrated in Figures 8 and 9 a linear reaction rate (slope $\cong$ 1) is observed for short times at 1800°F and below, with subsequent parabolic oxidation (slope $\cong$ 1/2) at longer times and/or higher temperatures. Further evidence for the existence of linear oxidation during the initial stages of oxidation was afforded by the straight lines produced in plots of W/A versus time. The parabolic regions of the rate curve were demonstrated by the excellent straight line fit obtained when $(\Delta W/A)^2$ was plotted as a function of time. There were instances in which the oxidation data were better represented by a "cubic" rate, but since this was not true in the majority of cases, the best fit to a "parabolic" rate(s) of oxidation was obtained. It is apparent from the curves that the linear rates which exist at 1600° and 1800°F are replaced by parabolic rates as time increases. At 1800°F and above, two parabolic rates appeared to be present, the second one being slower than the first. The oxidation rate constants computed from the data shown in Table IA, as well as the time intervals over which these rates apply are summarized in Table V. The initial ten minutes of oxidation was not included due to the effects of temperature and surface preparation during this stage of oxidation.

A plot of the rate constants in the normal Arrhenius form is shown in Figure 10 and includes both heats. The variation between Heats 1 and 2 during linear oxidation is evident and more scatter is observed in the data points for Heat 2. The validity of assigning activation energies to processes as complex as these may be questionable. However, the slopes of these curves suggest apparent activation energies of 36 K cal/mole for the linear rate and 45 and 29 K cal/mole for the two successive parabolic processes. The secondary parabolic process obtained from these results is observed only after long times at moderate temperatures or after relatively shorter times at the high temperatures where volatile reaction products were observed after testing, as indicated by a black condensate on the specimen hanger chain. It has also been demonstrated[43] that such factors as oxide porosity or densification, changing specimen geometry, and oxide interactions can produce deviations from ideal parabolic rate laws. Hence, the secondary parabolic rates observed may be representative of combined oxidation and volatilization processes which produce what appears to be a slower parabolic oxidation rate. If this is the case, the assignment of an activation energy to this latter process will have no significance with respect to determining the oxidation mechanism.
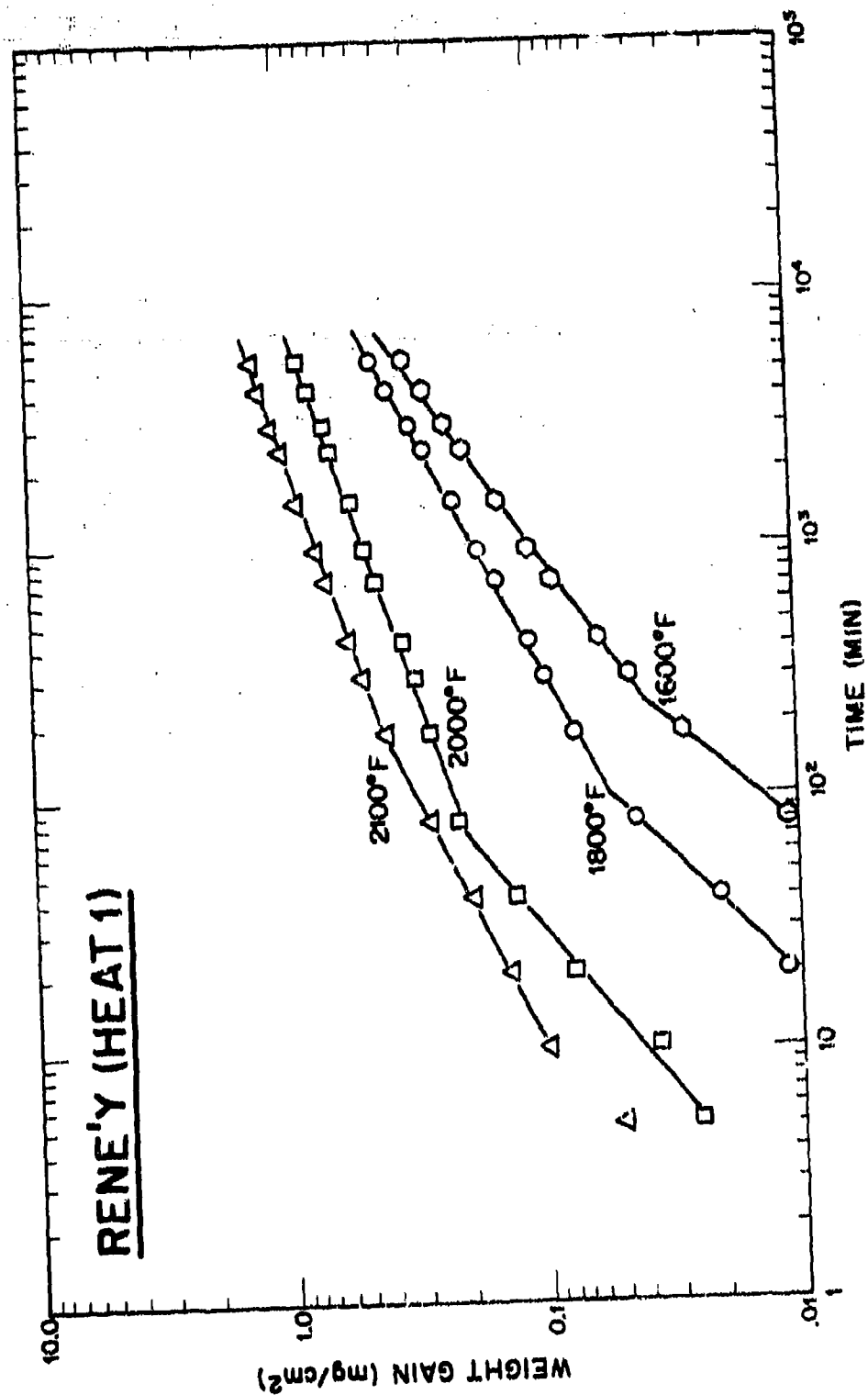
FIGURE 8  Typical Logarithmic Plot of Weight Gain Versus Time for René Y Heat 1

33

FIGURE 9  Typical Logarithmic Plot of Weight Gain Versus Time for René Y  Heat 2

34
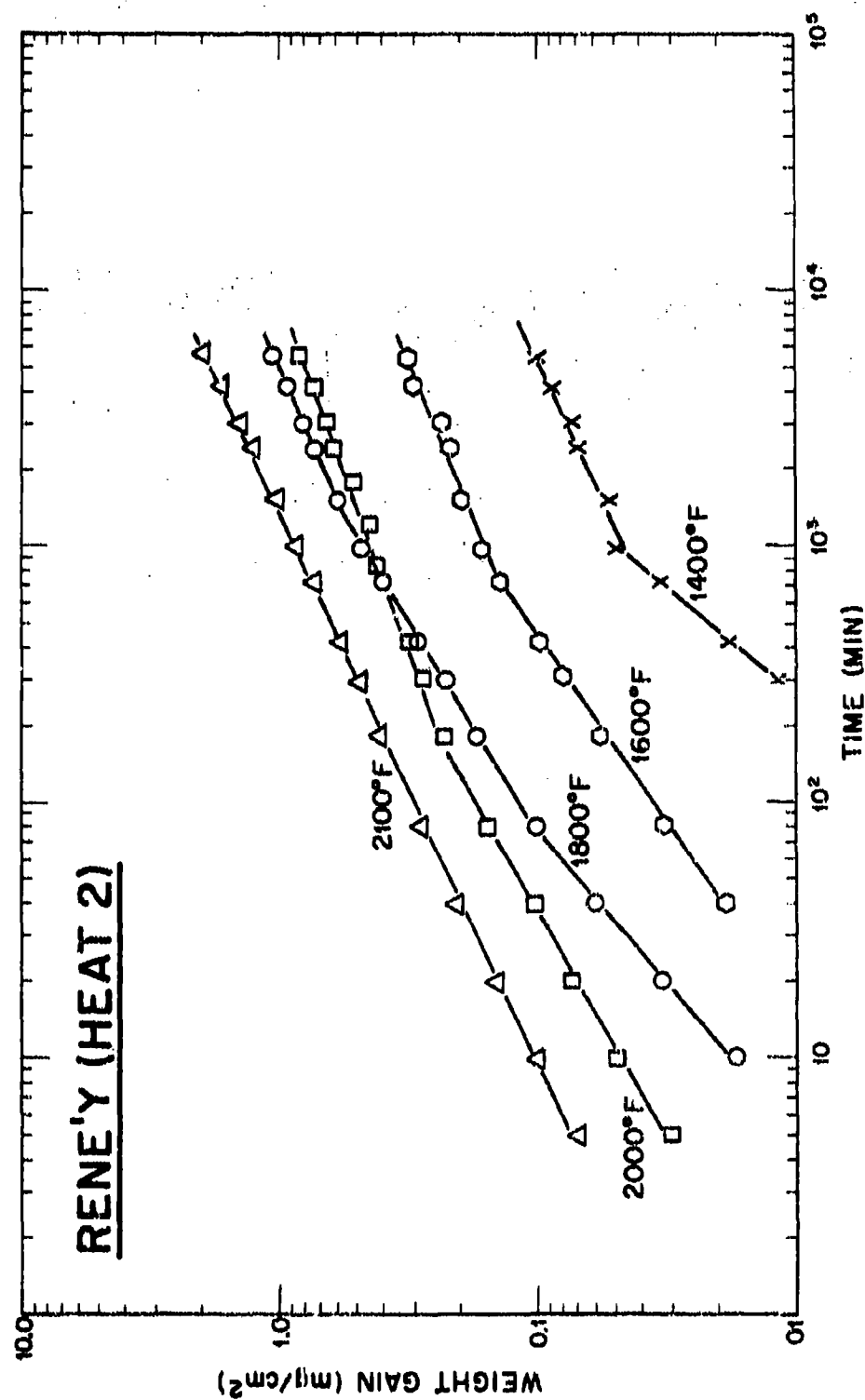
## TABLE V

### SUMMARY OF OXIDATION RATE CONSTANTS FOR RENÉ Y

**Heat #1 (64-711)**

| Temp °F | Test No. | $K_L$(a) | $K_{PI}$(b) | $K_{PII}$(c) |
|---|---|---|---|---|
| 1600 | 12 | $3.06 \times 10^{-6}$ (10-200 Min) | $3.38 \times 10^{-7}$ (400-6000 Min) | — |
| 1600 | 16 | $5.01 \times 10^{-6}$ (10-180 Min) | $4.52 \times 10^{-7}$ (180-3400 Min) | — |
| 1600 | 44 | $2.50 \times 10^{-6}$ (10-180 Min) | $3.09 \times 10^{-7}$ (400-6000 Min) | — |
| 1800 | 2 | -- | $2.08 \times 10^{-6}$ (40-1200 Min) | $1.13 \times 10^{-6}$ (1200-6000 Min) |
| 1800 | 23 | $8.67 \times 10^{-6}$ (10-100 Min) | $5.00 \times 10^{-7}$ (165-2200 Min) | $6.51 \times 10^{-7}$ (2200-6000 Min) |
| 1800 | 29 | $8.35 \times 10^{-6}$ (10-120 Min) | $8.75 \times 10^{-7}$ (200-800 Min) | $6.05 \times 10^{-7}$ (800-6000 Min) |
| 2000 | 7 | -- | $1.06 \times 10^{-5}$ (10-120 Min) | $2.08 \times 10^{-6}$ (700-6000 Min) |
| 2000 | 42 | -- | $5.60 \times 10^{-5}$ (10-120 Min) | $1.95 \times 10^{-6}$ (120-900 Min) |
| 2100 | 9 | -- | $1.58 \times 10^{-5}$ (10-180 Min) | $3.88 \times 10^{-6}$ (2000-6000 Min) |

**Heat #2 (65-590)**

| Temp °F | Test No. | $K_L$(a) | $K_{PI}$(b) | $K_{PII}$(c) |
|---|---|---|---|---|
| 1400 | 63 | $8.67 \times 10^{-7}$ (150-1000 Min) | $2.92 \times 10^{-8}$ (1200-6000 Min) | — |
| 1600 | 18 | $7.26 \times 10^{-6}$ (10-60 Min) | $5.30 \times 10^{-7}$ (100-1300 Min) | — |
| 1800 | 8 | $2.00 \times 10^{-5}$ (10-70 Min) | $2.67 \times 10^{-6}$ (70-400 Min) | — |
| 1800 | 10 | $2.37 \times 10^{-5}$ (10-60 Min) | $4.15 \times 10^{-6}$ (60-1800 Min) | — |
| 2000 | 5 | -- | $1.48 \times 10^{-5}$ (10-70 Min) | $2.79 \times 10^{-6}$ (150-2100 Min) |
| 2000 | 41 | -- | $5.22 \times 10^{-6}$ (10-150 Min) | $2.22 \times 10^{-5}$ (400-6000 Min) |
| 2100 | 11 | -- | $1.32 \times 10^{-5}$ (10-420 Min) | $1.84 \times 10^{-6}$ (1200-6000 Min) |
| 2100 | 15 | -- | $1.21 \times 10^{-5}$ (10-6000 Min) | -- |

(a) $K_L$ = linear rate constant (mg/cm²/sec)

(b) $K_{PI}$ = initial parabolic rate constant (mg²/cm⁴/sec)

(c) $K_{PII}$ = secondary parabolic rate constant (mg²/cm⁴/sec)

Values in parenthesis indicate duration which rate constant applies.

35
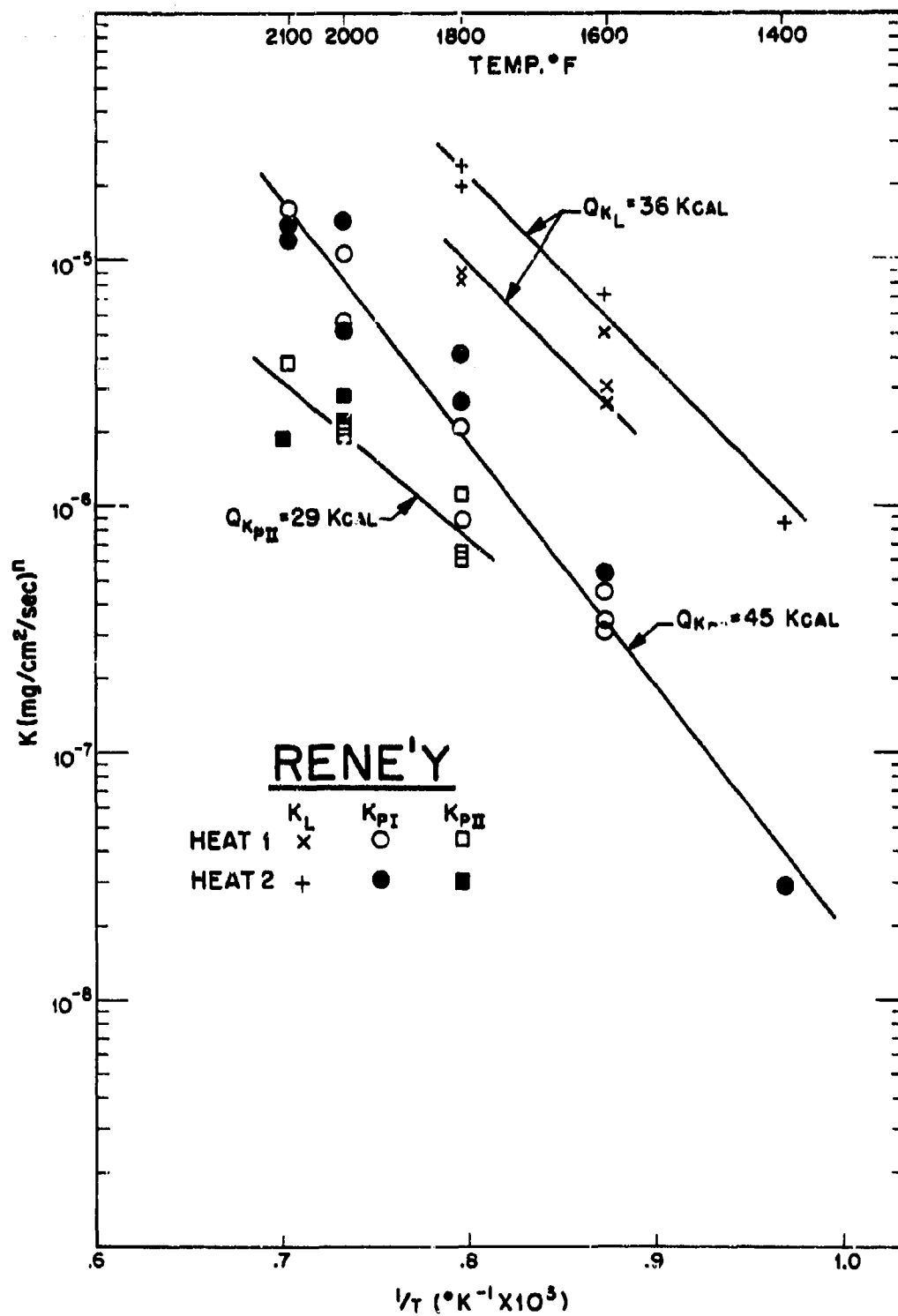
FIGURE 10  Arrhenius Plot of the Rate Constants for René Y

## 4.1.2 IN-100

The oxidation behavior of IN-100 is typified by the log-log plots of weight
gain versus time in Figures 11 and 12. The curves illustrate a combined
cubic/parabolic oxidation rate (slope $\cong$ 1/2 to 1/3) at the lower temperatures
or during the initial periods at high temperatures. These reaction rates
decrease after long times and/or high temperatures. The decrease in weight
gain rate is attributed to spalling losses which were actually observed
during testing. In some instances at 2100°F spalling was actually observed
during the first hour of testing.

The oxidation rate constants, as computed from the slopes of the "best-fit"
straight lines from $\Delta W/A$ or $(\Delta W/A)^3$ versus time plots, are summarized in
Table VI. Although parabolic rates were computed for comparative purposes,
the majority of data were best represented by cubic rate constants. The
absence of linear type oxidation at temperatures above 1400°F, the relatively
limited time interval for initial parabolic oxidation ($Kp_I$), and the existence
of a secondary parabolic oxidation rate ($Kp_{II}$) are all noteworthy features.

A plot of the rate constants in the normal Arrhenius form is shown in Figure
13. Considerable scatter is present in the data and above 2000°F some deviu-
tion from the straight line representing $Kp_I$ exists. From the straight line
formed during initial parabolic oxidation, a value for Q of 45 K cal was
computed, which is similar to that determined for René Y. It is doubtful,
however, that this value is the enthalpy required for oxidation in view of
the complex nature of the oxidation process. This value should rather be
considered an empirical constant which characterizes the initial stages of
oxidation below 2000°F.

As in the kinetic analysis for René Y, a dual parabolic oxidation process is
also observed for IN-100 above 1800°F. Since the value of $Kp_{II}$ does not vary
significantly with temperature, it is probably related to some mechanical
rather than a thermo-chemical process. Oxide spalling during exposure is
considered most likely responsible for this constant oxidation rate.

37
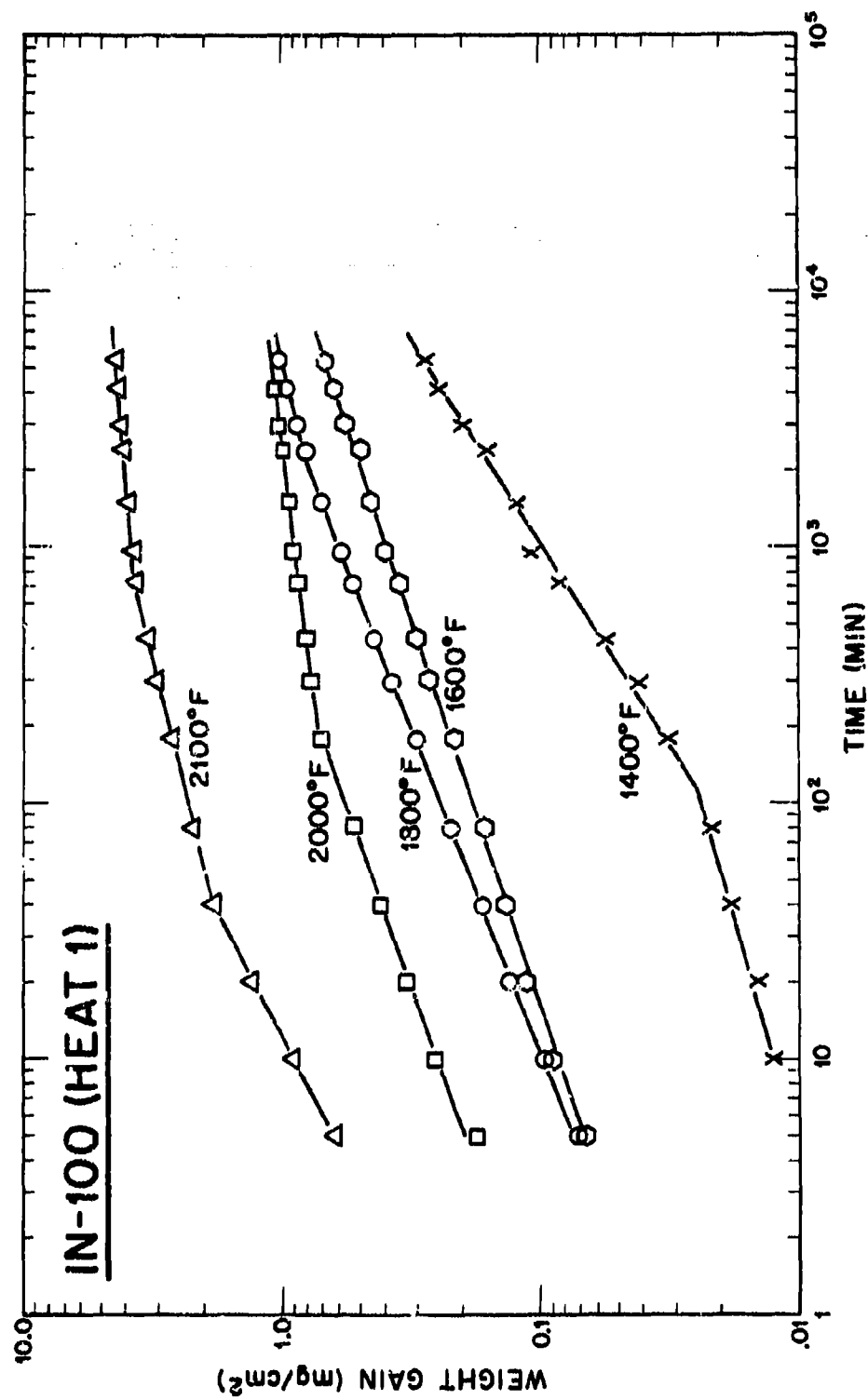
FIGURE 11   Typical Logarithmic Plot of Weight Gain Versus Time for IN-100  Heat 1

38
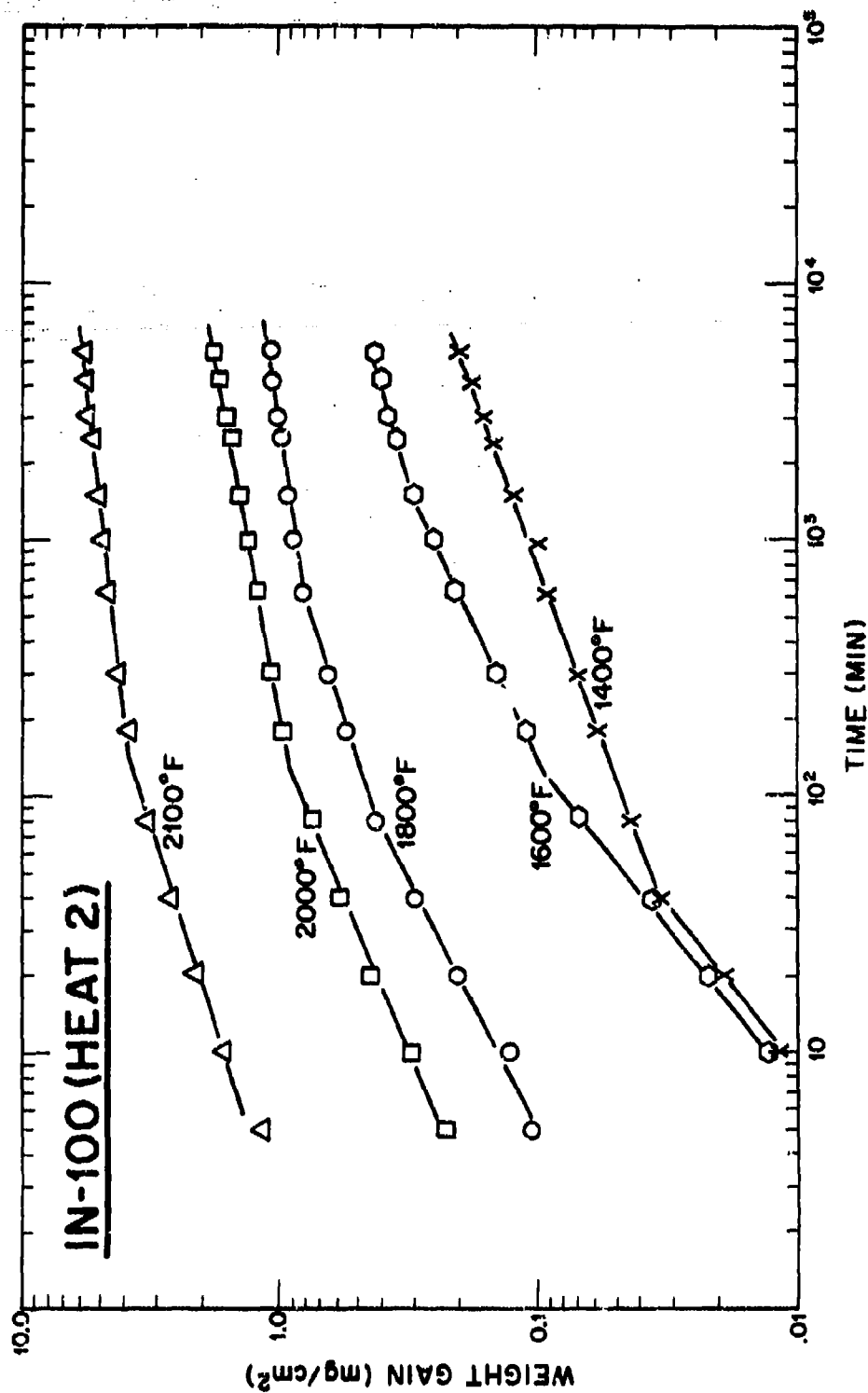
FIGURE 12   Typical Logarithmic Plot of Weight Gain Versus Time for IN-100   Heat 2

## TABLE VI

### SUMMARY OF OXIDATION RATE CONSTANTS FOR IN-100

#### Heat #1 (67V3261)

| Temp °F | Test No. | $K_L$ (a) | $K_{PI}$ (b) | $K_{PII}$ (c) |
|---|---|---|---|---|
| 1400 | 24 | $1.76 \times 10^{-5}$ (100-900 Min) | $2.57 \times 10^{-7}$ (900-6000 Min) | — |
| 1600 | 20 | — | $1.38 \times 10^{-6}$ (150-6000 Min) | — |
| 1800 | 21 | — | $9.05 \times 10^{-6}$ (10-400 Min) | $4.48 \times 10^{-6}$ (400-3000 Min) |
| 1800 | 49 | — | $2.00 \times 10^{-5}$ (10-100 Min) | $2.35 \times 10^{-6}$ (500-3300 Min) |
| 2000 | 19 | — | $4.18 \times 10^{-5}$ (15-200 Min) | $4.55 \times 10^{-6}$ (200-1600 Min) |
| 2000 | 27 | — | $6.78 \times 10^{-5}$ (10-125 Min) | $2.40 \times 10^{-6}$ (400-2500 Min) |
| 2100 | 17 | — | $3.13 \times 10^{-4}$ (60-400 Min) | $2.37 \times 10^{-5}$ (700-3300 Min) |

#### Heat #2 (VD582/3)

| Temp °F | Test No. | $K_L$ (a) | $K_{PI}$ (b) | $K_{PII}$ (c) |
|---|---|---|---|---|
| 1400 | 22 | $1.11 \times 10^{-5}$ (10-60 Min) | $1.56 \times 10^{-7}$ (80-6000 Min) | — |
| 1400 | 26 | $1.85 \times 10^{-5}$ (10-100 Min) | Erratic | — |
| 1600 | 14 | $1.39 \times 10^{-5}$ (10-80 Min) | $1.51 \times 10^{-6}$ (100-2000 Min) | — |
| 1800 | 4 | — | $1.70 \times 10^{-5}$ (40-400 Min) | $3.00 \times 10^{-6}$ (900-6000 Min) |
| 1800 | 6 | — | $3.3 \times 10^{-5}$ (15-80 Min) | Not Parabolic |
| 2000 | 3 | — | $1.03 \times 10^{-4}$ (15-120 Min) | $6.2 \times 10^{-5}$ (575-3600 Min) |
| 2000 | 25 | — | $4.79 \times 10^{-5}$ (10-140 Min) | $4.0 \times 10^{-6}$ (400-6000 Min) |
| 2100 | 13 | — | — | $5.97 \times 10^{-5}$ (400-6000 Min) |
| 2100 | 43 | — | — | $2.78 \times 10^{-5}$ (480-6000 Min) |

(a) $K_L$ = linear rate constant ($mg/cm^2/sec$)

(b) $K_{PI}$ = initial parabolic rate constant ($mg^2/cm^4/sec$)

(c) $K_{PII}$ = secondary parabolic rate constant ($mg^2/cm^4/sec$)

Values in parenthesis indicate duration which rate constant applies.
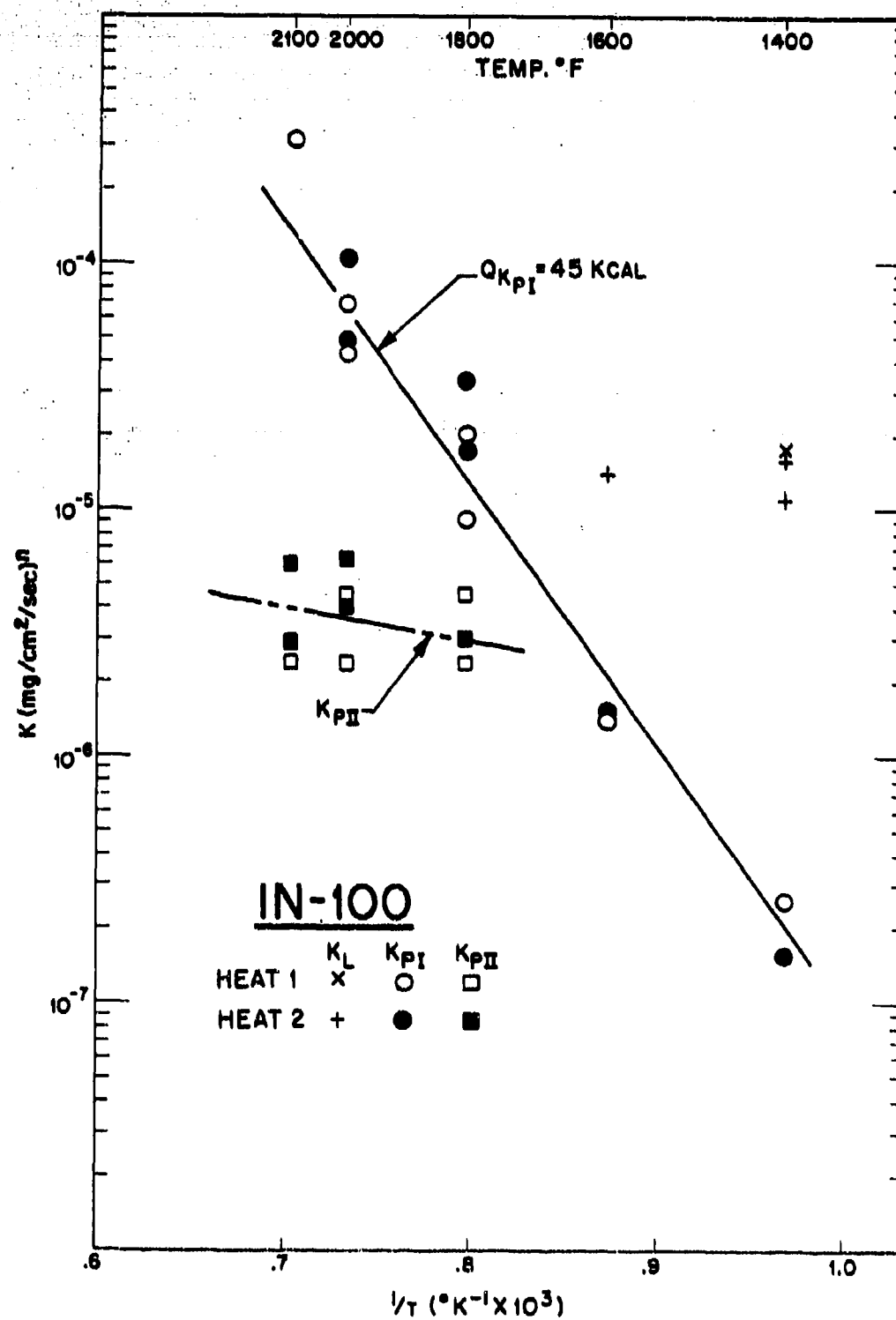
FIGURE 13   Arrhenius Plot of the Rate Constants for IN-100

41

### 4.1.3 SM-200

As observed in IN-100, the continuous weight gain curves for SM-200 (Figures 14 and 15) also deviate considerably from parabolic after long time high temperature exposures. In fact, prolonged exposures at 2100°F produced an apparent cessation in weight gain followed by a weight decrease. Since spalling was not evidenced during any of the tests, excessive vaporization was expected. An X-ray fluorescence analysis of the deposits scraped from the cooler sections of the specimen hanger chain indicated large amounts of chromium and tungsten*. However, an X-ray analysis of the same deposit produced an unidentifiable pattern.

The linear and parabolic rate constants derived from the various tests are summarized in Table VII and further illustrate the anomalous high temperature behavior. As with IN-100, the linear reaction rates ($K_{p_L}$) were limited to the first few hundred minutes of oxidation at temperatures greater than 1800°F. A plot of these reaction constants versus reciprocal temperature, shown in Figure 16, indicates a discontinuity in the initial parabolic process at approximately 1700°F. This suggests that two initial parabolic processes are operative, each of which is controlled by a different mechanism or combination of mechanisms.

### 4.1.4 INCO 713C

As illustrated in Figures 17 and 18 the oxidation behavior of this alloy displays more heat-to-heat variation than the other alloys tested. The large grain size of the test specimens and difficulties encountered in electropolishing the specimens may account for this behavior. However, the cause of the anomalous shape of the oxidation curves for both heats at 2000°F has not been established. Spalling and vaporization effects can be discounted since neither were observed during the tests. The behavior observed for this alloy may rather be associated with the relatively high aluminum content of the alloy and the dissolution of the aluminum-rich γ' phase at this temperature. This will be discussed further in another section.

The oxidation rate constants for this alloy which are summarized in Table VIII, are in general similar to the previous two cast alloys. The notable exception is the absence of any linear oxidation rates. The variation of the oxidation constants with reciprical temperatures is illustrated in Figure 19. The relation depicts two reasonably well defined parabolic processes.

---

* The analysis also identified lesser amounts of all the other constituents in the alloy.

42
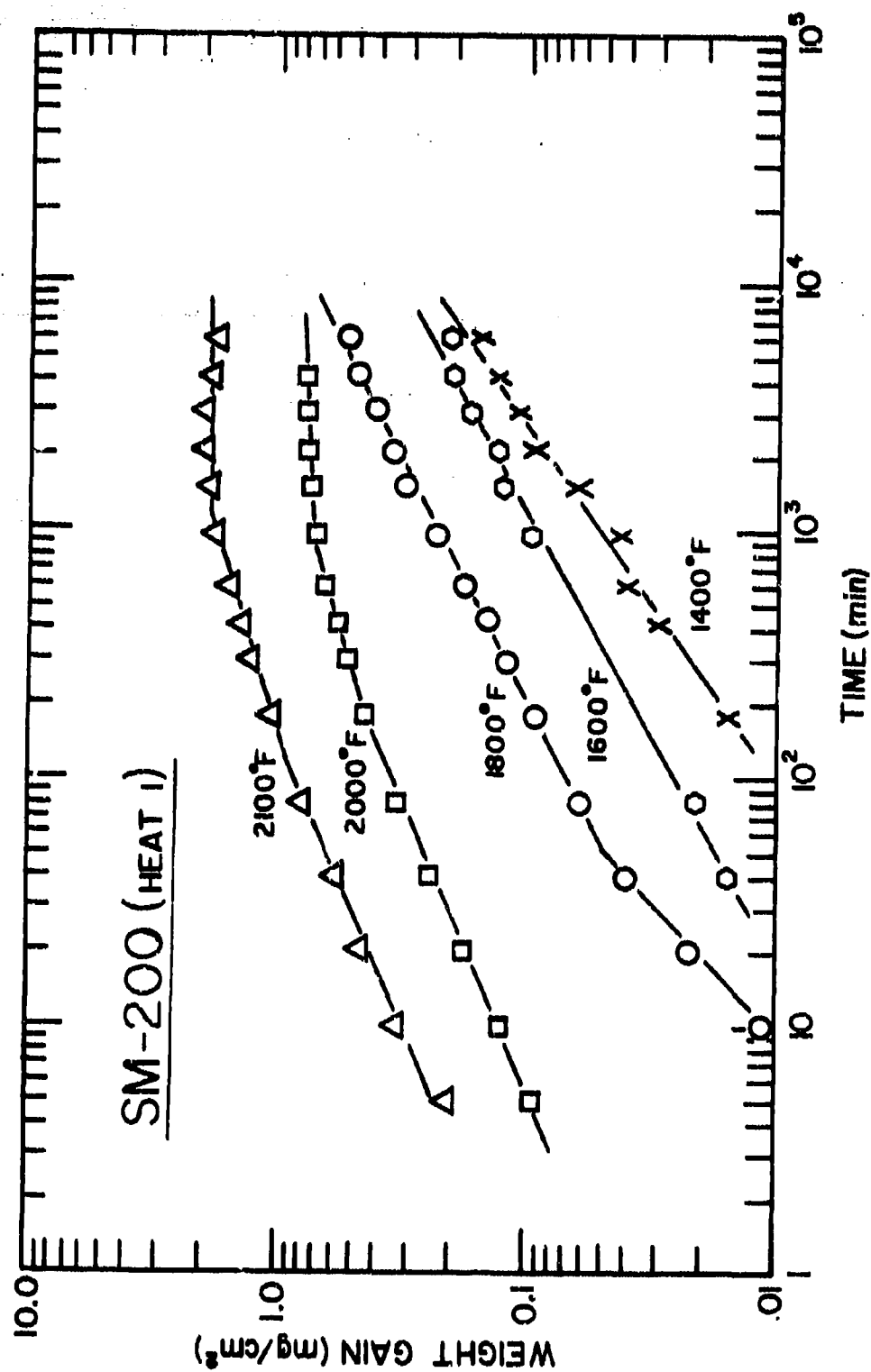
FIGURE 14  Typical Logarithmic Plot of Weight Gain Versus Time for SM-200  Heat 1

43
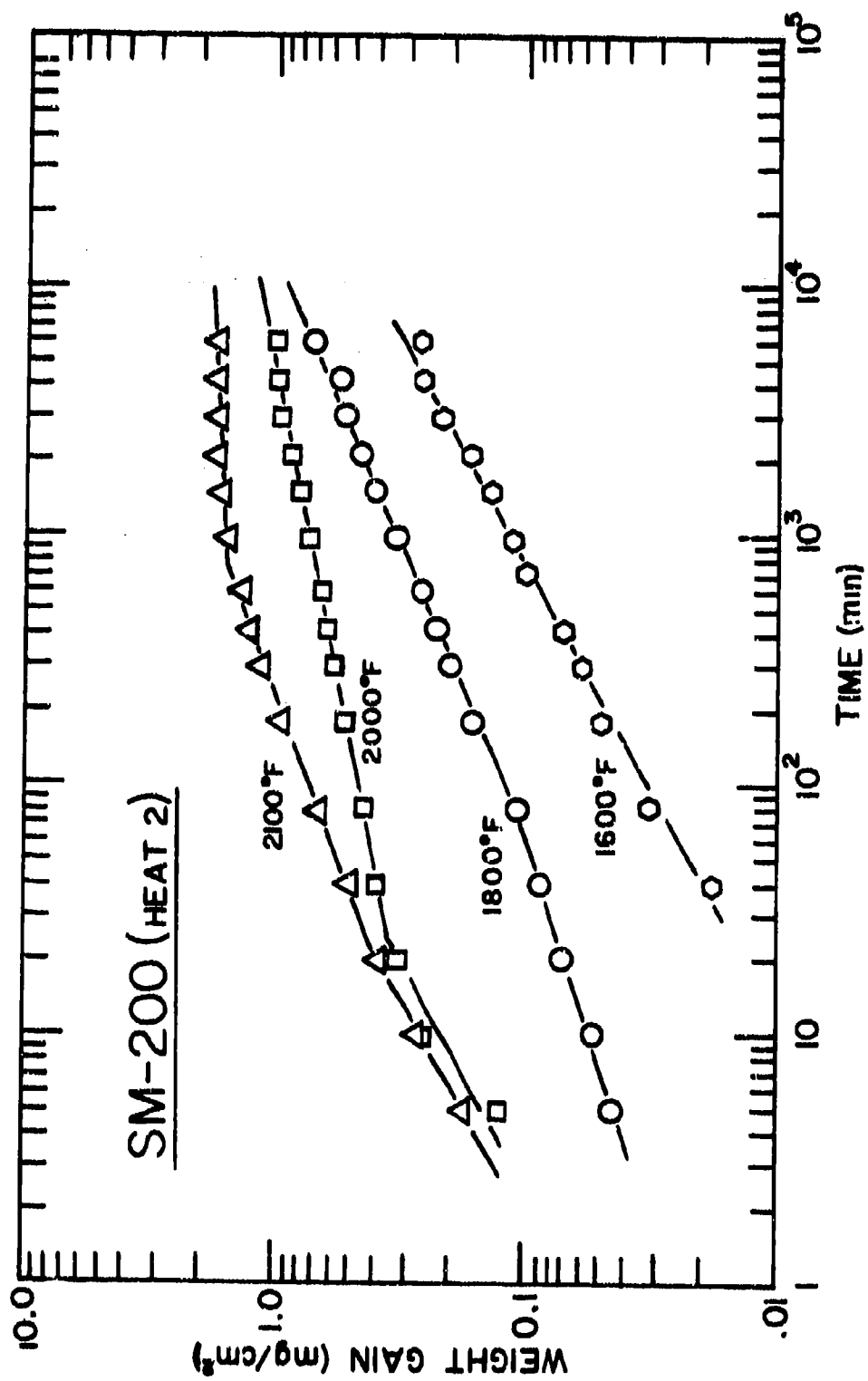
FIGURE 15   Typical Logarithmic Plot of Weight Gain Versus Time for SM-200  Heat 2

## TABLE VII

## SUMMARY OF OXIDATION RATE CONSTANTS FOR SM-200

### Heat #1 (34V2804)

| Temp °F | Test No. | $K_L$(a) | $K_{PI}$(b) | $K_{PII}$(c) |
|---|---|---|---|---|
| 1400 | 65 | $1.16 \times 10^{-6}$ (100-550 Min) | $6.95 \times 10^{-8}$ (1800-6000 Min) | --- |
| 1600 | 60 | $7.55 \times 10^{-6}$ (10-30 Min) | $1.57 \times 10^{-7}$ (50-4400 Min) | --- |
| 1800 | 34 | --- | $3.13 \times 10^{-6}$ (10-6000 Min) | --- |
| 1800 | 59 | $1.89 \times 10^{-5}$ (10-20 Min) | $9.62 \times 10^{-7}$ (35-6000 Min) | --- |
| 2000 | 36 | --- | $2.08 \times 10^{-5}$ (10-120 Min) | $9.17 \times 10^{-6}$ (120-750 Min) |
| 2100 | 31 | --- | $1.12 \times 10^{-4}$ (10-100 Min) | Not Parabolic |
| 2100 | 53 | --- | $5.16 \times 10^{-4}$ (10-100 Min) | Not Parabolic |

### Heat #2 (34V2865)

| Temp °F | Test No. | $K_L$(a) | $K_{PI}$(b) | $K_{PII}$(c) |
|---|---|---|---|---|
| 1400 | 66 | --- | $1.06 \times 10^{-7}$ (10-100 Min) | Erratic |
| 1600 | 64 | $7.4 \times 10^{-6}$ (10-100 Min) | $2.23 \times 10^{-7}$ (100-6000 Min) | --- |
| 1800 | 32 | --- | $1.69 \times 10^{-6}$ (10-3000 Min) | $4.78 \times 10^{-7}$ (3000-5000 Min) |
| 2000 | 51 | --- | $6.05 \times 10^{-5}$ (3-20 Min) | $6.67 \times 10^{-7}$ (150-2500 Min) |
| 2100 | 57 | --- | $9.85 \times 10^{-5}$ (20-700 Min) | Not Parabolic |
| 2100 | 35 | --- | $4.80 \times 10^{-5}$ (10-300 Min) | Not Parabolic |
| 2100 | 46 | --- | $7.35 \times 10^{-5}$ (10-125 Min) | Not Parabolic |

(a) $K_L$ = linear rate constant (mg/cm$^2$/sec)

(b) $K_{PI}$ = initial parabolic rate constant (mg$^2$/cm$^4$/sec)

(c) $K_{PII}$ = secondary parabolic rate constant (mg$^2$/cm$^4$/sec)

Values in parenthesis indicate duration which rate constant applies.

45
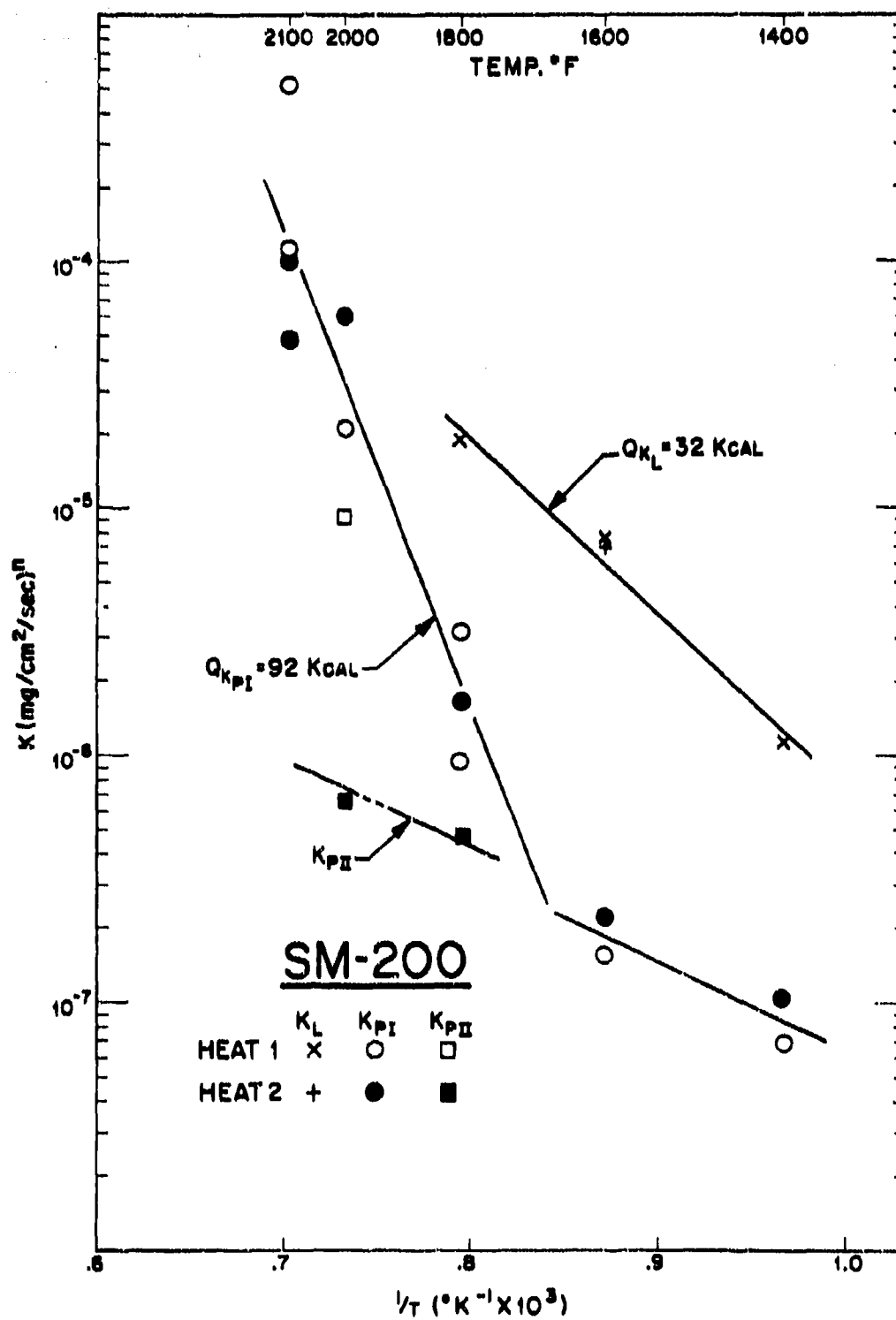
FIGURE 16  Arrhenius Plot of the Rate Constants for SM-200

46
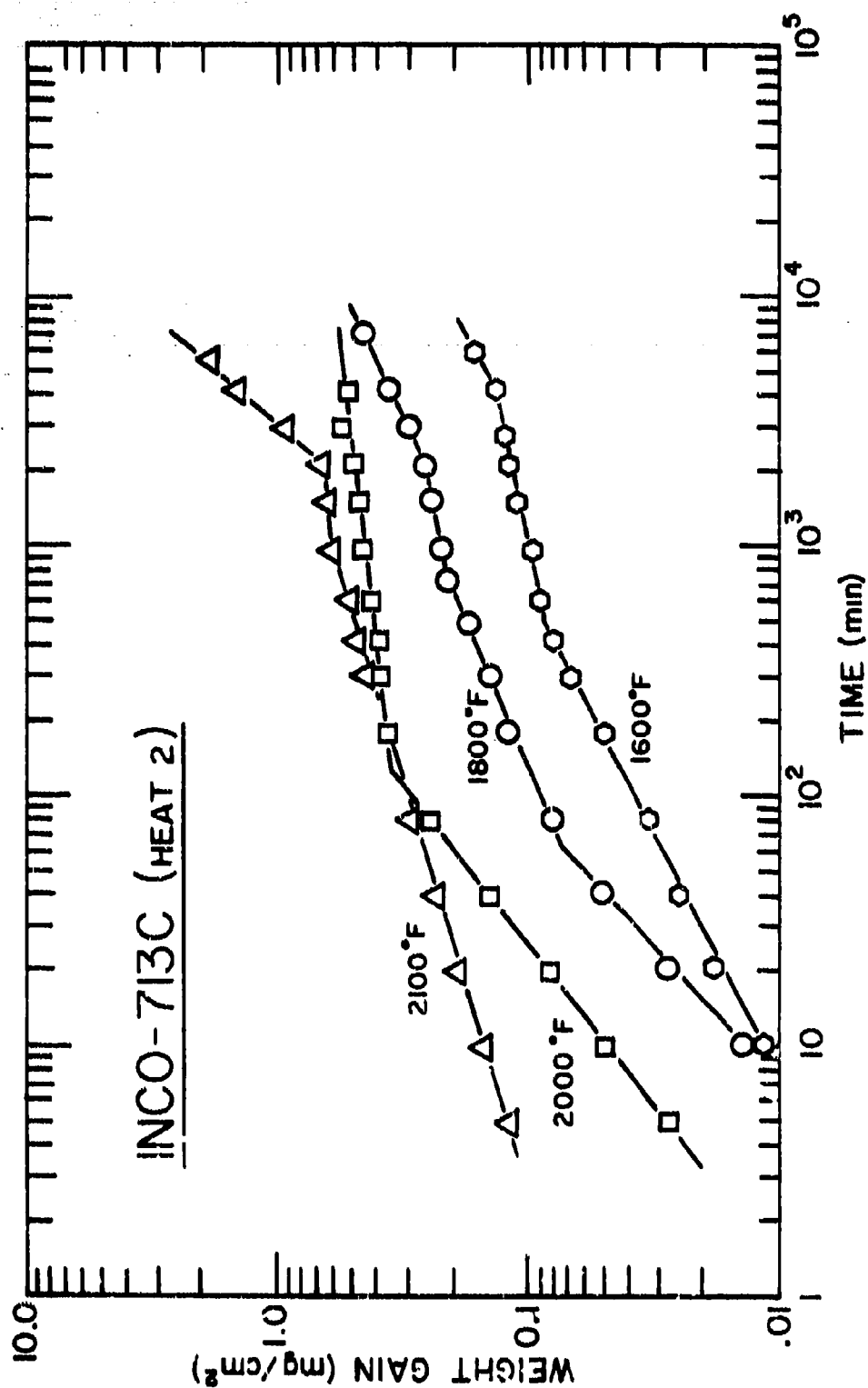
Figure 17 Typical Logarithmic Plot of Weight Gain Versus Time for Inco 713C Heat 1
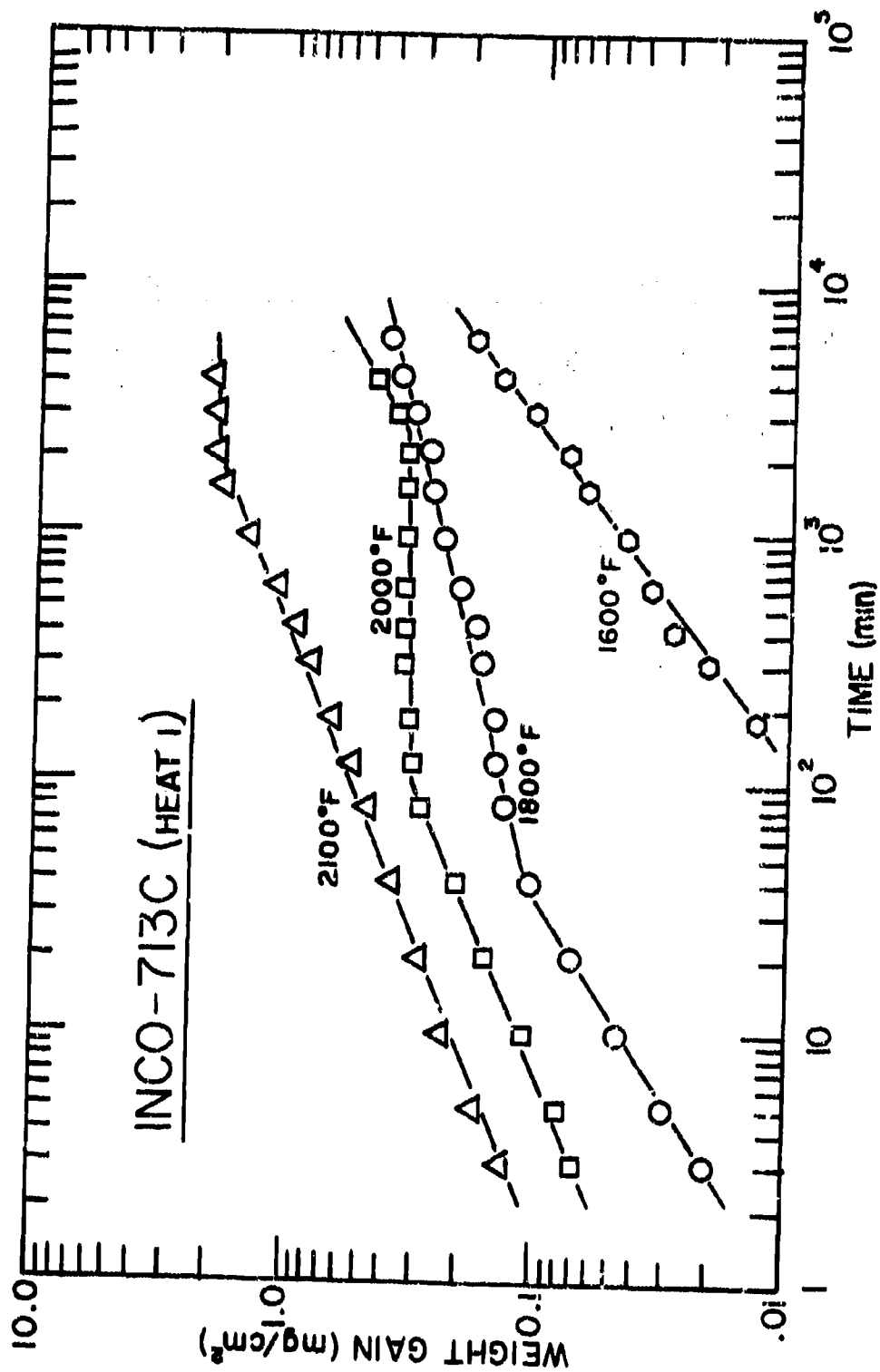
FIGURE 18   Typical Logarithmic Plot of Weight Gain Versus Time for Inco 713C   Heat 2

48

## TABLE VIII

### SUMMARY OF OXIDATION RATE CONSTANTS FOR INCO 713C

Heat #1 (601)

| Temp °F | Test No. | $K_L$ (a) | $K_{PI}$ (b) | $K_{PII}$ (c) |
|---|---|---|---|---|
| 1600 | 58 | Not Linear | $1.35 \times 10^{-7}$ (2000-6000 Min) | — |
| 1800 | 61 | -- | $5.65 \times 10^{-7}$ (10-35 Min) | $4.78 \times 10^{-7}$ (250-6000 Min) |
| 1800 | 45 | -- | $1.67 \times 10^{-6}$ (10-140 Min) | $6.22 \times 10^{-8}$ (600-6000 Min) |
| 2000 | 38 | -- | $1.59 \times 10^{-5}$ (10-100 Min) | Not parabolic |
| 2100 | 39 | -- | $3.51 \times 10^{-5}$ (10-2500 Min) | Not parabolic |
| 2100 | 52 | -- | $7.95 \times 10^{-5}$ (50-1400 Min) | Not parabolic |

Heat #2 (602)

| Temp °F | Test No. | $K_L$ (a) | $K_{PI}$ (b) | $K_{PII}$ (c) |
|---|---|---|---|---|
| 1600 | 56 | -- | $2.50 \times 10^{-7}$ (10-670 Min) | Not Parabolic |
| 1800 | 47 | -- | $1.15 \times 10^{-6}$ (50-500 Min) | $4.60 \times 10^{-7}$ (600-6000 Min) |
| 2000 | 40 | -- | $1.52 \times 10^{-5}$ (10-100 Min) | $1.19 \times 10^{-6}$ (100-2000 Min) |
| 2000 | 55 | -- | $1.92 \times 10^{-5}$ (10-120 Min) | $2.07 \times 10^{-6}$ (120-1200 Min) |
| 2100 | 37 | -- | $2.22 \times 10^{-5}$ (10-30 Min) | $2.60 \times 10^{-6}$ (225-2300 Min) |

(a) $K_L$ = linear rate constant (mg/cm²/sec)

(b) $K_{PI}$ = initial parabolic rate constant (mg²/cm⁴/sec)

(c) $K_{PII}$ = secondary parabolic rate constant (mg²/cm⁴/sec) –

Values in parenthesis indicate duration which rate constant applies.
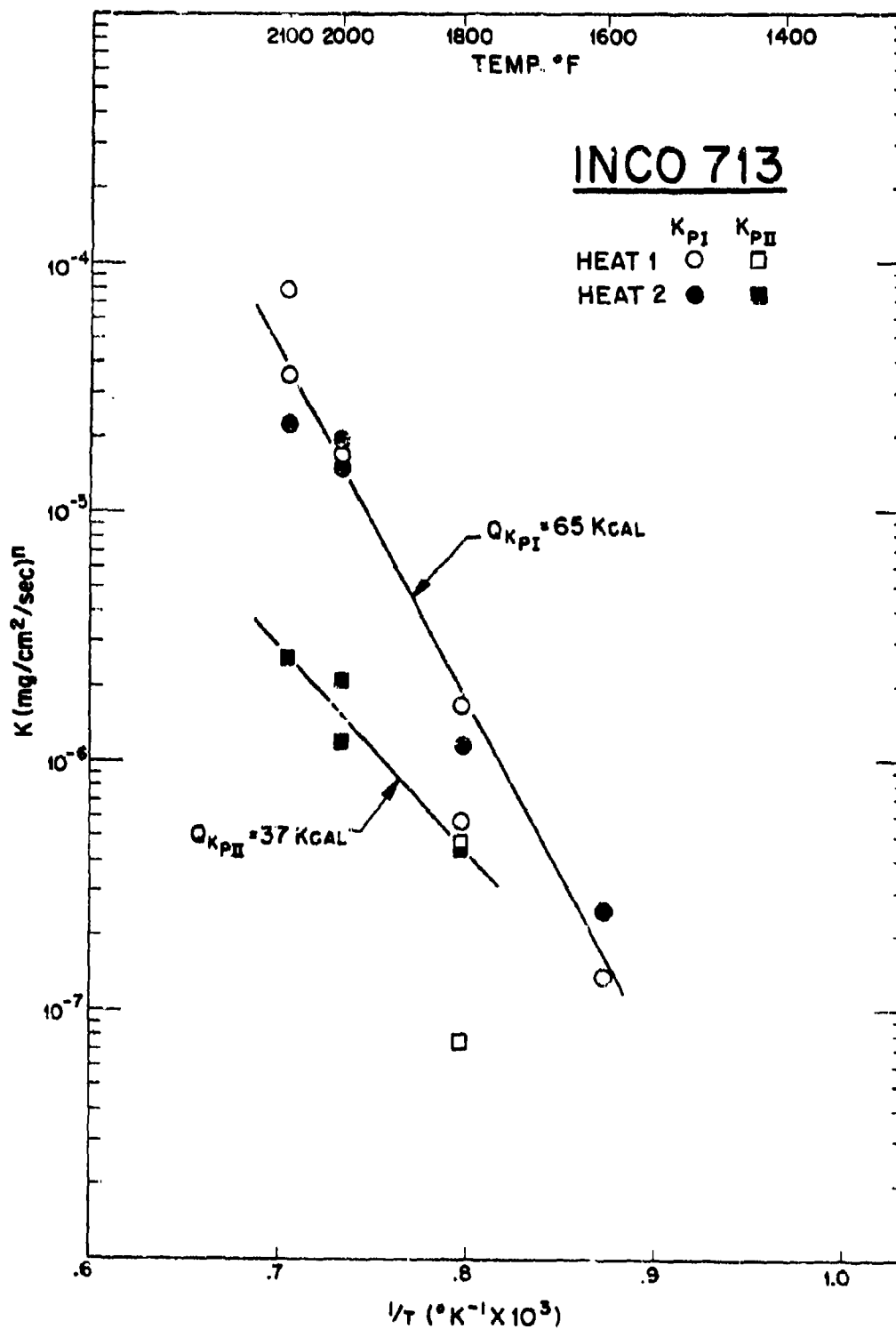
**FIGURE 19** Arrhenius Plot of the Rate Constants for Inco 713C

50

### 4.1.5 Comparison of Alloy Kinetics

The kinetic analyses performed in this investigation do indicate certain similarities in the oxidation mechanisms which dictate the behavior of these alloys. However, it is doubtful that the activation energies computed for the parabolic rates are representative of simple diffusion processes. The rate controlling oxidation mechanisms are probably much more complex. Although models have been developed to correct thermogravimetric data for the high temperature vaporization effects[13,14] the correlation obtained with the present data was poor, indicating that the assumptions of single phase oxide formation and parabolic oxidation kinetics are not valid for these alloys.

On the other hand, the oxidation data obtained in this investigation do denote gross differences in oxidation behavior of any alloy and thus serve to compare the oxidation rates of the alloys. Such a comparison is presented in Figure 20 for two extreme test temperatures. At 1600°F all the alloys oxidize similarly with no more than a factor of three difference in total weight gain after 100 hours exposure. All alloys except Inco 713C showed a linear reaction rate (slope $\cong$ 1) during the initital stage of oxide scale formation with subsequent parabolic (slope $\cong$ 1/2) or cubic oxidation (slope $\cong$ 1/3) after longer times. The relatively slow initial oxidation rate demonstrated by Inco 713C is not fully understood. At 2000°F the general weight gain behavior of the alloys are also similar and it is apparent that the linear rates which were prominent at 1600°F have been replaced by parabolic rates during the initial 100 minutes of oxidation. This can simply be construed as equivalent to the latter stages of oxidation at 1600°F where oxide growth is diffusion controlled. However, for times much greater than 100 minutes the oxidation rates decelerate. This behavior has been associated with excessive oxide deposits on the specimen hanger chain and throughout the oxidation test equipment with no corresponding observation of spalling losses. Hence, even in this slow flowing (1 liter/min) environment, oxide volatilization is considered primarily responsible for the oxidation behavior observed. At 1400°, 1800°, and 2100°F the alloys displayed oxidation rates which were either extremes of those illustrated in Figure 20 or transitional as was the case at 1800°F where some alloys displayed volatilization and others did not.

A comparison of the oxidation rates of these alloys is illustrated in Figure 21 where the initial parabolic rate constants ($K_{p_I}$) are plotted versus reciprocal temperature. Although a kinetic evaluation of René 41 and U-700 was not performed in this investigation their oxidation behavior has been previously characterized in a similar study.[2] The results are included here for a more complete comparison of the alloys. Considering the differences in

51
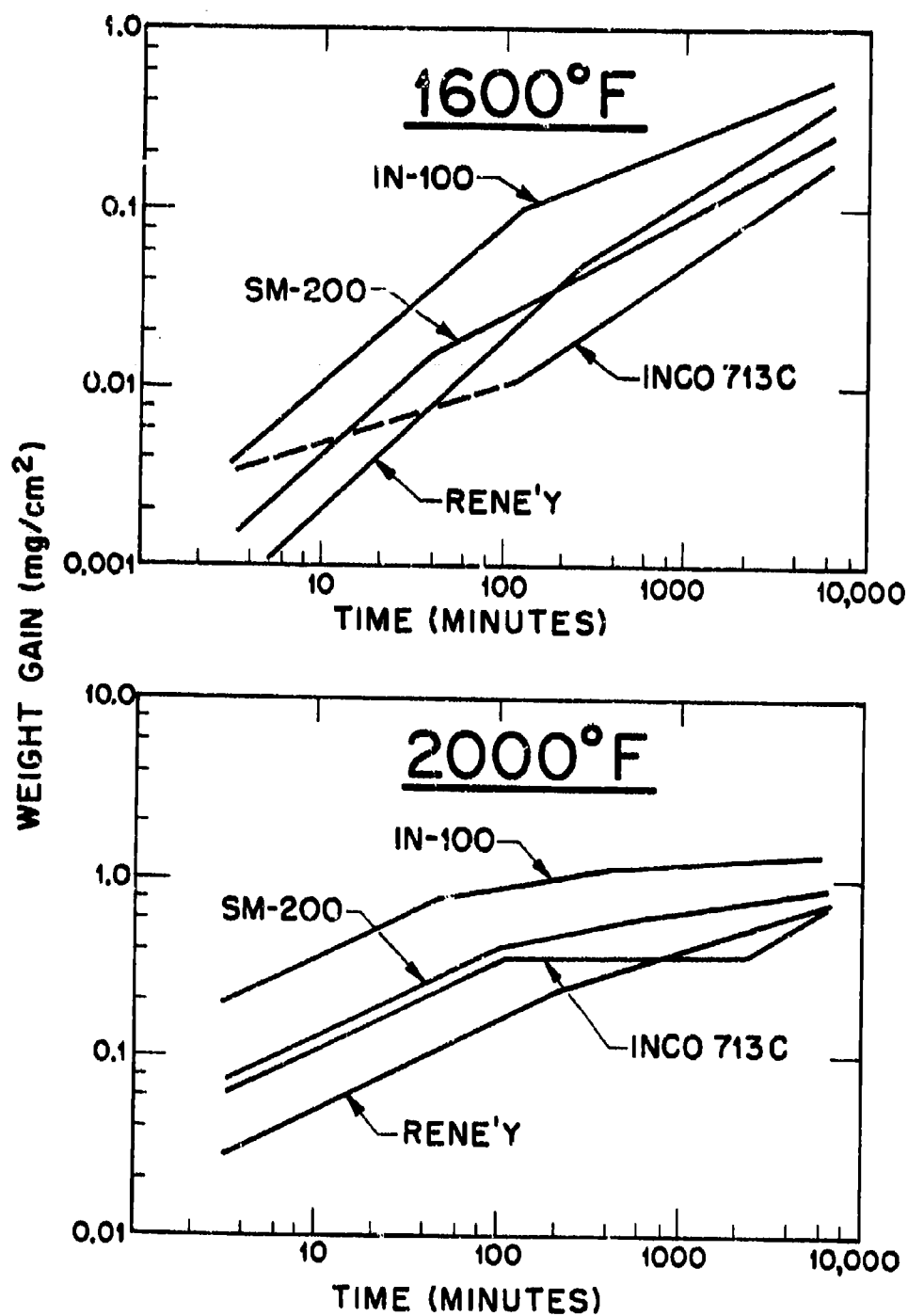
FIGURE 20 Comparison of the Oxidation Behavior of René Y, IN-100, SM-200 and Inco 713C at 1600 and 2000°F. Note the decreasing oxidation rate for all alloys at 2000°F (t > 100 min).
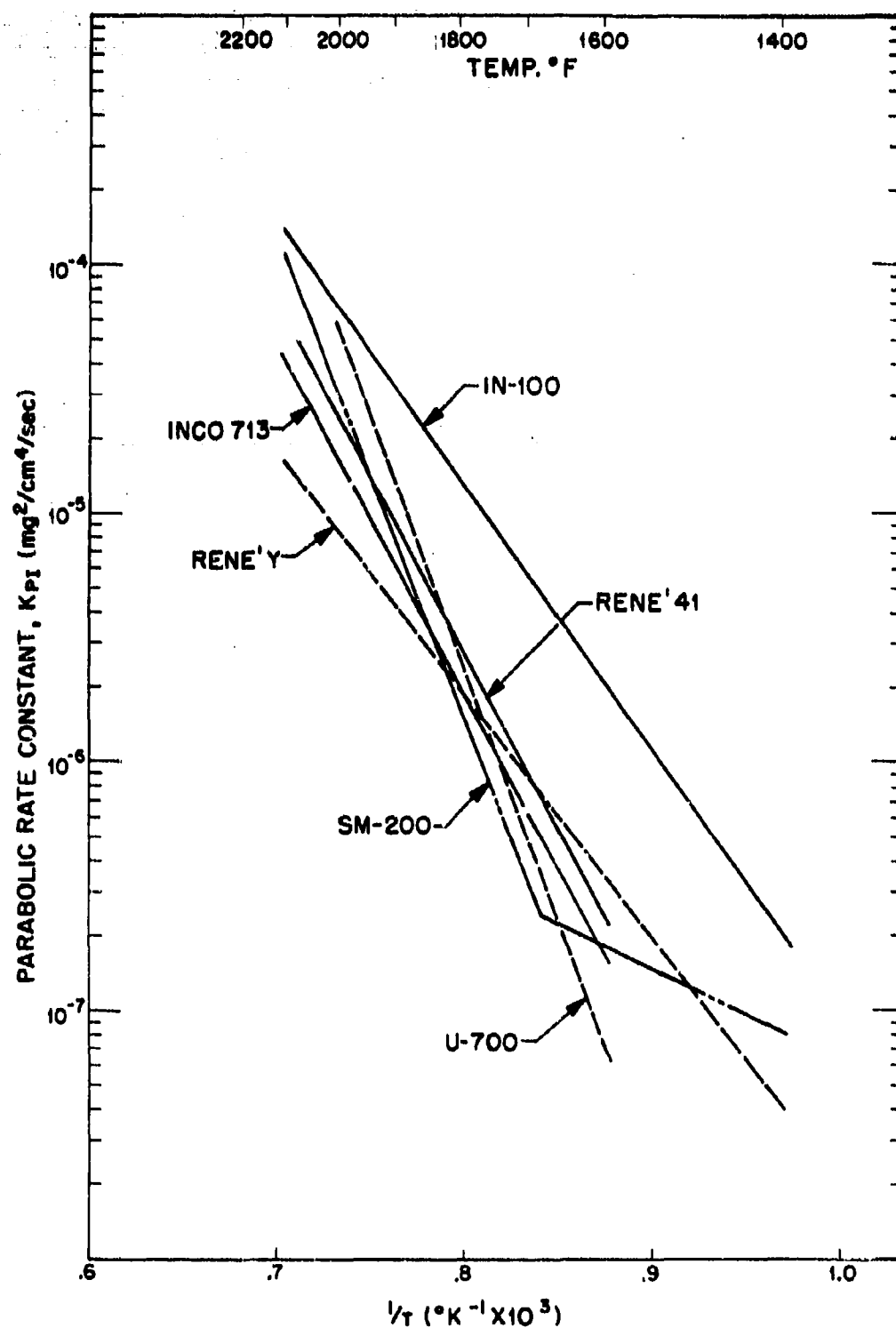
FIGURE 21   A Comparison of the Initial Parabolic Rate Constants of the Alloys

53

composition and activation energies displayed by this group of alloys the similarity in oxidation rate at 1800°F and below is pronounced. A notable exception is IN-100 which oxidizes five to ten times faster than the other alloys. If data scatter is considered and IN-100 excluded, there is essentially no difference in the initial oxidation rates of these alloys between 1600 and 1900°F. It should be noted, however, that the time interval over which this initial parabolic oxidation rate is applicable generally decreases with increasing temperature. Therefore, these curves only compare the initial oxidation behavior and should not be considered applicable for extended times above 1800°F.

## 4.2 Static Oxidation Behavior

The data presented here establish the type and extent of the oxidation reactions for René Y, SM-200, IN-100 and Inco 713C during static oxidation. For these studies, specimens were exposed in ambient air at 1600, 1800, and 2000°F for times of 5 minutes to 1000 hours. A relatively complete microstructural characterization of the oxidation products is presented, however, in some instances, details and apparent anomalies remain undefined.

### 4.2.1 Thin Film Studies

This study was conducted to determine the nature of the initial oxide films formed on these alloys. Information regarding this stage of oxidation is necessary to obtain an understanding of the subsequent longer time behavior. The progressive growth of the oxide scale during four hours exposure at 1600°F is illustrated for each alloy by the sequence of electron photomicrographs in Figure 22 through 25. Although some variation was observed in these thin films due to orientation and homogeneity effects, the areas selected are considered representative. For each alloy the base oxide film (5 minutes) is observed to mature with time as indicated by the crystallite development. The cast alloys all demonstrated at least one additional oxide phase which appears to protrude through the base oxide and subsequently grow or agglomerate. This behavior became more pronounced on thin films formed at 1800°F. It is this heterogeneous oxide formation and the combined action of the different oxidation modes operative which is considered responsible for the irregular oxidation kinetics observed in the previous section.

A summary of the oxide phase identification for these thin films is presented in Table IX along with the specific identification technique employed. As indicated, electron diffraction reflection techniques did not yield workable results. In most instances, the patterns were either too weak or diffuse to perform an analysis. Where patterns were obtained, arcing of the Debye
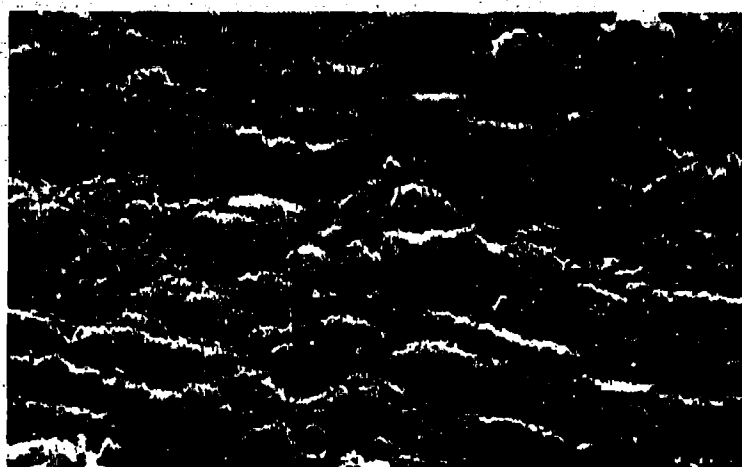
a) 5 Minutes (10,000X)

(698A)
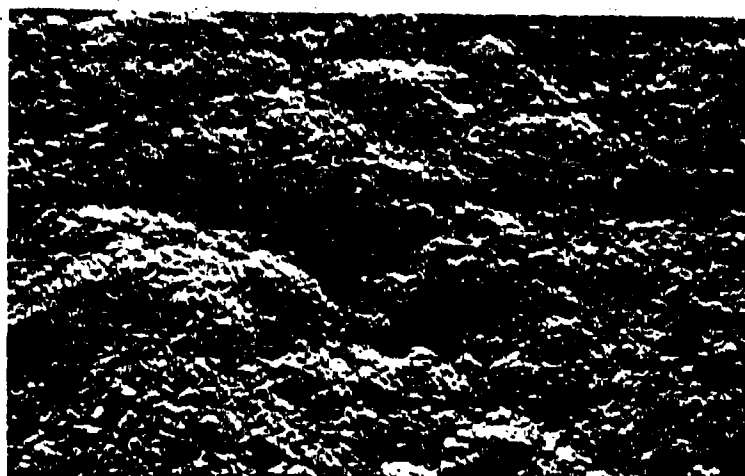
b) 30 Minutes (10,000X)

(698B)

c) 240 Minutes (10,000X)

(698C)

FIGURE 22    Initial Oxide Growth Morphology in René Y During Exposure at 1600°F. Shadowed replica as stripped for specimen surface.

55
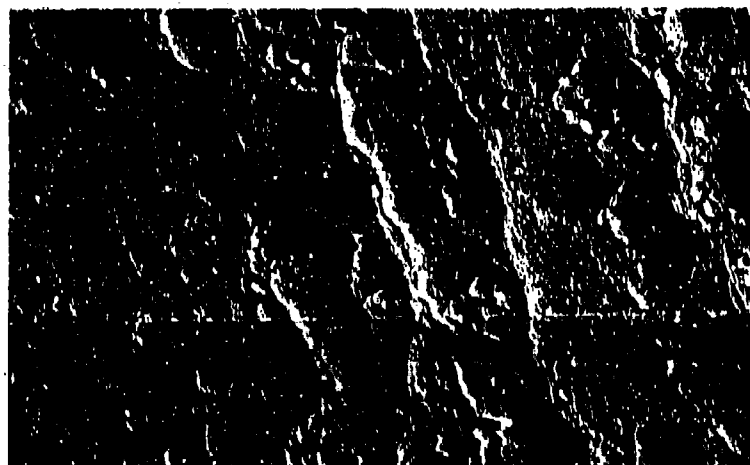
a)  5 Minutes
    (10,000X)

(699A)
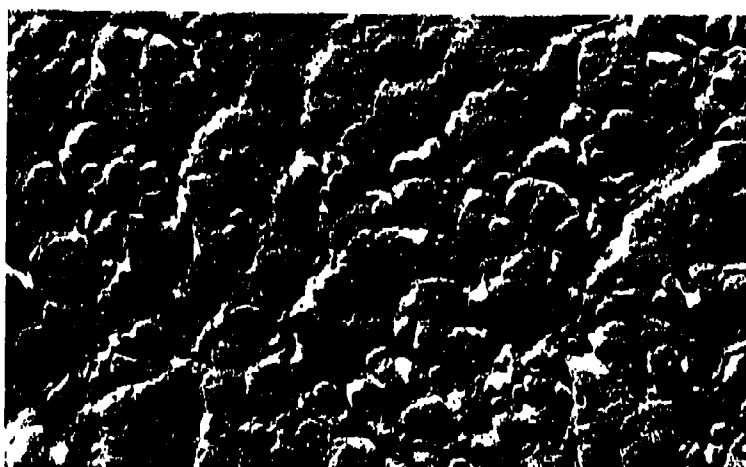
b)  30 Minutes
    (10,000X)

(699B)
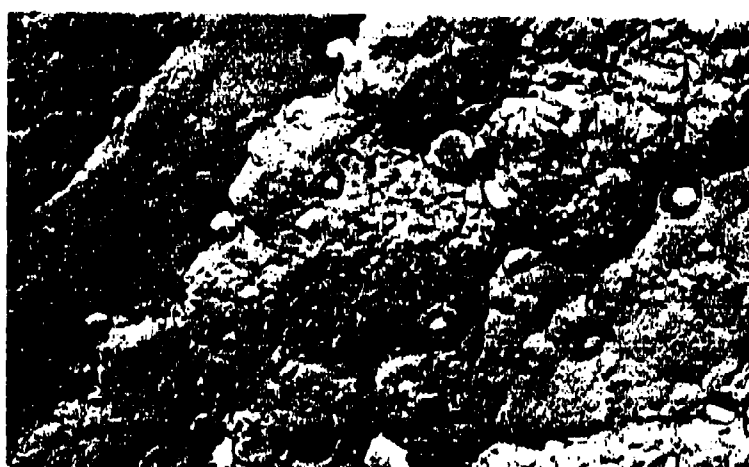
c)  240 Minutes
    (10,000X)

(699C)

FIGURE 23    Initial Oxide Growth Morphology in SM-200 During Exposure
             at 1600°F.  Shadowed Replica as stripped from specimen surface.

56
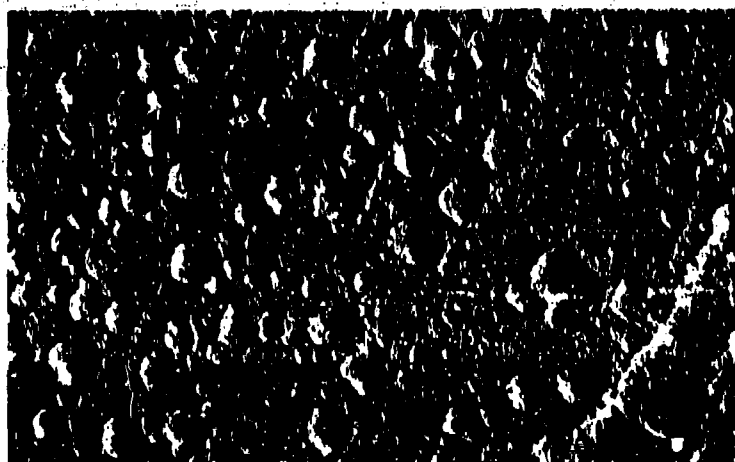
a) 5 Minutes
(10,000X)

(696A)
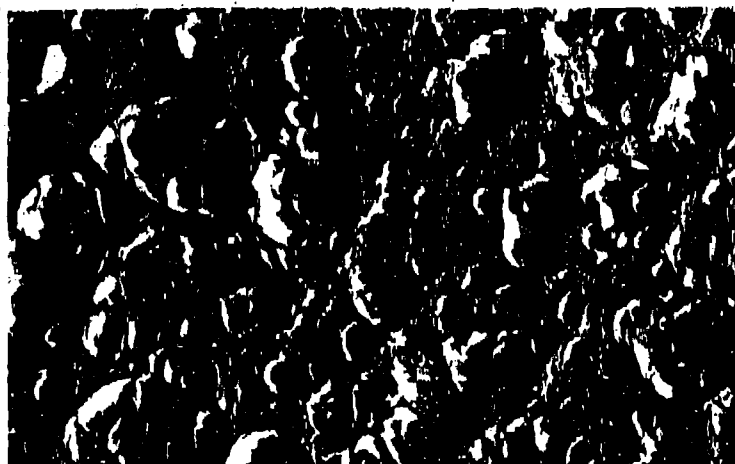
b) 30 Minutes
(10,000X)

(696B)
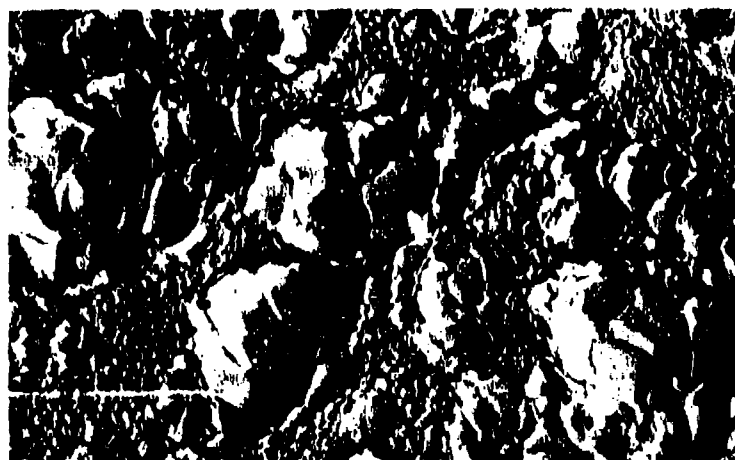
c) 240 Minutes
(10,000X)

(696C)

FIGURE 24    Initial Oxide Growth Morphology in IN-100 During Exposure at
1600°F.   Shadowed Replica as stripped from specimen surface.

57
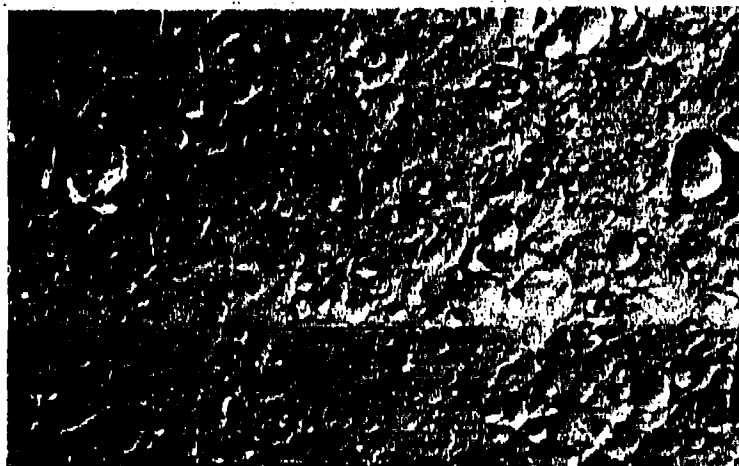
a) 5 Minutes
(10,000X)

(697A)

b) 30 Minutes
(10,000X)

(697B)
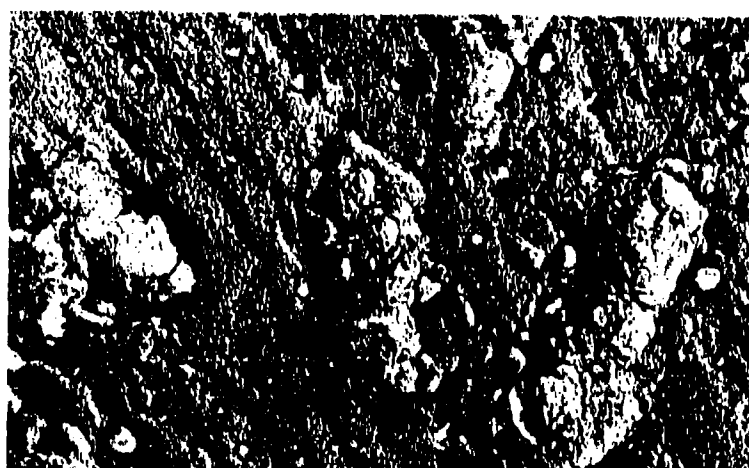
c) 240 Minutes
(10,000X)

(697C)

FIGURE 25    Initial Oxide Growth Morphology in Inco 713C During Exposure
at 1600°F.   Shadowed replica as stripped from specimen surface.

58

TABLE IX

## SUMMARY OF THIN FILM OXIDE IDENTIFICATION

| Alloy | Temp ($^\circ$F) | Time (mins) | Method | Products[a] |
|-------|------|------|--------|-------------|
| Rene' Y | 1600 | 5 | (b) | $Cr_2O_3$ |
|  | 1600 | 120 | (c) | $Cr_2O_3 + MnCr_2O_4$ ($a_0 = 8.41$Å) (W) |
|  | 1800 | 5 | (b) | $Cr_2O_3$ |
|  | 1800 | 30 | (c) | $Cr_2O_3 + MnCr_2O_4$ ($a_0 = 8.43$Å) (W) |
| SM-200 | 1600 | 5 | (b) | Spinel ($a_0 = 8.34$Å) |
|  | 1600 | 30 | (b) | Diffuse |
|  | 1600 | 120 | (c) | Spinel($a_0 = 8.24$Å) + $TiO_2$ (W) + $WO_3$ * |
|  | 1800 | 5 | (b) | Diffuse |
|  | 1800 | 30 | (c) | Spinel($a_0 = 8.34$Å) + NiO + $(Cr,Al)_2O_3 + TiO_2$ (VW) |
| Inco 713C | 1600 | 5 | (b) | No pattern |
|  | 1600 | 30 | (b) | Diffuse |
|  | 1600 | 120 | (c) | NiO($a_0 = 4.12$Å) + Spinel($a_0 = 8.24$Å) |
|  | 1800 | 5 | (b) | Diffuse |
|  | 1800 | 30 | (c) | NiO($a_0 = 4.15$Å) + Spinel($a_0 = 8.34$Å) + $Cr_2O_3$ |
| IN-100 | 1600 | 5 | (b) | No pattern |
|  | 1600 | 30 | (b) | Diffuse |
|  | 1600 | 120 | (c) | $(Ni,Co,V)O$($a_0 = 4.30$Å) + $TiO_2 + Cr_2O_3$ (W) + $Al_2O_3$ (W) |
|  | 1800 | 5 | (b) | Diffuse |

(a) Listed in order of decreasing intensity

(b) Electron diffraction reflection

(c) X-ray diffraction of electrolytically stripped oxide. Carbide phases not listed.

* Tentative identification

rings indicated some preferred orientation present. The accuracy of
electron diffraction transmission techniques was not considered sufficient
for oxide phase identification, therefore, most of the thin film identifi-
cation was performed using X-ray diffraction of electrolytically stripped
films. However, the identification of oxides employing this technique
was complicated by the presence of intermetallic phases from the metal
which were also extracted with the oxide. A typical X-ray pattern pro-
duced using this technique is shown in Table X.

Relating the thin film morphology and corresponding X-ray identification,
the various features of the structure can be characterized. To assist in
determining the chemical makeup of the spinel phases or oxides with distorted
parameters the composition of the matrix of each alloy was determined employing
a Phacomp analysis[16]. The results of this analysis are presented in Table VA.
These results indicate that for the majority of alloys the matrix is con-
siderably richer in Cr, Co, and Mo than the bulk chemical analysis shows.
This is due to intermetallic formation (i.e., $\gamma'$, carbides, borides) which
deplete the matrix of Ni, Al, Ti, and the strong carbide-forming elements.

For SM-200 (Figure 23) the base oxide is a cubic spinel whose lattice
parameter and matrix analysis suggests a $(Ni,Co)Cr_2O_4$ composition. This
oxide contains $TiO_2$ and possibly $WO_3$ protrusions which grow with time. The
position of these secondary phases indicates some relation with grain
boundaries and/or intermetallics in the alloy.

For IN-100 (Figure 24) the initial oxide is cubic $(Co, Ni)O$ lattice
further expanded by the solution of V. This oxide contains a random size
distribtuion of $TiO_2$ (rutile) protrusions which also grow rapidly with time.
After 4 hours exposure at 1600°F, the protrusions become massive and occupy
approximately 30% of the surface. There is also some evidence of $\alpha-Al_2O_3$
and $\alpha-Cr_2O_3$ type oxides but these (particularly the $Al_2O_3$) may be part of
the internal oxide.

Inco 713C (Figure 25) initially forms cubic NiO whose lattice parameter
indicates relatively high purity. After 4 hours exposure, crystalline
$Ni(Cr,Al)_2O_4$ type spinel protrusions are observed. The spinel phase forms
a pattern which indicates some relation with the matrix morphology.

In all instances, the cast alloys display thin films with multi-phase
oxides. However, the thin film morphology for René Y (Figure 22) displayed
a relatively uniform single phase oxide of rhombohedral $\alpha-Cr_2O_3$ and possibly
some homogeneous $(Mn,Ni)Cr_2O_4$ spinel overgrowths. After exposure at 1800
and 2000°F, the oxide remained uniform although significantly more developed

60

# TABLE X

## TYPICAL X-RAY DIFFRACTION PATTERN OF PRODUCTS ELECTROLYTICALLY STRIPPED FROM IN-100 AFTER 2 HOURS/1600°F

| d(Å) | I/I₀ | (Co,Ni,V)O Cubic (a₀=4.3Å) | TiO₂ Tetragonal a₀=4.59Å c₀=2.96Å | Al₂O₃ Rhomb | Cr₂O₃ Rhomb | M₂₃C₆ |
|------|------|------|------|------|------|------|
| 3.25 | M | - | 110 | - | - | - |
| 2.67 | VW | - | - | - | 104 | 400 |
| 2.55 | VW | - | - | 104 | - | - |
| 2.49 | S | 111 | 101 | - | 110 | - |
| 2.38 | VW | - | - | 110 | - | 420 |
| 2.30 | VW | - | 200 | - | - | - |
| 2.19 | VW | - | 111 | - | - | - |
| 2.15 | M | 200 | - | - | - | 422 |
| 2.05 | W | - | 210 | - | - | 511 |
| 1.80 | VW | - | - | - | - | 531 |
| 1.74 | VW | - | - | 024 | - | - |
| 1.68 | M | - | 211 | - | - | 620 |
| 1.66 | VW | - | - | - | 116 | - |
| 1.62 | W | - | 220 | - | - | 533 |
| 1.60 | VW | - | - | 116 | - | 622 |
| 1.56 | VW | - | - | - | - | - |
| 1.52 | M | 220 | - | - | - | - |
| 1.475 | VW | - | 002 | - | - | - |
| 1.450 | VW | - | 310 | - | - | - |
| 1.425 | VW | - | - | - | 300 | - |
| 1.400 | VW | - | - | - | - | - |
| 1.355 | W | - | 301 | - | - | - |
| 1.345 | VW | - | 112 | - | - | - |
| 1.299 | M | 311 | 311 | - | - | 644 |
| 1.256 | VW | - | - | - | - | - |
| 1.245 | W | - | 202 | - | - | - |
| 1.169 | VW | - | 321 | - | - | 840 |
| 1.150 | VW | - | 400 | - | - | - |
| 1.092 | VW | - | 222 | - | - | - |

11 more lines

S = strong; M = medium; W = weak; V = very

as illustrated in Figure 26. The microporosity noted at the edges of the
crystal faces (Figure 26(a)) may reflect the onset of oxide vaporization.
After the 2000°F exposure (Figure 26(b)), crystal growth is observed along
with rounding of the crystal edges. This latter effect is believed to
reflect an advanced stage of volatilization.

### 4.2.2 Macroscopic Oxide Morphology

To completely evaluate the oxidation mechanism of an alloy, the macroscopic
as well as the microscopic oxidation process must be understood. This is
particularly important for complex alloys where inhomogeneities can exist
and influence the oxidation behavior. For this reason, some attention was
devoted to evaluating the gross oxide morphology as a function of both time
and temperature.

The general oxide morphology of IN-100 continuous weight-gain specimens as
a function of testing temperature are illustrated in Figure 27. The
general thickening of the oxide with increasing oxidation temperature is
evident. The important feature, however, is the relation between the
interdendritic precipitates in the as-cast structure (Figure 27(a)) and
the excessive oxide buildup in these regions with increasing temperature,
which eventually leads to spalling. Figure 28 is presented to further
demonstrate the apparent relation which exists between precipitates within
as-cast SM-200 and Inco 713C and the subsequent oxide growth pattern.
Although the specific cause(s) of the oxide buildup on or in the vicinity
of original interdendritic precipitates was not established, it is no
doubt related to alloying element partitioning present in the cast alloys.
It also demonstrates that the heterogeneous oxidation observed during thin
film oxidation persists after longer exposures.

Figure 29 shows the general appearance of the oxides produced during the
static oxidation of René Y at 1800°F. Of significance here is the varia-
tion in oxide morphology exhibited between heats and the homogeneous
appearing oxide. Heat 1, which consistently displayed superior oxidation
resistance in oxidation tests, demonstrated the nucleation and subsequent
growth of oxide protrusions as a function of oxidation time. Heat 2, on the
other hand, shows no such effects. The protrusions, although tenacious,
were removed and analyzed using X-ray diffraction. With the exception of
additional NiO and matrix phase, the structure was the same as the adjoining
oxide. Further explanation regarding the cause or significance of this
phenomenon is presented in the following section.

82

589A

589B

(a) 100 Hrs/1800°F    Note Well-Developed Single
Crystalline Structure, Growth Steps, and Micro-Porosity.
(10,000X)

(b) 100 Hrs/2000°F    Note Additional Crystal Growth
And Rounding of Crystal Edges Due to Volatilization.
(10,000X)

FIGURE 26    Electron Microscopy Depicting the Topography of Thick Oxides Produced on René Y After Long-
Time Exposure to Air.  Shadowed Replica as Stripped from Oxidized Specimen Surface.

63

C65102617

C65102616

L5164

(a) Alloy as-cast - illustrating
    interdendritic precipitation

(b) 1400°F - Note oxide buildup
    on precipitates

(c) 1600°F - Additional oxide
    growth

C65102618

C65102619

C65102620

(d) 1800°F - Lateral oxide
    growth

(e) 2000°F - Massive oxide
    protrusions & spalling

(f) 2100°F - Gross spalling of
    oxide protrusions
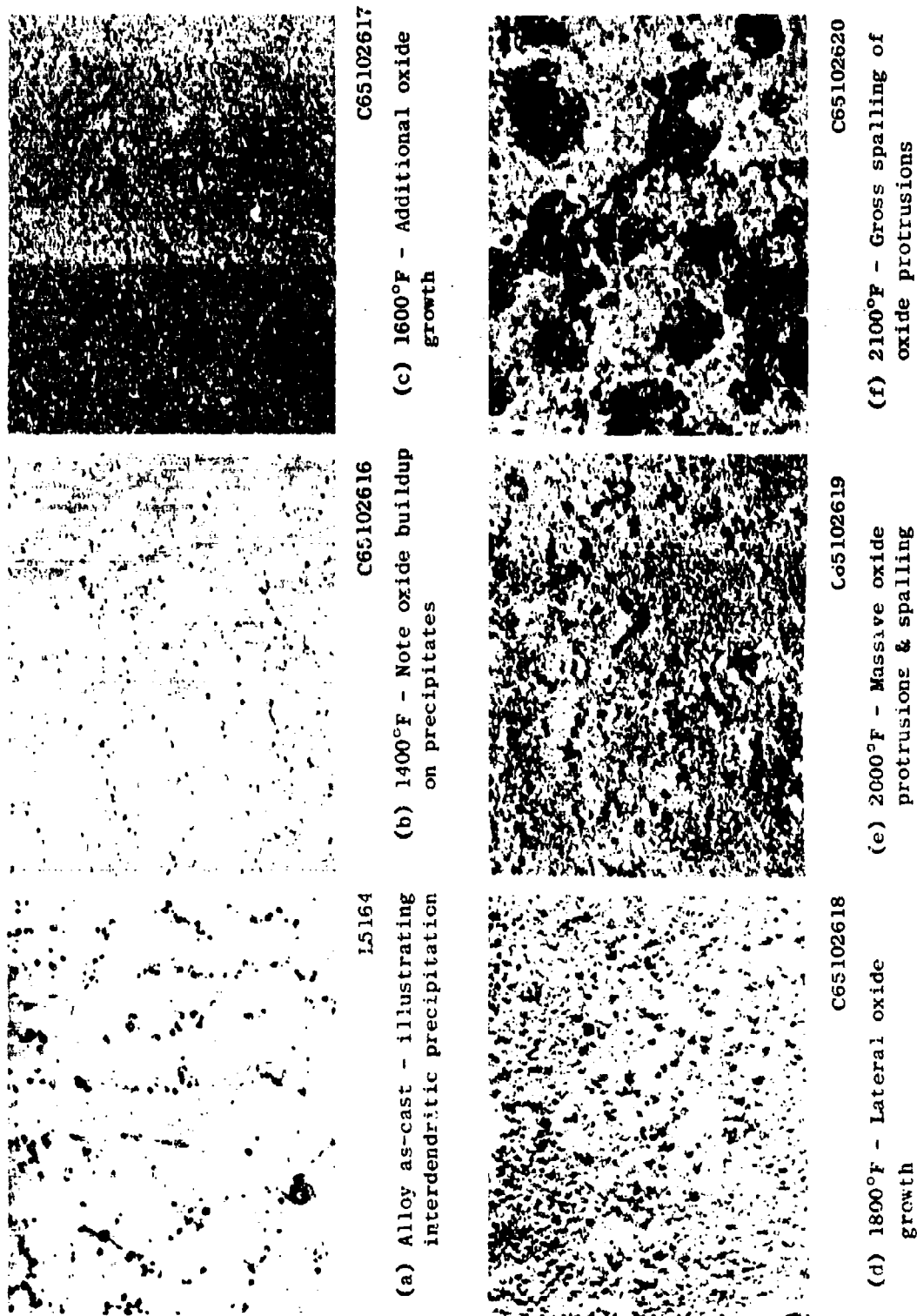
FIGURE 27    The general surface appearance of IN-100 (Heat #1) continuous weight-gain specimens oxidized
             100 hours at 1400, 1600, 1800, 2000, and 2100°F.  Note excessive oxide growth on what was
             originally interdendritic precipitates.                                              45x

64

C65112211

(c) SM-200 Ht. #1 At 1800°F

C65112209
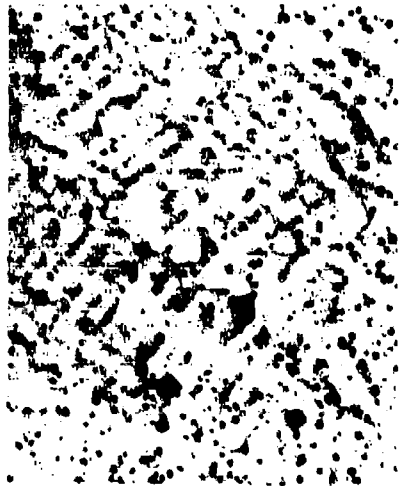
(f) INCO 713C Ht. #1 At 1800°F

C65112208

(b) SM-200 Ht. #1 At 1600°F

C65112207

(e) INCO 713C Ht. #1 At 1600°F

L5168

(a) SM-200 Ht. #1 As-Cast

L5167

(d) INCO 713C Ht. #1 As-Cast

Figure 28    General surface appearance of SM-200 and INCO 713C after 100 hour exposure in static air at 1600°F and 1800°F.  Note relation between regions of heavy oxide growth and original precipitates.
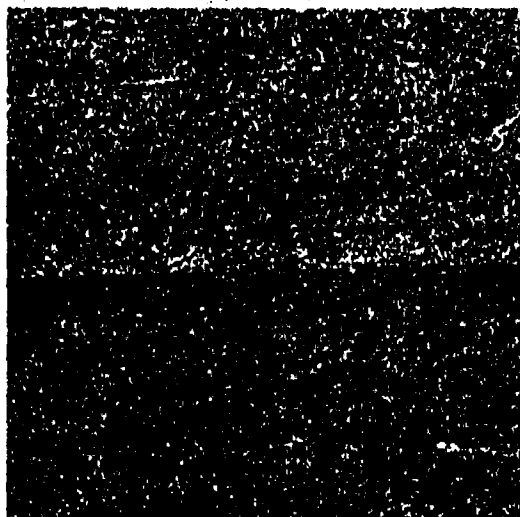
(a) Heat #1 - Oxidized 100 hours
Note nucleation of protrusions
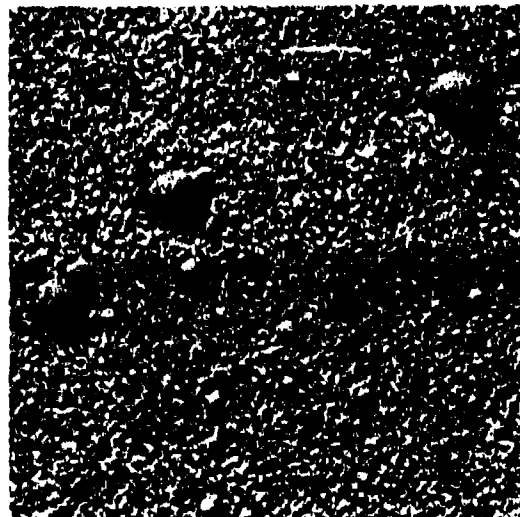
(b) Heat #1 - Oxidized 1000 hours
Note growth of protrusions
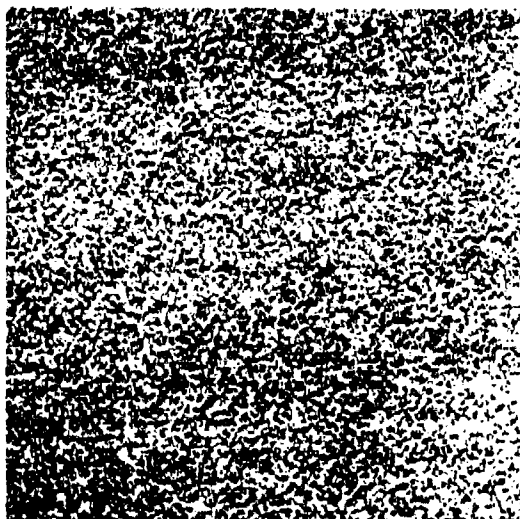
(c) Heat #2 - Oxidized 100 hours
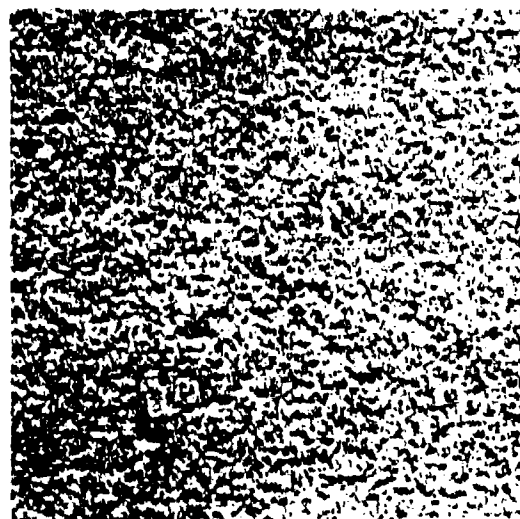
(d) Heat #2 - Oxidized 1000 hours

FIGURE 29   The general surface appearance and heat variations observed for
René Y oxidized in static air for various times at 1800°F.   Note
the formation and growth of oxide protrusions in Heat #1.

45x

### 4.2.3 René Y Oxidation

Typical microstructures depicting the morphology of the oxidation reactions for René Y after various times and temperatures are presented in Figures 30 and 31. The quantitative measurements indicating the extent of the reactions are given in Table XI. The oxide features consist of a relatively dense two-phase scale with semi-continuous grain boundary attack and a uniform I.O. or I.G.O. region. The oxide measurements indicate the following:

(1)  Greater oxidation resistance for Heat No. 1 (see Figure 30). This heat variation is considered a result of fabrication induced variables, since the chemical analysis of the two heats are essentially identical.

(2)  For each heat the scale thickness reached a maximum value and then remained constant or decreased with increasing time/temperature. The I.O., however, continued to increase with time and temperature attaining a depth two to four times greater than the scale thickness. This provided additional support for the hypothesis that vaporization of oxides is significant at temperatures greater than 1800°F.

(3)  The growth of I.O. follows parabolic kinetics within the accuracy of measurement (this will be covered in more detail in a subsequent section).

(4)  Only very slight spalling of surface oxides was observed after an exposure of 1000 hours at 2000°F.

(5)  Alloy depletion or $\gamma'$ dissolution was not detected since this alloy does not form $\gamma'$. However, a zone, irregular in thickness and depleted of carbides was found to exist below the oxide scale.

The results of X-ray diffraction studies of oxidized specimens obtained employing various techniques are summarized in Table XII while Tables XIII and XIV present typical X-ray diffraction patterns of the reaction products. Figure 32 summarizes the results of microprobe traverses through the oxide zone after exposures of 100 hours at 1600, 1800, and 2000°F.

By combining the results of the metallographic evaluation, X-ray identification and microprobe analysis, the nature of the oxidation reaction can be understood. During the initial stages of oxidation at 1600 and 1800°F, the rhombohedral phase, $\alpha-Cr_2O_3$, is the primary scale product with traces of $MnCr_2O_4$ spinel. X-ray diffraction of surface oxides in situ shows mixtures of the cubic spinel $MnCr_2O_4$ and $\alpha-Cr_2O_3$ at temperatures between 1600 and 2000°F for times up to 1000 hours. With increasing temperature or time at temperature, $MnCr_2O_4$ becomes the predominant oxide phase with a lattice parameter which varies from 8.49Å at 1600°F to 8.43Å at 2000°F. Correspondingly, the apparent abundance of $\alpha-Cr_2O_3$ decreases with increasing
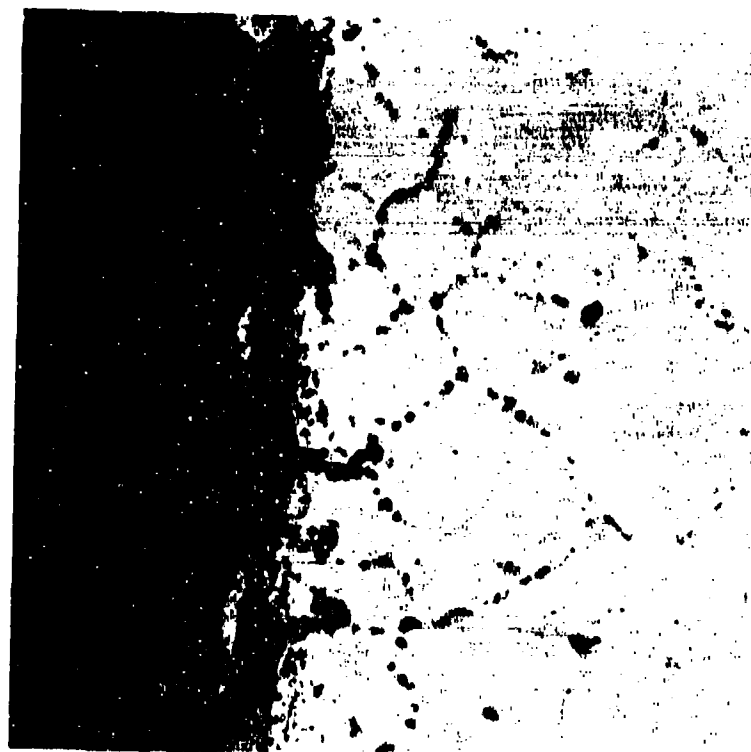
M1781

M1782

(a) Heat No. 1    Note Two-Phase Oxide Scale and
Metallic Inclusions.

(b) Heat No. 2    Note Thicker Oxide Scale and
Deeper I.O.

FIGURE 30    Typical Scale and Subscale Morphology for René Y Oxidized 1000 Hours at 1600°F Denoting
Scaling Differences Between Heats.  Mounted on 5:1 Taper Sections.  Unetched (500X)
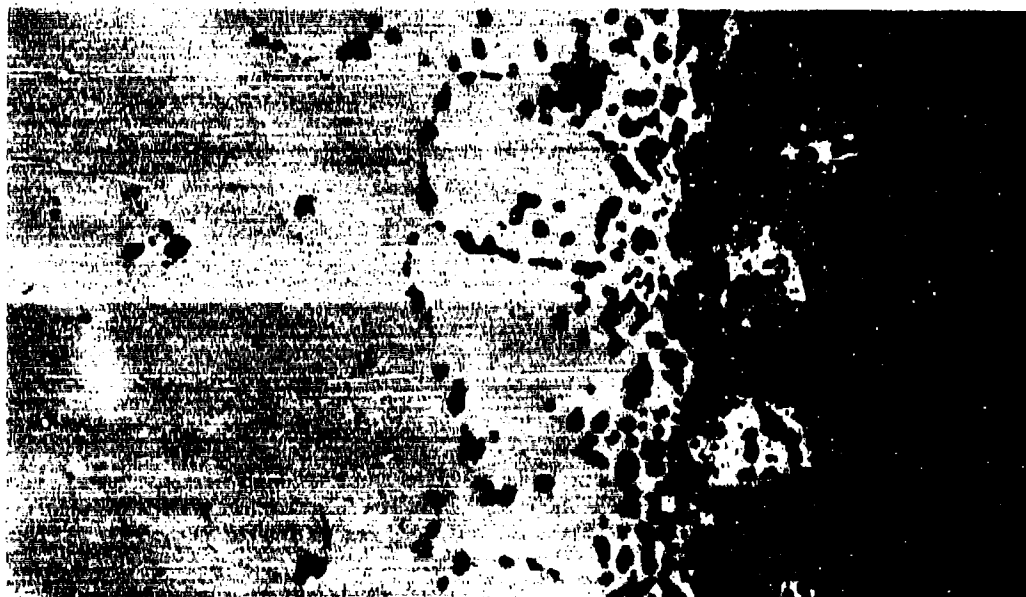
M1785

(a) 1000 Hrs/1800°F    Note Two-Phase Surface Oxide and Encirclement of
Metallic Grain.
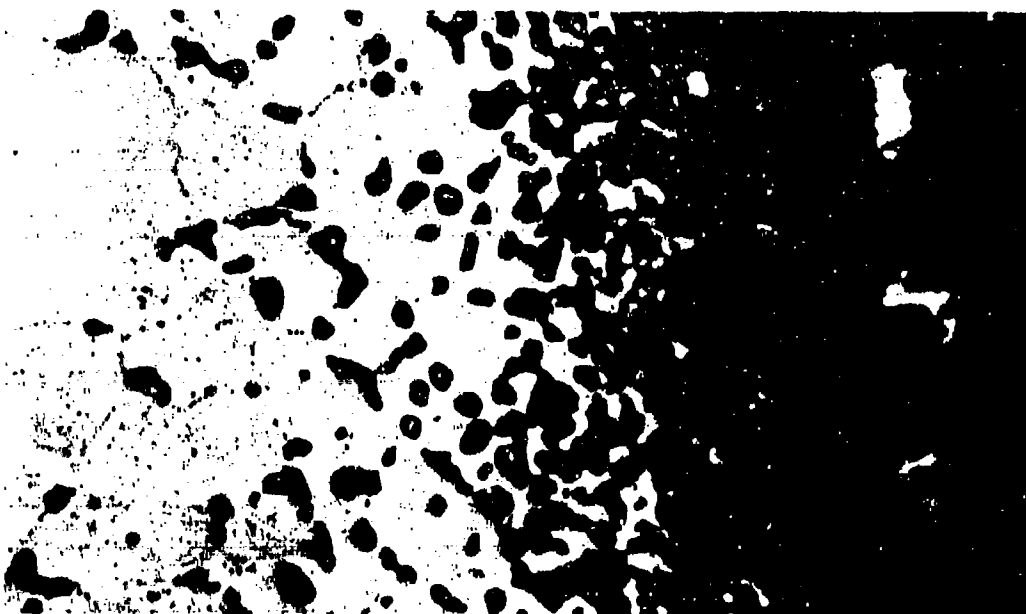


M1778

(b) 1000 Hrs/2000°F    Note Metallic Particles in Surface Scale.

FIGURE 31    Typical Scale and Subscale Morphology for René Y Oxidized
In a Static Atmosphere.  Mounted on 5:1 Taper Sections.
Unetched (500X).

## TABLE XI

### STATIC OXIDATION METALLOGRAPHIC RESULTS FOR RENÉ Y(a)

| Heat | Test Conditions Temp (°F) | Time (hrs) | Average Weight Gain(b) (mg/cm²) | Avg. Scale Thickness (mils/side) | Average I.O. (mils/side) | Metal Loss(d) (mils/side) | γ' Dissolution(c) (mils/side) |
|---|---|---|---|---|---|---|---|
| 1 | 1600 | 100 | 0.34 | 0.2 | 0.3 | 0.2 | 0 |
|   |      | 400 | 0.80 | 0.3 | 0.5 | - | 0 |
|   |      | 1000 | 0.85 | 0.4 | 0.7 | - | 0 |
| 2 | 1600 | 100 | 0.38 | 0.2 | 0.3 | - | 0 |
|   |      | 400 | 1.04 | 0.4 | 0.7 | - | 0 |
|   |      | 1000 | 1.35 | 0.5 | 1.0 | - | 0 |
| 1 | 1800 | 100 | 0.65 | 0.3 | 0.5 | 0.7 | 0 |
|   |      | 400 | 1.13 | 0.4 | 0.8 | - | 0 |
|   |      | 1000 | 1.28 | 0.5 | 1.1 | 0.9 | 0 |
| 2 | 1800 | 100 | 0.96 | 0.6 | 0.5 | 0.6 | 0 |
|   |      | 400 | 1.86 | 0.6 | 1.0 | - | 0 |
|   |      | 1000 | 2.22 | 0.6 | 1.2 | - | 0 |
| 1 | 2000 | 100 | 0.95 | 0.4 | 0.8 | 0.0 | 0 |
|   |      | 400 | 1.59 | 0.3 | 1.2 | - | 0 |
|   |      | 1000 | 2.72 | 0.5 | 1.5 | 0.5 | 0 |
| 2 | 2000 | 100 | 1.04 | 0.3 | 0.7 | - | 0 |
|   |      | 400 | 1.52 | 0.4 | 1.4 | - | 0 |
|   |      | 1000 | 2.69 | 0.5 | 2.0 | 0.0 | 0 |

(a) All metallographic measurements taken at 250X from tapered sections with a 5:1 magnification except as indicated.

(b) For reference purposes only.

(c) No γ dissolution observed but an undefinable region of carbide dissolution was noted.

(d) Vertical sections used with accuracy of ± 0.5 mil.

## TABLE XII

### X-RAY IDENTIFICATION OF REACTION PRODUCTS FOR RENÉ Y EXPOSED IN STATIC AIR

| Temp °F | Time Hrs. | Heat No. | Type Spec | Reaction Products[a] |
|---|---|---|---|---|
| 1600 | 100 | 1 | (b) | $Cr_2O_3$ + $MnCr_2O_4$ ($a_o$=8.49Å) |
| | 1000 | 1 | (b) | $Cr_2O_3$ + $MnCr_2O_4$ ($a_o$=8.49Å) |
| 1800 | 100 | 1 | (b) | $Cr_2O_3$ + $MnCr_2O_3$ ($a_o$=8.47Å) |
| | 400 | 1 | (b) | $MnCr_2O_3$ ($a_o$=8.48Å) + $Cr_2O_3$ |
| | 1000 | 1 | (b) | $MnCr_2O_4$ ($a_o$=8.45Å) + $Cr_2O_3$ + NiO (VVW) |
| 2000 | 100 | 1 | (b) | $MnCr_2O_4$ ($a_o$=8.45Å) + $Cr_2O_3$ |
| | 100 | 1 | (c) | $MnCr_2O_4$ ($a_o$=8.45Å) + $Cr_2O_3$ + $SiO_2$ |
| | 100 | 2 | (b) | $MnCr_2O_4$ ($a_o$=8.45Å) + $Cr_2O_3$ |
| | 1000 | 1 | (b) | $MnCr_2O_4$ ($a_o$=8.44Å) + $Cr_2O_3$ |
| | 1000 | 1 | (d) | $MnCr_2O_4$ ($a_o$=8.42Å) + $Cr_2O_3$ + NiO |
| | 1300 | 1 | (e) | $MnCr_2O_4$ ($a_o$=8.43Å) + $Cr_2O_3$ + NiO |
| 2100 | 100 | 1 | (b) | $MnCr_2O_4$ ($a_o$=8.44Å) + $Cr_2O_3$ + $SiO_2$ |

(a) Listed in order of decreasing predominance as indicated by X-ray intensities.

(b) Diffractometer trace of oxide in situ.

(c) Debye Scherrer analysis of electrolytically stripped oxide.

(d) Debye Scherrer analysis of spalled oxide.

(e) Debye Scherrer analysis of surface oxide protrusions.

**TABLE XIII**

TYPICAL X-RAY PATTERN OF SPALLED OXIDE FROM

RENÉ Y AFTER 1000 HOURS/2000°F IN STATIC AIR

| | | | h k l | | |
|---|---|---|---|---|---|
| $d(Å)$ | $I/I_0$ | Matrix (F.C.C.) | $\alpha$-$Cr_2O_3$ Rhomb ($a_0$=5.36Å) ($\alpha$=55°8") | $MnCr_2O_4$ Cubic ($a_0$=8.42Å) | NiO Cubic ($a_0$=4.17Å) |
| 3.60 | W | – | 012 | – | – |
| 2.95 | VVW | – | – | 220 | – |
| 2.65 | S | – | 104 | – | – |
| 2.53 | S | – | – | 311 | – |
| 2.47 | S | – | 110 | – | – |
| 2.42 | VVW | – | – | 222 | – |
| 2.40 | VW | – | – | – | 111 |
| 2.16 | W | – | 113 | – | – |
| 2.10 | VW | – | – | 400 | – |
| 2.075 | W | 111 | – | – | 200 |
| 1.810 | W | 200 | 024 | – | – |
| 1.720 | VVW | – | – | 422 | – |
| 1.665 | S | – | 116 | – | – |
| 1.619 | W | – | – | 511 | – |
| 1.571 | VVW | – | 112 | – | – |
| 1.488 | M | – | – | 440 | – |
| 1.473 | W | – | – | – | 220 |
| 1.462 | W | – | 214 | – | – |
| 1.429 | VS | – | 300 | – | – |
| 1.331 | VVW | – | – | 620 | – |
| 1.293 | W | – | 1·0·10 | – | – |
| 1.284 | W | – | – | 533 | – |
| 1.238 | W | – | 220 | – | – |
| 1.217 | VW | – | – | 444 | – |
| 1.210 | VW | – | 306 | – | – |
| 1.205 | W | – | – | – | 222 |
| 1.173 | VVW | – | 128,312 | – | – |

S = strong; M = medium, W = weak; V = very

## TABLE XIV

### TYPICAL X-RAY DIFFRACTION FROM SURFACE OXIDES
### FORMED ON RENÉ Y AFTER 100 HOURS/2100°F IN STATIC AIR

| | | h k l | |
|---|---|---|---|
| d(Å)* | I/I$_0$ | MnCr$_2$O$_4$ Spinel, Cubic (a$_0$=8.44Å) | $\alpha$-Cr$_2$O$_3$ Rhombohedral (a$_0$=5.37Å) ($\alpha$=55.4°) |
| **4.19 | 10 | – | – |
| 3.65 | 29 | – | 012 |
| 2.99 | 50 | 220 | – |
| 2.67 | 33 | – | 104 |
| 2.55 | 100 | 311 | – |
| 2.49 | 25 | – | 110 |
| 2.18 | 11 | – | 113 |
| 2.11 | 17 | 400 | – |
| 1.81 | 8 | – | 024 |
| 1.72 | 8 | 422 | – |
| 1.67 | 21 | – | 116 |
| 1.625 | 25 | 511,333 | – |
| 1.492 | 27 | 400 | – |
| 1.467 | 8 | 214 | – |
| 1.433 | 10 | 531 | 300 |
| 1.287 | 8 | 622 | 1·0·10 |

** Unidentified line – corresponds to strongest reflection from SiO$_2$ (cristobalite)

\* Reflections from base metal have been omitted
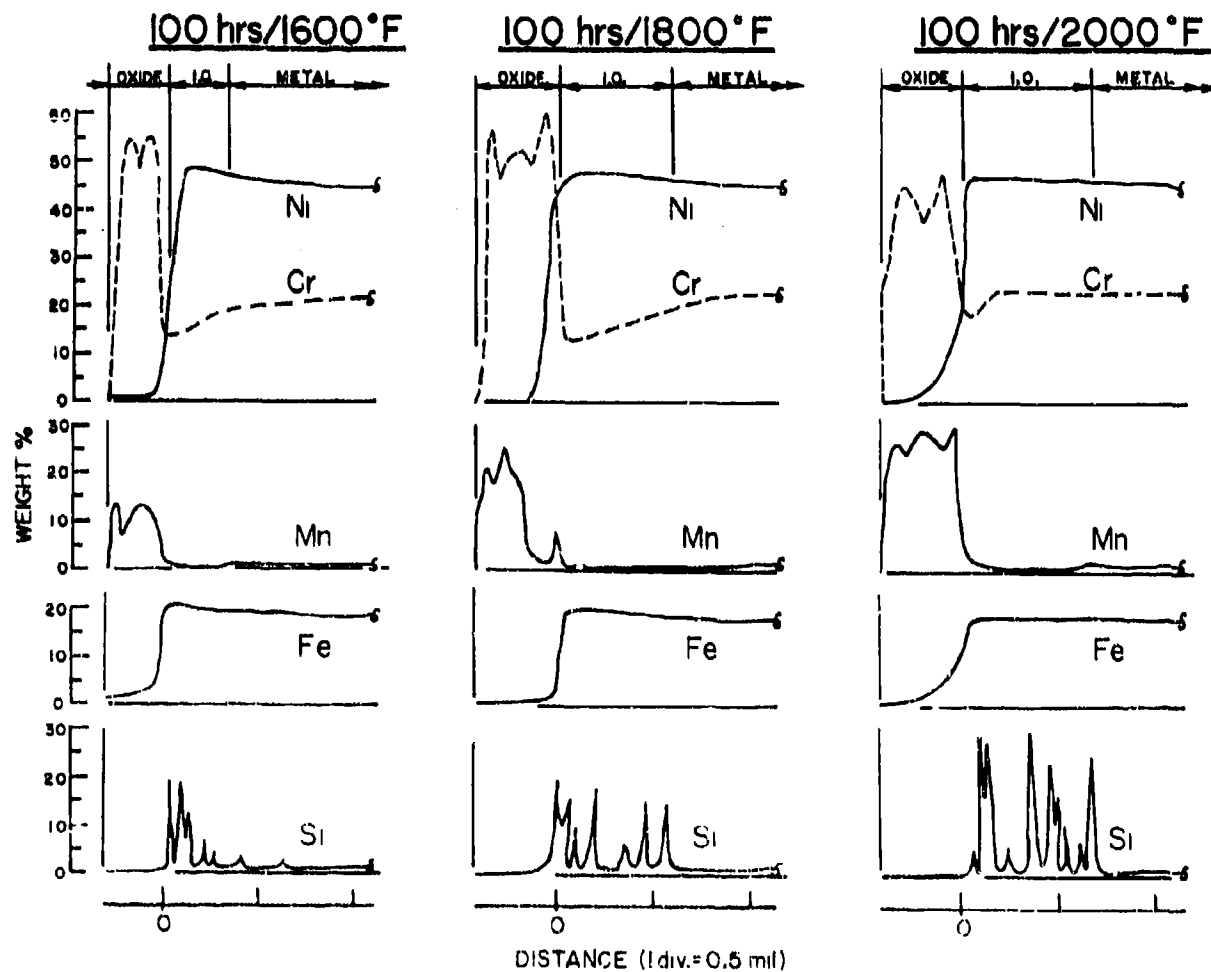
FIGURE 32 Microprobe Traverse Results for René Y (Heat No. 1) Static Oxidation Test Specimens

temperature and displays a lattice contraction to the theoretical value
at 2000°F. X-ray diffraction results of spalled oxide products and
protrusions formed at 2000°F indicate that $Cr_2O_3$ is overgrown with
$MnCr_2O_4$ spinel but is still present in significant quantities. This is
also evident from the microstructures (see Figures 30 and 31) where the
darker outer scale product is $MnCr_2O_4$. X-ray diffraction of electrolyti-
cally stripped oxides from specimens oxidized at 2000°F indicated trace
quantities of $SiO_2$ (cristobalite). This phase is amorphous at lower
temperatures and therefore not detectable by X-ray. The microprobe analysis
corroborates the X-ray data and indicates the following additional features:

(a)    The spinel phase is $MnCr_2O_4$ (24 w/o Mn and 46 w/o Cr) and overgrows
       the $Cr_2O_3$ phase which contains 65 w/o Cr.

(b)    $SiO_2$ with trace quantities of $Mn_xO_y$ are the primary internal oxides
       present. The stoichiometry of the $Mn_xO_y$ could not be ascertained.

(c)    The expansion of the $Cr_2O_3$ lattice parameter at the lower temperatures
       is due to the solubility of Mn and not Mo or Fe since the concentrations
       of these elements in the scale are negligible.

(d)    At 1600-1800°F there is an increase in the concentration of Fe and
       Ni just below the oxide scale. At 2000°F however, both Ni and Fe
       display some solubility in the oxide and may yield $(Mn,Ni)Cr_2O_4$ and
       $(Cr,Fe)_2O_3$ mixed oxide phases.

A summary chart for the reaction products formed on René Y as a function of
oxidation time and temperature is shown in Figure 33.

The cause of anomalous oxide protrusions previously illustrated (Figure 29)
during high (> 1800°F) temperature oxidation of René Y (Heat No. 1) has been
resolved. An X-ray analysis of these protrusions indicated the additional
presence of NiO and matrix. By referring to Figure 34 and 30(a), the
sequence of events resulting in these protrusions is apparent. At the higher
temperatures (Figure 30(a)) the $Cr_2O_3$ displays some preference for formation
in grain boundaries. This results in the isolation of grains, depletion
of chromium from the matrix through selective oxidation, subsequent reduction
in the oxidation resistance of the remaining matrix, and finally the forma-
tion of NiO at a significantly faster rate which promotes the "ballooning"
effect indicated in Figure 34. The fact that this phenomenon is not
observed for Heat No. 2 must be related to subtle differences in processing
(grain size, etc.,) or the distribution of elements between the two heats.

Additional information regarding the oxidation behavior of this alloy,
specifically the role of Mn and La additions will be covered in subsequent
sections.

75
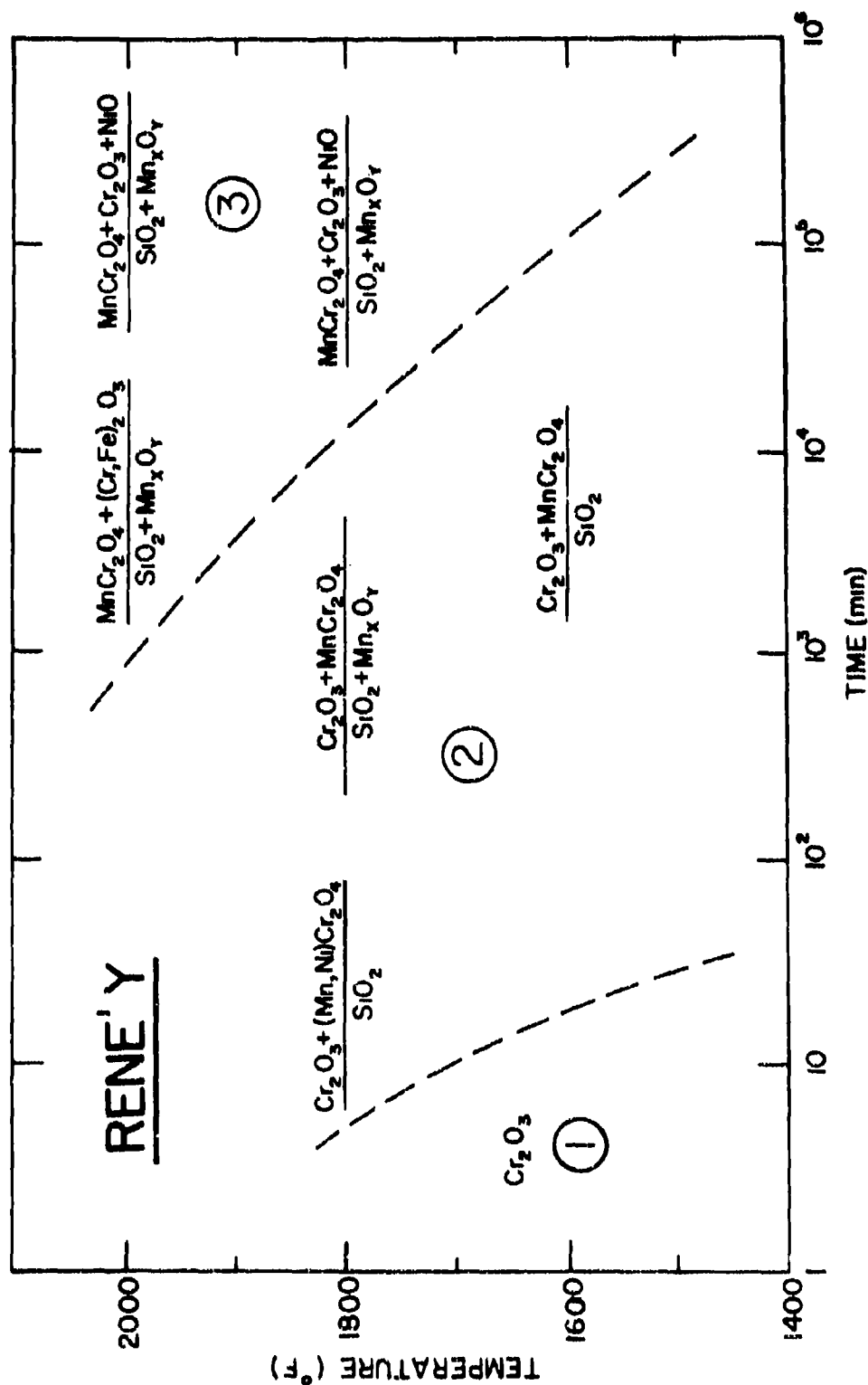
FIGURE 33    Simplified Summary of the Main Stages of Oxidation for Rene Y.  Phases present in the numerator are the scale constituents, those in the denominator are products of internal oxidation.
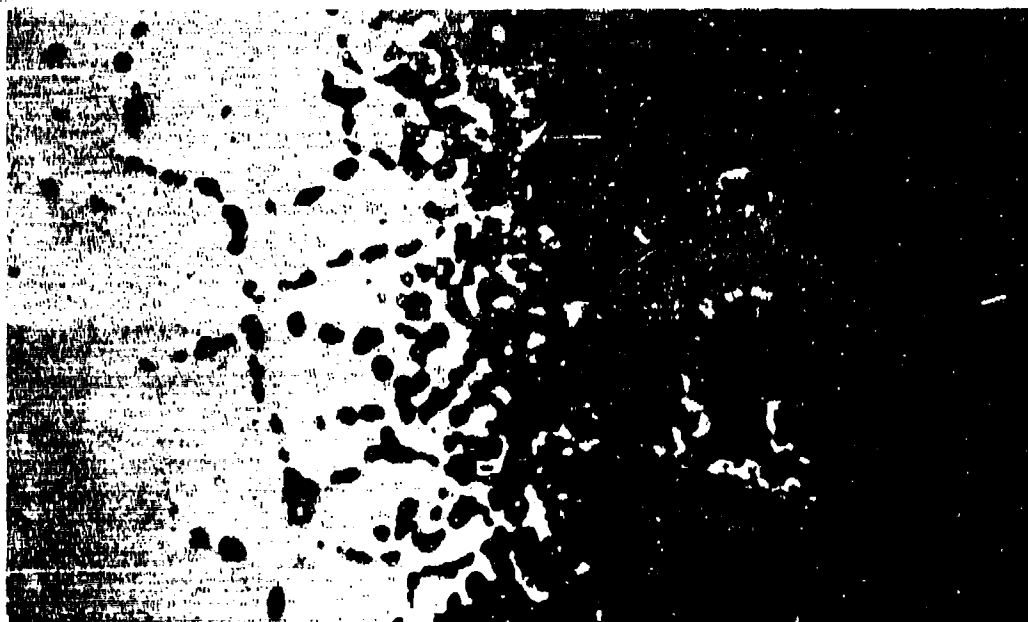
M1789

(a) 400 Hrs/2000°F    Early Stage of Growth Where Coherence With
Surface Oxide is Maintained.    (500X)



M1940

(b) 400 Hrs/2000°F    Latter Stage of Growth Displaying Lack of
Adherence.    (250X)

FIGURE 34    Latter Stages of Growth of Protrusions Formed on René Y
             During Oxidation.  Mounted on 5:1 Taper Sections.  Unetched.

### 4.2.4  SM-200 Oxidation

The oxidation reactions of this alloy are more complex than the previously discussed René Y.  This complexity can be attributed to:

(a)    Reactive element activities which are highly sensitive to temperature yielding internal and external oxidation which does not vary in a simple manner with temperature.

(b)    A heterogeneous oxide scale which results in oxide spalling and difficulty in determining the extent of oxidation and oxide morphology.

In general, the scaling and subscaling processes which occur during normal exposure compete for the solute elements.  If the solute activity is low and if it is much less noble than the major surface oxide constituent, internal oxidation or grain boundary oxidation will result.  If, however, the activity is sufficiently altered by an increased concentration of solute (as by enhanced diffusion) this will result in oxidation of the reactive element as a part of the surface scale.  The critical nature of this competition is well demonstrated by the microstructures of oxidized SM-200, shown in Figure 35.  Aside from illustrating the general morphology of the oxidation products and associated interaction with the base metal, the sequence displays the fine balance between surface oxide and internal oxide formation.  After 100 and 400 hours at 1600°F, (Figure 35(a)) the classical type salt and pepper I.O. (probably $Al_2O_3$) is formed.  After 1000 hours (Figure 35(b)) at temperature, the I.O. is still present but agglomeration has occurred which essentially produces a continuous internal scale of $Al_2O_3$, minimizing the formation of additional I.O. by providing a stable diffusion barrier.  After an exposure of 100 hours at 1800°F (Figure 35(c)), only remnants of I.O. are observed and finally at 2000°F no I.O. is noted.  At 1800°F and above, the enhanced diffusion rate, or perhaps the dissociation of $\gamma'$, increases the effective concentration of aluminum at the metal/scale interface making its incorporation into the scale more favorable.  The fact that traces of I.O. are observed at 1800°F may reflect inhomogeneities in the alloy, but clearly indicates the close balance which exists between scale and subscale formation.  It should be pointed out that in theory once oxygen and solute element concentration gradients are produced within the alloy which satisfy the conditions required for internal oxidation at a specific temperature, the internal oxide precipitation will continue to form regardless of the exposure time[18].  The practical exception to this rule is illustrated in Figure 35(b) where inhomogeneities in the alloy in the form of primary $\gamma'$ particles caused the apparent cessation of I.O.  The converse to the above statement does not necessarily hold.  That is, continued oxidation at a specific temperature where I.O. is not initially formed may yield conditions conducive to its formation due to compositional changes which occur in the subscale region.
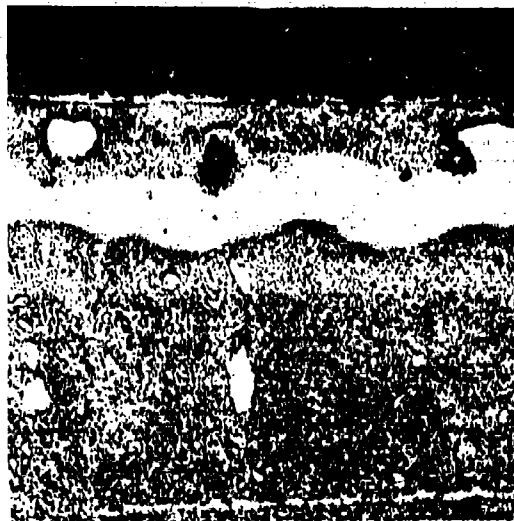
(a) 400 Hrs/1600°F    Note Classical
Salt and Pepper Type I.O.



(b) 1000 Hrs/1600°F    Note Cessation
Of I.O. Penetration by a Front of
Agglomerated I.O.



(c) 100 Hrs/1800°F    Note Only Remnants
Of I.O. at This Temperature.



(d) 100 Hrs/2000°F    Note Multi-Phase
Scale and Isolated Regions of I.O.
From I.G.A.

FIGURE 35    Typical Scale and Subscale Morphology Produced in SM-200 Oxidized
For Various Times and Temperatures in Static Air.  Mounted on
5:1 Taper Sections.  Etched in 2% Chromic (250X).

The measurements of the extent of reaction for this alloy are presented
in Table XV. As indicated by the weight-change data, the alloy was subject
to spalling during cooling from 1800°F and above. The extent of this
spalling may at first appear great so it should be emphasized that the
weight of the spalled products includes not only the oxygen gained to
form the oxide but also the weight of metal it combines with, whereas
weight-gain measurements with no spalling include only the weight gain
due to oxygen pickup. Therefore, only about one-third of the weight of
the spalled products can be attributed to oxygen. Due to the spalling
which occurred, identification of the original metal interface was difficult.
This in turn decreases the absolute accuracy of the I.O. and $\gamma'$ dissolution
measurements. An identification of the reaction products is also made dif-
ficult due to oxide spalling. This is particularly true for the microprobe
analysis where the spalled oxide is not included in the trace. In such
instances more reliance is placed upon X-ray results of spalled products
for an identification of the oxides present at temperature.

The results of X-ray diffraction studies conducted on this alloy are sum-
marized in Table XVI while Tables XVII, XVIII, and XIX illustrate typical
X-ray diffraction patterns of spalled and electrolytically stripped oxide
products. Figure 36 presents the microprobe traverse results of specimens
exposed for 100 hours at 1600, 1800, and 2000°F.

The oxidation of SM-200 cannot be considered as a progression of a certain
oxidation process with time and temperature but rather entirely different
modes of oxidation occur at each temperature which then progress with time.
The initial oxide formed at 1600°F is a spinel whose lattice dimensions
suggest $(Ni,Co)Cr_2O_4$. Continued exposure in the thin film region produces
a mixed $(Ni,Co)(Al,Cr)_2O_4$ type spinel with second phase protrusions of
$TiO_2$ and a tentatively identified tungstate $(WO_3)$. After 100 hours exposure,
an oxide scale rich in $Cr_2O_3$ with a heterogeneous* distribution of $NiCr_2O_4$
and $TiO_2$ and an I.O. zone containing primarily $Al_2O_3$ is observed. Continued
exposure to 1000 hours does not significantly alter the products but as
previously noted, does cause agglomeration of the I.O. products. During
the initial (thirty minutes) exposure at 1800°F a surface scale is formed
containing a heterogeneous mixture of $NiCr_2O_4$ spinel, $(Cr,Al)_2O_3$, NiO, and
$TiO_2$ in order of decreasing abundance. Increased exposure to 100 hours
produces $NiCr_2O_4 + NiAl_2O_4$ duplex spinel scale with dispersed $TiO_2$ and an
I.O. of $Al_2O_3$. After 1000 hours the notable addition of TiN and possibly a
tungstate phase to the subscale is observed. At 2000°F, the oxide scale
produced is extremely heterogeneous, as evidenced by visual observation
and the phase analysis. The data of Table XVIII illustrate the simultaneous

---

*The term "heterogeneous" used throughout this report does not indicate oxide layer
formation but rather an oxide mixture.

## TABLE XV

### STATIC OXIDATION METALLOGRAPHIC RESULTS FOR SM-200(a)(b)

| Heat | Test Conditions Temp (°F) | Time (hrs) | Average Weight Gain(c) (mg/cm²) | Avg. Scale Thickness (mils/side) | Gross I.O. or IGA (mils/side) | Maximum I.O. or IGA (mils/side) | γ′ Dissolution (mils/side) |
|---|---|---|---|---|---|---|---|
| 1 | 1600 | 100 | 0.40 | 0.20 | 0.20 | 0.25 | 0.30 |
|  |  | 400 | 0.70 | 0.20 | 0.22 | 0.30 | 0.40 |
|  |  | 1000 | 0.57 | 0.30 | 0.35 | 0.55 | 0.60 |
| 2 | 1600 | 100 | 0.62 | 0.18 | 0.20 | 0.40 | 0.39 |
|  |  | 400 | 1.70 | 0.20 | 0.30 | 0.50 | 0.50 |
|  |  | 1000 | 0.44 | 0.30 | 0.50 | 0.80 | 1.00 |
| 1 | 1800 | 100 | 0.79 | 0.30 | 0.30 | 0.45 | 0.50 |
|  |  | 400 | 1.38 (d) | 0.90 | 0.70 | 1.00 | 1.00 |
|  |  | 1000 | 0.72 (d) | 0.40 | 0.20 | - | 0.40 |
| 2 | 1800 | 100 | 0.83 | 0.35 | 0.40 | 0.60 | 0.50 |
|  |  | 400 | 1.50 (d) | 1.10 | 0.50 | 1.00 | 1.00 |
|  |  | 1000 | 1.01 (d) | 0.40 | 0.20 | - | 0.30 |
| 1 | 2000 | 100 | -0.32 (1.59) | - | 0.20 | 0.40 | 0.60 |
|  |  | 400 | -3.42 (2.22) | 0.60 | 0.50 | 1.00 | 0.80 |
|  |  | 1000 | -3.42 (3.11) | 0.60 | 0.40 | 0.80 | 1.00 |
| 2 | 2000 | 100 | -1.14 (1.92) | 0.35 | 0.50 | 1.00 | 0.60 |
|  |  | 400 | -3.50 (2.13) | 0.50 | 0.40 | 0.80 | 0.50 |
|  |  | 1000 | -2.02 (1.44) | 0.40 | 0.60 | 0.80 | 1.00 |

(a) All metallographic measurements taken at 250X from taper sections with a 5:1 magnification.

(b) Metal loss within accuracy of measurement ($\pm$ 0.5 mil), hence not reported.

(c) For reference purposes - value in parentheses includes specimen weight gain plus spalled products where spalling occurs.

(d) Spalling occurred but not measured.

TABLE XVI

X-RAY IDENTIFICATION OF REACTION PRODUCTS FOR SM-200 EXPOSED IN STATIC AIR

| Temp °F | Time Hrs. | Heat No. | Type Spec | Reaction Products[a] |
|---|---|---|---|---|
| 1600 | 100 | 1 | (b) | $Cr_2O_3$ + $TiO_2$ + Spinel |
| | 100 | 2 | (b) | $Cr_2O_3$ + $TiO_2$ + Spinel |
| | 1000 | 1 | (b) | $Cr_2O_3$ + $\alpha$-$Al_2O_3$ + Spinel + $TiO_2$ |
| 1800 | 100 | 1 | (b) | Spinel ($a_o$=8.36Å) + NiO + $Al_2O_3$ + $TiO_2$ |
| | 1000 | 1 | (c) | $TiO_2$ + $\alpha$-$Al_2O_3$ + Spinel ($a_o$=8.05Å) + TiN + unknown |
| 2000 | 100 | 1 | (c) | Spinel ($a_o$=8.02-8.30Å) + $\alpha$-$Al_2O_3$ + $TiO_2$ + unknown + TiN |
| | 100 | 1 | (d) | Spinel ($a_o$=8.28Å) + $\alpha$-$Al_2O_3$ + Spinel ($a_o$=8.06Å) + unknown + $NiTiO_3$ |
| | 1000 | 1 | (b) | $\alpha$-$Al_2O_3$ + Spinel ($a_o$=8.05Å) |
| | 1000 | 2 | (b) | Spinel ($a_o$=8.08Å) + $\alpha$-$Al_2O_3$ + Spinel ($a_o$=8.30Å) |
| | 1000 | 1 | (d) | Spinel ($a_o$=8.06Å) + Spinel ($a_o$=8.23Å) + $\alpha$-$Al_2O_3$ + $TiO_2$ |
| | 1000 | 1 | (e) | Spinel ($a_o$=8.26Å) + NiO + $\alpha$-$Al_2O_3$ + $TiO_2$ + Spinel ($a_o$=8 ?Å) |

[a] Listed in order of decreasing predominance as indicated by X-ray intensities

(b) Diffractometer trace of oxide in situ.

(c) Debye Scherrer analysis of electrolytically stripped oxide.

(d) Debye Scherrer analysis of spalled oxide.

(e) Debye Scherrer analysis of surface oxide protrusions.

**TABLE XVII**

TYPICAL X-RAY PATTERN OF PRODUCTS ELECTROLYTICALLY STRIPPED

FROM SM-200 AFTER 1000/1800°F IN STATIC AIR

| | | | h k l | | |
|---|---|---|---|---|---|
| | | | Spinel[a] | | |
| | | $\alpha$-Al$_2$O$_3$ | cubic | TiO$_2$ | TiN |
| d(Å) | I/I$_0$ | Trigonal | (a$_0$=8.05Å) | Tetragonal | Cubic |
| 4.65 | W | -- | 111 | -- | -- |
| *3.75 | VW | - | - | - | - |
| *3.60 | VW | - | -- | -- | - |
| 3.50 | M | 012 | - | -- | -- |
| 3.25 | M | - | - | 110 | - |
| 2.89 | M | - | 220 | - | -- |
| 2.55 | M | 104 | - | - | -- |
| 2.50 | S | - | - | 101 | - |
| 2.43 | S | - | 311 | - | 111 |
| 2.37 | W | 110 | - | - | - |
| 2.29 | VW | - | - | 200 | - |
| *2.26 | VW | - | - | - | - |
| 2.18 | S | - | - | 111 | - |
| 2.13 | W | - | - | - | 200 |
| 2.08 | M | 113 | -- | -- | - |
| 2.05 | VW | -- | - | 210 | - |
| 2.02 | M | - | 400 | - | - |
| 1.96 | VW | 202 | - | - | -- |
| *1.89 | VW | - | - | - | -- |
| 1.74 | M | 024 | - | - | - |
| 1.69 | W | -- | 422 | 211 | - |
| 1.60 | M | 116 | - | - | -- |
| 1.55 | M | - | 511 | - | -- |
| 1.535 | M | 211 | - | - | - |
| 1.460 | VW | - | - | - | 220 |
| 1.425 | W | - | 440 | - | - |
| 1.401 | W | 124 | - | - | -- |
| 1.370 | W | 030 | 531 | - | - |
| *1.315 | W | - | - | - | - |

S = strong; M = medium; W = weak; V = very

* Unknown phase, most probably a tungstate

(a) Most probably NiAl$_2$O$_4$

TABLE XVIII

## TYPICAL X-RAY PATTERN OF SPALLED OXIDE FROM
## SM-200 AFTER 100 HOURS/2000°F

| | | h, k, l | | | | |
|---|---|---|---|---|---|---|
| d(Å) | I/I$_0$ | Spinel[a] Cubic (a$_0$=8.28Å) | NiO Cubic | Spinel[b] Cubic (a$_0$=8.06Å) | α-Al$_2$O$_3$ Trigonal | NiT..O$_3$ Rhomb |
| 4.78 | W | 111 | - | - | - | - |
| *4.00 | VVW | - | - | - | - | - |
| 3.70 | VVW | - | - | - | - | 102 |
| *3.57 | VVW | - | - | - | - | - |
| 3.45 | VVW | - | - | - | 012 | - |
| *3.30 | VW | - | - | - | - | - |
| 3.22 | VVW | 220β | - | - | - | - |
| 2.93 | M | 220 | - | - | - | - |
| 2.88 | VVW | - | - | 220 | - | - |
| 2.75 | VVW | 311β | - | - | - | - |
| 2.71 | VVW | - | - | - | - | 104 |
| 2.53 | VVW | - | - | - | 104 | 110 |
| 2.49 | VS | 311 | - | - | - | - |
| 2.40 | W | - | 111 | 311 | - | - |
| 2.33 | VVW | - | - | - | 110 | - |
| 2.28 | VVW | - | - | - | - | - |
| 2.21 | VVW | - | - | - | - | 113 |
| 2.09 | W | - | 200 | - | 113 | - |
| 2.07 | W | 400 | - | - | - | - |
| 2.03 | VVW | - | - | 400 | - | - |
| 1.75 | VVW | - | - | - | 224 | - |
| 1.72 | VVW | - | - | - | - | 116 |
| 1.69 | W | 422 | - | - | - | - |
| 1.65 | VVW | - | - | 422 | - | - |
| 1.61 | VVW | 440β | - | - | - | - |
| 1.595 | M | 511 | - | - | 116 | - |
| 1.475 | VW | - | 220 | - | - | - |
| 1.467 | S | 440 | - | - | - | - |
| 1.311 | VW | 620 | - | - | - | - |
| *1.267 | W | - | - | - | - | - |
| 1.258 | VW | 533 | 311 | - | - | - |
| 1.252 | VVW | - | - | - | - | - |
| 1.206 | VVW | - | 222 | - | - | - |
| 1.196 | VVW | 444 | - | - | - | - |

S = strong; M = medium; W = weak; V = very

* Unidentified phase probably a tungstate

[a] Most probably NiCr$_2$O$_4$

[b] Most probably NiAl$_2$O$_4$

# TABLE XIX

## TYPICAL X-RAY PATTERN OF PRODUCTS ELECTROLYTICALLY STRIPPED

## FROM SM-200 AFTER 100 HOURS/2000°F IN STATIC AIR

| d(Å) | $I/I_0$ | Spinel[a] Cubic ($a_0 = 8.02$Å) | $\alpha$-$Al_2O_3$ Trigonal | $TiO_2$ Tetragonal | TiN Cubic |
|---|---|---|---|---|---|
| | | h k l | | | |
| 4.65 | W | 111 | - | - | - |
| *3.70 | VW | - | - | - | - |
| *3.58 | VW | - | - | - | - |
| 3.48 | VW | - | 012 | - | - |
| 3.25 | W | - | - | 110 | - |
| 2.88 | M | 220 | - | - | - |
| 2.54 | VW | - | 104 | - | - |
| 2.42/2.53 | S | 311 | - | 101 | 111 |
| 2.37 | VW | - | 110 | - | - |
| 2.30 | VW | - | - | 200 | - |
| 2.17 | W | - | 006 | 111 | - |
| 2.12 | VW | - | - | - | 200 |
| 2.08 | W | - | 113 | - | - |
| 2.02 | W | 400 | - | - | - |
| 1.95 | VW | - | 202 | - | - |
| *1.85 | VW | - | - | - | - |
| *1.78 | VW | - | - | - | - |
| 1.74 | W | - | 024 | - | - |
| 1.67 | W | - | - | 211 | - |
| 1.64 | VW | 422 | - | - | - |
| 1.595 | M | - | 116 | - | - |
| 1.550 | W | 511 | 211 | - | - |
| 1.425 | M | 440 | - | - | - |
| 1.400 | VW | - | 124 | - | - |
| 1.370 | W | 531 | 030 | - | - |
| *1.315 | W | - | - | - | - |
| 1.255 | W | 533 | - | 301 | - |
| 1.230 | W | - | 1·0·10 | - | - |
| 1.070 | VW | - | 134 | - | - |
| 1.050 | W | 731 | 226 | - | - |

S = strong; M = medium; W = weak; V = very

\* Unkown phase most probably a tungstate.

(a) Most probably $NiAl_2O_4$

FIGURE 36    Microprobe Traverse Results for SM-200 (Heat No. 1) Static
Oxidation Test Specimens

identification of $NiCr_2O_4$ and $NiAl_2O_4$ spinel phases as part of the spalled products. Since these two phases are mutually soluble, their separate identification indicates that the oxides form on different areas of the specimens. This would reflect local inhomogeneities within the material. These inhomogeneities when combined with the heterogeneous nature of the scales formed makes identification of the exact oxide position within the scale difficult. The majority of data indicate that after 100 hours exposure at 2000°F the $NiCr_2O_4$ spinel and the Ti containing oxide ($TiO_2$ or $NiTiO_3$) spall leaving an oxide rich in $NiAl_2O_4$, $\alpha-Al_2O_3$ and an unidentified tungsten rich phase. Increased exposure time to 1000 hours results in the exfoliation of almost all the oxide phases produced leaving primarily $\alpha-Al_2O_3$ and some $NiAl_2O_4$. Referring to the microprobe analysis (Figure 36) the tendency toward Al base oxide formation with increasing temperature is quite pronounced. Supplementary to this is the apparent decrease in the extent of Cr depletion and an increase in W content beneath the oxide scale. These latter two effects suggest that W provides a "diffusion barrier" to Cr.


A simplified phenomenological summary of the prime reaction products formed during oxidation of this alloy is illustrated in Figure 37.


### 4.2.5 IN-100 Oxidation

Microstructures depicting the morphology of the oxidation reaction for this alloy at the various times and temperatures are presented in Figure 38, while measurements showing the extent of reaction are given in Table XX. As described for SM-200 this alloy also exhibits a heterogeneous oxide scale which promotes spalling after testing for 1000 hours at 1600°F and above but shows essentially no I.O. and considerably deeper I.G.O. than SM-200. The heavy spalling exhibited by IN-100 made the microstructural characterization difficult. A summary of the microstructural features observed for this alloy is given below:

(a)   The variation between heats is not considered significant.

(b)   The onset of spalling occurs at a lower temperature than SM-200, but the amount of oxide spalled at any time/temperature is less.

(c)   Although the oxide scale of IN-100 is twice the thickness of René Y the gross I.G.O. penetration is of the same magnitude. However, there are isolated regions where the massive I.G.O. exhibited for IN-100 is more than twice the depth exhibited by René Y and at least five times greater than SM-200. For this reason both the gross and maximum depth of I.G.O. have been reported.

87

**SM-200**

NiCr$_2$O$_4$ + (Cr, Al)$_2$O$_3$ + NiO + TiO$_2$

Cr$_2$O$_3$

① 

② $\dfrac{\text{Ni(Cr,Al)}_2\text{O}_4 + \text{TiO}_2 + \text{NiO}}{\text{Al}_2\text{O}_3}$

③ $\dfrac{\text{Cr}_2\text{O}_3 + \text{NiCr}_2\text{O}_4 + \text{TiO}_2}{\text{Al}_2\text{O}_3}$

$\dfrac{\text{(S)}\ \text{NiCr}_2\text{O}_4 + \text{NiAl}_2\text{O}_4 + \text{TUNGSTATE} + \text{NiTiO}_3}{\text{Al}_2\text{O}_3 + \text{TiO}_2 + \text{TiN}}$

④ $\dfrac{\text{(S)}\ \text{NiCr}_2\text{O}_4 + \text{NiAl}_2\text{O}_4 + \text{TiO}_2}{\text{Al}_2\text{O}_3 + \text{TUNGSTATE} + \text{TiN}}$

TIME (min)

TEMPERATURE (°F)

2000   1800   1600   1400

10   10$^2$   10$^3$   10$^4$   10$^5$   10$^6$

FIGURE 37   Simplified Summary of the Main Stages of Oxidation for SM-200. Phases present in the numerator are scale constituents; those in the denominator are subscale products.

88

M4717

(a) 100 Hrs/1600°F    Note Irregular
Scale with Isolated I.O.



M4718

(b) 1000 Hrs/1600°F    Note
Excessive Porosity.



M4719

(c) 100 Hrs/1800°F    Note Decreased
Scale Thickness and Intergranular
Penetration.
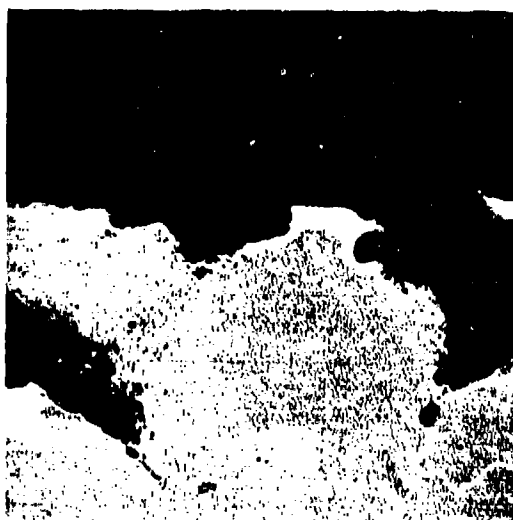


M4727

(d) 100 Hrs/2000°F    Note Multi-Phase
Oxide and Increased Intergranular
Penetration.

FIGURE 38    Typical Scale and Subscale Morphology for IN-100 Oxidized

In a Static Atmosphere.    Mounted on 5:1 Taper Section.

Etched in 2% Chromic.

## TABLE XX

### STATIC OXIDATION METALLOGRAPHIC RESULTS FOR IN-100(a)

| Heat | Test Conditions Temp (°F) | Time (hrs) | Avg. Weight Gain(b) (mg/cm²) | Avg. Scale Thickness (mils/side) | Gross I.O. or IGA (mils/side) | Maximum I.O. or IGA (mils/side) | Metal Loss(c) (mils/side) | γ' Dissolution (mils/side) |
|---|---|---|---|---|---|---|---|---|
| 1 | 1600 | 100 | 1.77 | 0.6 | 0.5 | 0.5 | 1.1 | 1.0 |
|   |      | 400 | 2.91 | 0.7 | 0.7 | 0.7 | - | 0.9 |
|   |      | 1000 | 3.11 (3.20) | 0.7 | 0.7 | 0.9 | - | 2.0 |
| 2 | 1600 | 100 | 1.86 | 0.6 | 0.5 | 0.5 | - | 0.6 |
|   |      | 400 | 2.33 | 0.5 | 0.7 | 0.7 | - | 1.2 |
|   |      | 1000 | 3.24 (3.27) | 0.8 | 1.0 | 1.1 | - | 1.2 |
| 1 | 1800 | 100 | 1.67 (1.73) | 0.6 | 0.3 | 0.6 | 1.3 | 1.0 |
|   |      | 400 | 1.83 (1.98) | 0.7 | 0.8 | 1.0 | - | 1.0 |
|   |      | 1000 | 0.94 (1.98) | 0.8 | 1.0 | 2.1 | 1.0 | 2.0 |
| 2 | 1800 | 100 | 1.88 (2.01) | 0.7 | 0.3 | 0.8 | 1.3 | 1.2 |
|   |      | 400 | 2.08 (2.30) | 1.0 | 1.0 | 1.0 | - | 1.2 |
|   |      | 1000 | 1.73 (2.68) | 1.0 | 1.2 | 2.0 | - | 1.4 |
| 1 | 2000 | 100 | -0.25 (1.80) | 0.7 | 1.3 | 1.5 | 0.5 | 1.5 |
|   |      | 400 | 0.03 (2.91) | 0.6 | 1.8 | 4.0 | - | 2.0 |
|   |      | 1000 | 0.03 (4.64) | - | 2.0 | 5.0 | 0.5 | 3.0 |
| 2 | 2000 | 100 | 0.11 (1.88) | 0.7 | 1.4 | 2.0 | - | 1.6 |
|   |      | 400 | -0.35 (3.27) | 0.6 | 2.0 | 4.0 | - | 2.0 |
|   |      | 1000 | 0.19 (5.17) | - | 2.0 | 5.0 | - | 3.0 |

(a) All metallographic measurements taken at 250X from tapered sections with a 5:1 magnification except as indicated.

(b) For reference purposes - value in parenthesis includes specimen weight gain plus spalled products where spalling occurs.

(c) Vertical sections used with accuracy of $\pm$ 0.5 mil.

90

(d)  The microstructures are notably free from the classical type I.O.
     which was observed for the other nickel-base alloys during some
     stage of the oxidation process.


The results of the microprobe traverses through the oxide are summarized
in Figure 39. Of interest is the high nickel, titanium, and aluminum con-
centrations in the scale and the correspondingly low chromium content. The
X-ray results are summarized in Table XXI while Table XXII illustrates the
X-ray pattern of a synthesized $NiTiO_3$ perovskite-type oxide used for a more
precise oxide identification. Tables XXIII and XXIV present actual diffraction
patterns obtained from spalled and scraped oxide specimens. All of this
analysis when combined with observations of the general microstructural
appearance yields a relatively complete characterization of IN-100 oxidation
as follows:

Thin film studies at 1600°F (see Section 4.2.1) vividly displayed the
multi-phase oxide formed during short-time exposures. The copious amount
of $TiO_2$ which initially forms within the (Ni,Co)O base oxide appears to
have significant bearing on the relatively poor oxidation resistance of
this alloy. After 100 hours at 1600°F the prime surface oxide remained
cubic (Ni,Co)O containing approximately 20% Co (as verified by the increased
NiO lattice parameter and microprobe results) but considerable "perovskite"
$NiTiO_3$ and $NiCr_2O_4$ type spinel phases were also detected. The subscale con-
tained small amounts of $Al_2O_3$ and $TiO_2$. Increased exposure at 1800°F to
1000 hours produced little change in the oxides present, however, the $NiCr_2O_4$
and $NiTiO_3$ overgrowths became separated from the subscale by a relatively
continuous string of voids. The formation of an acicular precipitate,
previously identified as TiN was also observed. Oxidation behavior at
1800°F was generally characterized by a decrease in the abundance of NiO
which no doubt combined to form the more predominant compound oxides
$NiCr_2O_4$ and $NiTiO_3$. The subscale oxide still contained $Al_2O_3$ and $TiO_2$.
Increased exposure at 1800°F produced considerable oxide spalling. An
analysis of the spalled products indicated primarily $NiCr_2O_4$ spinel and
$NiTiO_3$ and trace quantities of NiO. This implies that spalling occurs at
the interface between the $NiCr_2O_4$/$NiTiO_3$ and the $Al_2O_3$/$TiO_2$ subscale.
Therefore, under cyclic operation where spalling may result, $Al_2O_3$ and
$TiO_2$ would be exposed to the environment. X-ray analysis taken from the
surfaces of spalled specimens also indicates the presence of $NiTiO_3$. Since
$TiO_2$ is one of the original phases formed and that reaction with NiO will
readily produce $NiTiO_3$, it is suspected that the formation of this phase
is responsible for the massive intergranular attack characteristic of IN-100.
Oxidation at 2000°F is very complex and implies extremely heterogeneous
oxidation. After 100 to 400 hours exposure the spalled products contain
$NiCr_2O_4$, $NiTiO_3$, NiO, and trace quantities of a $Ni(Cr,Al)_2O_4$, $Al_2O_3$, $TiO_2$,
and $NiTiO_3$. Here again spalling appears to occur between the compound
oxides (i.e., $NiCr_2O_4$, $NiTiO_3$) and the simple subscale oxides (i.e., $Al_2O_3$
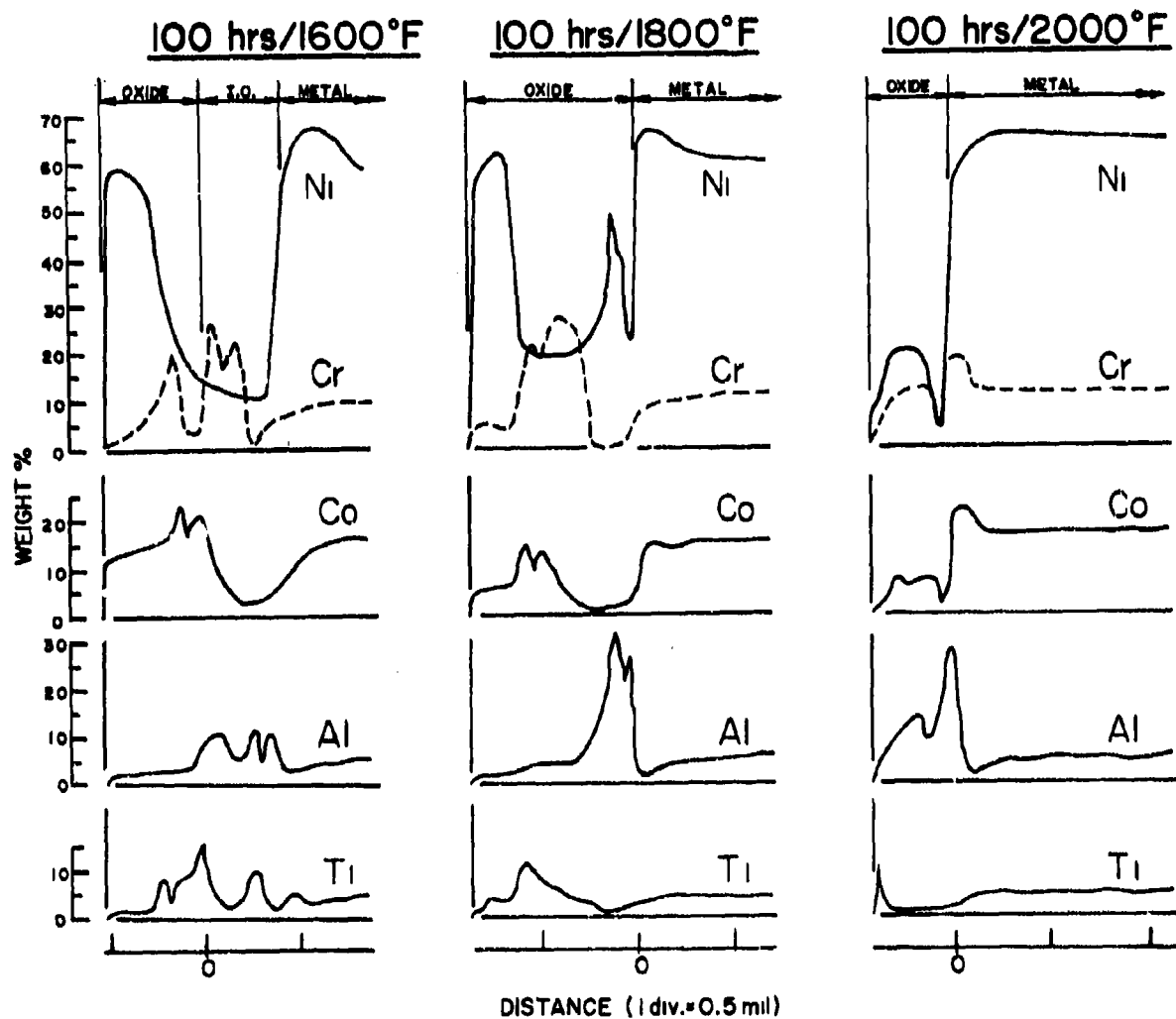
**FIGURE 39** Microprobe Traverse Results for IN-100 (Heat No. 1) Static Oxidation Test Specimens

92

## TABLE XXI

## X-RAY IDENTIFICATION OF REACTION PRODUCTS FOR IN-100 IN STATIC AIR

| Temp °F | Time Hrs. | Heat No. | Type Spec | Reaction Products[a] |
|---------|-----------|----------|-----------|----------------------|
| 1600 | 100 | 1 | (b) | NiO ($a_0$=4.20Å) + spinel ($a_0$=8.32Å) + NiTiO$_3$ + TiO$_2$ (VVW) |
|  | 100 | 2 | (b) | NiO ($a_0$=4.20Å) + spinel ($a_0$=8.35Å) + NiTiO$_3$ + TiO$_2$ (VVW) |
|  | 400 | 1 | (b) | NiO ($a_0$=4.20Å) + spinel ($a_0$=8.35Å) + NiTiO$_3$ |
|  | 1000 | 1 | (b) | NiO ($a_0$=4.20Å) + spinel ($a_0$=8.35Å) + NiTiO$_3$ + Al$_2$O$_3$ |
| 1800 | 100 | 1 | (b) | Spinel ($a_0$=8.31Å) + NiO ($a_0$=4.19Å) + NiTiO$_3$ + TiO$_2$ + Al$_2$O$_3$ |
|  | 1000 | 1 | (b) | Spinel ($a_0$=8.34Å) + NiTiO$_3$ + TiO$_2$ + Al$_2$O$_3$ |
|  | 1000 | 1 | (d) | Spinel ($a_0$=8.30Å + NiTiO$_3$ |
| 2000 | 100 | 2 | (b) | Matrix(s) + TiO$_2$ + NiTiO$_3$ + Al$_2$O$_3$ |
|  | 100 | 1 | (d) | Spinel ($a_0$=8.32Å) + NiTiO$_3$ + NiO + Spinel ($a_0$=8.12Å) |
|  | 400 | 1 | (b) | Spinel ($a_0$=8.14Å) + α-Al$_2$O$_3$ + TiO$_2$ + NiO (VVW) |
|  | 1000 | 1 | (b) | Spinel ($a_0$=8.15Å) + α-Al$_2$O$_3$ + TiO$_2$ + TiN + NiTiO$_3$ |
|  | 1000 | 2 | (b) | Spinel ($a_0$=8.15Å) + α-Al$_2$O$_3$ + TiO$_2$ (VVW) |
|  | 1000 | 2 | (c) | Spinel ($a_0$=8.09Å) + α-Al$_2$O$_3$ + TiO$_2$ |
|  | 1000 | 1 | (d) | Spinel ($a_0$=8.09Å) + Spinel ($a_0$=8.29Å) + α-Al$_2$O$_3$ + NiTiO$_3$ + TiO$_2$ |
|  | 2000 | 2 | (e) | Spinel ($a_0$=8.10Å) + TiO$_2$ ($a_0$=4.59Å, c=2.96Å) + NiTiO$_3$ + α-Al$_2$O$_3$ |
|  | 1000 | 1 | (f) | Spinel ($a_0$=8.27Å) + NiO + TiO$_2$ + α-Al$_2$O$_3$ + NiTiO$_3$ |

(a) Listed in order of decreasing predominance as indicated by X-ray intensities.

(b) Diffractometer trace of oxide in situ.

(c) Debye Scherrer analysis of electrolytically stripped oxide.

(d) Debye Scherrer analysis of spalled oxide.

(e) Debye Scherrer analysis of scraped oxide.

(f) Debye Scherrer analysis of surface oxide protrusions.

TABLE XXII

## X-RAY IDENTIFICATION OF NiTiO$_3$

| hkl | ASTM Card* #3-1157 d(Å) | I/J$_0$ | Synthesized d(Å) | I/I$_0$ |
|---|---|---|---|---|
| 102 | 3.71 | 40 | 3.708 | 28 |
| 104 | 2.716 | 80 | 2.718 | 100 |
| 110 | 2.532 | 80 | 2.525 | 65 |
| 113 | 2.212 | 60 | 2.214 | 29 |
| 204 | 1.852 | 60 | 1.845 | 40 |
| 116 | 1.704 | 80 | 1.702 | 64 |
| 108,212 | 1.607 | 40 | 1.605 | 12 |
| 214 | 1.490 | 100 | 1.489 | 28 |
| 300 | 1.459 | 80 | 1.455 | 31 |
| 208 | 1.358 | 20 | – | – |
| 1·0·10 | 1.318 | 80 | 1.317 | 15 |
| 217,220 | 1.265 | 80 | 1.259 | 7 |
| 306 | 1.234 | 40 | 1.229 | 4 |
| 218,312 | 1.193 | 60 | 1.193 | 6 |
| 2·0·10 | 1.169 | 60 | 1.167 | 7 |
| 314 | 1.145 | 60 | 1.142 | 8 |
| 226 | 1.107 | 80 | 1.104 | 10 |
| 2·1·10,309 | 1.060 | 80 | 1.058 | 9 |
| 318,322 | 0.993 | 60 | – | – |
| 1·0·14,324 | 0.963 | 100 | 0.960 | 10 |
| 410 | 0.954 | 60 | 0.951 | 6 |
| | | | 0.909 | 8 |
| | | | 0.879 | 9 |
| | | | 0.845 | 8 |
| | | | 0.838 | 5 |
| | | | 0.809 | 5 |
| | | | 0.801 | 4 |

* Indexed as hexagonal (rhom. div.) S.G. $C_{3i}^2$ $R\bar{3}$
a$_0$ = 5.448, $\alpha$ = 55°0"

## TABLE XXIII

### TYPICAL X-RAY PATTERN OF SPALLED OXIDES FROM
### IN-100 AFTER 1000 HOURS/2000°F IN STATIC AIR

| | | h k l | | | | |
|---|---|---|---|---|---|---|
| $d(Å)$ | $I/I_0$ | Spinel[a] cubic ($a_0$=8.09Å) | Spinel[b] cubic ($a_0$=8.29Å) | $NiTiO_3$ Rhom | $\alpha$-$Al_2O_3$ Trigonal | $TiO_2$ Tetragonal |
| 4.70 | VW | 111 | 111 | - | - | - |
| 3.68 | VVW | - | - | 102 | - | - |
| 3.45 | VVW | - | - | - | 012 | - |
| *3.38 | VVW | - | - | - | - | - |
| 3.22 | VW | - | - | - | - | 110 |
| 2.91 | VW | - | 220 | - | - | - |
| 2.85 | W | 220 | - | - | - | - |
| 2.69 | W | - | - | 104 | - | - |
| 2.50 | W | - | - | 110 | 104 | - |
| 2.48 | W | - | 311 | - | - | 101 |
| 2.43 | S | 311 | - | - | - | - |
| 2.20 | VW | - | - | 113 | - | - |
| 2.19 | VVW | - | - | - | - | 111 |
| 2.08 | VVW | - | - | - | 113 | - |
| 2.06 | VVW | - | 400 | - | - | - |
| 2.02 | M | 400 | - | - | - | - |
| 1.84 | VW | - | - | 204 | - | - |
| 1.74 | VVW | - | - | - | 024 | - |
| 1.695 | W | - | 422 | 116 | - | - |
| 1.685 | VW | - | - | - | - | 211 |
| 1.650 | VVW | 422 | - | - | - | - |
| *1.620 | VW | - | - | - | - | - |
| 1.600 | VW | - | 511 | 212 | 116 | - |
| *1.581 | VW | - | - | - | - | - |
| 1.555 | W | 511 | - | - | - | - |
| 1.485 | VW | - | - | 214 | - | - |
| 1.465 | VW | - | 440 | - | - | - |
| 1.450 | W | - | - | 300 | - | - |
| 1.430 | M | 440 | - | - | - | - |
| 1.400 | VVW | - | - | - | 124 | - |
| 1.372 | VVW | - | - | - | 030 | - |
| 1.359 | VVW | 531 | - | 208 | - | 301 |
| *1.345 | VVW | - | - | - | - | - |
| 1.312 | VVW | - | 620 | 1·0·10 | - | - |
| 1.278 | VVW | 620 | 533 | - | - | - |

S = strong; M = medium; W = weak; V = very

* Unknown lines

[a] Most probably $NiAl_2O_4$

[b] Most probably $NiCr_2O_4$

95

**TABLE XXIV**

**TYPICAL X-RAY PATTERN OF OXIDE SCRAPPED FROM**

**IN-100 AFTER 1000 HOURS/2000°F IN STATIC AIR**

| | | | h k l | | |
| | | Spinel[a] cubic ($a_O = 8.09$Å) | $TiO_2$ Tetragonal ($a_O = 4.59$Å) ($c_O = 2.97$Å) | $\alpha$-$Al_2O_3$ Trigonal | $NiTiO_3$ Rhom |
| d(Å) | $I/I_0$ | | | | |
|------|------|------|------|------|------|
| 4.69 | W | 111 | -- | - | - |
| 3.49 | VW | - | -- | 012 | - |
| 3.23 | M | - | 110 | -- | - |
| 2.86 | M | 220 | - | - | -- |
| 2.70 | M | - | -- | - | 104 |
| 2.54 | VW | - | - | 104 | 110 |
| 2.49 | VW | - | 101 | - | 110 |
| 2.43 | S | 311 | - | - | -- |
| 2.19 | VW | - | 111 | -- | 113 |
| 2.08 | VW | - | - | 113 | - |
| 2.02 | M | 400 | - | - | - |
| 1.84 | VW | 331 | - | - | 204 |
| 1.74 | VW | -- | - | 024 | -- |
| 1.69 | M | - | 211 | -- | 116 |
| 1.65 | VW | 422 | - | -- | -- |
| 1.62 | VW | -- | 220 | - | -- |
| 1.60 | W | - | - | 116 | -- |
| 1.55 | M | 511 | -- | - | 108 |
| 1.485 | VW | - | 002 | - | 214 |
| 1.450 | VW | - | 310 | - | 300 |
| 1.430 | M | 440 | -- | -- | -- |
| 1.365 | VW | 531 | - | 030 | - |
| 1.235 | W | 533 | -- | 1·0·10 | - |
| 1.170 | W | - | 321 | -- | -- |
| 1.080 | VW | 642 | - | - | -- |
| 1.054 | W | 731 | -- | -- | -- |
| 1.014 | VW | 800 | - | - | -- |
| 0.935 | VW | -- | - | - | - |
| 0.826 | VW | 844 | - | - | -- |

S = strong; M = medium; W = weak; V = very

[a] Most probably $NiAl_2O_4$

$TiO_2$). As indicated previously for SM-200, the simultaneous identification of Ni-Cr and Ni-Al spinel oxides indicates the existence of local alloy inhomogeneities. During the 1000 hour exposure, massive protrusions also became apparent on the specimen surface. An X-ray analysis of these "pocks" indicated the presence of $Ni(Al,Cr)_2O_4$, $TiO_2$, $NiTiO_3$ and $\alpha-Al_2O_3$. Metallographic evidence exists which associates these "pocks" with the deep intergranular penetration of oxide into the parent metal. The high Ti content of these oxides is noteworthy.

A summary of the reaction products formed on IN-100 as a function of time and temperature is presented in Figure 40. It should again be emphasized that these products represent those expected while at temperature.

### 4.2.6 Inco 713C Oxidation

The microstructures of representative oxidation specimens of Inco 713C exposed at various times and temperatures are illustrated in Figure 41. The accompanying microstructural measurements are summarized in Table XXV.

This alloy exhibits the same general features as the other cast alloys, namely, oxide spalling and heterogeneous oxidation. Some specific features observed during the evaluation are

(a)   The heat-to-heat variation is negligible.

(b)   Although the total weight gain is notably less for this alloy as compared to SM-200 and IN-100, the oxide phase coherency also appears to be less since spalling occurs after a much lower total weight gain.

(c)   The type of scale formed and the extent of internal attack is more similar to SM-200 than IN-100 although the internal oxidation typified by the low-temperature oxidation of SM-200 was not observed (Figure 41(a)). The type of internal oxidation produced was more typical of I.G.O. which is distorted by the taper mounting procedures employed (Figure 41(c)).

(d)   The interactions between oxides and/or metal inhomogeneities produced a heterogeneous surface scale as shown in Figure 41(b) where the subscale is illustrated protruding through the original surface oxide scale.

The results of the X-ray diffraction studies for Inco 713C are summarized in Table XXVI, while Tables XXVII and XXVIII represent typical X-ray diffraction patterns obtained from spalled and electrolytically stripped oxide specimens. The quality of the X-ray diffractometer patterns obtained for this material was not always considered optimum. The large grain size of the starting material and the associated anisotropy of film growth yielded results difficult to interpret. This was particularly true for specimens oxidized at 1600°F.
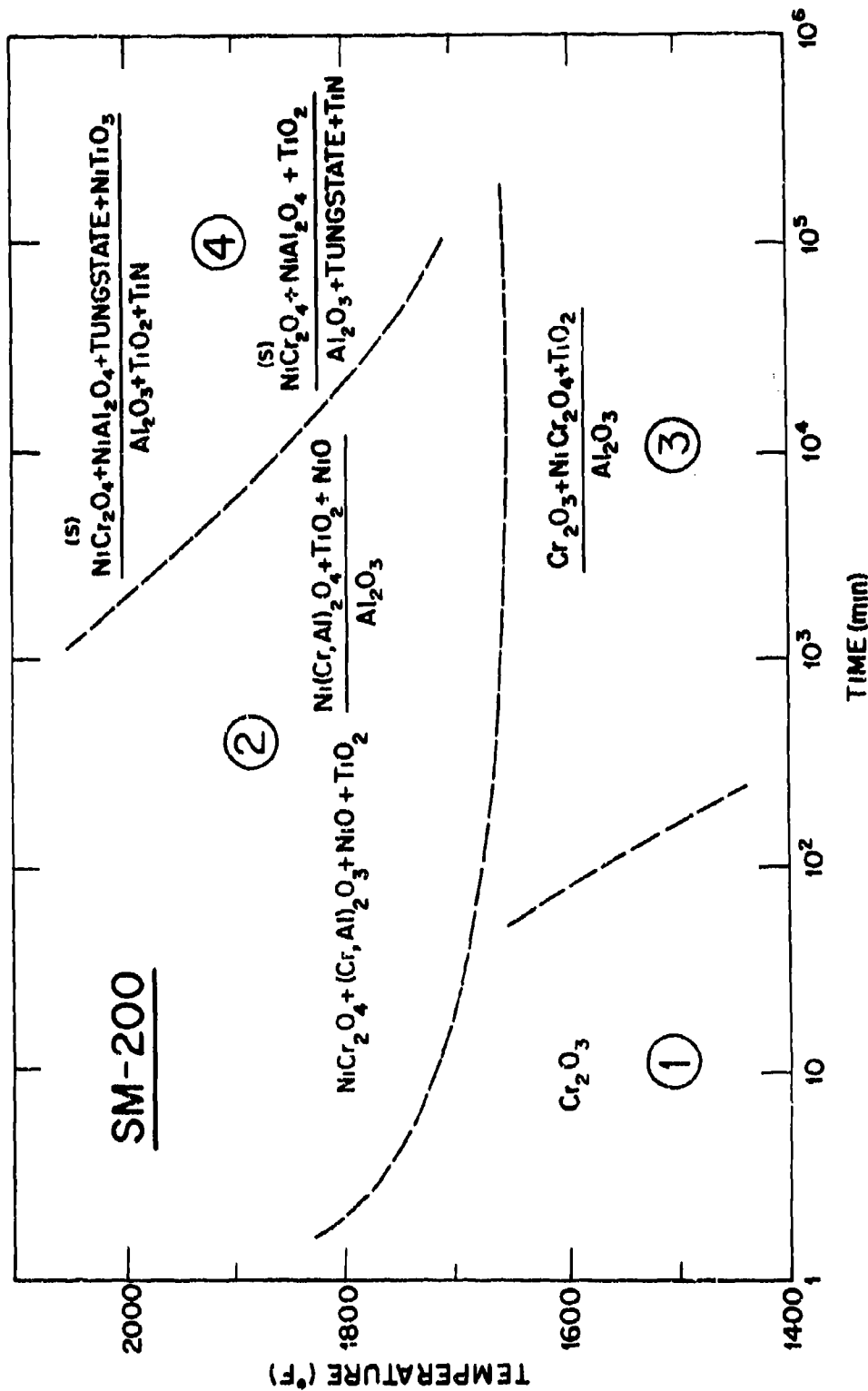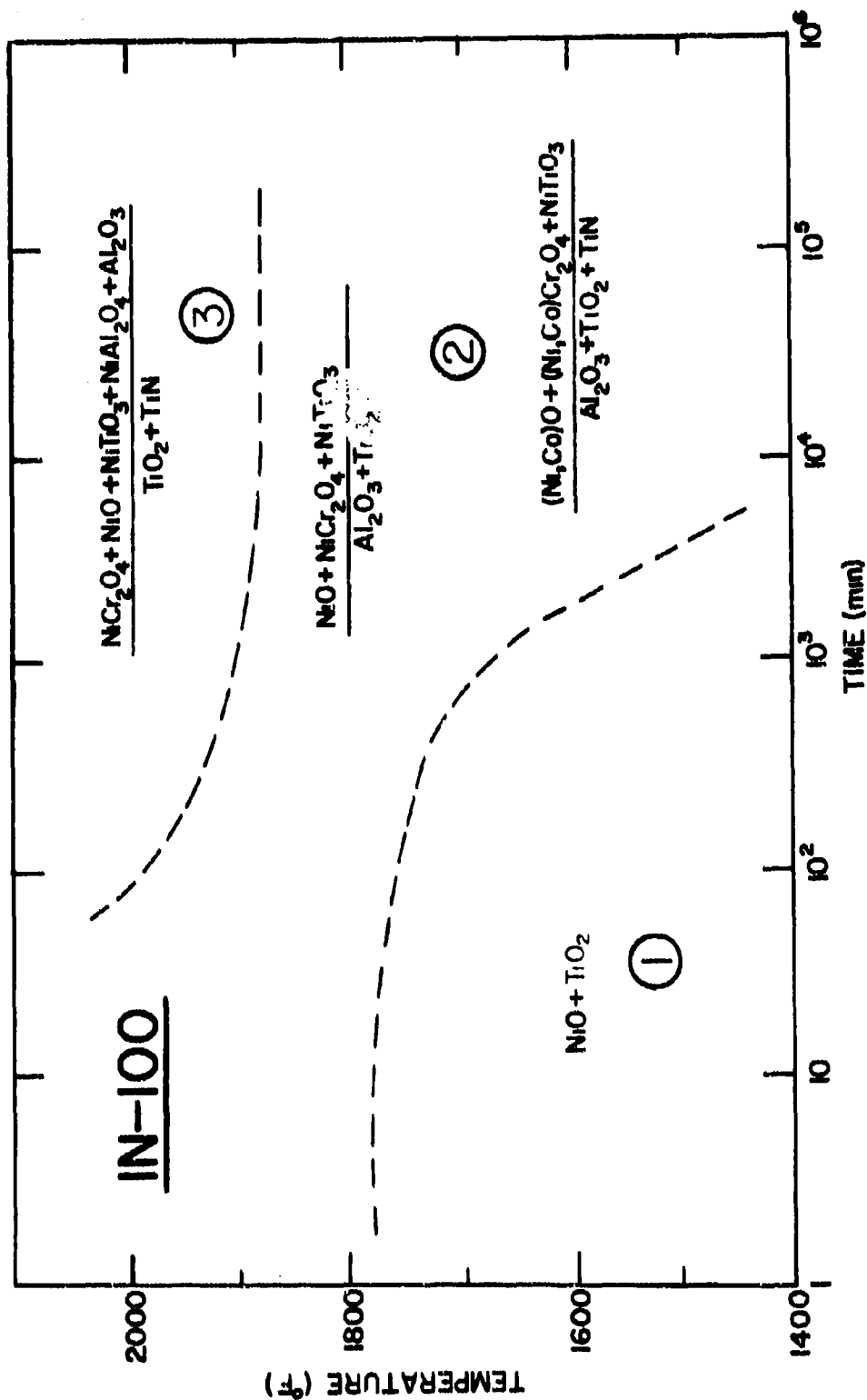
FIGURE 40   Simplified Summary of the Main Stages of Oxidation for IN-100. Phases present in the numerator are scale constituents; those in the denominator are subscale products.

M4713

(a) 100 Hrs/1600°F    Note Relatively
Thin Oxide Scale.

M4604

(b) 100 Hrs/1800°F    Note Subscale
Protruding through Original Oxide
Scale.

M4716

(c) 1000 Hrs/1800°F    Note Irregular
Oxide Scale.
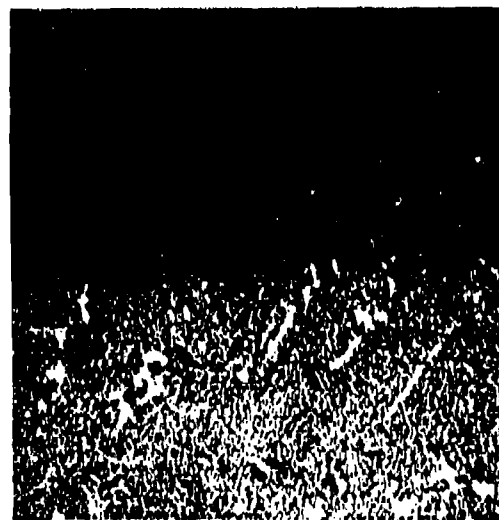
M3951

(d) 1000/2000°F    Note Multi-Phase
Oxide and Coarsened γ'.

FIGURE 41    Typical Scale and Subscale Morphology Produced in INCO 713C
Oxidized for 100 Hours in Static Air.  Mounted on 5:1 Tapers.
Etched with 2% Chromic (250X).

# TABLE XXV

## STATIC OXIDATION METALLOGRAPHIC RESULTS FOR INCO 713C (a)(b)

| Heat | Test Conditions Temp (°F) | Time (hrs) | Average Weight Gain(c) (mg/cm²) | Avg. Scale Thickness (mils) | Gross I.O. or IGA (mils/side) | Maximum I.O. or IGA (mils/side) | Gross γ′ Dissolution (mils/side) |
|------|------|------|------|------|------|------|------|
| 1 | 1600 | 100 | 0.34 | 0.13 | 0.12 | - | 0.30 |
|   |   | 400 | 0.85 | 0.20 | 0.20 | 0.40 | 0.40 |
|   |   | 1000 | 0.40 | 0.15 | 0.17 | 0.35 | 0.20 |
| 2 | 1600 | 100 | 0.61 | 0.20 | 0.20 | - | 0.30 |
|   |   | 400 | 0.77 | 0.40 | 0.20 | 0.40 | 0.40 |
|   |   | 1000 | 0.37 | 0.20 | 0.15 | 0.40 | 0.30 |
| 1 | 1800 | 100 | 0.87 | 0.18 | 0.28 | 0.64 | 0.30 |
|   |   | 400 | 0.64 (d) | 0.25 | 0.25 | 0.40 | 0.30 |
|   |   | 1000 | 1.02 (d) | 0.60 | 0.30 | 2.00 | 0.30 |
| 2 | 1800 | 100 | 1.06 | 0.40 | 0.30 | 0.50 | 0.40 |
|   |   | 400 | 0.70 (d) | 0.20 | 0.30 | - | 0.45 |
|   |   | 1000 | 0.70 (d) | 0.40 | 0.80 | 1.60 | 0.50 |
| 1 | 2000 | 100 | 0.27 (0.52) | 0.20 | 0.30 | 1.60 | 0.30 |
|   |   | 400 | -0.84 (1.20) | 0.40 | 0.34 | 1.40 | 0.40 |
|   |   | 1000 | 0.92 (1.43) | 1.00 | 0.60 | 1.80 | 0.60 |
| 2 | 2000 | 100 | 0.86 (1.18) | 0.10 | 0.40 | 1.40 | 0.45 |
|   |   | 400 | -1.75 (1.23) | 0.50 | 0.50 | 1.40 | 0.60 |
|   |   | 1000 | -1.12 (2.05) | 0.80 | 0.60 | 1.80 | 0.60 |

(a) All metallographic measurements taken at 250X from taper sections with a 5:1 magnification.

(b) Metal loss within accuracy of measurement ($\pm$ 0.5 mil), hence not reported.

(c) For reference purposes - value in parentheses includes specimen weight gain plus spalled products where spalling occurs.

(d) Spalling occurred but not measured.

TABLE XXVI

## X-RAY IDENTIFICATION OF REACTION PRODUCTS FOR INCO 713C EXPOSED IN STATIC AIR

| Temp °F | Time Hrs. | Heat No. | Type Spec | Reaction Products[a] |
|---|---|---|---|---|
| 1600 | 100 | 1 | (b) | $\alpha$-$Cr_2O_3$ + Spinel ($a_0$=8.32Å) |
| | 1000 | 1 | (b) | Spinel ($a_0$=8.34Å) + $\alpha$-$Cr_2O_3$ |
| 1800 | 100 | 1 | (b) | Spinel ($a_0$=8.35Å) + $(Al,Cr)_2O_3$ + unknown |
| | 100 | 2 | (b) | Spinel ($a_0$=8.36Å) + $\alpha$-$Cr_2O_3$ + unknown + $Al_2O_3$ (VVW) |
| | 1000 | 1 | (b) | Spinel ($a_0$=8.36Å) + $\alpha$-$Al_2O_3$ + unknown |
| 2000 | 100 | 1 | (c) | $\alpha$-$Al_2O_3$ + Spinel ($a_0$=8.08Å) + $TiO_2$ + TiN |
| | 100 | 1 | (d) | Spinel ($a_0$=8.29Å) + $\alpha$-$Al_2O_3$ + Spinel ($a_0$=8.08Å) |
| | 400 | 1 | (e) | $\alpha$-$Al_2O_3$ + Spinel ($a_0$=8.04Å) + $TiO_2$ + $Cr_2O_3$ |
| | 1000 | 1 | (b) | $\alpha$-$Al_2O_3$ + Spinel ($a_0$=8.08Å) + $\alpha$-$Cr_2O_3$ |
| | 1000 | 1 | (d) | $\alpha$-$Al_2O_3$ + Spinel ($a_0$=8.06Å) |
| 2100 | 100 | 1 | (f) | Spinel ($a_0$=8.20Å) + Spinel ($a_0$=8.08Å) + NiO + $Cr_2O_3$ + $TiO_2$ |

[a] Listed in order of decreasing predominance as indicated by X-ray intensities.

(b) Diffractometer trace of oxide in situ.

(c) Debye Scherrer analysis of electrolytically stripped oxide.

(d) Debye Scherrer analysis of spalled oxide.

(e) Debye Scherrer analysis of scraped oxide.

(f) Debye Scherrer analysis of surface oxide protrusions.

TABLE XXVII

### TYPICAL X-RAY PATTERN OF PRODUCTS SPALLED
### FROM INCO 713C AFTER 100 HOURS/2000°F IN STATIC AIR

| | | h k l | | |
| | | Spinel[a] cubic ($a_0 = 8.29$Å) | $\alpha$-$Al_2O_3$ Trigonal | Spinel[b] cubic ($a_0 = 8.08$Å) |
| d(Å) | $I/I_0$ | | | |
|------|---------|------|------|------|
| 3.46 | VVW | – | 012 | – |
| 2.92 | VVW | 220 | – | – |
| 2.85 | VVW | – | – | 220 |
| 2.54 | VW | – | 104 | – |
| 2.49 | S | 311 | – | – |
| 2.43 | M | – | – | 311 |
| 2.37 | VW | – | 110 | – |
| *2.20 | VVW | – | – | – |
| 2.08 | VW | – | 113 | – |
| 2.03 | VW | – | – | 400 |
| *1.90 | VVW | – | – | – |
| 1.73 | VVW | – | 024 | – |
| 1.69 | VVW | 422 | – | – |
| 1.67 | VVW | – | – | 422 |
| 1.60 | W | 511 | 116 | – |
| 1.56 | VVW | – | – | 511 |
| 1.54 | VVW | – | 211 | – |
| *1.525 | VVW | – | – | – |
| 1.465 | VW | 440 | – | – |
| *1.440 | VVW | – | – | – |
| 1.430 | VW | – | – | 440 |
| 1.403 | VW | – | 124 | – |
| 1.373 | VW | – | 030 | – |
| 1.360 | VVW | – | – | 531 |
| 1.238 | VVW | – | 1·0·10 | 533 |

S = strong; M = medium; W = weak; V = very

* Unidentified lines

[a] Most probably $NiCr_2O_4$

[b] Most probably $NiAl_2O_4$

# TABLE XXVIII

## TYPICAL X-RAY PATTERN OF PRODUCTS ELECTROLYTICALLY STRIPPED FROM INCO 713C AFTER 100 HOURS/2000°F IN STATIC AIR

| | | | h k l | | |
| | | | Spinel(a) | | |
| d(Å) | I/I_0 | $\alpha$-Al$_2$O$_3$ Trigonal | Cubic ($a_0$=8.10Å) | TiO$_2$ Tetragonal | TiN Cubic |
|---|---|---|---|---|---|
| 4.70 | M | -- | 111 | - | - |
| 3.50 | M | 012 | - | - | - |
| 3.27 | M | - | - | 110 | - |
| 2.87 | W | - | 220 | - | - |
| 2.55 | S | 104 | - | - | - |
| 2.51 | W | -- | - | 101 | -- |
| 2.45 | S | - | 311 | - | 111 |
| 2.38 | W | 110 | - | - | - |
| 2.30 | VW | - | - | 200 | - |
| *2.26 | VW | - | - | - | - |
| 2.20 | VW | - | - | 111 | -- |
| 2.13 | W | - | -- | - | 200 |
| 2.08 | S | 113 | - | - | - |
| 2.02 | M | - | 400 | -- | - |
| 1.96 | VW | 202 | - | -- | - |
| 1.74 | M | 024 | - | -- | - |
| 1.70 | M | - | - | 211 | .. |
| 1.65 | VW | - | 422 | - | - |
| 1.63 | VW | - | - | 220 | - |
| 1.60 | S | 116 | - | - | - |
| 1.56 | W | - | 511 | - | -- |
| 1.51 | W | 018 | - | - | - |
| 1.465 | VW | - | - | 310 | - |
| 1.431 | S | - | 440 | - | - |
| 1.405 | M | 124 | - | -- | - |
| 1.371 | S | 030 | 531 | - | -- |
| 1.310 | VW | - | - | 311 | - |
| 1.23C | M | 1·0·10 | 533 | -- | - |
| 1.190 | VW | - | - | 212 | - |
| 1.125 | VW | -- | 640 | - | - |
| 1.079 | W | 134 | - | -- | - |
| 1.055 | VW | 226 | - | - | - |

\* Unidentified

(a) Most probably NiAl$_2$O$_4$

The microprobe analysis data which is summarized in Figure 42 when combined with the x-ray phase analysis and general microstructures indicate the following oxidation behavior for this alloy.

As indicated in section 4.2.1, short-time exposures at 1600°F produce NiO with Ni(Cr,Al)$_2$O$_4$ overgrowths. Increasing the exposure to 100 hours yields a surface scale containing mixed $\alpha$-Cr$_2$O$_3$ and NiCr$_2$O$_4$ spinel oxide and an aluminum-rich subscale (probably Al$_2$O$_3$). After an exposure of 1000 hours little change occurs. At 1800°F the (Al,Cr)$_2$O$_3$ subscale protrudes through the original NiCr$_2$O$_4$ oxide in isolated regions see Figure 41(b) which induces spalling. After 1000 hours a heterogeneous scale is produced containing NiCr$_2$O$_4$, $\alpha$-Al$_2$O$_3$ and an unknown phase*. Since the alloy contains considerable Cb, oxides containing this element were suspect. A microprobe analysis was performed but no increase in Cb was detected in the oxide. Exposure for 100 hours at 2000°F produced spalling between the Ni-Cr rich (NiCr$_2$O$_4$) and the Al containing oxides (Al$_2$O$_3$ and NiAl$_2$O$_4$). Continued exposure produces increased amounts of $\alpha$-Al$_2$O$_3$, NiAl$_2$O$_4$ and internal oxides of Cr$_2$O$_3$, TiO$_2$ and TiN. Although this alloy contains less than 1$^W$/$_o$ Ti, an analysis of oxide protrusions formed after 1000 hours indicated sufficient TiO$_2$ for detection (> 10$^V$/$_o$).

Referring to the microprobe analysis of this alloy (Figure 42) three features are noteworthy:

(a) increased Al in the scale with increasing temperature.

(b) the elimination of suboxide Cr depletion at 2000°F. In fact, there are indications of Cr$_2$O$_3$ internal oxide formation.

(c) the absence of Mo in the oxide and the obvious concentration buildup below the oxide scale.

A summary of the main stages of oxidation for this alloy as a function of time and temperature are given in Figure 43.


### 4.2.7  U-700 and René 41 Oxidation

A thorough evaluation of the scale and subscale processes and their rates of formation have previously been determined for U-700 and René 41[a]. Therefore, these studies were conducted to determine some of the features of their oxidation behavior to establish a base line for other studies which were performed. Of prime interest are the general microstructures and oxidation measurements for later comparison with flame tunnel and surface preparation test specimens.

104
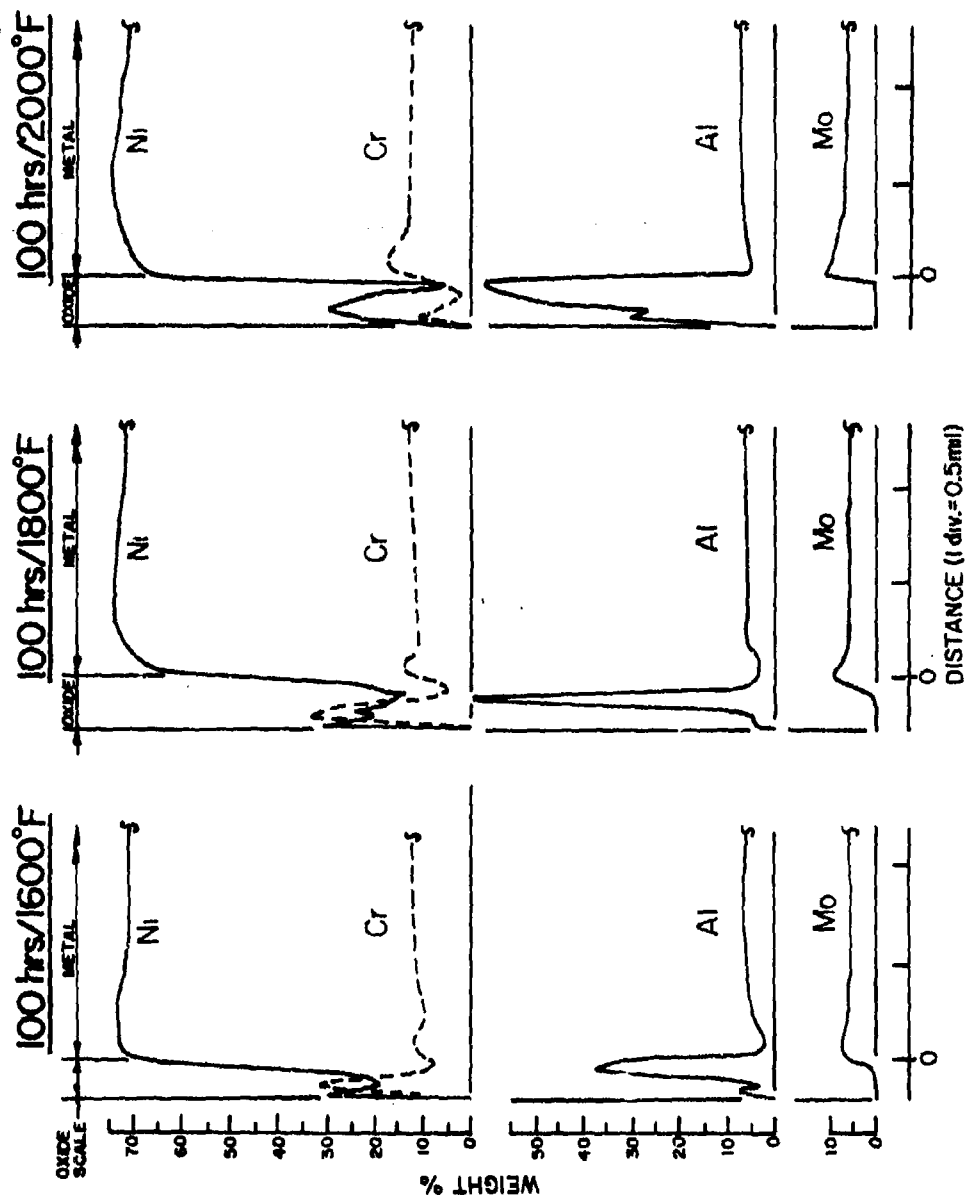
FIGURE 42  Microprobe Traverse Results for Inco 713C (Heat No. 1) Static
Oxidation Test Specimens
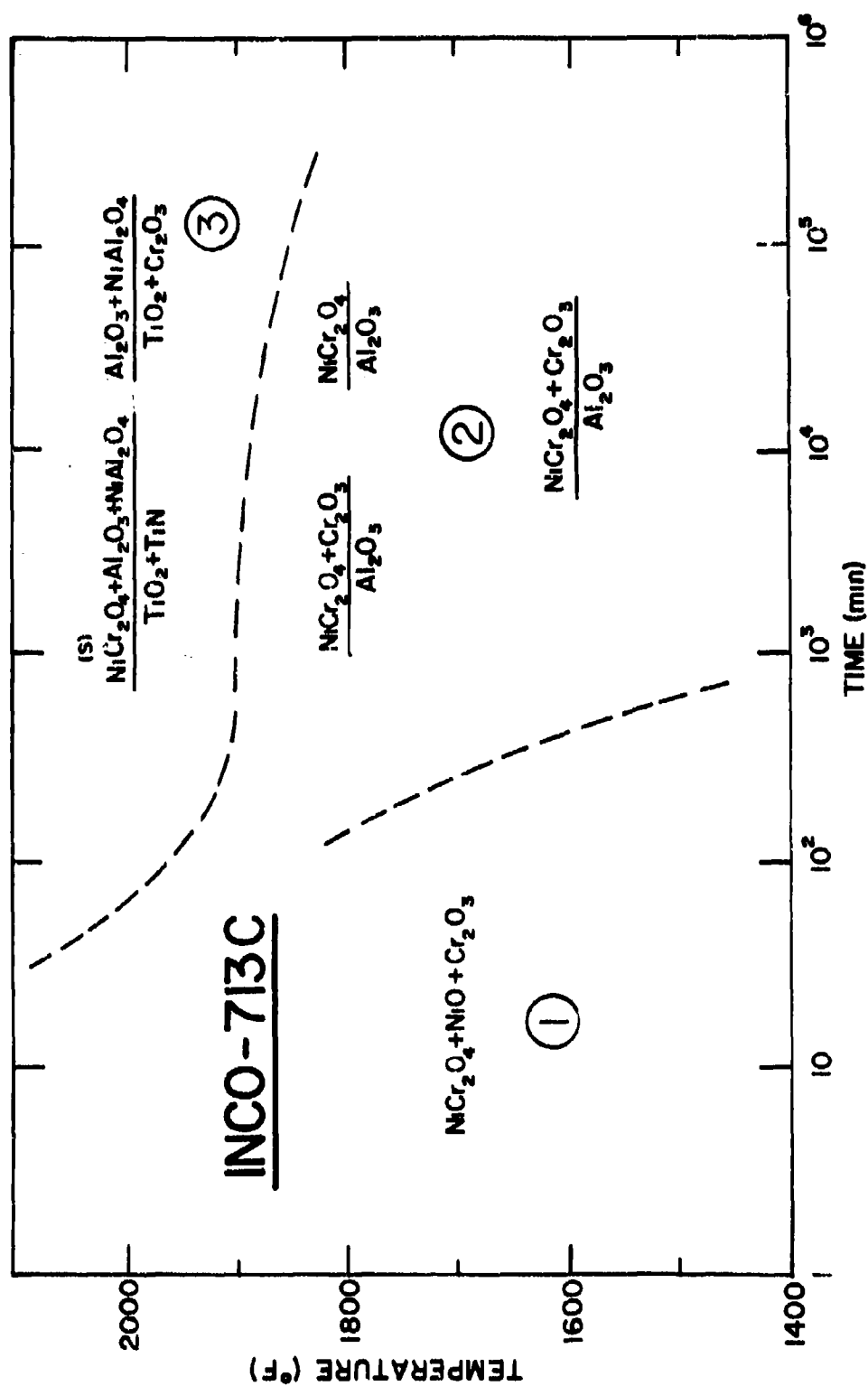
FIGURE 43  Simplified Summary of the Main Stages of Oxidation for Inco 713C.  Phases present in the numerator are scale constituents; those in the denominator are subscale products.

106

Figure 44 shows the typical oxide morphology and Table XXIX summarizes the metallographic measurements for U-700. This sequence of microstructures depicts the marked influence of less noble element activities on the subscale morphology and the subsequent oxidation behavior. A microprobe analysis taken from the same specimens is illustrated in Figure 45 and shows the respective compositional changes that occur in the oxide film. At 1600°F the scale is primarily $Cr_2O_3$, $NiCr_2O_4$ with trace quantities of $TiO_2$ or $NiTiO_3$. The internal oxide consists of a fine dispersion of $Al_2O_3$. The activity of the Al in solution is thus considered relatively low as compared to Cr. At 1800°F the scale still contains Cr-and Ti-base oxides but the activity of Al has increased considerably. This latter effect is evidenced by the shallowness of the internal oxide penetration and the agglomeration of $Al_2O_3$ along sub-grain boundaries. Since internal oxidation is controlled by both cation and anion diffusion, this I.O. thickening implies accelerated Al diffusion at this temperature. At 2000°F the activity of Al has increased to the point where scale formation is thermodynamically favored. The microprobe analysis clearly indicates the formation of a dense $Al_2O_3$ subscale. The fact that there is no Cr depletion in the subscale region is further evidence that Cr-base oxide formation is no longer favored. The absence of internal oxides at this temperature is not unusual since the subscale oxide contains the least noble constituent in the alloy and there are no elements available which will reduce $Al_2O_3$ at the scale/metal interface to form internal oxides. The increased aluminum activity observed with increasing temperature is considered a result of $\gamma'$ dissolution as indicated by the measurements in Table XXIX. Hence at 1800°F sufficient $\gamma'$ dissolution occurs to produce a relatively dense I.O. network. It should be emphasized that the sequence of microstructures shown in Figure 44 is not to be alternately considered representative of the progressive oxidation at any one temperature. Each of the structures shown is representative of that temperature and increased test time influences only the magnitude of the re- actions indicated.

The typical scale and subscale reactions for René 41 after various time- temperature exposures are shown in Figure 46. The corresponding metallographic measurements are presented in Table XXX and the results of the microprobe analysis are summarized in Figure 47. The extent of internal oxidation displayed by this alloy is greater than any of the other alloys evaluated. In contrast to U-700 behavior, the type of internal oxidation observed is independent of temperature. However, this behavior may also be explained by considering the thermodynamics of the system. Constitutionally René 41 contains more Cr, one third the Al and the same Ti content as U-700. It is the activity balance between Cr and Al which dictates the nature of the oxidation process. Hence, although $\gamma'$ dissolution also occurs in this alloy the aluminum activity never surpasses the large Cr activity and a $Cr_2O_3$ oxide scale and an $Al_2O_3$ internal oxidation zone prevails at all temperatures and times. In fact, it is this moderate concentration of the less noble aluminum that causes the excessive internal oxidation, since $Cr_2O_3$ will always dissociate at the oxide/metal interface providing $O^=$ for the formation of a

107

M3191

(a) 100 Hrs/1600°F
Note Classical Type I.O.

M3192

(b) 100 Hrs/1800°F
Note Agglomeration of I.O.

M3193

(c) 100 Hrs/2000°F
Note Absence of I.O. and Existence
of Multi-Phase Oxide.

FIGURE 44    Typical Scale and Subscale Morphology Produced in U-700 Oxidized for 100 Hours in Static
Air.  Mounted on 5:1 Tapers.   Unetched (500x)

# TABLE XXIX

## STATIC OXIDATION METALLOGRAPHIC RESULTS FOR U-700(a)(b)

| Test Conditions Temp (°F) | Time (hrs) | Average Weight Gain(c) (mg/cm²) | Avg. Scale Thickness (mils) | Gross I.O. or IGA (mils/side) | Maximum I.O. or IGA (mils/side) | γ' Dissolution (mils/side) |
|---|---|---|---|---|---|---|
| 1600 | 100 | 0.35 | 0.3 | 0.3 | 0.5 | 0.4 |
| | 400 | 0.84 | 0.6 | 0.4 | 0.8 | 0.5 |
| | 1000 | 0.97 | 0.6 | 0.6 | 1.2 | 0.8 |
| 1800 | 100 | 0.47 | 0.4 | 0.4 | 1.0 | 0.4 |
| | 400 | 0.67 (d) | 0.3 | 0.4 | 0.5 | 0.4 |
| | 1000 | 0.71 (d) | 0.5 | 0.6 | 0.8 | 0.6 |
| 2000 | 100 | 1.45 (1.67) | 0.8 | 0.4 | 0.8 | 1.0 |
| | 400 | 1.37 (4.83) | 1.2 | 0.8 | 1.2 | 2.8 |
| | 1000 | 1.87 (6.31) | 1.3 | 1.8 | 2.4 | 3.0 |

(a) All metallographic measurements taken from taper sections with a 5:1 magnification.

(b) Metal loss within accuracy of measurement, hence not reported.

(c) For reference purposes - value ir parentheses includes specimen weight gain plus spalled products where spalling occurs.

(d) Spalling occurred but not measured.
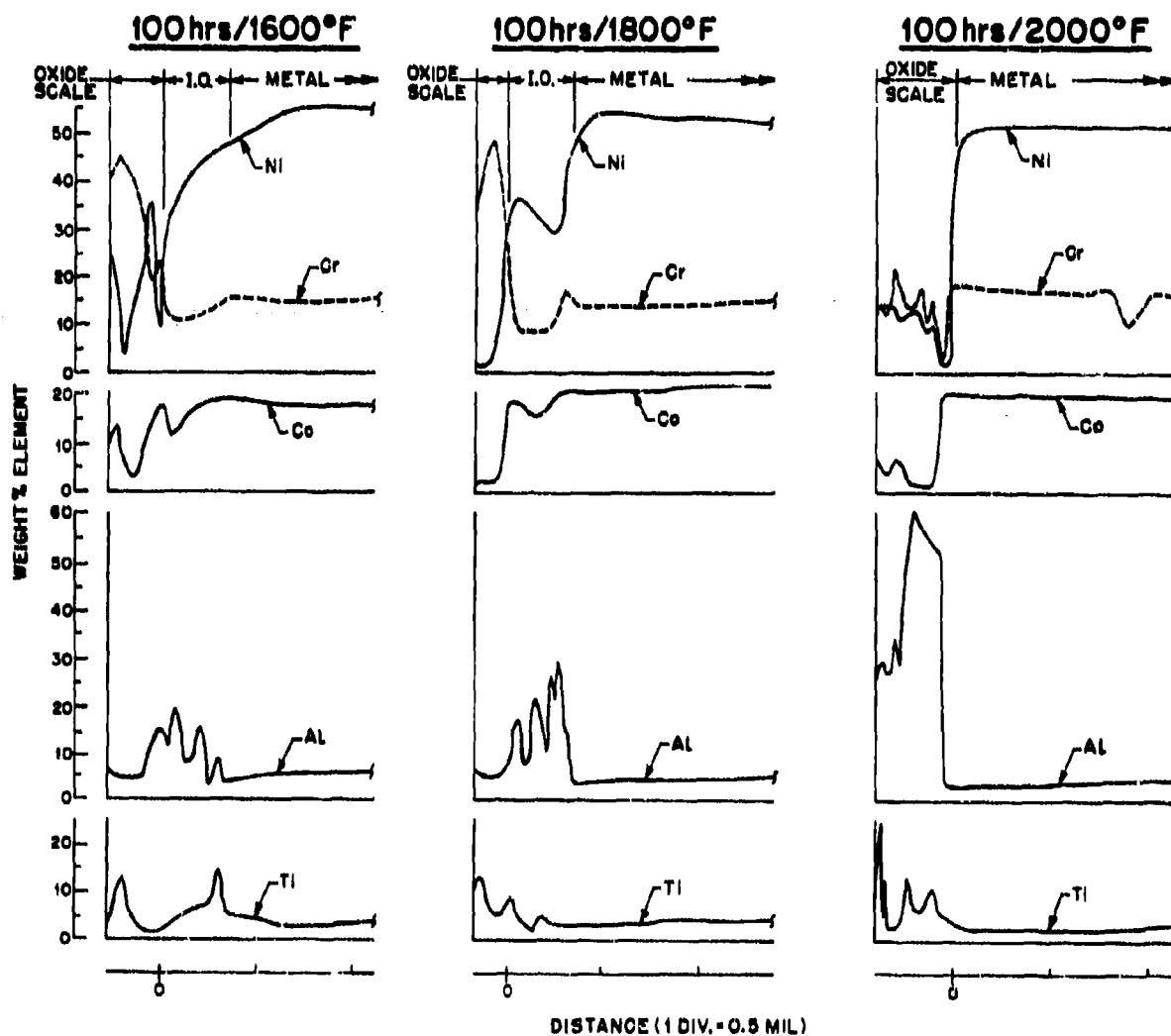
**FIGURE 45   Microprobe Traverse Results for U-700 Static Oxidation Test Specimens**

(a) 1000 Hr/1600°F
250X

M-2635

(b) 1000 Hr/1800°F
250X

M-2626
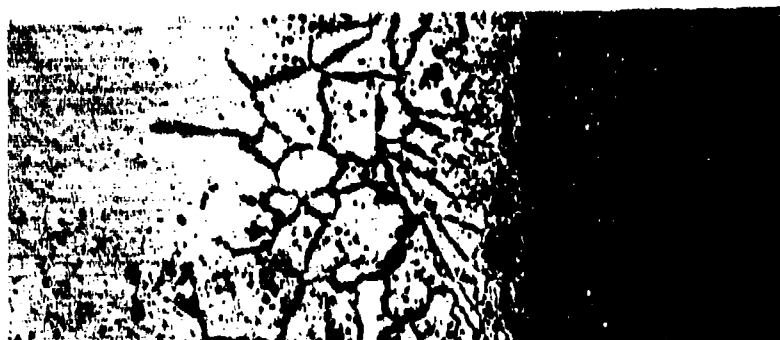
(c) 100 Hr/2000°F
250X

M-2627
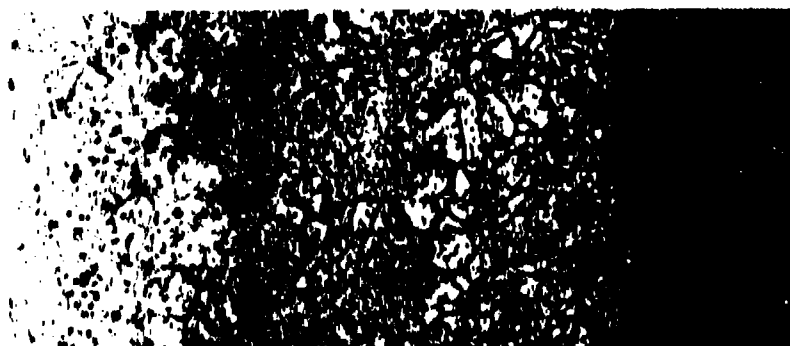
(d) 1000 Hr/2000°F
100X

M-4012

FIGURE 46    Typical Scale and Subscale Morphology for René 41 Oxidized for
Various Times and Temperatures in Static Air.  Etched in 2% Chromic
Mounted on 5:1 Taper Section.

111

## TABLE XXX

### STATIC OXIDATION METALLOGRAPHIC RESULTS FOR RENÉ 41

| Heat | Test Conditions Temp (°F) | Time (hrs) | Average Weight Gain(a) (mg/cm²) | Average Scale Thickness (mils/side) | Gross I.O. (mils/side) | Metal Loss (mils/side) | γ' Dissolution (mils/side) |
|---|---|---|---|---|---|---|---|
| 1 | 1600 | 100 | 0.95 | 0.4 | 0.5-0.6 | 0.2 | 0.6 |
|  |  | 400 | 1.77 | 0.7 | 0.8-0.9 | - | 1.0 |
|  |  | 1000 | 3.23 | 0.7 | 1.0 | - | 1.6 |
| 1 | 1800 | 100 | 2.36 | 0.8 | 1.0-1.6 | - | 1.5 |
|  |  | 400 | 0.09 (3.93) | 1.1 | 1.4 | - | 1.8 |
|  |  | 1000 | 0.01 (7.64) | 0.8 | 2.4 | 0.7 | 4.4 |
| 1 | 2000 | 100 | 4.07 (4.96) | 0.8 | 1.4-1.6 | 0.5 | 4.0 |
|  |  | 400 | - 6.00 (9.07) | 1.0 | 3.6 | - | 15.0 |
|  |  | 1000 | -10.96 (12.12) | 1.0 | 5.0-6.0 | 1.1 | 17.0 |

(a) For reference purpose only – value in parentheses includes specimen weight plus spalled products where spalling occurs.

All metallographic measurements taken from tapered sections with a 5:1 magnification.
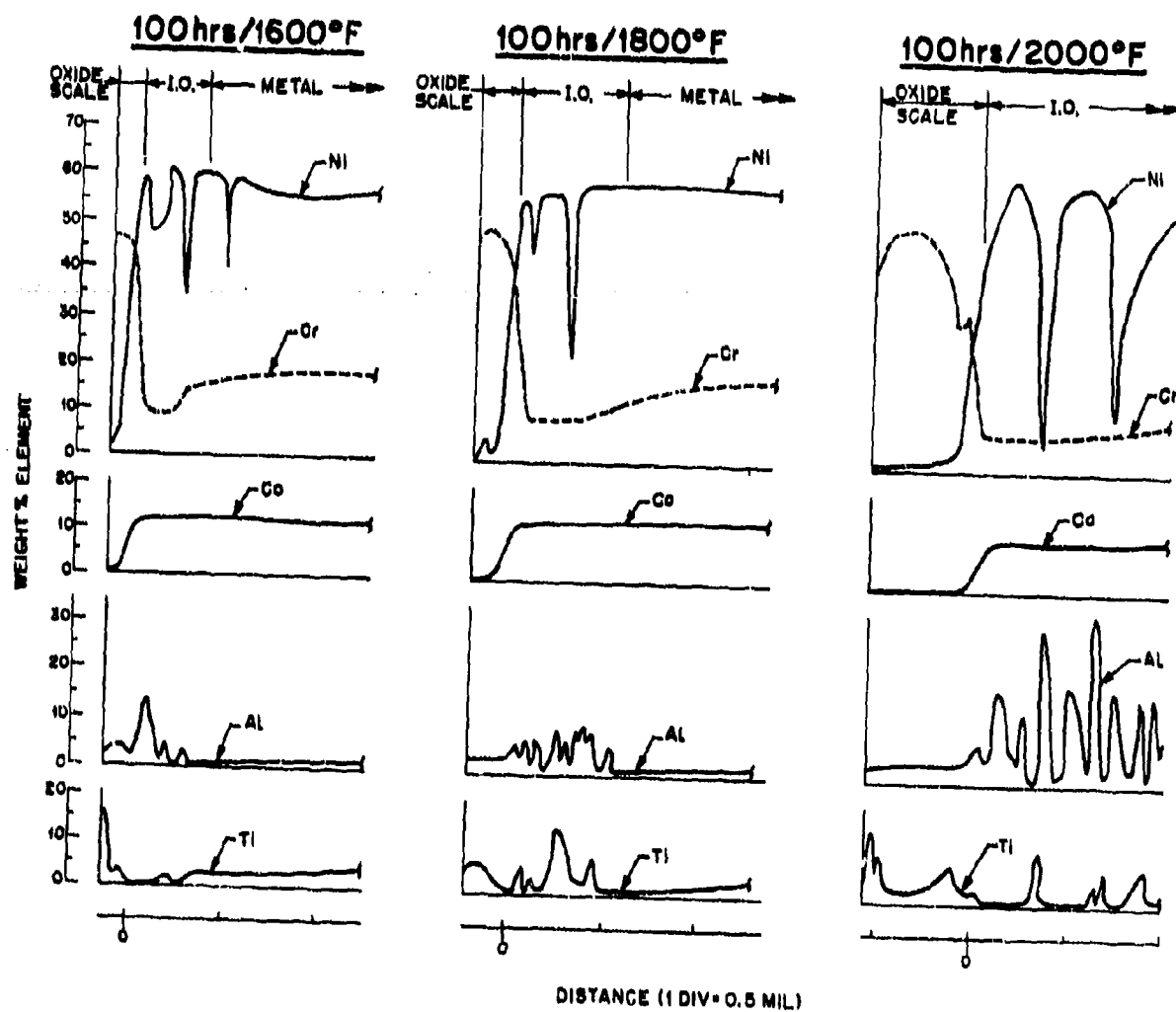
FIGURE 47    Microprobe Traverse Results for René 41 Static Oxidation Test Specimens

113

more stable $Al_2O_3$ oxide. The morphology of the internal oxides does imply control by Al diffusion as discussed in the following section.

### 4.2.8  Internal Oxidation Kinetics for René Y and René 41

The two sheet alloys René Y and René 41 were the only alloys studied which exhibited a continuous internal oxidation zone over the time and temperature range of oxidation studied. If the formation of these internal products is diffusion controlled, the advance of the internal oxidation front should follow parabolic kinetics defined by the following equation:

$$\xi^2 = 2Kt + C \qquad (1)$$

Where $\xi$ = depth of I.O. or I.G.O. from metal oxide interface in mils/side(assumes metal/oxide interface equals original metal surface and interface movement $\ll \xi$ )

K = parabolic rate constant (mils$^2$/hr)

t = time in hours

C = constant

The parabolic nature of the process is demonstrated for these alloys by the linear relation between $\xi^2$ versus t shown in Figures 48 and 49. The resultant rate constants (K) calculated from the slopes of these curves are tabulated below:

Rate Constant "K" (Mil$^2$/Hr)

| Temp °F | René 41 | René Y |
|---|---|---|
| 1600 | $5.45 \times 10^{-4}$ | $1.95 \times 10^{-4}$ |
| 1800 | $2.41 \times 10^{-3}$ | $4.80 \times 10^{-4}$ |
| 2000 | $1.52 \times 10^{-2}$ | $1.37 \times 10^{-3}$ |

The relation between "K" and temperature is given by the general rate equation:

$$K = A \exp\left(-\frac{H}{RT}\right) \qquad (2)$$

A plot of log K versus 1/T yields a straight line illustrated in Figure 50, the slope of which represen the activation energy for the process. By combining Equations (1) and (2) empirical equations may be derived representing

114
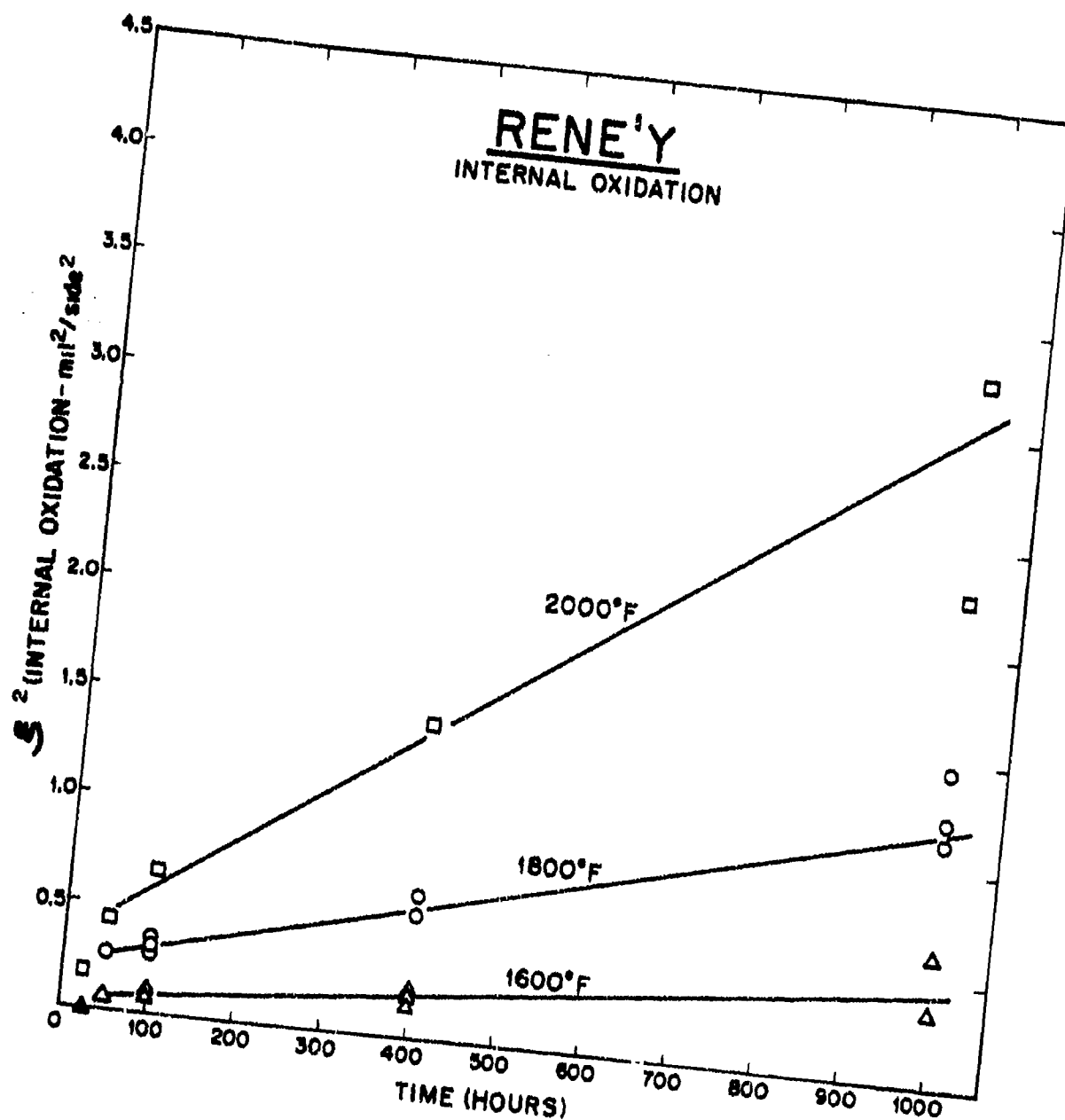
FIGURE 48    Parabolic Internal Oxidation of René Y

115
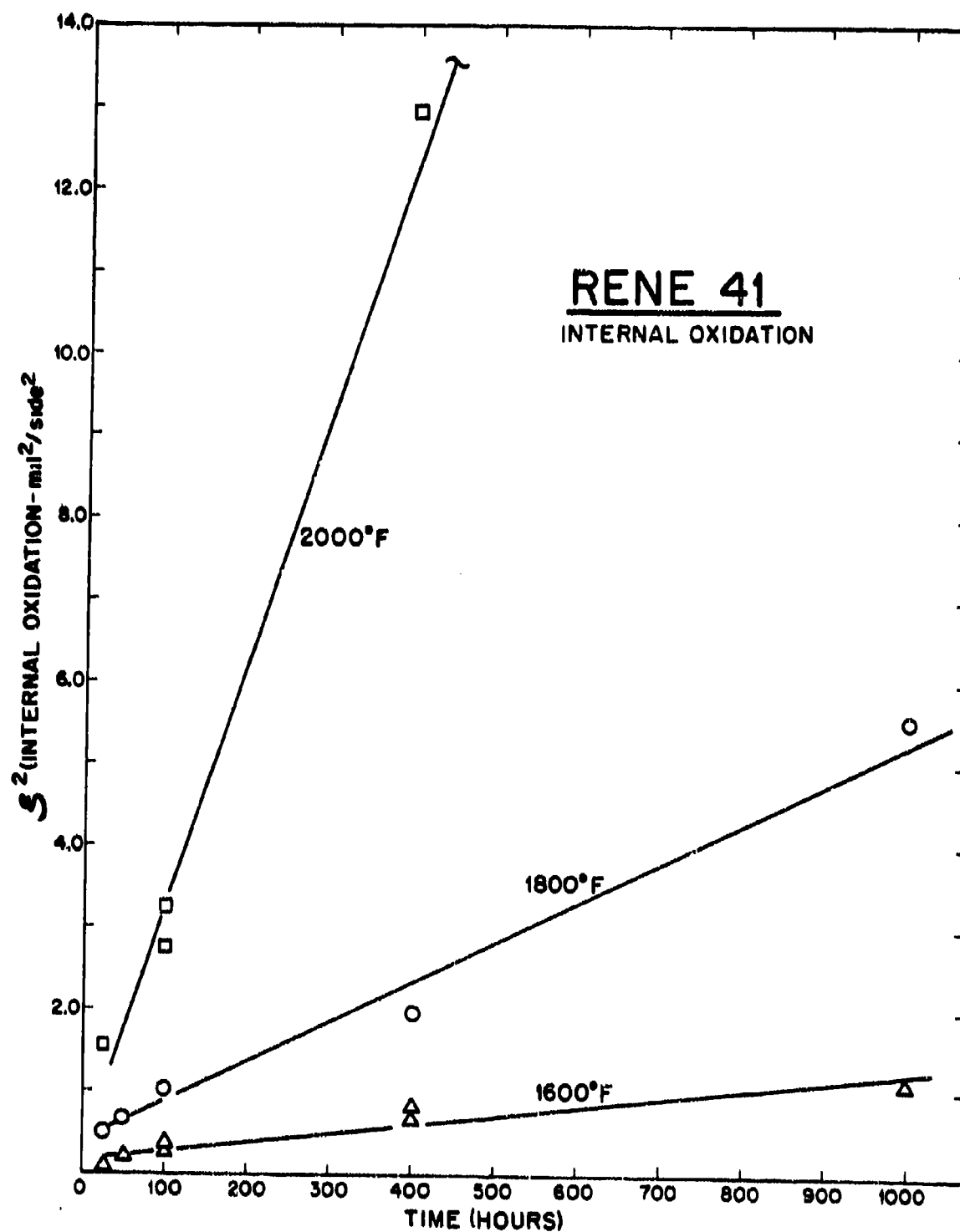
**FIGURE 49    Parabolic Internal Oxidation of René 41**
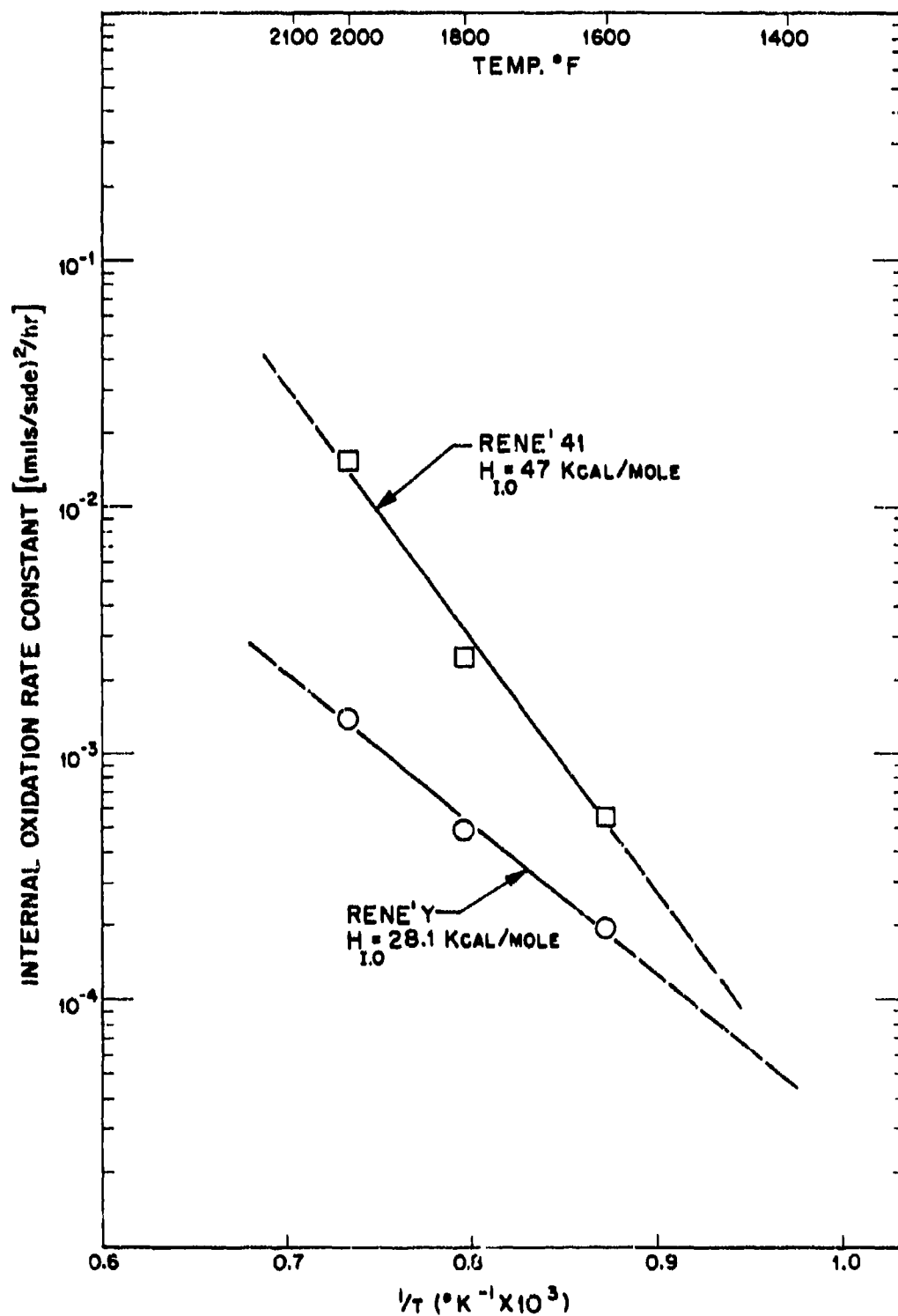
FIGURE 50    Arrhenius Plot of the Rate Constants for the Internal Oxidation
of René Y and René 41.

117

the depth of internal oxidation as a function of time and temperature:

For René 41    $\xi^3 = [8.91 \times 10^5 \exp - \left( \dfrac{47,000}{RT} \right)]t + 0.30$

For René Y     $\xi^3 = [8.32 \exp - \left( \dfrac{28,000}{RT} \right)]t + 0.20$

These equations are considered valid between 1600 and 2000°F for 50-1000 hours with an accuracy of ± 0.25 mil/side.

It can reasonably be assumed that internal oxidation occurs in these alloys by dissociation of the surface oxide scale ($Cr_2O_3$ in both cases) at the oxide/metal interface. Further, assuming that the oxide/metal interface is stationary ($<< \xi$), the partial pressure of oxygen above the internal oxide region is maintained at the dissociation pressure of the lowest oxide of the base metal and the problem could be reduced to one in which the surface oxide can be neglected. Rapp[16] has shown that where oxygen diffusion through the matrix is much greater than the cation diffusion;

$$ \xi^3 \ \alpha \ \frac{N_O \ D_O \ t}{N_B} \tag{3} $$

Where $N_O$ = mole fraction of oxygen at the external surface (oxide/metal interface)

$D_O$ = diffusivity of oxygen through base metal

t = time

$N_B$ = mole fraction of less noble solute which forms IGO

This would suggest similar activation energies for both alloys since $N_O$ $D_O$ products are nearly equivalent. But the computed activation energies for the two alloys are considerably different indicating that in René 41, cation($Al^{+++}$) diffusion may be a governing factor. Evans[17] has cited examples of internal oxide segregation at grain boundaries similar to René 41. He indicates that the presence of minor constituents with a great affinity for oxygen (i.e., Al) will favor grain boundary penetration at a parabolic growth rate. The activation energy of 47 K cal is therefore considered to represent control by $Al^{+++}$, not $O^=$ diffusion. It should be pointed out, however, that the Al diffusion in the bulk metal is not the same as that in the $\gamma'$ dissolution zone due to the larger concentration gradient present in the latter. The activation energy for René Y may more closely represent $O^=$ diffusion control.

### 4.2.9  Cyclic Oxidation

To better define the extent of oxide spalling which might be experienced during jet-engine operation, cyclic oxidation tests were performed. Although these tests were to be conducted only on IN-100 at 2000°F, the practical importance of this aspect of the oxidation behavior warranted additional evaluation. Therefore, cyclic tests were conducted for 400 hours on IN-100 at 1600, 1800, and 2000°F. In addition, Inco 713C was tested at 2000°F and comparative tests were conducted on René Y and Hastelloy X at 1800 and 2000°F.

The weight change results after eighteen 22-hour cycles compared to similarly treated isothermal test specimens are shown in Table XXXI. Thermal cycling promoted spalling and as a result increased the rate of material degradation. Cycling promoted spalling of IN-100 at 1600, 1800, and 2000°F, but was particularly deleterious to Inco 713C where all the oxide formed was lost. Measurements on these two alloys after cyclic exposure at 2000°F indicated $9.5 \pm 0.5$ mils/side metal loss. The I.O. and $\gamma'$ dissolution zones were similar to the isothermal specimens. In view of the fact that metal loss measurements for the isothermal specimens were almost nil (within the accuracy of measurement) cyclic effects can markedly influence the load-bearing capacity of a material.

X-ray identification of the spalled products from both the cast alloys showed only $NiO$ and $Ni(Cr,Al)_2O_4$, indicating that the surface became enriched in Al and Ti oxides. The excessive spalling, which is no doubt associated with the heterogeneous oxide formation, may be more directly related to incoherency between Ni-Cr and Al-base oxides. However, a detailed evaluation of the cyclic effect would be required before a more specific mechanism can be defined.

The results of the cyclic tests performed on René Y (Hastelloy X + La + Mn) and Hastelloy X clearly shows the improved scale adherence and oxidation resistance achieved by minor additions of lanthanum and manganese.

119

## TABLE XXXI

### CYCLIC OXIDATION WEIGHT CHANGE AFTER 400 HOURS EXPOSURE

#### IN-100

| Temperature (°F) | Specimen Number | Weight Change (mg/cm²) Isothermal | Weight Change (mg/cm²) Cyclic[a] | Cyclic Spalled Product (mg/cm²) |
|---|---|---|---|---|
| 1600[b] | 1 | 2.94 | + 1.86* (+ 2.43) | |
| | 2 | 2.87 | + 1.75* (+ 2.77) | 1.80 |
| | Average | 2.91 | + 1.80* (+ 2.60) | |
| 1800[b] | 1 | +1.65* (+1.90) | - 7.72* (+ 3.25) | |
| | 2 | +2.00* (+2.06) | - 8.43* (+ 2.85) | 11.12 |
| | Average | +1.83* (+1.98) | - 8.07* (+ 3.08) | |
| 2000 | 1 | -0.24* (+1.85) | - 4.74* (+ 4.39) | |
| | 2 | -0.26* (+1.74) | - 4.26* (+ 4.08) | 8.73 |
| | Average | -0.25* (+1.80) | - 4.50* (+ 4.23) | |

#### INCO 713C

| Temperature (°F) | Specimen Number | Isothermal | Cyclic[a] | Cyclic Spalled Product (mg/cm²) |
|---|---|---|---|---|
| 2000 | 1 | +0.21* (+0.45) | -21.30* (+11.70) | |
| | 2 | +0.32* (+0.58) | -28.29* (+12.19) | 36.74 |
| | Average | +0.27* (+0.52) | -24.79* (+11.95) | |

#### René Y

| Temperature (°F) | Specimen Number | Isothermal | Cyclic[a] | Cyclic Spalled Product (mg/cm²) |
|---|---|---|---|---|
| 1800 | 1 | +1.21* (+1.36) | + 1.44* (+ 1.46) | 0.02 |
| 2000 | 1 | +1.88* (+1.98) | + 1.60* (+ 1.67) | 0.07 |

#### Hast X

| Temperature (°F) | Specimen Number | Isothermal | Cyclic[a] | Cyclic Spalled Product (mg/cm²) |
|---|---|---|---|---|
| 1800 | 1 | +1.80* (+1.86) | + 0.15* (+ 1.31) | 1.16 |
| 2000 | 1 | -0.19* (+3.14) | - 0.15* (+ 3.29) | 3.44 |

[a] Eighteen 22-Hour Cycles to Room Temperature

[b] Isothermal data from previously conducted static oxidation tests.

* Indicates spalling with value in parentheses the W/A of specimen plus spalled products.

120

### 4.2.10 Comparison of General Oxidation Behavior

To permit an evaluation of the gross oxidation behavior of the alloys bar charts have been compiled which compare the average extent of attack. Both weight gain and internal oxidation effects are presented since neither by itself provides a good measure of oxidation resistance.

Figures 51 through 53 compare the total oxidation weight gain of the alloys as a function of time at 1600, 1800, and 2000°F, respectively (see Table VIA for actual data). The bars represent the weight change of specimen, including any spalling produced during cooling from temperature. At 1600°F the weight gains of all alloys except IN-100 and René 41 are similar. Except for SM-200 and Inco 713C, the total weight gain also increases with exposure time. The apparent decrease in weight change for SM-200 and Inco 713C after 1000 hours may indicate oxide volatilization. At 1800 and 2000°F spalling is observed for all alloys except René Y. Also, the fact that the weight-gain values actually decrease with increasing temperature for some alloys indicates that oxide volatilization may even occur in relatively static air. Therefore, weight-gain measurements should not be used as a conclusive means of assessing the oxidation resistance of these superalloys.

Figures 54 through 56 illustrate the extent of internal oxidation produced in the alloys as a function of time at 1600, 1800, and 2000°F. The metal loss has purposely been omitted from these charts since the observed thickness changes for all alloys was within the accuracy of measurement (± 0.5 mil/side). As reported for the weight-gain results, some discontinuities were also observed in the internal oxidation measurements at 2000°F or after long times at 1800°F. In general, these apparent anomalies can be attributed to difficulties in identifying the initial oxide/metal interface due to the spalling that occurs. Also, in many cases the I.O. that exists at low temperature is converted to suboxide at the higher temperatures, as previously pointed out for SM-200 and U-700.

### 4.3 Flame Tunnel Oxidation

#### 4.3.1 General Appearance

The general appearances of the alloys after 300 and 1000 hours exposure to high velocity combustion products of natural gas at 1600 and 2000°F are illustrated in Figures 57 and 58, respectively. The specimens tested at 1600°F displayed relatively thin oxides whose anisotropic growth revealed the grain structure of the cast alloys.
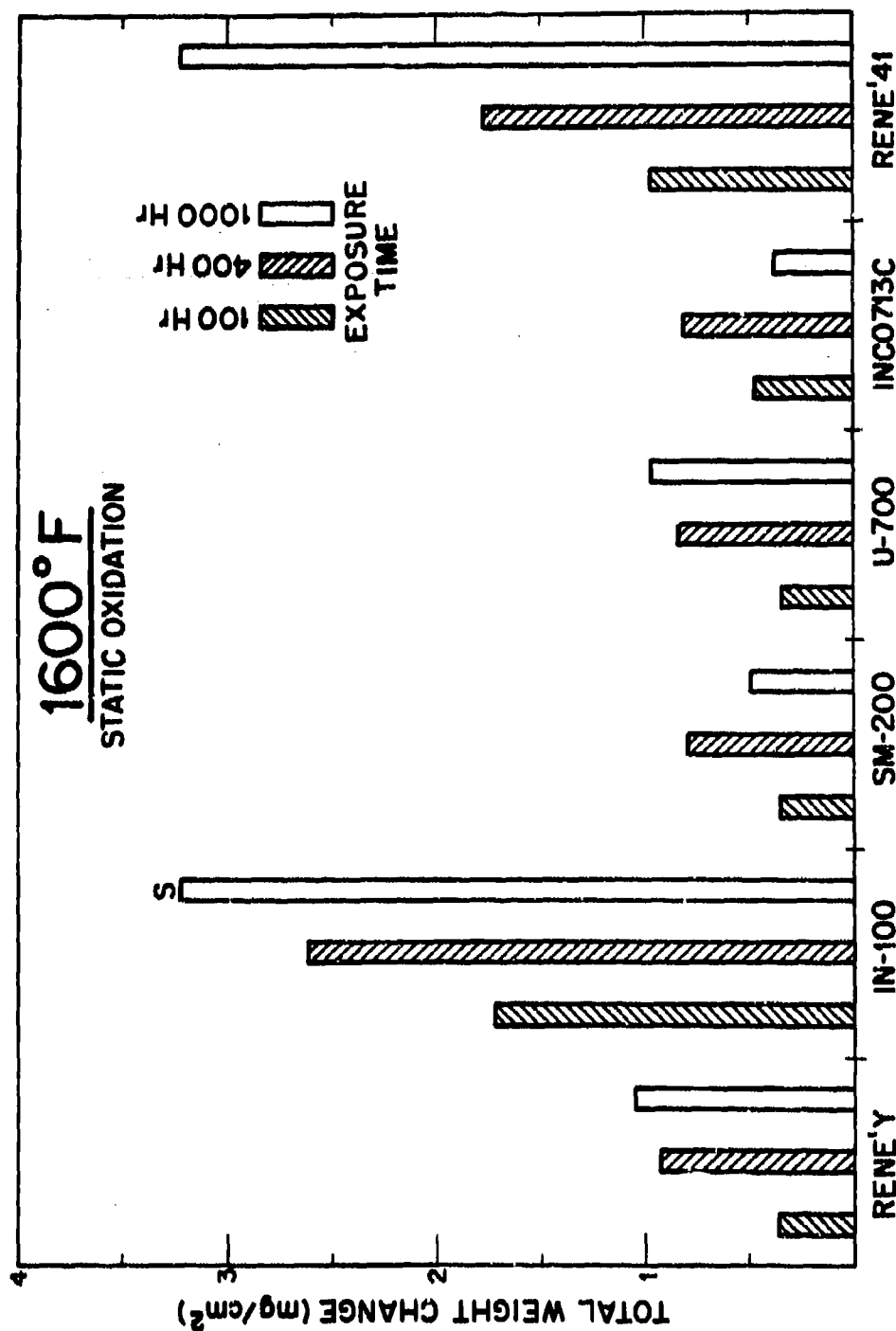
FIGURE 51    Comparison of the Average Weight-Gains During Static Air Oxidation at $1600^{\circ}$F.
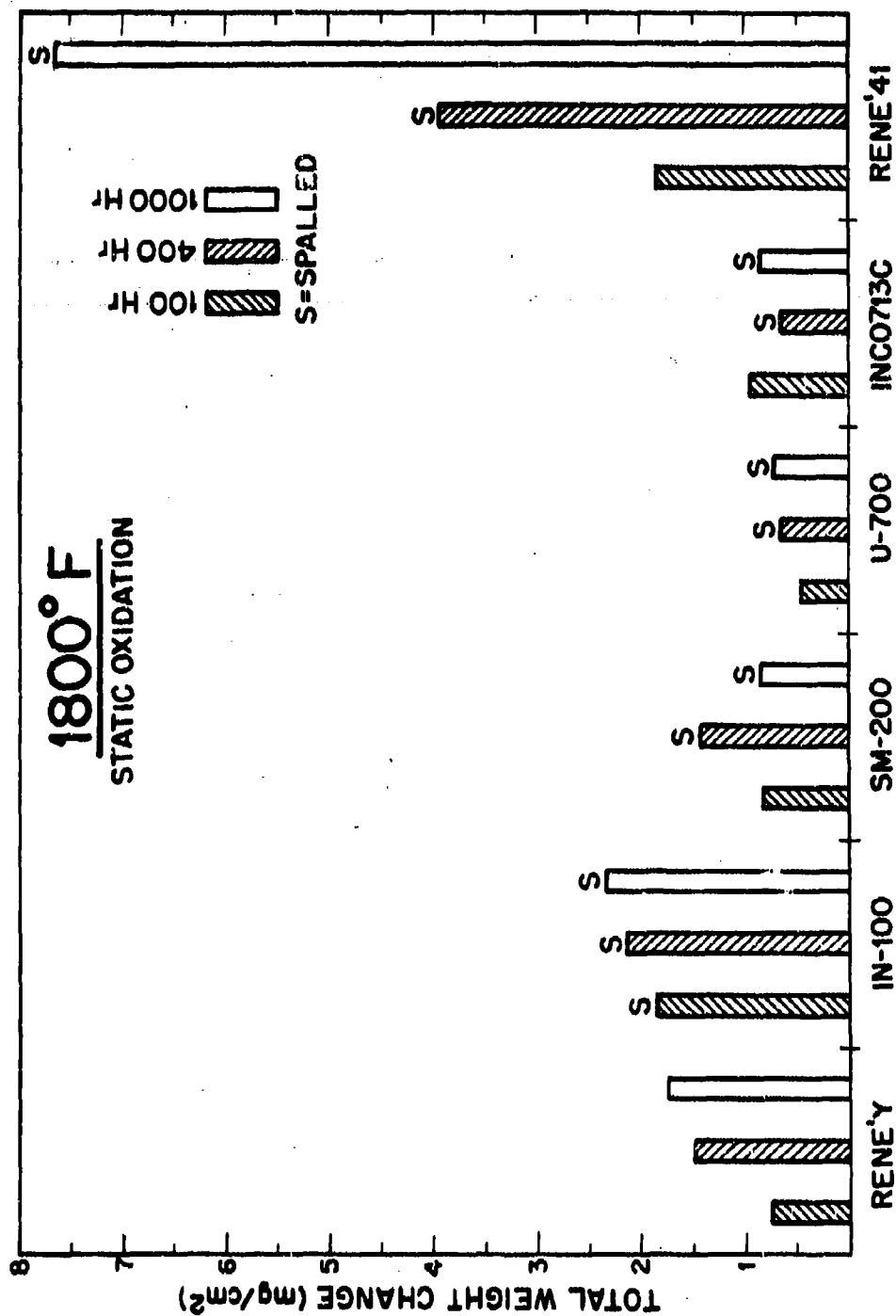
FIGURE 52    Comparison of the Average Weight-Gains During Static Air Oxidation at 1800°F.
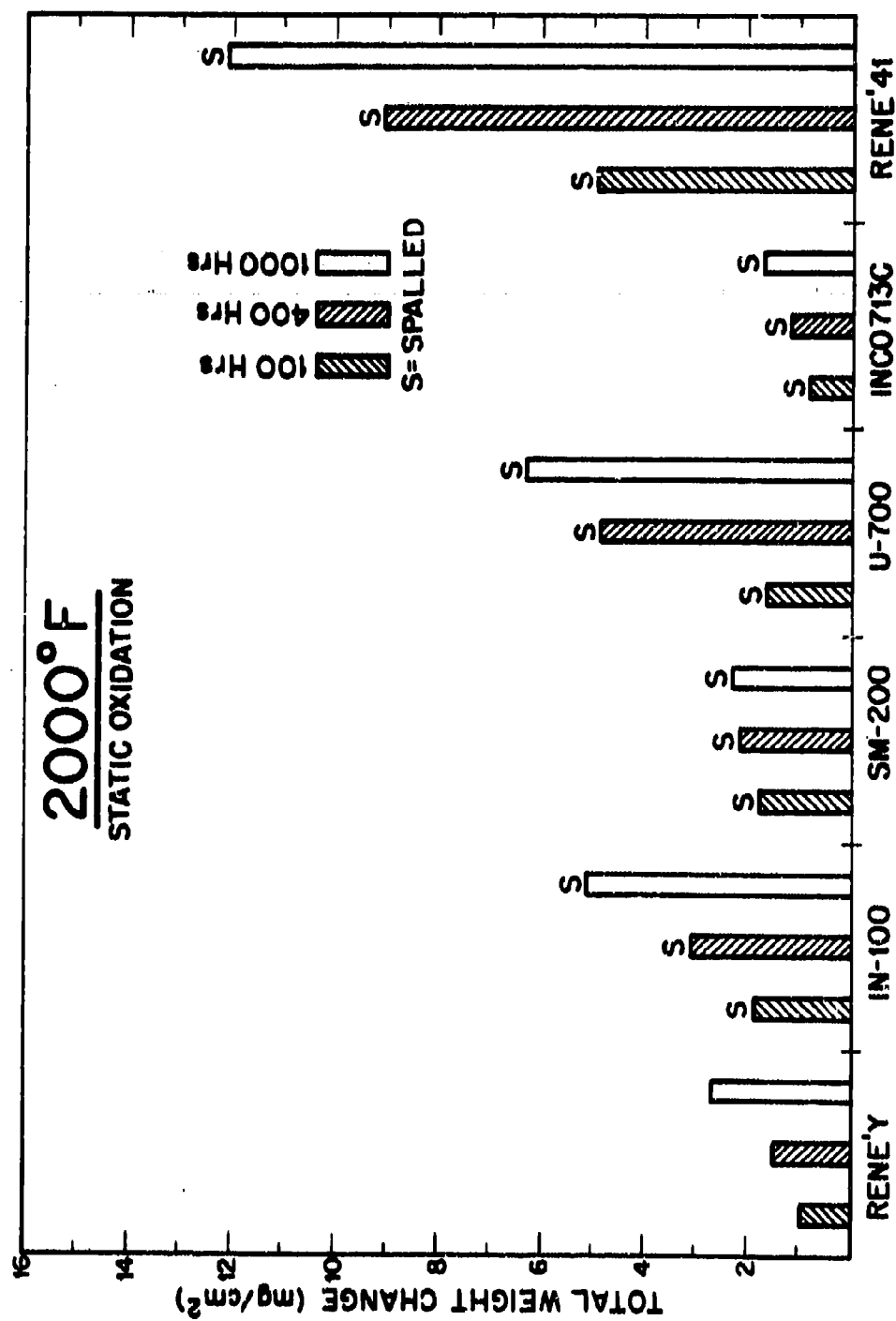
FIGURE 53    Comparison of the Average Weight-Gains During Static Air Oxidation at 2000°F.
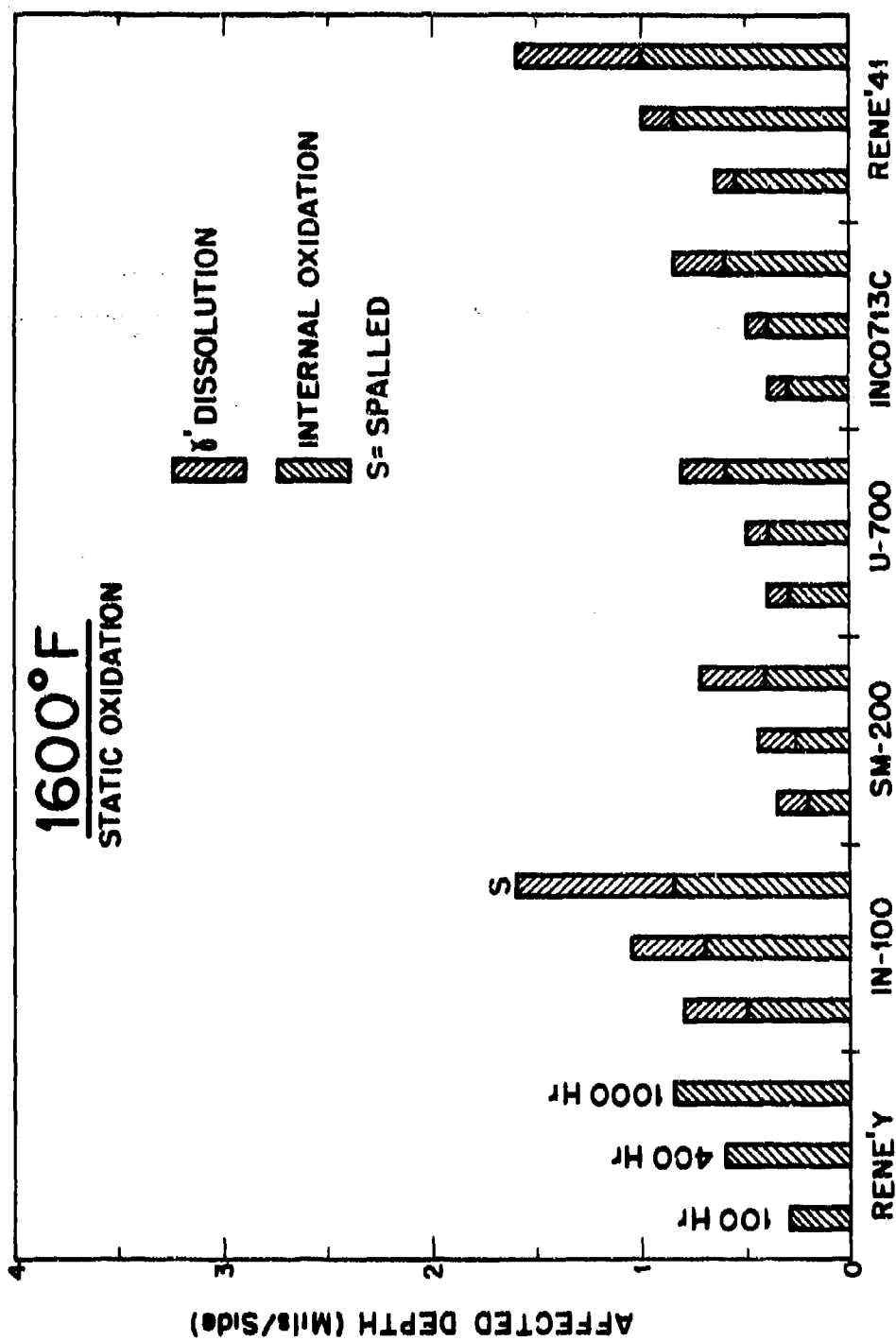
FIGURE 54   Comparison of the Internal Effects Produced During Static Air Oxidation at 1600°F.

125
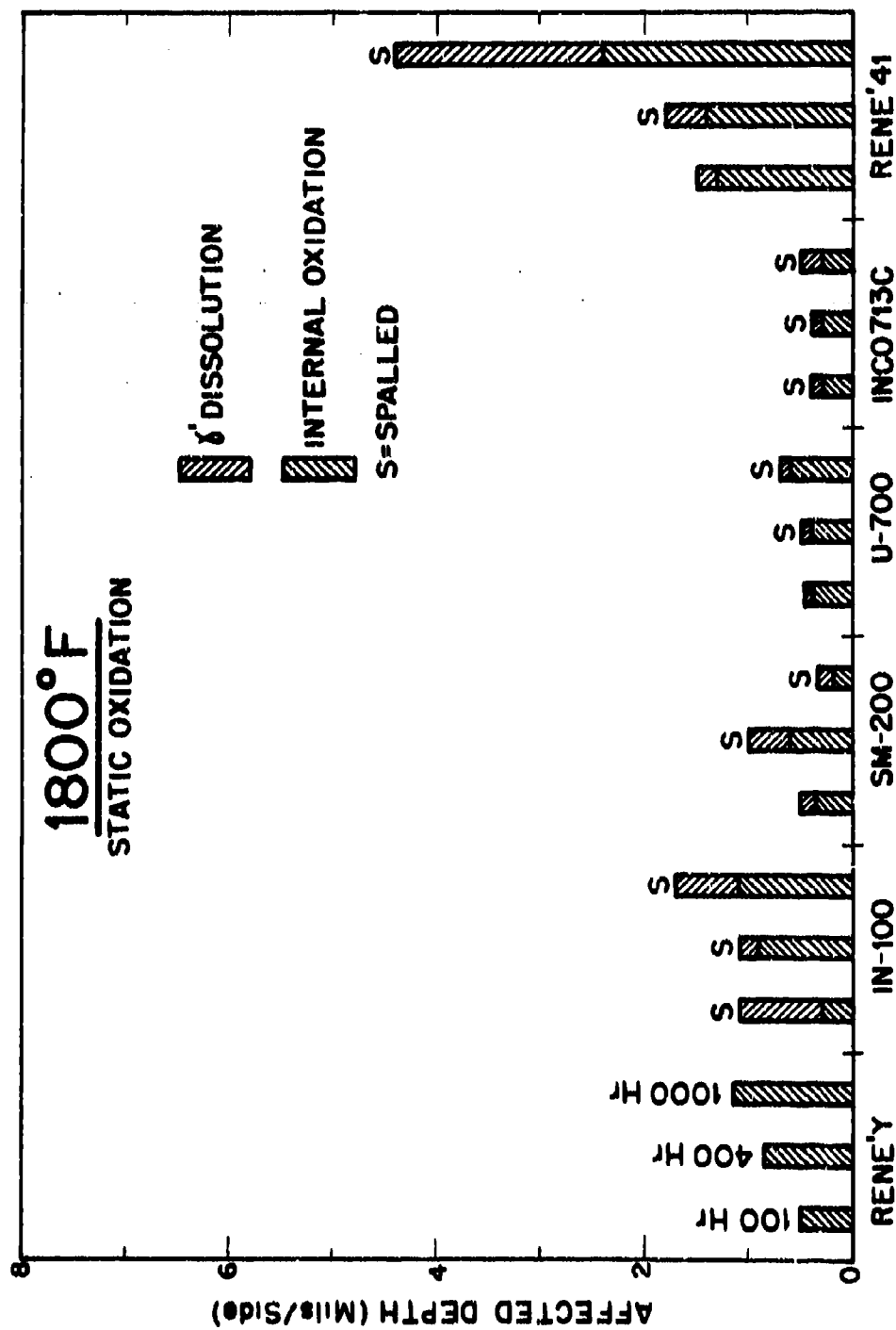
Figure 55    Comparison of the Internal Effects Produced During Static Air Oxidation at 1800°F.
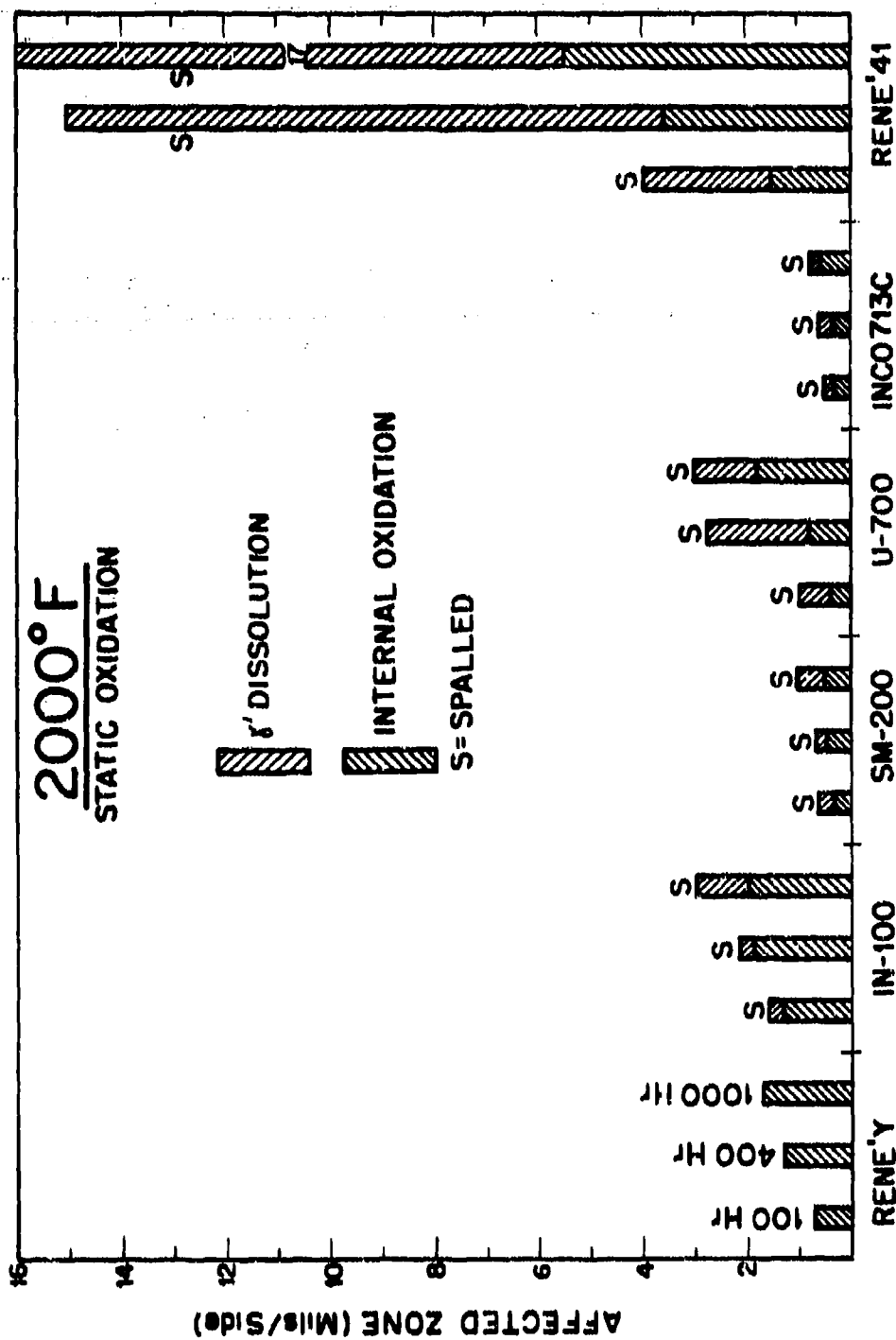
FIGURE 56    Comparison of the Internal Effects Produced During Static Air Oxidation at 2000° F.

SM-200
(34V2804)
C66050803

René Y
(64-711)

U-700
(6-4084)

300 Hours

René 41
(TV-394)

Inco 713C
(601)
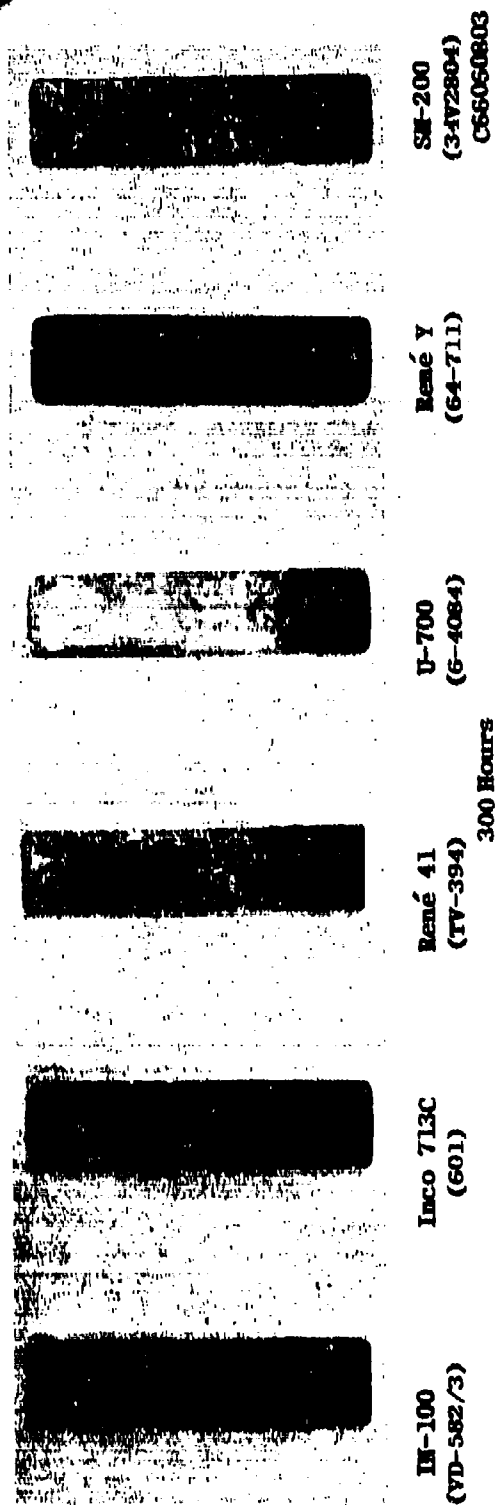
IN-100
(YD-582/3)
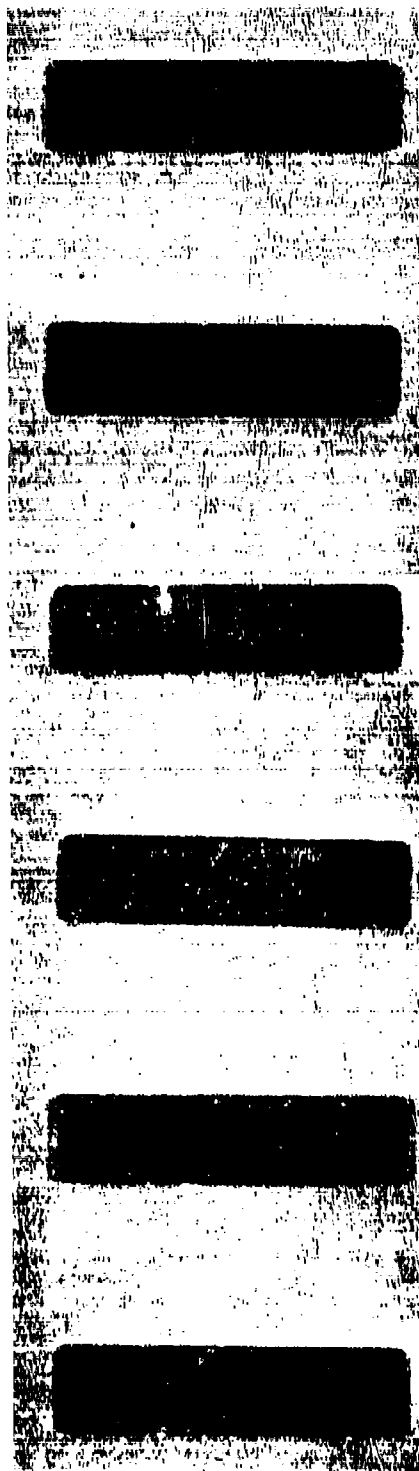
1000 Hours

C66050316

FIGURE 57    The General Appearance of the Alloys After 100 and 1000 Hours Exposure to High Velocity
Combustion Products of Natural Gas at 1600°F.

128

C6606339

C6612610

SM-200
(34V2804)

René Y
(64-71i)

U-700
(6-4084)

René 41
(TV-394)

100 Hours

Inco 713C
(601)

IN-100
(AD-582/3)
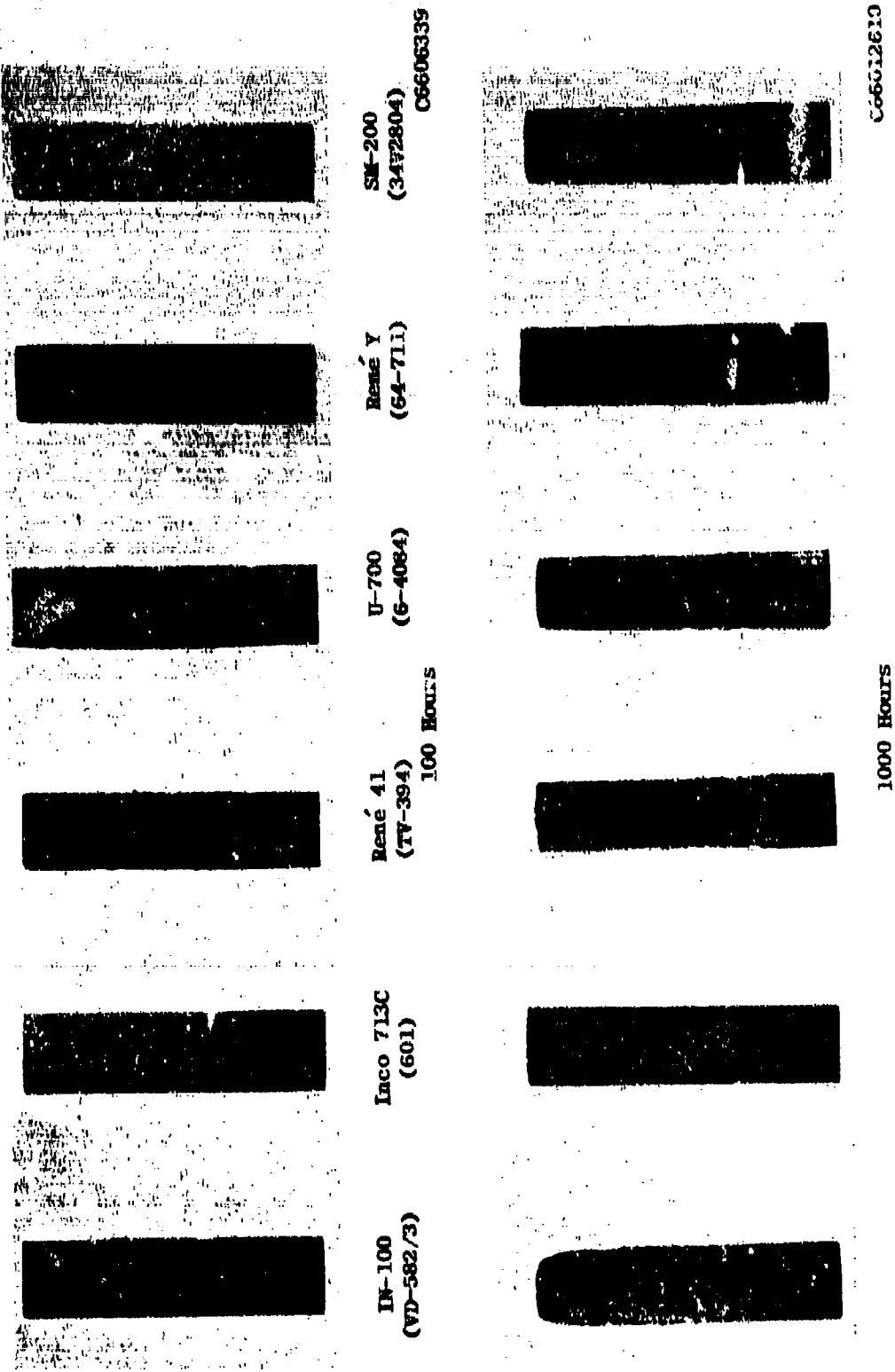
1000 Hours

FIGURE 58    The General Appearance of the Alloys After 100 and 1000 Hours Exposure to High Velocity
Combustion Products of Natural Gas at 2000°F.

At 2000°F both similarities and large differences were observed in the macroscopic appearance of oxides produces on those alloys. René Y, which exhibited the greatest oxidation resistance (based on weight-gain data), also displayed the most tenacious oxide scale. This oxide scale was generally black with some brown scaling oxide which became evident on the edges during the last 200 hours of testing. In-100, SM-200, and Inco 713C exhibited similar-appearing oxides with characteristic greenish-brown oxide protrusions in a silver and green oxide background. IN-100 contained the least amount of oxide overgrowth and Inco 713C the most. U-700 exhibited an oxide mixture of varying shades of green. René 41 exhibited a brownish oxide base with a green oxide overgrowth which was porous. All alloys displayed some evidence of oxide spalling or erosion after 1000 hours exposure with René Y and Inco 713C least susceptible and René 41 and IN-100 showing the greatest attack.

### 4.3.2 Weight Changes

The average incremental and total weight change which occurred during the first 400 hours of test at both 1600 and 2000°F is tabulated in Table VIIA. The 1000-hour weight change data for the 1600 and the 2000°F tests are given in Tables VIIIA and IXA, respectively. Summary curves showing the variation in weight with test time at 1600 and 2000°F are presented in Figures 59 and 60, respectively. A summary of the surface reaction products formed during flame tunnel exposure at these two temperatures is given in Table XXXII.

At 1600°F (Figure 59), with the exception of René Y, the alloys exhibited little difference in weight-gain behavior. René Y was the only alloy which displayed a weight loss for each 100-hour test increment. In view of the test variables which include thermal cycling to 1000°F, the weight change measured must be considered a result of:

(a)  Increased weight due to oxygen and nitrogen reaction.

(b)  Decreased weight due to vaporization of oxides where the weight loss is at least double the gain of oxygen.

(c)  Decreased weight due to oxide spalling and/or erosion where the losses can again be more than double the oxygen weight gain.

At 1600°F the spalling and erosion effect is assumed negligible, hence the weight change can be considered the result of (a) minus (b).

130
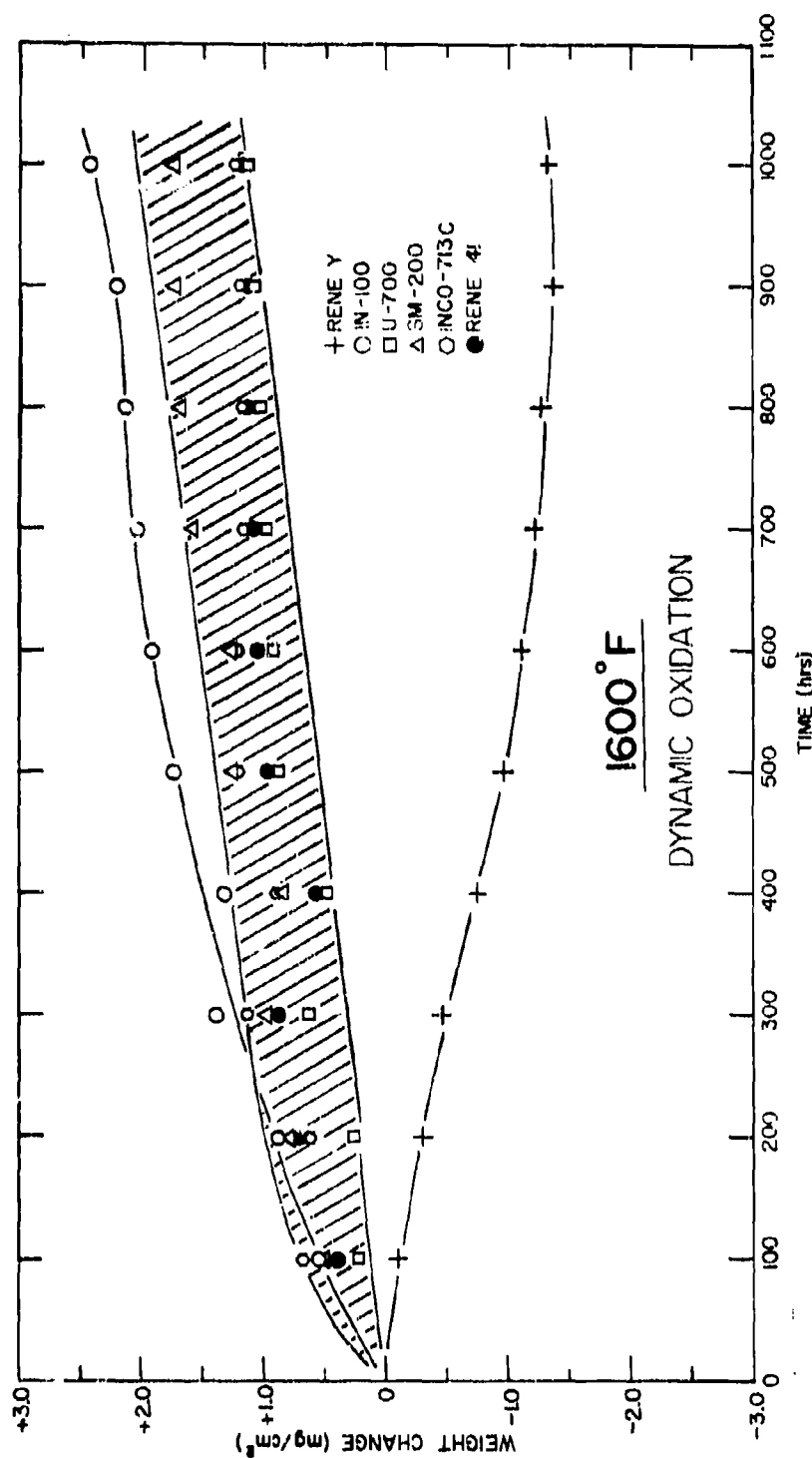
FIGURE 59    Weight Change During Oxidation in High Velocity Natural Combustion Gas Products at 1600°F.

131
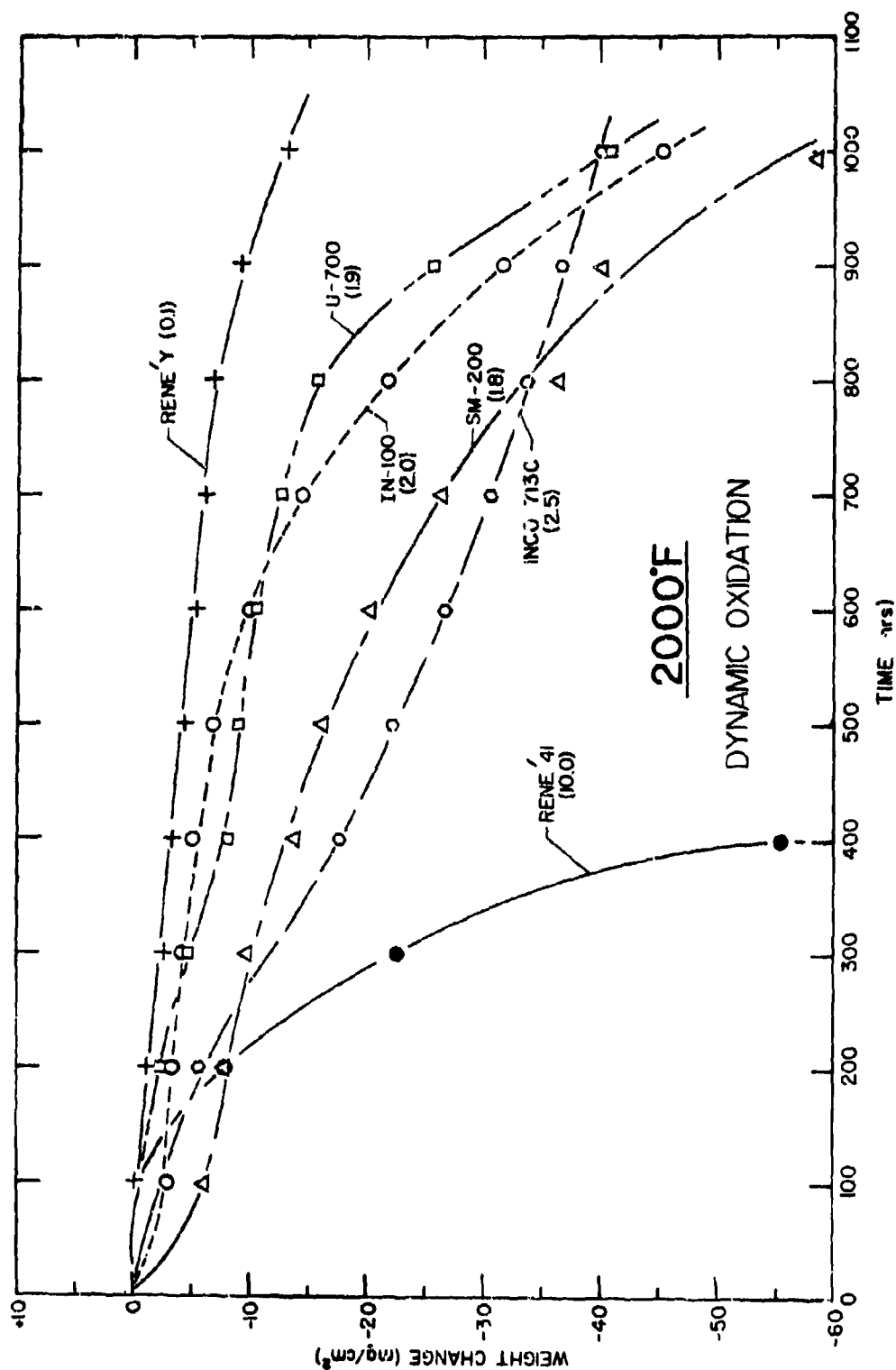
FIGURE 60   Weight Change During Oxidation in High Velocity Natural Gas Combustion
Products at 2000°F

Values in parenthesis represent the metal loss (mils/side) after
1000 hours exposure.

132

## TABLE XXXII

## X-RAY IDENTIFICATION OF REACTION PRODUCTS FORMED ON VARIOUS ALLOYS

## DURING FLAME-TUNNEL EXPOSURE

| Temp °F | Time Hrs. | Type Spec | Reaction Products[a] |
|---------|-----------|-----------|----------------------|
| | | | **René Y** |
| 1600 | 400 | (b) | $MnCr_2O_4$ ($a_C$=8.44Å) + $\alpha Cr_2O_3$ |
| | 1000 | (b) | $MnCr_2O_4$ ($a_O$=8.43Å) + $\alpha Cr_2O_3$ |
| 2000 | 100 | (b) | $MnCr_2O_4$ ($a_O$=8.44Å) + $\alpha Cr_2O_3$ |
| | 1000 | (b) | $MnCr_2O_4$ ($a_O$=8.42Å) + $\alpha Cr_2O_3$ + unidentified lines |
| | | | **IN-100** |
| 1600 | 400 | (b) | $NiO$ ($a_O$=4.20Å) + Spinel ($a_O$=8.35Å) |
| | 1000 | (b) | $NiO$ ($a_O$=4.19Å) + $NiTiO_3$ + Spinel ($a_O$=8.24Å) |
| 2000 | 100 | (b) | Spinel ($a_O$=8.14Å) + $NiTiO_3$ |
| | 1000 | (b) | $NiO$ + Spinel ($a_O$=8.10Å) + $Al_2O_3$ + TiN |
| | | | **SM-200** |
| 1600 | 400 | (b) | $NiO$ + Spinel ($a_O$=8.39Å) + $TiO_2$ + $\alpha Al_2O$ (VVW) |
| | 1000 | (b) | $NiO$ + $NiTiO_3$ |
| 2000 | 100 | (c) | $NiO$ + Spinel ($a_O$=8.26Å) + $NiTiO_3$ + Spinel ($a_O$=8.07Å) |
| | 1000 | (b) | $NiO$ + Spinel ($a_O$=8.24Å) + $NiTiO_3$ + Spinel ($a_O$=8.16Å) |
| | | | **Inco 713C** |
| 1600 | 400 | (b) | $NiO$ + $\alpha Cr_2O_3$ + Spinel ($a_O$=8.34Å) |
| | 1000 | (b) | $NiO$ + $\alpha Al_2O_3$ + Spinel ($a_O$=8.34Å) |
| 2000 | 100 | (c) | $NiO$ + $\alpha Al_2O_3$ + Spinel ($a_O$=8.08-8.34Å) + $TiO_2$ |
| | 1000 | (b) | $NiO$ + $\alpha Al_2O_3$ + Spinel ($a_O$=8.20Å) |
| | | | **U-700** |
| 1600 | 400 | (b) | $NiO$ ($a_O$=4.17Å) + Spinel ($a_O$=8.37) + $Cr_2O_3$ |
| | 1000 | (b) | $NiO$ ($a_O$=4.20Å) + Spinel |
| 2000 | 100 | (b) | $NiTiO_3$ + $(Al,Cr)_2O_3$ |
| | 1000 | (b) | Spinel ($a_O$=8.30Å) + $NiO$ ($a_O$=4.16Å) + $NiTiO_3$ + $Cr_2O_3$ |
| | | | **René 41** |
| 1600 | 400 | (b) | $NiO$ ($a_O$=4.17Å) + Spinel ($a_O$=8.38Å) + $\alpha Cr_2O_3$ + TiN |
| | 1000 | (b) | $NiO$ ($a_O$=4.19Å) + Spinel + $\alpha Cr_2O_3$ |
| 2000 | 1000 | (b) | $NiO$ ($a_O$=4.19Å) + Spinel ($a_O$=8.36Å) + $\alpha Cr_2O_3$ + $NiTiO_3$ |

[a] Listed in order of decreasing predominance as indicated by X-ray intensities

[b] Diffractometer trace of oxides in situ.

[c] Debye Scherrer analysis of scraped oxide.

Referring to the nature of the reaction products formed on these alloys, René Y is observed to form oxides based on $Cr_2O_3$, whereas the other alloys contain NiO or Ni-Al-Cr base oxides. The volatilization of $Cr_2O_3$-base oxides as compared to NiO or Ni-Al-Cr oxides is therefore considered responsible for the slight weight loss exhibited by René Y. The volatilization rate constant of $Cr_2O_3$ when exposed to static oxygen has a temperature dependence given by

$$K_V = 0.214 \exp(-48,800 \pm 3,000/RT) \text{ gm/cm}^2 \text{ sec}^{-1} \text{[18]}$$

Since the oxide scale on René Y is approximately 90% $Cr_2O_3$, a calculated volatilization weight loss of -0.65 mg/cm$^2$ would occur during the 1000-hour test at 1600°F. However, assuming an oxygen weight gain for the same period of +0.85 mg/cm$^2$ (from static test data) the net weight change during the flame tunnel test should have been +0.20 mg/cm$^2$, which is considerably higher than the -1.33 mg/cm$^2$ observed. Since erosion and spalling effects are not considered responsible for the additional weight loss, the dynamic atmosphere apparently promoted volatilization. The extent of volatilization for the other alloys is illustrated in Table XXXIII, indicating that those alloys rich in chromium are most subject to volatilization. However, this does not imply that those alloys showing a net weight gain were not also subjected to volatilization losses. The presence of predominantly NiO rather than a $Cr_2O_3$-base oxide indicates that the weight gain by oxygen reaction was simply greater than the volatilization loss. For the cast alloys the net gain was greater than that measured after equivalent static oxidation testing. Considering that it requires the reaction of approximately four moles of $O_2$ to compensate for the weight loss due to volatilization of one mole of $Cr_2O_3$ (or $CrO_3$), the oxidation rates of the alloys in the flame tunnel must also be significantly increased at 1600°F.

Figure 60 illustrates that exposure in the flame tunnel at 2000°F yields net weight losses for all alloys with René Y being the least susceptible. A 1000-hour exposure produces a weight loss for René Y which is one-third that of the next best alloy (Inco 713C, -40.2 mg/cm$^2$) and that predicted employing $Cr_2O_3$ vaporization data[18], assuming 90% $Cr_2O_3$ in the oxide scale. Hence, very little erosion or spalling occurs for this alloy, as verified by the appearance. If the flame-tunnel atmosphere increases the oxidation rate at 1600°F, it will also increase it at 2000°F and therefore probably enhance spalling. Thus the large weight losses for the other alloys may be attributed primarily to volatilization and spalling. The fact that oxide buildup and spalling occurs predominantly at the edges and corners of specimens accounts for the alteration in the shape of the coupons observed after test.

## TABLE XXXIII

### VOLATILIZATION DURING FLAME TUNNEL TESTING

| Alloy | $mg/cm^2$ for 1000 hr/1600°F Static[a] | Dynamic | Volatilization Weight Loss $(mg/cm^2)$ | Prime Reaction Products at 1600°F |
|---|---|---|---|---|
| Rene' Y | + 0.85 | - 1.35 | - 2.10 | $MnCr_2O_4$, $Cr_2O_3$ |
| IN-100 | + 3.20 | + 2.45 | - 0.75[b] | NiO, spinel |
| SM-200 | + 0.57 | + 1.10 | - | NiO, spinel, $\alpha-Al_2O_3$ |
| U-700 | + 0.97 | + 1.75 | - | NiO, spinel, $Al_2O_3$ |
| INCO 713C | + 0.40 | + 1.25 | - | NiO, $\alpha-Al_2O_3$, spinel |
| Rene' 41 | + 3.23 | + 1.15 | - 2.08 | NiO, spinel, $Cr_2O_3$ |

(a) From static weight gain data.

(b) May be increased spalling since spalling is observed in the static test after 1000 hr/1600°F.

### 4.3.3 Oxidation Reactions

The morphology of the reaction products on the alloys after exposure to high velocity combustion products at 1600°F are illustrated in Figures 61 through 63. The extent of the internal oxidation features as a function of time at 1600 and 2000°F are presented in Tables XXXIV and XXXV, respectively. A bar graph summarizing the depth of affected metal in the alloys after 1000 hours exposure at 1600 and 2000°F is given in Figure 64. A comparison of these data with comparable static oxidation test results indicates the extent of oxidation in the flame-tunnel atmosphere to be significantly more severe. The best measure of degradation is obtained by combining the metal loss and I.O. measurements. This permits the following ranking of alloys in order of decreasing resistance to the flame-tunnel atmosphere:

| Ranking | 1600°F | 2000°F |
|---|---|---|
| 1 | Inco 713C | René Y |
| 2 | SM-200 | SM-200 |
| 3 | René Y | U-700 |
| 4 | U-700 | Inco 713C |
| 5 | René 41 | IN-100 |
| 6 | IN-100 | René 41 |

All alloys rank similarly at the two test temperatures with the major exception of Inco 713C which shows lower resistance at the high temperature because of excessive oxide spalling and deep internal oxidation. However, if all facets of oxidation are considered (weight gain, appearance, and internal effects) René Y displays superior resistance to the flame-tunnel atmosphere. It is of interest to note from the above ranking that contrary to some views the resistance to a dynamic atmosphere is not solely dependent upon the Cr content of the alloy.

The microstructural features observed during exposure at 1600°F (Figures 61 through 63) do not differ significantly from those observed after an equivalent static oxidation test.

The reaction products formed during the high velocity flame-tunnel tests after 1000 hours at 1600 and 2000°F, as identified by X-ray diffraction (see Table XXXII) and microprobe analysis, are summarized in Table XXXVI. For comparison purposes the reaction products formed during equivalent time static oxidation tests have been included. A considerable difference is observed between the static reaction products and those produced in a dynamic atmosphere. With the exception of René Y which displays little alteration in the form of oxide products, the prime difference is the lack of chromium-rich oxides after dynamic testing. This is attributed to volatilization of $CrO_3$. René Y is not subjected to such depletion due to the formation of a protective layer of $MnCr_2O_4$ spinel.

136
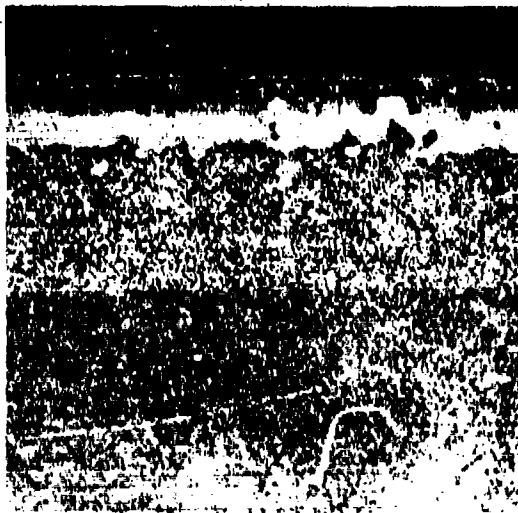
250X             M4019            250X               M3175

a)    Inco 713C After 100 Hours        b)    Inco 713C After 1000 Hours
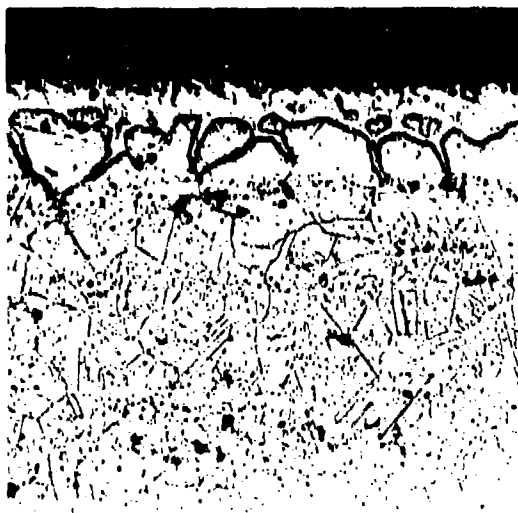
250X             M4027            250X               M3184
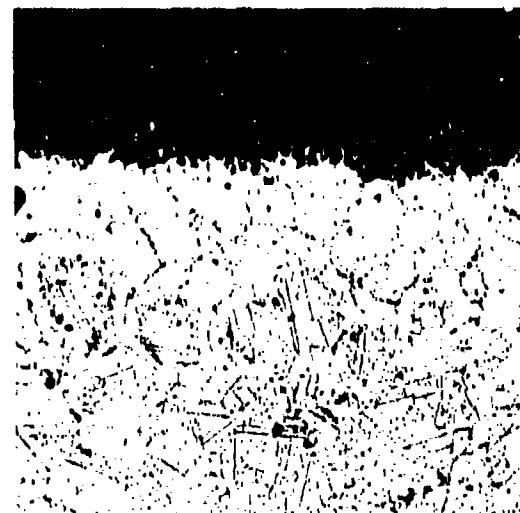
a) René Y After 100 Hours          b) René Y After 1000 Hours

FIGURE 61      Typical Oxide Morphology Produced in Inco 713C and René Y After
Exposure to High Velocity Natural Gas Combustion Products at
1600°F. Mounted on 5:1 Taper Section. Etched in 2% Chromic.

137
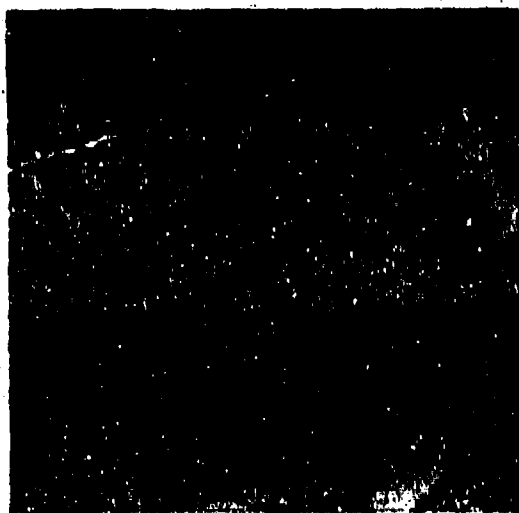
250X           M4025      250x           M3183

a)    IN-100 After 100 Hours        b)    IN-100 After 1000 Hours

250x           M4024      250x           M3182
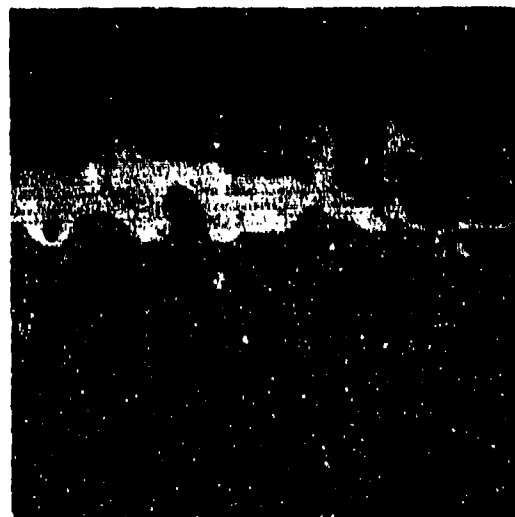
a)    SM-200 After 100 Hours        b)    SM-200 After 1000 Hours

FIGURE 62      Typical Oxide Morphology Produced in IN-100 and SM-200 after
Exposure to High Velocity Natural Gas Combustion Products at
1600°F.   Mounted on 5:1 Taper Section.   Etched in 2% Chromic.

138

250X       M4023       250X       M3181

a)   U-700 After 100 Hours       b)   U-700 After 1000 Hours

250X       M4020       250X       M3179

a) René 41 After 100 Hours       b) René 41 After 1000 Hours

FIGURE 63       Typical Oxide Morphology Produced in U-700 and René 41 After Exposure to High Velocity Natural Gas Combustion Products at 1600°F. Mounted on 5:1 Taper Section. Etched in 2% Chromic.

TABLE XXIV

MEASUREMENTS OF INTERNAL REACTION FOR FLAME TUNNEL SPECIMENS TESTED AT 1600°F[a]

| Alloy | Time (hrs) | Gross Scale Thickness (mils/side) | Maximum Scale Thickness (mils/side) | Gross I.O. or IGO (mils/side) | Maximum I.O. or IGO (mils/side) | Average γ' Dissolution (mils/side) | Metal Loss[b] (mils/side) |
|---|---|---|---|---|---|---|---|
| René Y | 100 | 0.1 | - | 0.1 | - | 0.3 | - |
| | 400 | 0.2 | 0.4 | 0.4 | 0.7 | 0.6 | +0.2 |
| | 1000 | 0.2 | 0.4 | 0.8 | 1.0 | 0.9 | +0.3 |
| IN-100 | 100 | 0.2 | 0.4 | 0.3 | 0.4 | 0.4 | - |
| | 400 | 0.7 | 1.0 | 1.2 | 1.6 | 1.8 | -1.3 |
| | 1000 | 0.7 | 1.0 | 0.8 | 1.6 | 1.0 | -1.2 |
| SM-200 | 100 | 0.1 | - | 0.1 | - | 0.2 | - |
| | 400 | 1.1 | - | 0.2 | 0.8 | 0.8-1.2 | -1.2 |
| | 1000 | 0.2 | 0.8 | 0.1 | 0.2 | 0.4 | -0.5 |
| U-700 | 100 | 0.3 | 0.4 | 0.4 | - | 0.9 | - |
| | 400 | 0.1 | 0.2 | 0.6 | - | 0.8 | -1.3 |
| | 1000 | 0.6 | 0.8 | 0.4 | 0.6 | 1.0 | -1.2 |
| Inco 713C | 100 | 0.1 | 0.2 | 0.1 | 0.2 | 0.3 | - |
| | 400 | 0.4 | 0.8 | 0.3 | 0.4 | 0.8 | +0.6 |
| | 1000 | 0.1 | 0.2 | 0.2 | 0.5 | 0.4 | +0.5 |
| René 41 | 100 | 0.2 | 0.4 | 0.2 | 0.3 | 0.4 | - |
| | 400 | 0.3 | 0.6 | 0.8 | 1.2 | 1.2-1.6 | -1.4 |
| | 1000 | 0.3 | 0.4 | 0.8 | 1.2 | 0.8 | -1.2 |

(a) All metallographic measurements taken from taper sections with a 5:1 magnification.

(b) Measurements taken from vertical sections.

# TABLE XXV

## MEASUREMENTS OF INTERNAL REACTION FOR FLAME TUNNEL SPECIMENS TESTED AT 2000°F

| Alloy | Time (hrs) | Gross Scale Thickness (mils/side) | Maximum Scale Thickness (mils/side) | Gross I.O. or IGO (mils/side) | Maximum I.O. or IGO (mils/side) | Average $\gamma'$ Dissolution (mils/side) | Metal Loss(b) (mils/side) |
|---|---|---|---|---|---|---|---|
| René Y | 100 | 0.2 | 0.4 | 0.4 | -- | 0.5 | -- |
|  | 400 | 0.4 | 1.0 | 1.0 | -- | 1.2 | -- |
|  | 1000 | 0.4 | -- | 3.0 | -- | 3.2 | 0.1 |
| IN-100 | 100 | 0.1 | 0.2 | 1.0 | -- | 0.4 | -- |
|  | 400 | 0.8 | 1.2 | 2.0 | 3.0 | 2.0 | -- |
|  | 1000 | 1.0 | -- | 2.0 | 7.0 | 4.0 | 2.0 |
| SM-200 | 100 | 0.2 | 0.4 | 0.3 | 0.6 | 0.4 | -- |
|  | 400 | 0.5 | 0.8 | 0.6 | 0.8 | 0.8 | -- |
|  | 1000 | 1.0 | 1.5 | 1.5 | 2.5 | 1.2 | 1.8 |
| U-700 | 100 | 0.3 | 0.4 | 0.4 | -- | 1.0 | -- |
|  | 400 | 0.6 | 0.8 | 0.5 | 1.0 | 2.0 | -- |
|  | 1000 | 1.0 | -- | 1.0 | 2.0 | 3.0 | 1.9 |
| Inco 713C | 100 | 0.4 | -- | 0.5 | 0.8 | 0.6 | -- |
|  | 400 | 0.2 | 0.4 | 0.6 | 10.0 | 1.0 | -- |
|  | 1000 | 1.0 | -- | .2.5 | -- | 5.3 | 2.5 |
| René 41 | 100 | 0.6 | -- | 2.4 | 3.0 | 1.4 | -- |
|  | 400 | 1.3 | -- | 10.0 | 12.0 | 5.0 | -- |
|  | 1000 | 1.0 | -- | 15.0 | -- | 8.0 | 10.0 |

(a) All metallographic measurements taken from taper sections with a 5:1 magnification.

(b) Measured from vertical sections.

# 1600°F & 2000°F

DYNAMIC OXIDATION

(a) 1600°F
(b) 2000°F

γ' DISSOLUTION

INTERNAL OXIDATION

METAL LOSS

AFFECTED DEPTH (Mils/Side)

16  14  12  10  8  6  4  2  0

RENE'Y    IN-100    SM-200    U-700    INCO713C    RENE'41

(a) (b)  (a) (b)  (a) (b)  (a) (b)  (a) (b)  (a) (b)
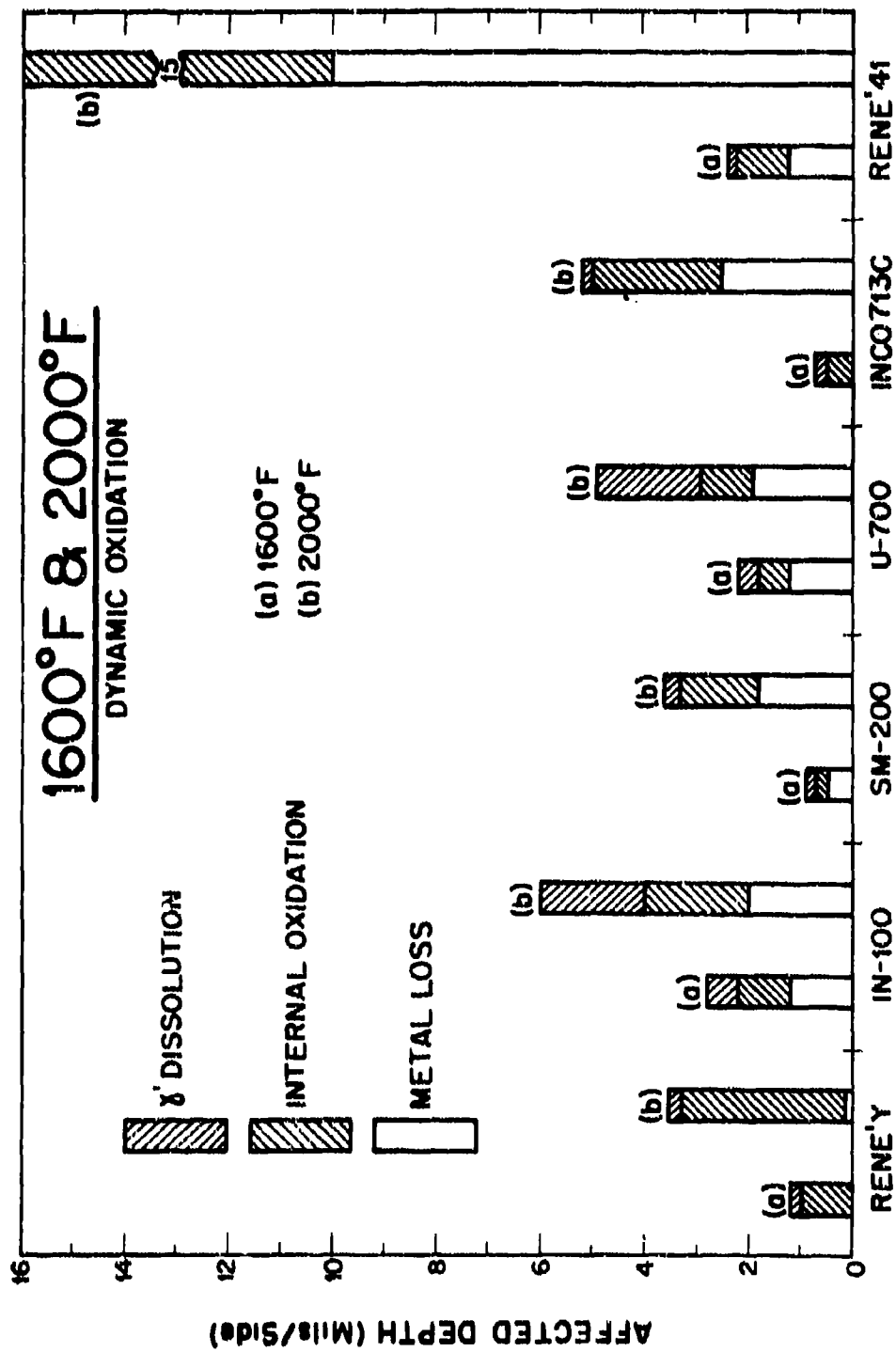
FIGURE 64    Summary of the Depth of Affected Zone after 1000 Hours Exposure in the Flame Tunnel.

## TABLE XXVI

### COMPARISON OF OXIDATION REACTION PRODUCTS AFTER 1000-HOUR EXPOSURE[a] IN STATIC AND DYNAMIC ENVIRONMENTS

| Alloy | 1600°F Static | 1600°F Dynamic | 2000°F Static | 2000°F Dynamic |
|---|---|---|---|---|
| René Y | $\dfrac{Cr_2O_3+MnCr_2O_4}{SiO_2}$ | $\dfrac{MnCr_2O_4+(Cr,Fe)_2C_3}{SiO_2}$ | $\dfrac{MnCr_2O_4+Cr_2O_3+NiO}{SiO_2+Mn_xO_y}$ | $\dfrac{MnCr_2O_4+Cr_2O_3}{SiO_2}$ |
| René 41 | $\dfrac{Cr_2O_3+NiCr_2O_4}{Al_2O_3+TiO_2+TiN}$ [b] | $\dfrac{NiO+NiCr_2O_4+Cr_2O_3}{Al_2O_3+TiN}$ | $\dfrac{Cr_2O_3+NiCr_2O_4+NiO}{Al_2O_3+TiO_2+TiN}$ | $\dfrac{NiO+NiCr_2O_4+Cr_2O_3}{Al_2O_3+TiN+AlN}$ |
| IN-100 | $\dfrac{NiO+(Ni,Co)Cr_2O_4+NiTiO_3}{Al_2O_3+TiO_2+TiN}$ | $\dfrac{NiO+Ni(Cr,Al)_2O_4+NiTiO_3}{Al_2O_3}$ | $\dfrac{Ni(Cr,Al)_2O_4+Al_2O_3+NiTiO_3}{TiO_2+TiN}$ | $\dfrac{NiO+Ni(Al,Cr)_2O_4}{Al_2O_3+TiN}$ |
| SM-200 | $\dfrac{Cr_2O_3+NiCr_2O_4+TiO_2}{Al_2O_3}$ | $\dfrac{NiO+NiCr_2O_4+NiTiO_3}{Al_2O_3}$ | $\dfrac{NiCr_2O_4+NiAl_2O_4+Tungstate}{Al_2O_3+TiO_2+TiN}$ | $\dfrac{NiO+Ni(Cr,Al)_2O_4+NiTiO_3}{Al_2O_3+TiN}$ |
| Inco 713C | $\dfrac{NiCr_2O_4+Cr_2O_3}{Al_2O_3}$ | $\dfrac{NiO+NiCr_2O_4}{Al_2O_3}$ | $\dfrac{NiAl_2O_4+Al_2O_3+NiCr_2O_4}{TiO_2+Cr_2O_3}$ | $\dfrac{NiO+Al_2O_3+Ni(Al,Cr)_2O_4}{TiO_2}$ |
| U-700 | $\dfrac{Cr_2O_3+NiCr_2O_4}{Al_2O_3+TiO_2+TiN}$ [b] | $\dfrac{N_2O+NiCr_2O_4}{Al_2O_3}$ | $\dfrac{NiCr_2O_4+NiAl_2O_4+Al_2O_3}{TiO_2+TiN}$ | $\dfrac{Ni(Cr,Al)_2O_4+NiO+Cr_2O_3}{TiO_2+TiN}$ |

(a) Reaction products are expressed in order of decreasing X-ray intensity or relative amount determined by electron microprobe analysis. Those products in the numerator represent the surface scale and those in the denominator indicate the internal oxidation or subscale products.

(b) Estimate based on previous work.

143

## 4.4 Oxidation of René Y

The superior oxidation resistance displayed by René Y during the course of
this investigation has prompted additional studies to determine the basis for
its behavior.

### 4.4.1 René Y Versus Hastelloy X

René Y is basically a modified Hastelloy X containing 0.15 w/o lanthanum and
additional manganese to 1.0 w/o. Although the modifications are slight, the
following improved oxidation features were observed in the course of this
investigation:

      (a)   Increased scale adherence

      (b)   Stabilized oxide scale in a dynamic environment

      (c)   Decreased oxidation rate

To establish if differences in the composition of the oxide scales could promote
this improved behavior, electron microprobe and X-ray fluorescence analyses
were conducted. EMX traces obtained from both Hastelloy X and René Y after
a static air exposure at 2000°F for 100 hours are illustrated in Figure 65.
Although the base metal compositions are similar, the composition of the
oxide phases differed considerably. The 1.0 w/o manganese originally present
in René Y builds up in the oxide to 20-30 w/o as verified by X-ray emission
analysis, whereas the 0.7 w/o manganese present in Hastelloy X concentrates
to only 6 w/o in the oxide scale. Similarly, the concentration of chromium
and nickel in the oxide scale of René Y is considerably less than Hastelloy X.
Thus, René Y exhibits an oxide of $Cr_2O_3$ overgrown with $MnCr_2O_4$ with no nickel
in solution. Hastelloy X, on the other hand, exhibits an oxide consisting of
$NiCr_2O_4$ spinel overgrown with $(Cr,Mn)_2O_3$. On the basis of flame tunnel tests
conducted on these two materials, it can be concluded that the $MnCr_2O_4$ spinel
overgrowth minimizes the volatilization of $Cr_2O_3$ and stabilizes the oxide scale.

The increase in the concentration of manganese in the oxide scale of René Y
is not considered simply the result of additional manganese since it contains
only 0.2 w/o more than Hastelloy X. Rather, it is postulated that the activity
of the manganese is increased by the small amount of lanthanum present in the
alloy. The microprobe analysis also shows that lanthanum effectively reduces
the participation of nickel in the oxide scale. Previous studies at this
laboratory on a René Y alloy with lanthanum but without manganese support
this hypothesis since a $Cr_2O_3$ oxide was promoted with no evidence of a $NiCr_2O_4$
spinel, which would be the expected oxide product.

144
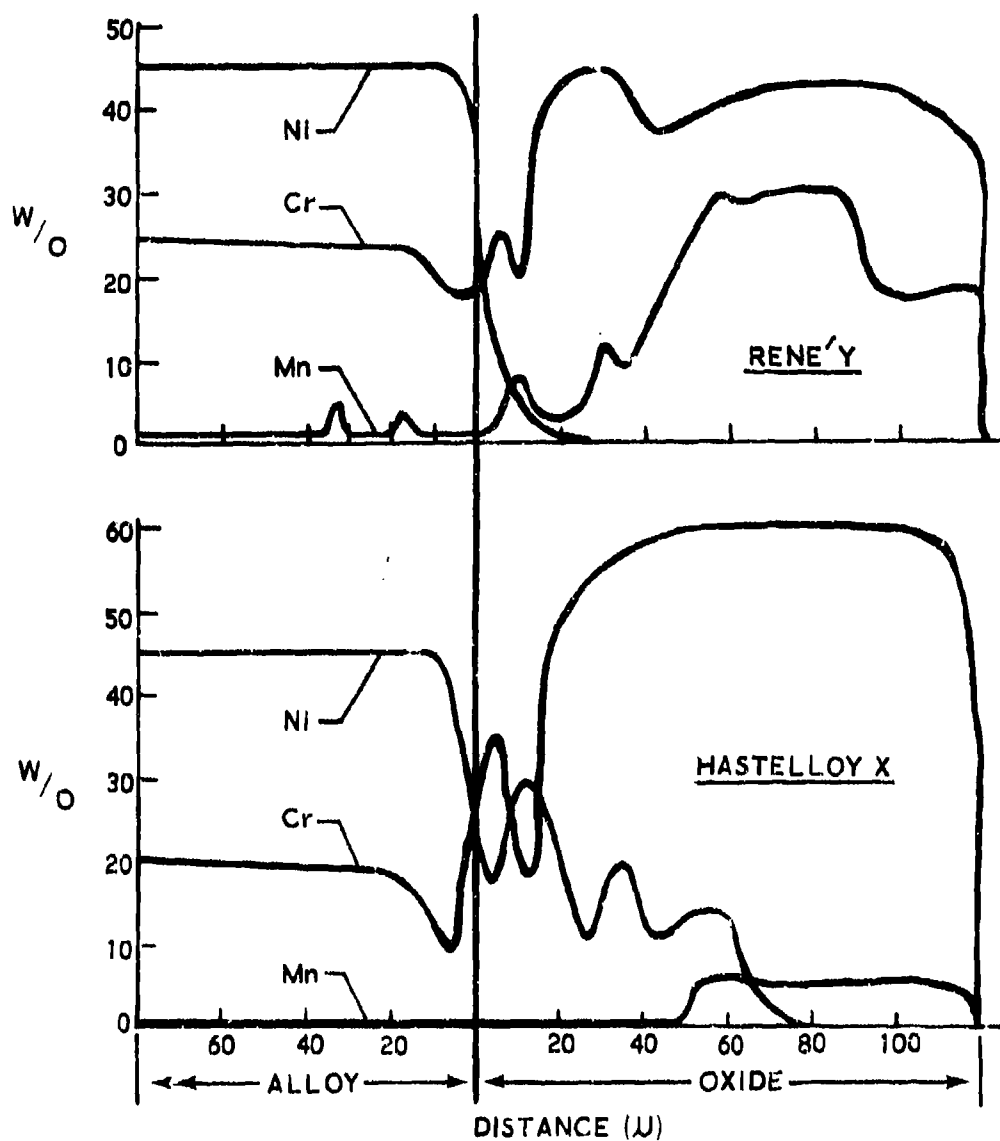
**FIGURE 65**   Results of Microprobe Analysis for René Y and Hastelloy X After 100 Hours Exposure at 2000°F

Observe the Presence of $MnCr_2O_4$ Spinel Oxide (24 w/o Mn + 46 w/o Cr) on the surface at René Y versus a $Cr_2O_3$ oxide (60 w/o Cr + 5 w/o Mn) on the surface of Hastelloy X. Both alloys have comparable amount of Mn.

19

### 4.4.2 Role of Lanthanum in René Y

A study was also made to determine the distribution of lanthanum in René Y and the manner in which it participates in the oxidation reaction. This study was considered necessary to determine the role of lanthanum in improving the oxidation behavior of Hastelloy X.

A thorough analysis of the René Y base material employing the microprobe revealed lanthanum-rich particles (which were not oxides) located primarily in grain boundaries and associated with base metal carbides. A wavelength scan across the particles indicated relatively high concentrations of molybdenum, silicon, lanthanum, and carbon. The fact that the lanthanum-rich particles revealed no more oxygen than the matrix and the absence of particle fluorescence when probed by the EMX was considered sufficient evidence to indicate that the particles were not oxides. The particles could be detected metallographically but always appeared diffuse or in relief. Attempts to extract the particles for X-ray diffraction analysis were not successful since an X-ray fluorescence analysis of the extracted residues did not detect La. Since the rare-earth carbides do decompose in air to form acetylene, it is postulated that the lanthanum-containing particles are complex Mo-Si-La carbides which are not stable when exposed to air.

A number of microprobe analyses were conducted on the surface oxide and at the oxide/metal interface to determine the lanthanum distribution. The results of this investigation are summarized schematically in Figure 66. In the center of this figure is a schematic of the oxide formed on René Y. Each numbered dashed line represents probe traces for lanthanum with the lanthanum concentration profile presented parallel to the trace. The results showed significant lanthanum concentrations only in the cusps or fingers of the oxide scale which extend into the matrix metal and not in the internal grain boundary oxides or the scale per se. These results were verified by taking microprobe analyses across several locations along the scale/metal interface. Thus, the results support grain boundary "keying" as the mechanism for increased scale adherency. Investigations were also conducted using the electron microscope to determine if La-containing oxide films were formed along the oxide/metal interface. No indications of such films were found.

On the basis of these findings, the following mechanism is postulated to explain the enhanced oxidation resistance of René Y. The lanthanum originally present as a carbide phase goes into solution during oxidation providing a continuing source of lanthanum. The lanthanum diffuses to the oxide/metal interface where it concentrates at the grain boundary cusps adjacent to the oxide. These La-rich cusps then serve as mechanical "keys" with the matrix

FIGURE 66    Microprobe Analysis of René Y for La Detection

C66061737

147

to minimize the interfacial oxide/metal shear stress and improve oxide adherence. The lanthanum also alters the activity and/or diffusivity of the nickel, chromium, and manganese in the alloy yielding a more stable spinel oxide, $MnCr_2O_4$ in the case of René Y. The latter reaction decreases oxide volatilization and improves oxidation resistance, particularly in dynamic environments.

## 4.5 Effects of Surface Preparation

A limited study was initially intended to establish if variations in surface finish grossly affect the oxidation behavior of Ni-base alloys. Due to the complexity of the behavior actually observed, however, the scope was expanded considerably to characterize the main factors which govern the effects of surface preparation.

### 4.5.1 Static and Continuous Weight Gain Oxidation

Specimens used for this study were given three different finishes which resulted in different degrees of roughness and surface deformation. They were electropolished, dry grit blasted, and coarse wet ground. The roughness of the resulting surfaces were measured with a Profilometer and the average values obtained are listed below:

| | | |
|---|---|---|
| Electropolished | | $3\mu \pm 1$ RMS |
| Grit Blasted | (150 grit $Al_2O_3$) | $55\mu \pm 10$ RMS |
| Wet Ground | (50 grit $SiO_2$) | $130\mu \pm 20$ RMS |

The scatter in the measured roughness not only reflects variations in the abrasion resistance of the alloys but also the extent of surface finish reproducibility. Specimens were lightly rinsed in methanol-10% HCl, rinsed in ethanol, and oxidized in electric box furnaces for 100 and 400 hours at 1600, 1800, and 2000°F.

The appearance of the specimens after testing showed:

(a) Significant differences in the color of the oxides produced on specimens with different finishes. The largest differences were observed between electropolished and grit blasted specimens.

(b) Generally, specimens in the electropolished condition displayed the greatest degree of oxide spalling, at times exhibiting gross exfoliation of the surface scale.

148

The weight changes, amount of oxidation, and $\gamma'$ dissolution were measured
for each alloy as a function of time, temperature, and surface finish and
are presented in Table XXXVII. These data did not exhibit consistent
effects as a function of the test variables. However, there were general
trends and some specific data indicating that grit-blasted finishes produced
accelerated attack. The apparent conflicts in the results were of such a
nature as to necessitate a metallographic re-evaluation on the anomalous
specimens. The extent of oxidation in these duplicates were found to
reasonably agree with the original measurements. Hence, specimen mis-identification
was discounted as the cause of the apparent anomalies. It was noted, however,
that grit blasting and coarse grinding did produce a more irregular type of
attack which in some cases made assessment of the extent of attack difficult.

There were certain instances where oxidation behavior was definitely affected
by surface preparation. A typical example is illustrated by IN-100 in
Figures 67 and 68. In this instance a grit blasted surface produced exces-
sive grain boundary oxidation after 400 hours at 1800°F, however the effect
was not observed after shorter times of exposure and was minimized after
exposure to 2000°F (see Figure 67 and 68). A similar behavior was observed
in cast Inco 713C but not in the wrought alloys U-700 and René 41.

The results of X-ray diffraction analysis to identify the oxides formed as
a function of surface preparation (namely electropolished and grit blasted)
are summarized in Table XXXVIII after 400 hours exposure at 1600, 1800, and
2000°F. Contrary to expectation, large differences were not observed in the
oxides formed on the two extreme surface finishes. There were indications,
however, that Cr-base oxides were favored on grit-blasted surfaces for all
alloys except IN-100. For IN-100 an increase in Al and Ti-containing oxides
was indicated for the grit blasted specimens. However, microprobe traces
obtained from identical specimens did not display any pronounced scale
composition differences as compared to fine ground specimens. In an attempt
to clarify the behavior reflected in these observations, the following
additional tests were performed:

(a) Continuous weight-gain testing of grit-blasted IN-100 and Inco 713C
    at 1800°F to further establish the effect of $O_2/N_2$ pickup and determine if a
    transition time existed for good to poor oxidation resistance.

(b) Static oxidation of both cast and wrought U-700 to determine if the form
    of the alloy was an influencing factor.

(c) Oxidation of grit blasted IN-100 and Inco 713C for 400 hours at 1800°F
    with a pre-oxidation argon anneal (8 hours at 2000°F) to establish if
    surface roughness per se or cold work was responsible for the detrimental
    effect observed.

149

## TABLE XXXVII

### EFFECT OF SURFACE PREPARATION ON OXIDATION[a]

| Time/ Temp °F | Type Preparation | IN-100 Weight Gain mg/cm² | Average IO Mils/Side | γ' Dissolution Mils/Side | Inco 713C Weight Gain mg/cm² | Average IO Mils/Side | γ' Dissolution Mils/Side | U-700 Weight Gain mg/cm² | Average IO Mils/Side | γ' Dissolution Mils/Side | René 41 Weight Gain mg/cm² | Average IO Mils/Side | γ' Dissolution Mils/Side |
|---|---|---|---|---|---|---|---|---|---|---|---|---|---|
| 100/1600 | Electropolish | 0.52 | 0.10 | 0.35 | 0.14 | 0.25 | 0.25 | 0.43 | 0.40 | 0.55 | - | 0.80 | 1.00 |
|  | Coarse Ground | 1.85 | 0.55 | 0.55 | 0.44 | 0.15 | 0.20 | 0.39 | 0.40 | 0.55 | - | 1.20 | 1.60 |
|  | Grit Blast | 2.91 | 0.50 | 0.70 | 0.37 | 0.30 | 0.55 | 0.40 | 0.50 | 0.60 | - | 0.50 | 0.80 |
| 400/1600 | Electropolish | 1.50(s) | 0.35 | 0.80 | 0.39(s) | 0.02 | 0.10 | 0.55(s) | 0.55 | 0.75 | - | - | - |
|  | Coarse Ground | 2.10 | 0.65 | 1.00 | 1.23 | 0.15 | 0.25 | 1.59 | 0.50 | 0.80 | - | - | - |
|  | Grit Blast | 1.18 | 0.60 | 1.00 | 0.75 | 0.10 | 0.20 | 1.41 | 0.65 | 0.80 | - | - | - |
| 100/1800 | Electropolish | 0.93 | 0.45 | 0.65 | 0.27(s) | 0.20 | 0.20 | - | 0.50(b) | 0.30 | 1.82 | 1.00 | 1.20 |
|  | Coarse Ground | 1.08 | 0.55 | 0.85 | 0.28 | 0.10 | 0.20 | - | - | - | 1.83 | 0.90 | 1.00 |
|  | Grit Blast | 0.83 | 0.30 | 0.65 | 0.93 | 0.20 | 0.35 | - | 0.00 | 0.30 | 1.93 | 1.20 | 1.40 |
| 400/1800 | Electropolish | 1.69(s) | 0.10 | 0.30 | 0.76(s) | 0.20 | 0.40 | - | 0.00 | 0.20 | 3.68(s) | 1.50 | 2.10 |
|  | Coarse Ground | 1.15(s) | - | 0.35 | 1.05(s) | - | 0.20 | - | 0.00 | 0.30 | 3.36(s) | 1.65 | 2.00 |
|  | Grit Blast | 5.70(ss) | 1.75 | 2.75 | 2.61(s) | 1.50 | 2.50 | - | 0.00 | 0.50 | 2.65(s) | 1.90 | 2.60 |
| 100/2000 | Electropolish | 0.53(s) | 0.10 | 0.25 | 0.48(s) | 0.25 | 0.35 | 0.94(s) | 0.25 | 1.70 | - | - | - |
|  | Coarse Ground | 0.89(s) | 0.35 | 0.50 | 0.35(s) | 0.15 | 0.40 | 1.36(s) | 0.30 | 1.45 | - | - | - |
|  | Grit Blast | 0.83(s) | 0.50 | 0.80 | 0.79(s) | 0.50 | 0.80 | 1.10(s) | 0.45 | 1.10 | - | - | - |
| 400/2000 | Electropolish | 1.41(ss) | 0.60 | 0.80 | 0.93(ss) | 0.20 | 0.40 | 2.63(s) | 0.70 | 2.40 | - | - | - |
|  | Coarse Ground | 1.85(ss) | 1.00 | 1.20 | 0.75(s) | 0.80 | 0.80 | 2.29(s) | 0.80 | 2.60 | - | - | - |
|  | Grit Blast | 2.17(ss) | 0.50 | 0.60 | 1.22(s) | 0.60 | 0.80 | 2.91(ss) | 0.80 | 2.00 | - | - | - |

(s) - Spalled; (ss) - Severe Spalling

(a) - All metallographic measurements are averages of two specimens mounted on taper and vertical sections. (Accuracy = ± 0.25 Mil)

(b) - Primarily IGO

150

IN-100 Grit Blasted (100X)    N-162

IN-100 Electropolished (250X)    F-3976

FIGURE 67    The Effect of Surface Preparation on the Internal Oxidation of IN-100 Exposed
400 Hrs/1800°F in Air.  4:1 Taper Etched In 2% Chromic.
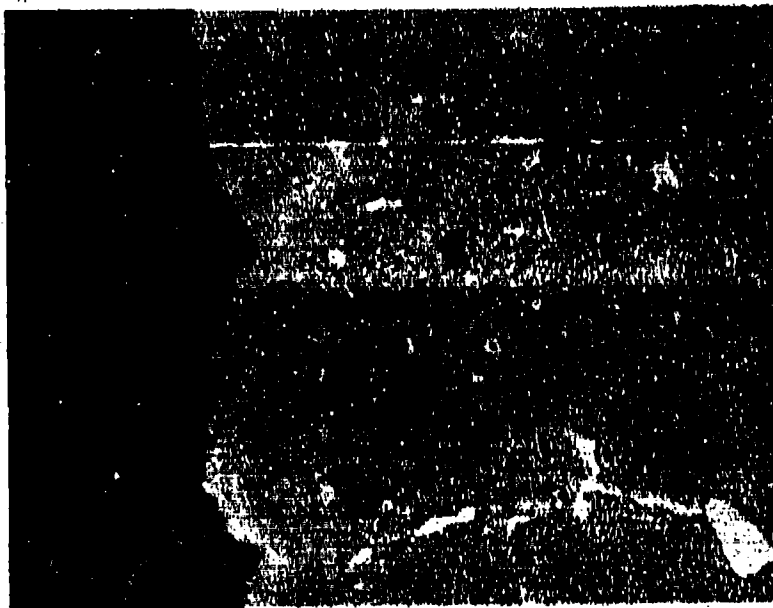
N-169

IN-100 Electropolished



N-167

IN-100 Grit Blasted

FIGURE 68    Effect of Surface Preparation on Oxidation of IN-100 After 400 Hrs/2000°F Exposure in Air.
250X    4:1 Taper    Etched in 2% Chromic

TABLE XXXVIII

## OXIDES FORMED AS A FUNCTION OF SURFACE PREPARATION

| Alloy | Time/Temp (Hrs)(°F) | Surface Condition | Oxides |
|---|---|---|---|
| Inco 713C | 400/1600 | Electropolish | $\alpha$-Al$_2$O$_3$, Cr$_2$O$_3$, TiO$_2$, NiAl$_2$O$_4$ (a$_0$=8.12), NiCr$_2$O$_4$ (a$_0$=8.32) |
| | | Grit Blast | $\alpha$-Al$_2$O$_3$, Cr$_2$O$_3$, TiO$_2$, NiCr$_2$O$_4$ (a$_0$=8.32) |
| | 400/1600 | Electropolish | $\alpha$-Al$_2$O$_3$, NiAl$_2$O$_4$ (a$_0$=8.11), Cr$_2$O$_3$, TiO$_2$ |
| | | Grit Blast | Cr$_2$O$_3$, $\alpha$-Al$_2$O$_3$, TiO$_2$, Ni(Cr,Al)$_2$O$_4$ (a$_0$=8.24) |
| | 400/2000 | Electropolish | $\alpha$-Al$_2$O$_3$, NiAl$_2$O$_4$ (a$_0$=8.06), TiO$_2$ |
| | | Grit Blast | $\alpha$-Al$_2$O$_3$, NiAl$_2$O$_4$ (a$_0$=8.06), TiO$_2$, NiO, NiCr$_2$O$_4$ (a$_0$=8.35) |
| IN-100 | 400/1600 | Electropolish | NiO, NiCr$_2$O$_4$ (a$_0$=8.32), TiO$_2$, NiTiO$_3$ |
| | | Grit Blast | TiO$_2$, NiCr$_2$O$_4$ (a$_0$=8.32), NiTiO$_3$, $\alpha$-Al$_2$O$_3$ |
| | 400/1800 | Electropolish | TiO$_2$, NiAl$_2$O$_4$ (a$_0$=8.07), NiCr$_2$O$_4$ (a$_0$=8.26), $\alpha$-Al$_2$O$_3$, Cr$_2$O$_3$*, AlN* |
| | | Grit Blast | TiO$_2$, Ni(AlCr)$_2$O$_4$ (a$_0$=8.21), NiTiO$_3$ |
| | 400/2000 | Electropolish | NiCr$_2$O$_4$ (a$_0$=8.31), NiAl$_2$O$_4$ (a$_0$=8.09), NiTiO$_3$, TiO$_2$ |
| | | Grit Blast | NiAl$_2$O$_4$ (a$_0$=8.15), TiO$_2$, NiTiO$_3$, NiCr$_2$O$_4$ |
| U-700 | 400/1600 | Electropolish | TiO$_2$, $\alpha$-Al$_2$O$_3$, Cr$_2$O$_3$ |
| | | Grit Blast | Cr$_2$O$_3$, TiO$_2$, $\alpha$-Al$_2$O$_3$, NiCr$_2$O$_4$ (a$_0$=8.30) |
| | 400/2000 | Electropolish | TiO$_2$, Ni(Cr,Al)$_2$O$_4$ (a$_0$=8.18), $\alpha$-Al$_2$O$_3$, Cr$_2$O$_3$ |
| | | Grit Blast | TiO$_2$, Ni(Cr,Al)$_2$O$_4$ (a$_0$=8.12), $\alpha$-Al$_2$O$_3$, Cr$_2$O$_3$ |
| René 41 | 400/1800 | Electropolish | Cr$_2$O$_3$, TiO$_2$, NiCr$_2$O$_4$ (a$_0$=8.29) |
| | | Grit Blast | Cr$_2$O$_3$ |

*The Cr$_2$O$_3$ and AlN phases indicated are coincident with NiTiO$_3$.

153

(d) High velocity flame tunnel tests on all alloys at 1800°F in the grit
blasted and fine gound condition to determine if the surface preparation
effect persisted in a high velocity air flow.


The continuous weight-gain data for grit-blasted IN-100, Inco 713C, and
U-700 (sheet) are presented in Table XA. Log-log plots of the results for
IN-100 and Inco 713C are shown in Figure 69 and compared to results from
electropolished specimens. Grit-blasted IN-100 displayed results which
contradicted the static test results after 100 hours. This test also
indicated a significant effect of surface preparation on both weight change
and weight-gain kinetics. The oxidation rate of the grit-blasted specimen
was near linear, whereas the electropolished specimen displayed near parabolic
oxidation. This would indicate that the grit-blasted specimen did not form a
protective oxide. This fact is supported by metallographic observations where
excessive nitride formation was also observed. Continuous weight-gain tests
of Inco 713C and U-700 indicated little or no effect of surface preparation, in
agreement with previous static test results after 100 hours exposure.


Tests were also conducted to establish if the effect observed was caused by
surface roughness per se or if the resultant surface deformation was a prime
factor. Prior to exposure, Inco 713C and IN-100 specimens were grit blasted
and one set annealed for 8 hours in argon. This yielded surfaces of equivalent
roughness but with different degrees of surface deformation. The results of
internal oxidation measurements after testing are presented in Table XXXIX,
which indicates that the surface preparation effect is largely attributed to
cold work and not roughness per se. The effect is vividly illustrated by the
microstructures shown in Figure 70. To further establish differences in the
surface deformation with each type of preparation (grit blast, fine grinding,
and coarse grinding), back reflection Lave X-ray diffraction patterns were
taken of the surfaces. In the fine ground condition (600 grit) Debye rings
and spots were observed. Patterns of coarse ground surfaces (50 grit) produced
a more diffuse pattern with only faint remnants of Debye rings. The grit-blasted
specimen, however, gave no pattern at all, indicating a highly cold-worked
surface. The extent of this cold work was sufficient to produce recrystal-
lization of the alloys. With the proper etching procedure a fine grained,
evidently recrystallized, structure could be observed in the $\gamma'$ depletion zone.
This structure seemed most prevalent in cast materials.


The influence of surface preparation effects on alloys of different form (i.e.,
wrought and cast) is demonstrated by tests performed on wrought and cast U-700.
The internal oxidation measurements obtained after exposures of 100 and 400
hours at 1800°F are presented in Table XL and representative microstructures
illustrated in Figure 71. These results indicated that for relatively short
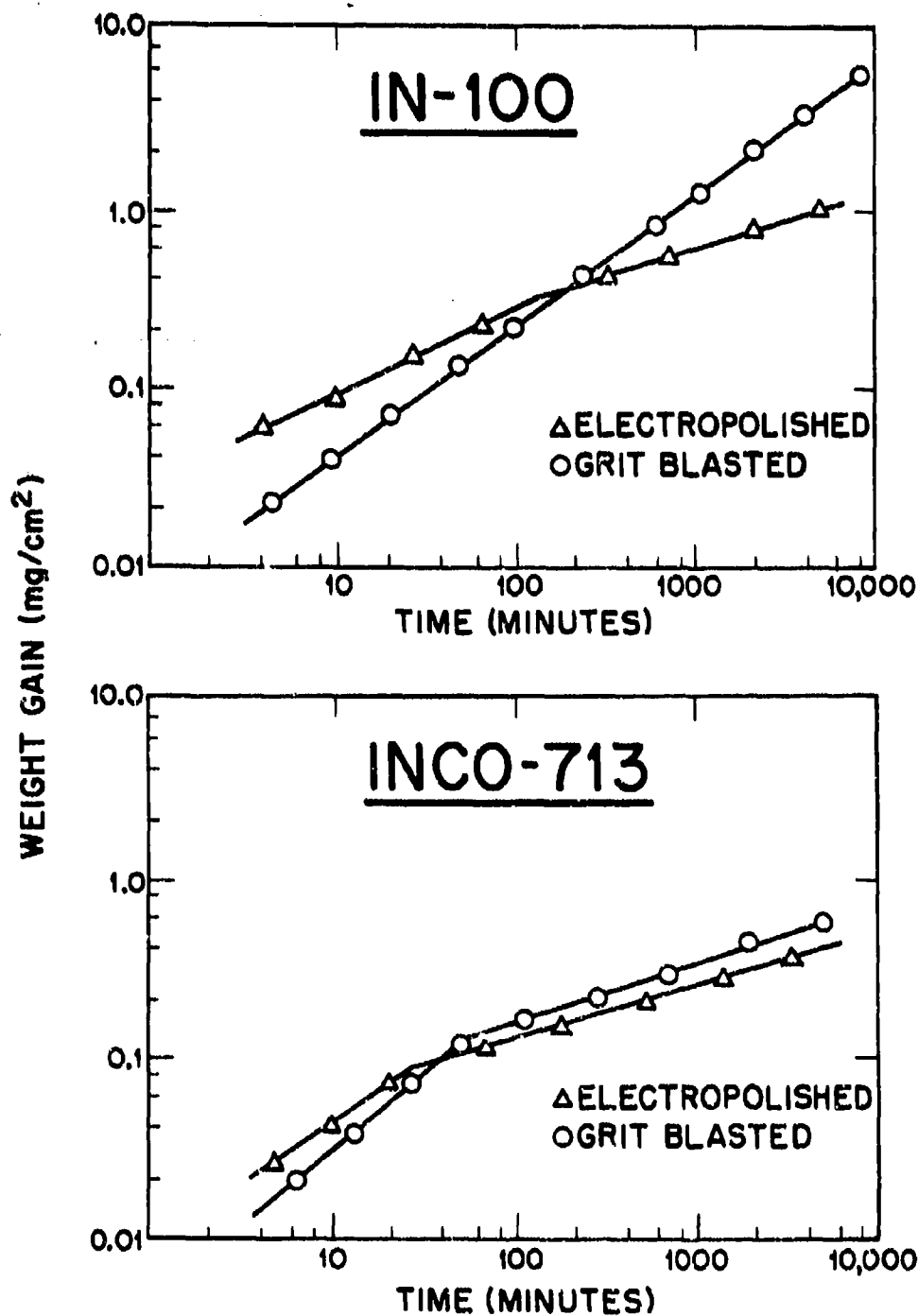
FIGURE 69   The Continuous Weight-Gain Behavior of IN-100 and Inco 713C
As A Function of Surface Preparation

155

## TABLE XXXIX

### INFLUENCE OF HEAT TREATMENT ON SURFACE PREPARATION EFFECT

#### INCO 713C

| Time/Temp (Hrs)(°F) | Condition | Average I.O. Mils/Side | $\gamma'$ Dissolution Mils/Side |
|---|---|---|---|
| 100/1800 | Grit Blast + Heat Treated * | 0.00 | 0.30 |
| 100/1800 | Grit Blast | 0.20 | 0.35 |
| 400/1800 | Grit Blast + Heat Treated * | 0.00 | 0.40 |
| 400/1800 | Grit Blast | 1.50 | 2.50 |

#### IN-100

| Time/Temp (Hrs)(°F) | Condition | Average I.O. Mils/Side | $\gamma'$ Dissolution Mils/Side |
|---|---|---|---|
| 100/1800 | Grit Blast + Heat Treated * | 0.00 | 1.00 |
| 100/1800 | Grit Blast | 0.30 | 0.65 |
| 400/1800 | Grit Blast + Heat Treated * | 0.50 | 1.20 |
| 400/1800 | Grit Blast | 1.75 | 2.75 |

* Heat treated 8 hours at 2000°F in argon prior to exposure.
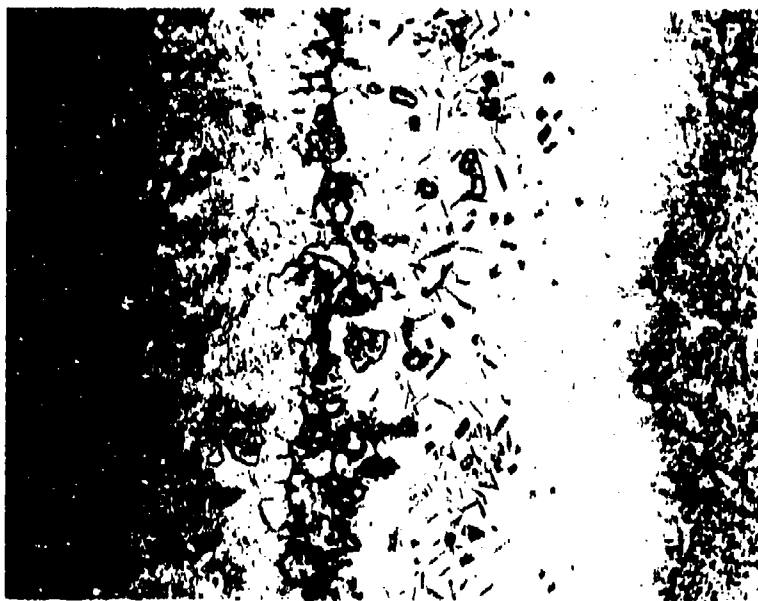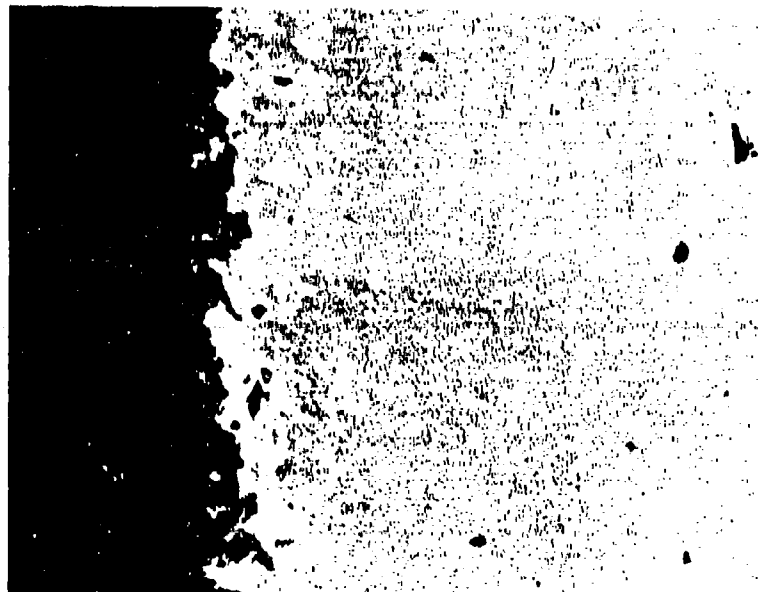
M-7014

Inco 713C  Grit Blasted Plus
HT 8 Hrs/2000°F in Argon



M-4226

Inco 713C  Grit Blasted

FIGURE 70  Removal of Surface Preparation Effect by Heat Treatment. Exposed 400 Hrs/1800°F in Air.
250x  4:1 Taper  Etched in 2% Chromic

**TABLE XL**

## INFLUENCE OF ALLOY FORM ON SURFACE PREPARATION EFFECT

| Time/Temp (Hrs)(°F) | Surface Condition | Wrought U-700 | | Cast U-700 | |
|---|---|---|---|---|---|
| | | Average I.O. Mils/Side | γ' Dissolution Mils/Side | Average I.O. Mils/Side | γ' Dissolution Mils/Side |
| 100/1800 | Electropolished | 0.50(a) | 0.30 | 1.20 | 0.80 |
| 100/1800 | Grit Blast | 0.00 | 0.30 | 2.50(a) | 0.80 |
| 400/1800 | Electropolished | 0.00 | 0.20 | 0.00 | 0.30 |
| 400/1800 | Grit Blast | 0.00 | 0.50 | 0.00 | 0.50 |
| 400/1800 | Coarse Ground | 0.00 | 0.30 | 4.00(a)(b) | 2.50(a) |

(a) Irregular

(b) Primarily I.G.O.
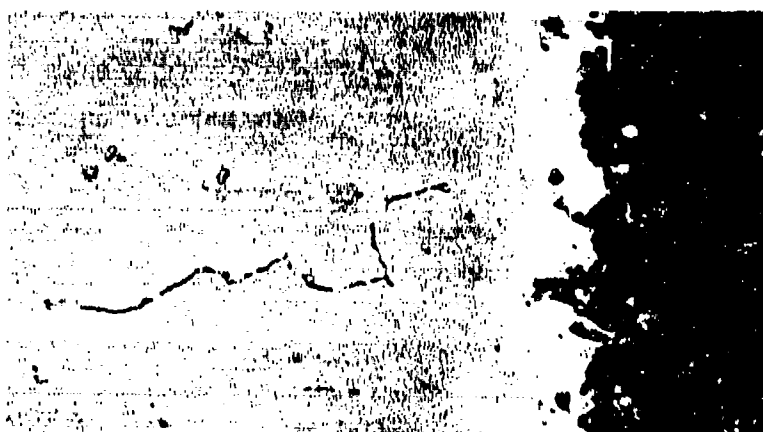
U-700 Cast
Grit Blasted
100/1800°F

M-7019
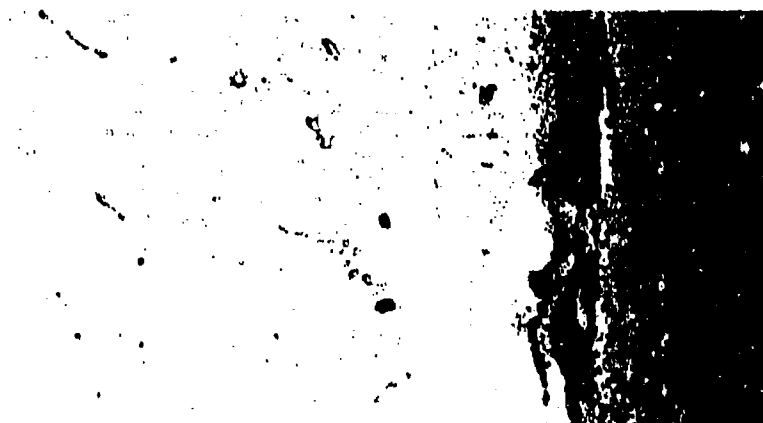
U-700 Cast
Electropolished
100/1800°F

M-6585
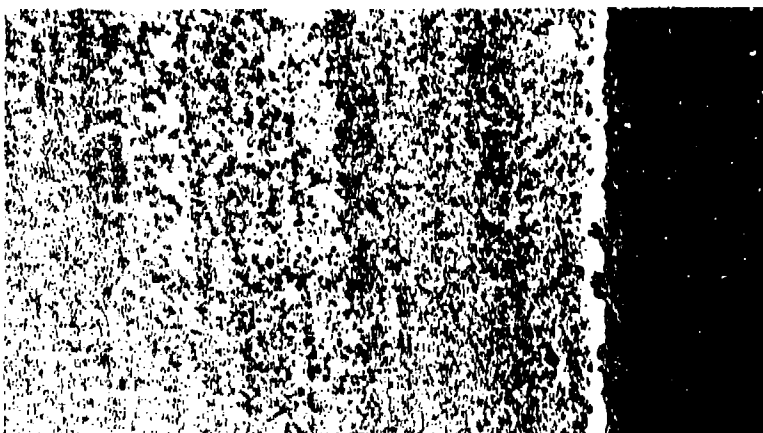
U-700 Wrought
Electropolished
100/1800°F

M-6581

FIGURE 71     Influence of Alloy Form on Surface Preparation Effect
250X     4:1 Taper     Etched in 2% Chromic

exposures the cast alloy was most susceptible to deformation-induced oxidation but the effect appeared to vanish after longer exposure times. The type of attack usually casued by surface deformation of U-700 was highly localized and usually present as I.G.O. as typified by Figure 71. It was also observed that for equivalent surface preparations the cast material always displayed inferior resistance.

### 4.5.2 Flame Tunnel Oxidation

The influence of surface preparation on the oxidation behavior of René Y, René 41, U-700 (sheet), IN-100, SM-200, and Inco 713C in high velocity natural gas combustion products was evaluated. The general appearance of the specimens after 100 hours exposure at 1800°F is illustrated in Figure 72 and the weight change results for the cast and wrought alloys are plotted in Figures 73 and 74, respectively. For the wrought alloys, increased surface deformation/roughness caused an increase in weight gain. Since the shapes of the weight-gain curves for the grit-blasted and fine-ground specimens were similar for each alloy, the effect could simply be attributed to the larger effective surface area of the grit-blasted specimen. The cast alloys, on the other hand, displayed an opposite trend. Except for Inco 713C, the fine gound surface exhibited a greater net weight gain. However, the appearance of the grit-blasted specimens showed more severe oxidation, indicating that weight change may not be a good measure of oxidaton resistance in the flame tunnel test.

The extent of internal oxidation exhibited by each alloy for the two surface finishes are shown in Figures 75 through 80. The effect of surface preparation on internal reaction is less severe in a dynamic as compared to a static atmosphere. As in the latter case, the specific effect of surface prepation is unpredictable. For example, grit blasting appeared to promote internal oxidation for IN-100 and Inco 713C but the opposite effect was observed for SM-200. Also, grit blasting produced increased internal oxidation and recrystallization for René 41 and U-700, but for René Y produced a noticeable decrease in the intergranular type oxidation which normally forms.

The reaction produces which formed during the flame tunnel exposure were identified employing Debye Scherrer patterns of scraped oxides. The results are tabulated in Table XXXXI. The absence of Cr-base oxides and the predominance of the perovskite-type $NiTiO_3$ oxide are the main features displayed. With two exceptions, no gross differences are noted in the reaction products formed as a function of surface treatment. The two alloys which displayed the greatest difference in the type of reaction products formed, namely U-700 and Inco 713C, were the two most similar alloys with respect to weight gain.

C66102720

IN-100
(VD-582/3)

Inco 713C
(601)

René 41
(TV-394)

U-700
(Ast. Sheet)

René Y
(64-711)

SM-200
(34V2804)

600 Grit

Grit Blast
(150 Grit)
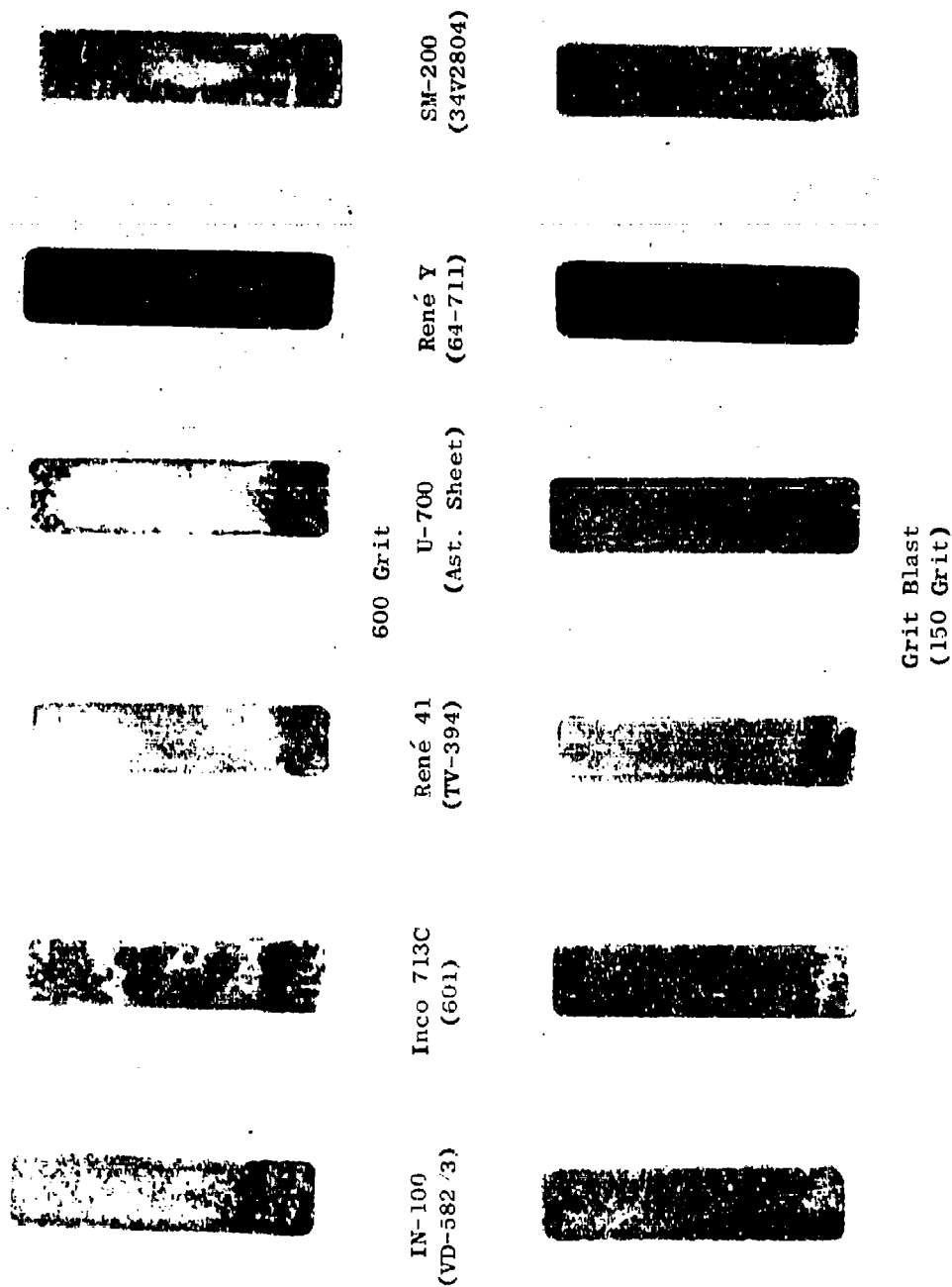
FIGURE 72   Effect of Surface Finish on the General Appearance During 100-Hour Exposure in the Flame Tunnel
At 1800°F.

161
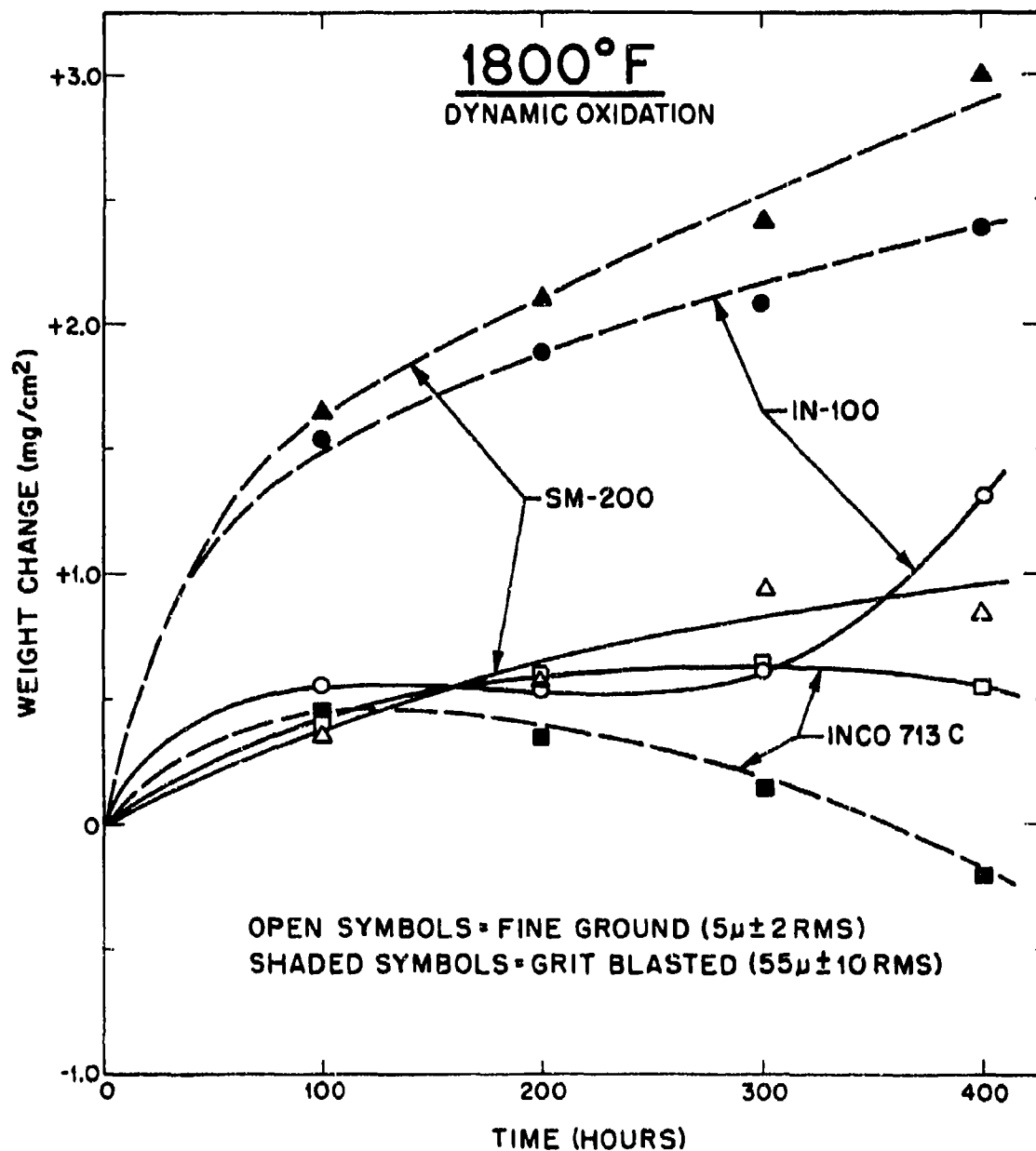
**FIGURE 73** The Effect of Surface Preparation on the Weight-Gain Behavior of Cast Alloys During Flame Tunnel Exposure at 1800°F
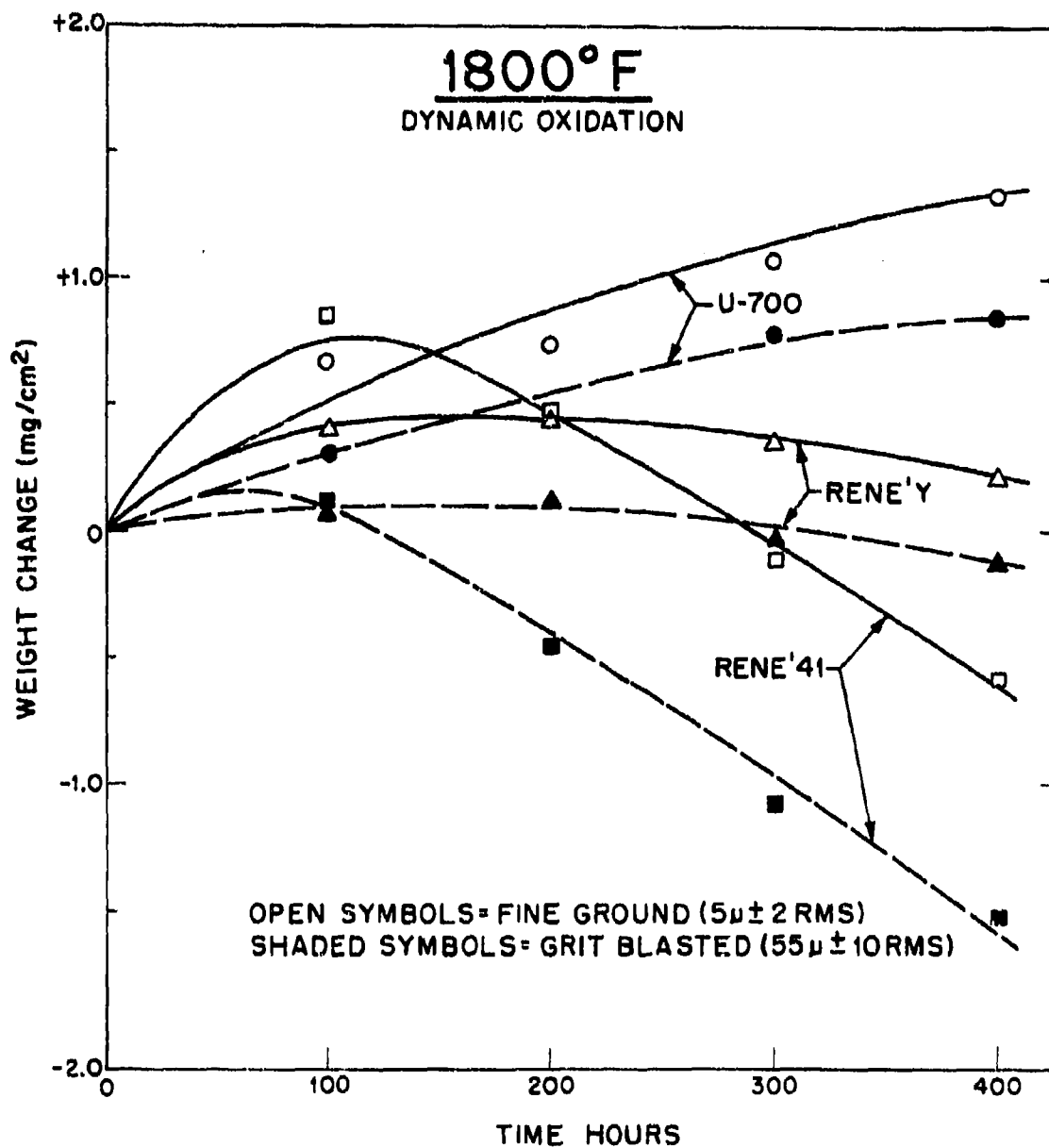
FIGURE 74    The Effect of Surface Preparation on the Weight-Gain Behavior
of Wrought Alloys During Flame Tunnel Exposure at 1800°F

163

(a)   René Y Fine Ground Surface

N-68



(b)   René Y Grit Blasted Surface

N-69

FIGURE 75    Typical Scale and Internal Reaction as a Function of Surface
             Preparation for René Y After 200 Hr. Exposure in the Flame
             Tunnel at 1800°F      2% Chromic      500X      4:1 Taper

164

N-116

(a)  U-700 Fine Ground Surface



N-118

(b)  U-700 Grit Blasted Surface

FIGURE 76    Typical Scale and Internal Reaction As A Function of Surface
             Preparation for U-700 After 200 Hr. Exposure in the Flame
             Tunnel at 1800°F        2% Chromic        250X      4:1 Taper

N-111

(a) René 41 Fine Ground Surface
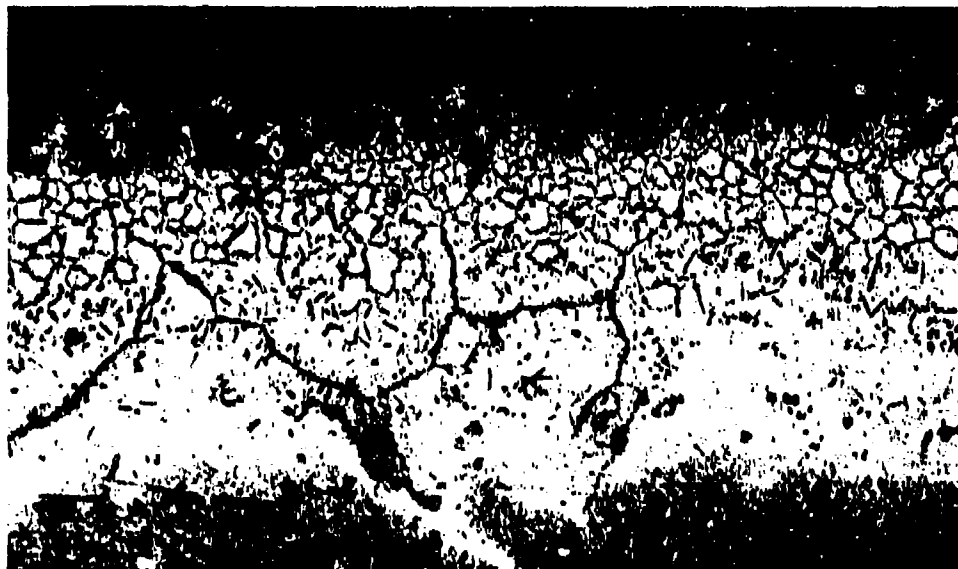


N-112

(b) René 41 Grit Blasted Surface

FIGURE 77   Typical Scale and Internal Reaction As a Function of Surface
Preparation for René 41 After 200 Hr. Exposure in the Flame
Tunnel at 1800°F.   2% Chromic   250X   4:1 Taper
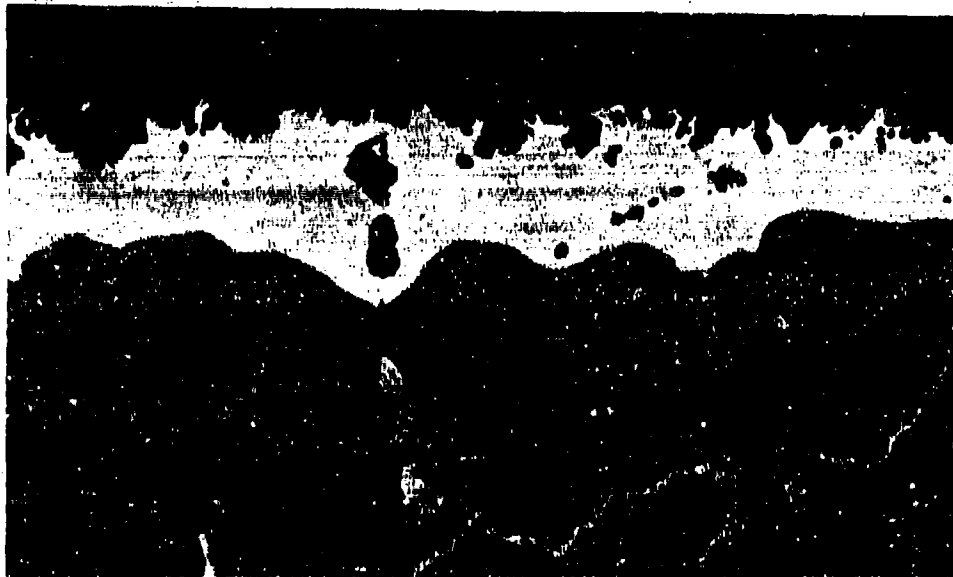
N-126

(a)  IN-100 Fine Ground Surface



N-127

(b)  IN-100 Grit Blasted Surface

FIGURE 78    Typical Scale and Internal Reaction as a Function of Surface
             Preparation for IN-100 After 200 Hr. Exposure in the Flame
             Tunnel at 1800°F              2% Chromic           250x    4:1 Taper

(a) SM-200 Fine Ground Surface

(b) SM-200 Grit Blasted Surface

FIGURE 79    Typical Scale and Internal Reaction As a Function of Surface
Preparation for SM-200 After 200 Hr. Exposure in the Flame
Tunnel at 1800°F.        2% Chromic        250X        4:1 Taper

N-113

(a)   Inco 713C Fine Ground Surface
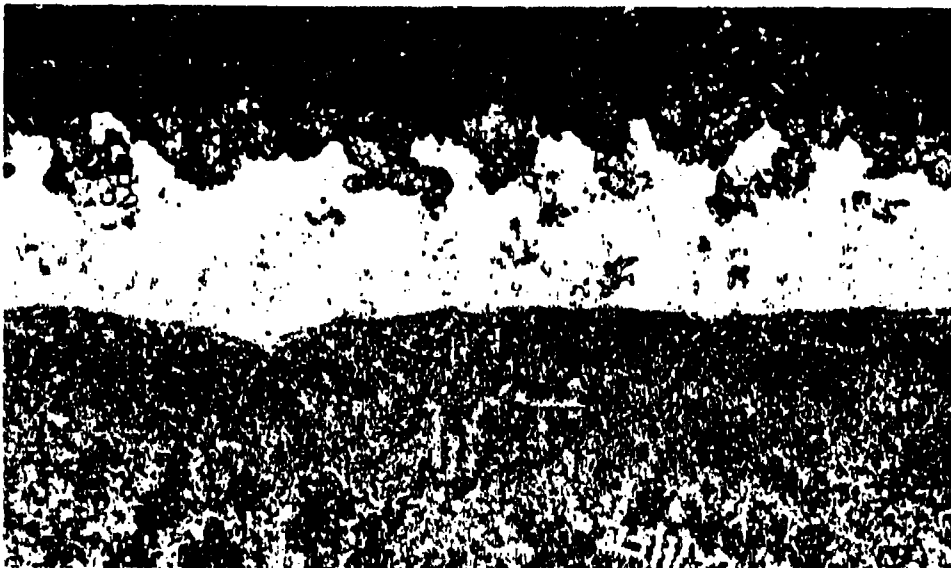


N-114

(b)   Inco 713C Grit   Blasted Surface

FIGURE 80   Typical Scale and Internal Reaction As a Function of Surface
Preparation for Inco 713C After 200 Hr. Exposure in the Flame
Tunnel at 1800°F.        2% Chromic          250X        4:1 Taper

## TABLE XLI

### X-RAY DIFFRACTION IDENTIFICATION OF REACTION PRODUCTS

### FORMED AS A FUNCTION OF SURFACE PREPARATION AFTER A 200 HR. EXPOSURE IN THE FLAME TUNNEL AT 1800°F

| Alloy | Condition | Reaction Products* |
|---|---|---|
| René Y | FG | $\alpha\text{-}Cr_2O_3$, $MnCr_2O_4$ ($a_O=8.47\text{Å}$) |
|  | GB | $\alpha\text{-}Cr_2O_3$, $MnCr_2O_4$ ($a_O=8.45\text{Å}$) |
| U-700** | FG | NiO ($a_O=4.24\text{Å}$), Spinel ($a_O=8.35\text{Å}$), $NiTiO_3$, $TiO_2$ |
|  | GB | $NiTiO_3$, $Ni(Cr,Al)_2O_4$ ($a_O=8.298\text{Å}$), $TiO_2$ |
| IN-100 | FG | $NiTiO_3$, $TiO_2$, Spinel |
|  | GB | $NiTiO_3$, Spinel ($a_O=8.29\text{Å}$), $TiO_2$ |
| SM-200 | FG | NiO, Spinel, $NiTiO_3$ |
|  | GB | NiO, $NiTiO_3$, Spinel ($a_O=8.365\text{Å}$) |
| Inco 713C | FG | NiO, $NiCr_2O_4$, $NiTiO_3$, $(Cr,Al)_2O_3$ |
|  | GB | $Al_2O_3$, $NiTiO_3$, $NiAl_2O_4$ ($a_O=8.08\text{Å}$), $Cr_2O_3$, NiO |

*As determined from Debye Scherrer patterns of scraped oxides.

**Sheet

170

From the combined results of static and dynamic tests the following general observations can be cited regarding the effect of surface preparation on the oxidation behavior:

(a) Effects produced by the various surface finishes can be attributed primarily to surface deformation and not to roughness per se.

(b) Increased surface deformation promotes internal oxidation. The effect is less severe in a dynamic atmosphere.

(c) The effect of surface deformation is most pronounced in cast as compared to wrought alloys.

(d) No large differences in the oxide scale composition have been noted as a function of surface deformation.

Although the general effects of surface preparation on the oxidation of these alloys have been determined, the specific mechanism(s) responsible for the effects has not been defined. The mechanism no doubt involves deformation-induced diffusion but establishing the exact mode would be difficult. This difficulty stems from the inconsistent results obtained and the many variables which appear to affect the process. Among the variables causing this complex behavior are:

(a) Temperature and time

(b) Alloy form (cast-vs-wrought)

(c) Alloy composition

(d) Uniformity of the surface finish

(e) Type of atmosphere (static-vs-dynamic)

A more critically designed experiment is considered necessary to separate these variables and characterize the surface preparation effect. Such an experiment was beyond the scope of this program.

171

# V  DISCUSSION

The results of the kinetics analyses performed indicated definite
similarities in the oxidation behavior of the alloys.  However, a true
kinetic characterization of the oxidation mechanisms was masked by the
complex interplay of heterogeneous oxidation, spalling, and oxide
volatilization.  In general, the linear oxidation observed reflects the
spontaneous nucleation or penetration of oxide colonies through the
initial oxide layer and subsequent coalescence or lateral growth to form
a relatively continuous phase as observed in the thin film studies.  The
parabolic oxidation rate is associated with continued oxide growth by
diffusion processes.  The slower parabolic or cubic rates observed are
indications of oxide interactions, porosity formation, and volatilization.
The decelerating kinetics observed for IN-100 and in some cases SM-200 and
Inco 713C denote oxide spalling or excessive volatilization.  The heter-
ogeneous nature of the oxidation observed on the cast alloys suggests that
two or more of these processes are occurring simultaneously at different
locations on the surface, thus further complicating the measured kinetics.
Hence, even if the atomic processes governing oxide growth could be ascertained
such models would be of little value in view of the intermixture of oxides
present.


It is well to emphasize here the lack of a direct relation between weight-gain
data and the extent of internal oxidation reactions.  The internal oxidation
process involves reactions between the less noble constituents of the alloy
and oxygen which has already reacted with the surface to form a scale.  The
weight gain reflects the amount of oxygen required to form the surface scale.
Subsequent solution of $O^=$ at the oxygen/metal interface through scale dis-
sociation and its diffusion into the metal to react with the least noble
solute it encounters involves no increase of mass by the sample and thus no
additional weight gain.  Hence, the weight gain does not reflect the extent
of internal oxidation per se.  This does not infer, however, that internal
oxidation reactions do not affect the scaling process indirectly by either
tying up the most reactive cations before they can be concentrated and
incorporated as part of the surface oxide or by providing a sink for the
oxygen ions which in effect causes a reduction in the scale thickness.

The microstructural changes observed in this study denote a critical relation between the scale and subscale reactions. In fact, the two processes are considered to be in direct conflict with each other with the final scale/subscale morphology controlled by thermodynamic factors. The affinities of the various constituents present in these alloys for oxygen and nitrogen at 1800°F are compiled in Table XXXXII[19]. Thermodynamically, the competitive oxidation reaction can be simply expressed as

$$AO_x + B \rightarrow BO_x + A$$

for which:

$$\Delta F_T = \Delta F_T^° + RT \ln \frac{a_{BO_x} \, a_A}{a_{AO_x} \, a_B}$$

Since the oxide activities can be assumed unity, the free energy change at a specific temperature is dependent upon the affinity of each element for oxygen and their corresponding activities in the alloy. Thus, although the concentration* (activity) of a specific element may be relatively low, its high affinity for oxygen may be sufficient to cause preferential oxide formation. The same is also true for elements with relatively low affinities for oxygen but high activities in the alloy. The oxide which is most thermodynamically favored will form first and exist as the surface oxide. Elements with lower concentrations but high affinities for oxygen will then oxidize internally if the decomposition of the surface oxide at the oxide/metal interface yields a higher partial pressure of oxygen than the dissociation pressure of the internal oxide being formed.

Specific examples of the critical nature of this scale/subscale reaction process have been demonstrated during this investigation. In the alloys studied, the elements most critical in the scale/subscale competition are Cr, Al, and to a lesser extent, Ti. During the oxidation of IN-100 (10.0 Cr, 5.8 Al, and 4.3 Ti) the relatively low activity of Cr and the high combined activities of Al and Ti resulted in the incorporation of the latter elements as subscale. No internal oxidation resulted because the dissociation pressures of $Al_2O_3$ and $TiO_2$ were less than any other oxide that could form. In fact, the high Ti content of the suboxide is considered responsible for the observed inferior oxidation behavior. SM-200 (10 Cr, 4.4 Al, and 2.0 Ti) on the other hand, displayed the same relative Cr activity as IN-100, but lower

---

*It is assumed for the sake of this discussion that concentration and activity are synonymous

173

TABLE XLII

THERMODYNAMIC PROPERTIES OF THE OXIDES AND NITRIDES AT 1800°F

| Element | Oxide $\Delta F$[a] | | $P$[b] | Nitride $\Delta F$ | | $P$[b] |
|---|---|---|---|---|---|---|
| Al | -207 | $Al_2O_3$ | $10^{-36}$ | -89.1 | AlN | $3 \times 10^{-16}$ |
| Ti | -177 | $TiO_2$ | $10^{-31}$ | -94.6 | TiN | $4 \times 10^{-17}$ |
| Si | -161 | $SiO_2$ | $10^{-28}$ | -32.0 | $Si_3N_4$ | $3 \times 10^{-8}$ |
| Cr | -135 | $Cr_2O_3$ | $10^{-23}$ | -19.5 | $Cr_2N$ | $4 \times 10^{-4}$ |
| Mo | -102 | $MoO_3$ | $2 \times 10^{-18}$ | | Unstable | |
| Fe | -83.5 | $Fe_2O_3$ | $3 \times 10^{-15}$ | | Unstable | |
| Co | -72.5 | CoO | $2 \times 10^{-13}$ | | Unstable | |
| Ni | -66.9 | NiO | $2 \times 10^{-12}$ | | Unstable | |
| Spinel | $-100$[c] | $NiCr_2O_4$ | $4 \times 10^{-15}$[c] | | Unstable | |

[a] Free energy of formation per mole of oxygen or nitrogen in K cal

[b] Dissociation pressure in atmospheres

[c] Estimated from data on $FeCr_2O_4$

Al and particularly Ti activities. Therefore, during low-temperature oxidation (1600°F) where the Al was still tied up as $\gamma'$, the thermodynamic activity was too low for scale formation and $Cr_2O_3$ scale formation and $Al_2O_3$ internal oxidation existed. At higher temperatures the effective activity of Al was increased sufficiently (due to $\gamma'$ dissolution and increased diffusion) to form an Al-rich oxide. The result was elimination of internal oxidation and Al subscale formation. The Al and Ti activities in U-700 (15 Cr, 4 Al, and 3.6 Ti) would be similar to those in SM-200 but the Cr activity was higher. The higher Cr activity actually favored the formation of Cr-base oxides and essentially increased the temperature range at which internal oxidation and Al suboxide formation would persist. The influence of high Cr activity was also demonstrated by René 41 (19 Cr, 1.4 Al, 3 Ti) in which $Cr_2O_3$ oxide scale predominated at all temperatures. This naturally resulted in excessive amounts of internal oxidation.

In view of present findings, it may be possible to thermodynamically design alloys with greater surface stability. Unfortunately, much of the required data for this type of design is lacking, particularly those pertaining to Al and Ti activities. Also, the Al activity as a function of temperature would probably differ for each superalloy due to differences in the $\gamma'$ stability and Al diffusion. However, since Al-base oxides are inherently more stable than those based on Cr, oxidation resistance can be improved by increasing the Al/Cr ratio. Increasing the Al level would, of course, increase the Al/Cr ratio at the expense of ductility. Decreasing the Cr while maintaining the usually high Al level content should produce the same net effect with no loss in ductility. Hence, alloys with lower Cr (6 to 9 w/o) and high Al (4 to 6 w/o) contents are suggested to increase surface stability. This should not cause unfavorable alloy properties.

In a practical sense, all the alloys studied, with the exception of René Y, displayed similar oxidation resistance and, in general, the same undesirable features. The major factors which contribute to increase oxidation and therefore most likely to reduce component life and reliability in turbine applications are:

Oxide spalling

Excessive localized intergranular Oxidation

Oxide volatilization

During cooling of isothermal oxidation test specimens from temperatures of 1800°F or greater, spalling of the surface oxide was always observed for IN-100, SM-200, and Inco 713C when the oxygen uptake exceeded 1.7, 1.5, and 1.0 $mg/cm^2$, respectively. Considering that a weight gain of 1.0 $mg/cm^2$

constitutes only approximately $1.0 \times 10^{-4}$ in./side of metal consumed, the effect of spalling at first appears insignificant. However, during exposure of these materials under service conditions, oxide spalling would be enhanced by the cyclic temperatures and "thermal fatigue" conditions which would prevail. Since spalling of the surface oxide scale causes the material to resume oxidation at the usually faster initial rate, considerable metal can be consumed by this mechanism. The load-bearing capacity and consequently service life or reliability will thus be impaired. The potential severity of cyclic temperature on the scale adherence and subsequent metal consumption for IN-100 and Inco 713C was illustrated by the comparative results of isothermal and cyclic oxidation tests. As indicated in these studies, thermal cycling-induced spalling can produce excessive material degradation in these cast alloys as compared to René Y, which is notably immune.

The spalling tendencies displayed by the cast alloys are attributed to the nature and morphology of the oxides formed during oxidation. As illustrated, the scaling and subscaling processes which occur during the exposure of these alloys are complex, leading to the formation of a heterogeneous mixture of oxides which results in spalling. The most obvious and ideal solution to this problem of excessive spalling involves the formation of a single-phase tenacious oxide scale which possesses compatibility with the base metal. This can be attained theoretically through control of the competition which exists between scale and subscale reactions by the addition of elements which increase the effective activity of desirable constituents, such as aluminum, for their eventual incorporation into the surface oxide. The rare earth elements, which are less noble than any element present in these superalloys, could be used for sacrificial internal oxidation and in the process increase the concentration of otherwise subscale components into the surface scale. Although theoretically feasible, this approach may not offer any significant advantage in practice due to the localized segregation which exists in these cast alloys.

The metallographic examination of IN-100, SM-200, and Inco 713C subsequent to oxidation testing above 1600°F revealed the presence of massive localized intergranular oxidation whose severity varied with alloy and exposure. A ranking of alloys would indicate IN-100 the most susceptible to this form of attack, and Inco 713C and SM-200 equally susceptible, but less than IN-100. Strength under fatigue loading, where failure is very surface sensitive, is reduced by the metallurgical notch effect produced by this type continuous grain boundary oxide. If, however, the internal oxides formed a fine particulate, non-continuous layer of oxides, they may, in fact, produce a dispersion strengthening effect. The uniform $\gamma'$ dissolution region usually associated with the fine I.O. region, may also be beneficial. Without this relatively ductile layer, low in solute and usually free of second phase, the internal reaction products could produce higher stress concentrations.

The cause of the undesirable intergranular oxide formation is attributed
to the segregation of strong oxide formers, particularly titanium.  It is
possible to minimize this type of internal oxidation by small additions
of elements less noble than titanium or aluminum, which could be finely
dispersed to serve as preferred elements in the competition for internal
oxidation formation.  This could theoretically increase the effective
activity of the titanium and aluminum sufficiently to prevent the formation
of I.G.O. to allow their inclusion in the surface oxide.  Among the few elements
which are less noble than titanium or aluminum are the rare earths and the
Group IIIB metals.

During the isothermal oxidation testing of these alloys at 2000°F, all alloys
with the exception of René Y displayed some degree of oxide vaporization.
However, during oxidation in high velocity (75 ft/sec), natural gas combustion
products, oxide volatility was markedly accelerated.  This effect can be con-
sidered somewhat analogous to that produced by spalling with similar consequences
to the material.  Although volatilization does not produce more rapid oxidation
by fresh metal exposure as in the case of spalling, evidence indicates that in
the process the protective constituents, namely $Cr_2O_3$, are removed from the
scale yielding a less protective oxide, a higher oxidation rate, and a
resultant increase in metal consumption.  The extent of volatilization has
been shown to be proportional to the amount of chromium-rich oxides in the scale
with the exception of René Y.  The amount of metal loss also increases with
increasing $Cr_2O_3$ content or the amount of chromium-rich oxides in the surface
scale.  The lack of volatilization from oxide scales formed on René Y, which
results in superior resistance to high velocity gas flow, is attributed to
the formation of a protective surface layer of La-induced $MnCr_2O_4$ spinel.

Oxide volatilization can therefore be minimized by the formation of either
surface oxide: with a minimal chromium content or protective chromium-bearing
spinels such as $MnCr_2O_4$.  Here again, as indicated for the other detrimental
factors, "rare earth" additions may provide the solution to this problem
by altering the dominant oxidation mode, yielding more stable oxidation
products.  The lower dissociation pressure of these newly formed surface
oxides, such as those based on $Al_2O_3$, would greatly enhance the surface
stability of the alloy.

The marked improvement in oxidation behavior provided by minor additions
of La and Mn to Hastelloy X (René Y) affords an excellent example of the
benefit to be derived using minor element additions.  In this alloy the
addition of La apparently alters the scaling process by decreasing the
effective Ni activity in the oxide and subsequently increasing the Cr and Mn

177

activities to produce a protective manganese chromate spinel oxide. This spinel phase displays a high resistance to volatilization. The La addition also produces greater scale adherence by concentrating at the grain boundary cusps formed at the oxide/metal interface producing an oxide which apparently reduces the interfacial stresses. In alloys with relatively high aluminum concentration (4 to $7^W/_O$) an w Cr content ($5-13^W/_O$) surface oxides of aluminum would probably be enhanced yielding a tenacious oxide.

In summary, it may be possible to minimize the deficiencies pointed out above by major alloying modifications. However, applying this approach to the complex high strength alloys would undoubtedly alter the already critical structural stability and hence mechanical properties of the base alloy which in turn would require a major alloy development effort to avoid adverse effects while improving surface stability. The René Y modifications offer a promising technique for improving surface stability without major property changes. This has been accomplished by the addition of small quantities of the "rare earth" type elements and manganese. The suggested approach toward increasing surface stability is particularly attractive since these additions not only appear to promote the effectiveness of major alloying elements already present in the alloy by producing protective oxide scales, but the amount of addition required is usually small enough to have an insignificant effect on mechanical properties.

APPENDIX

# APPENDIX I-A

## CONTINUOUS WEIGHT-GAIN OXIDATION TEST DATA FOR RENÉ Y

### Weight Gain/Area (mg/cm²)

| Time Min. | René Y Heat #1 (64-711) 1600°F (#12) | 1600°F (#16) | 1600°F (#44) | 1800°F (#23) | 1800°F (#29) | 2000°F (#7) | 2000°F (#42) | 2100°F (#9) | René Y Heat #2 (65-590) 1400°F (#63) | 1600°F (#18) | 1800°F (#8) | 1800°F (#10) | 2000°F (#5) | 2000°F (#41) | 2100°F (#11) | 2100°F (#15) |
|---|---|---|---|---|---|---|---|---|---|---|---|---|---|---|---|---|
| 3 | - | - | - | 0.002 | - | - | - | - | - | - | - | - | - | - | - | - |
| 5 | 0.001 | 0.002 | 0.001 | 0.003 | 0.001 | 0.010 | 0.167 | 0.051 | - | 0.002 | 0.014 | - | - | 0.061 | 0.067 | 0.070 |
| 10 | 0.002 | 0.005 | 0.002 | 0.005 | 0.003 | 0.026 | 0.179 | 0.099 | 0.0005 | 0.005 | 0.028 | 0.016 | 0.119 | 0.078 | 0.096 | 0.099 |
| 15 | 0.003 | 0.006 | 0.002 | 0.007 | 0.007 | 0.036 | 0.196 | 0.120 | - | 0.008 | 0.039 | 0.032 | 0.163 | 0.099 | 0.117 | 0.120 |
| 20 | 0.004 | 0.007 | 0.003 | 0.011 | 0.010 | 0.079 | 0.207 | 0.138 | 0.0008 | 0.010 | 0.048 | 0.047 | 0.197 | 0.122 | 0.137 | 0.140 |
| 30 | 0.005 | 0.009 | 0.004 | 0.016 | 0.012 | 0.110 | 0.215 | 0.169 | 0.0011 | 0.013 | 0.063 | 0.060 | 0.226 | 0.138 | 0.168 | 0.169 |
| 40 | 0.006 | 0.018 | 0.006 | 0.020 | 0.019 | 0.131 | 0.221 | 0.194 | 0.0015 | 0.019 | 0.075 | 0.083 | - | 0.150 | 0.192 | 0.194 |
| 60 | 0.008 | 0.028 | 0.010 | 0.029 | 0.023 | 0.158 | 0.244 | 0.240 | 0.0021 | 0.026 | 0.096 | 0.103 | - | 0.179 | 0.229 | 0.231 |
| 80 | 0.012 | 0.036 | 0.011 | 0.043 | 0.032 | 0.179 | 0.259 | 0.278 | 0.0027 | 0.032 | 0.112 | 0.119 | - | 0.201 | 0.261 | 0.266 |
| 100 | 0.017 | 0.045 | 0.016 | 0.050 | 0.042 | 0.221 | 0.272 | 0.315 | 0.0034 | 0.037 | 0.124 | 0.133 | - | 0.222 | 0.287 | 0.294 |
| 120 | 0.021 | 0.055 | 0.019 | 0.056 | 0.050 | 0.248 | 0.301 | 0.351 | 0.0039 | 0.042 | 0.133 | 0.169 | 0.269 | 0.234 | 0.313 | 0.317 |
| 180 | 0.032 | 0.083 | 0.028 | 0.074 | 0.058 | 0.263 | 0.326 | 0.413 | 0.0063 | 0.059 | 0.151 | 0.200 | 0.298 | 0.275 | 0.378 | 0.382 |
| 240 | 0.046 | 0.099 | 0.035 | 0.086 | 0.073 | 0.279 | 0.344 | 0.461 | 0.0091 | 0.070 | 0.167 | 0.227 | 0.316 | 0.305 | 0.429 | 0.440 |
| 300 | 0.049 | 0.106 | 0.044 | 0.097 | 0.088 | 0.300 | 0.372 | 0.502 | 0.012 | 0.081 | 0.185 | 0.282 | 0.351 | 0.324 | 0.473 | 0.492 |
| 360 | 0.065 | 0.111 | 0.052 | 0.103 | 0.102 | 0.315 | 0.385 | 0.568 | 0.015 | 0.091 | 0.218 | 0.354 | 0.406 | - | 0.515 | 0.538 |
| 420 | 0.074 | 0.120 | 0.057 | 0.110 | 0.116 | 0.351 | 0.398 | 0.645 | 0.018 | 0.100 | 0.271 | 0.397 | 0.432 | 0.367 | 0.552 | 0.578 |
| 480 | 0.085 | - | 0.064 | 0.117 | 0.130 | 0.422 | 0.410 | 0.695 | - | 0.110 | 0.295 | 0.434 | 0.453 | - | 0.594 | 0.623 |
| 540 | 0.102 | 0.130 | 0.072 | 0.125 | 0.143 | 0.443 | 0.424 | 0.727 | 0.023 | 0.119 | 0.319 | 0.471 | 0.485 | - | 0.648 | 0.687 |
| 600 | 0.114 | 0.133 | 0.076 | 0.132 | 0.154 | 0.464 | 0.438 | 0.763 | 0.027 | 0.128 | 0.343 | 0.523 | 0.519 | 0.412 | 0.709 | 0.758 |
| 720 | 0.127 | 0.145 | 0.089 | 0.146 | 0.164 | 0.480 | 0.449 | 0.820 | 0.034 | 0.144 | 0.409 | 0.600 | 0.543 | 0.440 | 0.810 | 0.814 |
| 800 | 0.155 | - | 0.098 | 0.159 | 0.184 | 0.511 | 0.460 | 0.682 | 0.040 | 0.156 | 0.448 | 0.654 | 0.564 | 0.457 | - | 0.868 |
| 960 | 0.174 | 0.166 | 0.108 | 0.171 | 0.198 | 0.543 | 0.481 | 0.934 | 0.050 | 0.166 | 0.505 | 0.694 | 0.582 | 0.473 | 0.868 | 0.953 |
| 1200 | 0.184 | 0.188 | 0.127 | 0.189 | 0.213 | 0.580 | 0.504 | - | 0.053 | 0.188 | 0.534 | 0.733 | 0.615 | 0.506 | 0.998 | 1.042 |
| 1500 | - | 0.208 | 0.146 | 0.210 | 0.226 | 0.664 | 0.524 | 1.025 | 0.053 | 0.202 | 0.582 | - | - | 0.528 | 0.930 | 1.136 |
| 1800 | - | 0.238 | 0.163 | 0.229 | 0.245 | 0.691 | 0.532 | 1.100 | 0.055 | 0.207 | - | 0.809 | 0.658 | 0.561 | 0.957 | 1.220 |
| 2100 | - | - | - | 0.249 | 0.274 | 0.749 | 0.532 | 1.170 | 0.065 | 0.214 | 0.668 | - | - | - | 0.975 | 1.289 |
| 2400 | 0.193 | 0.249 | 0.181 | 0.274 | 0.303 | 0.794 | 0.561 | 1.220 | 0.071 | 0.219 | - | 0.872 | 0.699 | 0.652 | - | - |
| 3000 | - | 0.257 | 0.192 | 0.313 | 0.319 | - | 0.607 | 1.239 | 0.075 | 0.241 | 0.744 | 0.925 | 0.733 | 0.699 | 1.030 | 1.455 |
| 3600 | - | 0.296 | 0.227 | 0.350 | 0.347 | - | 0.652 | 1.288 | 0.092 | 0.288 | 0.799 | - | - | 0.734 | 1.055 | - |
| 4200 | 0.279 | 0.308 | 0.263 | 0.390 | 0.379 | - | 0.664 | 1.327 | 0.089 | 0.312 | 0.839 | 0.991 | 0.822 | 0.770 | 1.083 | 1.579 |
| 4800 | 0.312 | 0.320 | 0.275 | 0.407 | 0.395 | 0.812 | 0.756 | - | 0.093 | 0.319 | 0.875 | 1.025 | 0.857 | 0.792 | 1.207 | 1.715 |
| 5400 | 0.328 | 0.338 | 0.301 | 0.427 | 0.427 | 0.854 | 0.866 | - | 0.101 | 0.319 | 0.929 | - | 0.865 | 0.522 | - | 1.923 |
| 6000 | 0.325 | 0.360 | 0.307 | 0.437 | 0.414 | 0.886 | 0.917 | - | - | 0.319 | - | - | - | - | - | 1.986 |
| Specimen Surface Area (cm²) | 9.7562 | 5.6131 | 9.3589 | 9.6879 | 9.7395 | 9.4757 | 9.3823 | 9.7556 | 17.588* | 9.7073 | 9.8246 | 9.5393 | 9.4795 | 8.1734 | 10.0490 | 9.9414 |

*Double Specimen Used

## CONTINUOUS WEIGHT-GAIN OXIDATION TEST DATA FOR IN-100

### Weight Gain/Area (mg/cm²)

| Time Min. | IN-100 – Heat #1 (67V3261) | | | | | | IN-100 – Heat #2 (YD-582/583) | | | | | | | | |
|---|---|---|---|---|---|---|---|---|---|---|---|---|---|---|---|
| | 1400°F (#24) | 1600°F (#20) | 1800°F (#21) | 2000°F (#19) | 2000°F (#27) | 2100°F (#17) | 1400°F (#22) | 1400°F (#26) | 1600°F (#14) | 1800°F (#4) | 1800°F (#6) | 2000°F (#3) | 2000°F (#25) | 2100°F (#13) | 2100°F (#43) |
| 3 | 0.005 | 0.051 | 0.046 | 0.141 | 0.147 | 0.446 | 0.008 | - | - | 0.031 | 0.053 | 0.207 | 0.196 | 0.932 | 0.810 |
| 5 | 0.010 | 0.065 | 0.063 | 0.178 | 0.178 | 0.654 | 0.010 | 0.008 | 0.005 | 0.046 | 0.101 | 0.264 | 0.224 | 1.180 | 0.941 |
| 10 | 0.012 | 0.087 | 0.098 | 0.258 | 0.254 | 0.944 | 0.013 | 0.144 | 0.012 | 0.088 | 0.128 | 0.352 | 0.310 | 1.656 | 1.070 |
| 15 | 0.013 | 0.102 | 0.117 | 0.305 | 0.300 | 1.173 | 0.016 | - | 0.016 | 0.119 | 0.206 | 0.435 | 0.351 | 1.936 | 1.220 |
| 20 | 0.014 | 0.113 | 0.129 | 0.334 | 0.336 | 1.339 | 0.020 | 0.026 | 0.022 | 0.139 | 0.258 | 0.487 | 0.382 | 2.174 | 1.300 |
| 30 | 0.016 | 0.125 | 0.146 | 0.381 | 0.388 | 1.619 | 0.027 | 0.037 | 0.031 | 0.181 | 0.299 | 0.559 | 0.425 | 2.484 | 1.520 |
| 40 | 0.018 | 0.134 | 0.162 | 0.416 | 0.424 | 1.816 | 0.031 | 0.047 | 0.036 | 0.215 | 0.328 | 0.622 | 0.464 | 2.681 | 1.650 |
| 60 | 0.020 | 0.150 | 0.191 | 0.480 | 0.466 | 2.210 | 0.038 | 0.062 | 0.052 | 0.248 | 0.356 | 0.725 | 0.527 | 3.028 | 1.800 |
| 80 | 0.021 | 0.162 | 0.216 | - | 0.491 | 2.296 | 0.047 | 0.072 | 0.070 | 0.279 | 0.408 | 0.798 | 0.581 | 3.269 | 1.930 |
| 100 | 0.022 | 0.171 | 0.237 | 0.579 | 0.509 | 2.412 | 0.050 | 0.080 | 0.076 | 0.331 | 0.451 | 0.860 | 0.633 | 3.437 | 2.050 |
| 120 | 0.025 | 0.185 | 0.254 | 0.619 | 0.528 | 2.582 | 0.053 | 0.087 | 0.087 | 0.383 | 0.485 | 0.901 | 0.674 | 3.571 | 2.140 |
| 180 | 0.032 | 0.216 | 0.299 | 0.706 | 0.561 | 2.803 | 0.062 | 0.107 | 0.122 | 0.424 | 0.550 | 0.969 | 0.736 | 3.871 | 2.350 |
| 240 | 0.039 | 0.241 | 0.338 | 0.752 | 0.590 | 2.984 | 0.068 | 0.122 | 0.128 | 0.526 | 0.600 | 1.020 | 0.742 | 4.068 | 2.510 |
| 300 | 0.042 | 0.258 | 0.368 | 0.785 | 0.609 | 3.135 | 0.072 | 0.131 | 0.146 | 0.601 | 0.743 | 1.064 | 0.764 | 4.208 | 2.610 |
| 360 | 0.050 | 0.275 | 0.397 | 0.806 | 0.621 | 3.269 | 0.079 | 0.132 | 0.157 | 0.676 | - | - | 0.782 | 4.311 | 2.680 |
| 420 | 0.056 | 0.291 | 0.428 | 0.815 | 0.637 | 3.393 | 0.086 | 0.138 | 0.172 | 0.792 | 0.727 | 1.133 | 0.800 | - | 2.740 |
| 480 | 0.063 | 0.307 | 0.450 | 0.837 | 0.650 | 3.476 | 0.092 | 0.139 | 0.194 | 0.870 | - | - | 0.816 | - | 2.770 |
| 540 | 0.069 | 0.313 | 0.468 | 0.848 | 0.658 | 3.540 | 0.094 | 0.111 | - | 0.901 | - | 1.191 | 0.834 | - | 2.830 |
| 600 | 0.073 | 0.324 | 0.483 | 0.858 | 0.666 | 3.594 | 0.096 | 0.144 | 0.212 | 0.971 | 0.799 | 1.212 | 0.842 | 4.580 | 2.870 |
| 720 | 0.087 | 0.341 | 0.520 | 0.879 | 0.683 | 3.685 | 0.102 | 0.152 | 0.228 | 1.005 | 0.815 | 1.253 | 0.868 | 4.647 | 2.920 |
| 840 | 0.101 | 0.357 | 0.550 | 0.897 | 0.700 | 3.754 | 0.104 | 0.158 | 0.244 | 1.036 | 0.851 | 1.279 | 0.892 | 4.704 | 2.950 |
| 960 | 0.112 | 0.370 | 0.573 | 0.913 | 0.716 | 3.820 | 0.105 | 0.160 | 0.256 | 1.039 | 0.872 | 1.303 | 0.913 | 4.748 | 3.000 |
| 1200 | 0.117 | 0.390 | 0.633 | 0.943 | 0.724 | 3.897 | 0.105 | 0.160 | 0.278 | 1.120 | 0.903 | 1.362 | 0.942 | 4.832 | 3.030 |
| 1500 | 0.126 | 0.409 | 0.696 | 0.973 | 0.742 | 3.977 | 0.132 | 0.160 | 0.299 | 1.178 | 0.919 | 1.401 | 0.992 | 4.937 | 3.100 |
| 1800 | 0.146 | 0.425 | 0.744 | 0.990 | 0.760 | 4.070 | 0.143 | 0.170 | 0.322 | 1.225 | 0.920 | 1.408 | 1.040 | 5.035 | 3.130 |
| 2100 | 0.156 | 0.453 | 0.782 | 1.008 | 0.787 | 4.135 | 0.172 | 0.177 | 0.343 | 1.262 | - | 1.440 | 1.074 | 5.135 | 3.250 |
| 2400 | 0.167 | 0.495 | 0.816 | 1.011 | 0.797 | 4.203 | - | 0.187 | 0.350 | 1.254 | - | 1.488 | 1.099 | 5.236 | 3.320 |
| 3000 | 0.206 | 0.567 | 0.855 | 1.054 | 0.805 | 4.294 | - | 0.223 | 0.382 | 1.298 | 1.004 | - | 1.142 | 5.409 | 3.490 |
| 3600 | 0.226 | 0.594 | 0.908 | 1.090 | 0.807 | 4.317 | - | - | 0.393 | 1.346 | 1.347 | 1.639 | 1.192 | 5.597 | 3.640 |
| 4200 | 0.235 | 0.617 | 0.941 | 1.090 | - | 4.347 | 0.188 | 0.294 | 0.403 | 1.362 | 1.070 | 1.724 | 1.232 | 5.662 | 3.460 |
| 4800 | 0.256 | 0.639 | 0.979 | 1.090 | 0.807 | - | 0.210 | - | 0.409 | - | 1.065 | - | - | - | 3.880 |
| 5400 | 0.268 | 0.658 | 1.004 | 1.090 | 0.807 | - | - | 0.325 | 0.414 | - | 1.070 | - | 1.294 | - | 4.000 |
| 6000 | 0.279 | - | - | - | - | - | - | - | - | - | - | - | - | - | - |
| Specimen Surface Area (cm²) | 9.6711 | 9.7214 | 9.7008 | 9.7073 | 9.6606 | 9.6363 | 9.6640 | 9.6673 | 9.1609 | 9.6550 | 9.6079 | 9.6539 | 9.6885 | 9.6602 | 9.6247 |

181

CONTINUOUS WEIGHT-GAIN OXIDATION TEST DATA FOR SM-200

Weight Gain/Area (mg/cm²)

| Time Min. | SM-200 Heat #1 (34V2804) | | | | | | | SM-200 Heat #2 (34V2863) | | | | | | |
| --- | --- | --- | --- | --- | --- | --- | --- | --- | --- | --- | --- | --- | --- | --- |
| | 1400°F (#63) | 1600°F (#60) | 1800°F (#34) | (#59) | 2000°F (#36) | 2100°F (#1) | (#53) | 1400°F (#66) | 1600°F (#64) | 1800°F (#32) | 2000°F (#51) | 2100°F (#57) | (#35) | (#46) |
| 3 | - | - | 0.058 | - | 0.074 | 0.30 | 0.236 | - | - | - | 0.134 | 0.119 | 0.083 | 0.120 |
| 5 | - | - | 0.074 | 0.005 | 0.095 | 0.206 | 0.349 | - | - | 0.039 | 0.170 | 0.182 | 0.125 | 0.150 |
| 10 | 0.001 | 0.004 | 0.096 | 0.01. | 0.125 | 0.319 | 0.554 | 0.0052 | 0.004 | 0.046 | 0.237 | 0.291 | 0.270 | 0.240 |
| 15 | - | - | 0.107 | 0.016 | 0.155 | 0.102 | 0.718 | - | - | 0.055 | 0.283 | 0.353 | 0.333 | 0.290 |
| 20 | 0.001 | 0.009 | 0.117 | 0.022 | 0.180 | 0.453 | 0.852 | 0.0078 | 0.009 | 0.067 | 0.315 | 0.468 | 0.390 | 0.330 |
| 30 | 0.001 | 0.014 | 0.127 | 0.020 | 0.216 | 0.528 | 1.090 | 0.0099 | 0.015 | 0.072 | 0.360 | 0.515 | 0.470 | 0.400 |
| 40 | 0.002 | 0.016 | 0.136 | 0.038 | 0.245 | 0.584 | 1.220 | 0.012 | 0.018 | 0.080 | 0.384 | 0.598 | 0.515 | 0.440 |
| 60 | 0.003 | 0.020 | 0.155 | 0.052 | 0.294 | 0.697 | 1.450 | 0.015 | 0.027 | 0.087 | 0.412 | 0.734 | 0.617 | 0.540 |
| 80 | 0.005 | 0.021 | 0.175 | 0.063 | 0.333 | 0.776 | 1.650 | 0.018 | 0.031 | 0.098 | 0.443 | 0.834 | 0.695 | 0.620 |
| 100 | 0.007 | 0.022 | 0.188 | 0.071 | 0.363 | 0.840 | 1.810 | 0.019 | 0.037 | 0.109 | 0.453 | 0.932 | 0.755 | 0.680 |
| 120 | 0.008 | - | 0.203 | 0.079 | 0.390 | 0.891 | 1.960 | 0.019 | 0.040 | 0.121 | 0.475 | 0.980 | 0.811 | 0.730 |
| 180 | 0.016 | - | 0.238 | 0.095 | 0.454 | 1.040 | 2.260 | 0.019 | 0.050 | 0.132 | 0.526 | 1.170 | 0.942 | 0.860 |
| 240 | 0.019 | - | 0.262 | 0.108 | 0.491 | 1.160 | 2.400 | 0.017 | 0.056 | 0.164 | 0.556 | 1.330 | 1.050 | 0.960 |
| 300 | 0.020 | - | 0.280 | 0.126 | 0.527 | 1.260 | 2.490 | 0.013 | 0.060 | 0.187 | 0.580 | 1.430 | 1.120 | 1.030 |
| 360 | 0.027 | - | 0.296 | 0.132 | 0.553 | 1.240 | 2.560 | 0.013 | 0.064 | 0.205 | 0.607 | 1.530 | 1.180 | 1.090 |
| 420 | 0.030 | - | 0.312 | 0.146 | 0.580 | 1.490 | 2.590 | 0.007 | 0.070 | 0.216 | 0.615 | 1.630 | 1.240 | 1.140 |
| 480 | 0.032 | - | 0.331 | 0.156 | 0.604 | 1.460 | 2.620 | 0.005 | 0.072 | 0.222 | 0.629 | 1.710 | 1.290 | 1.180 |
| 540 | 0.036 | - | 0.345 | 0.168 | 0.629 | 1.510 | 2.640 | 0.008 | 0.076 | 0.237 | 0.647 | 1.790 | 1.330 | 1.220 |
| 600 | 0.040 | - | 0.362 | 0.178 | 0.644 | 1.560 | 2.660 | 0.007 | 0.084 | 0.249 | 0.659 | 1.860 | 1.370 | 1.260 |
| 720 | 0.040 | - | 0.395 | 0.201 | 0.680 | 1.650 | 2.670 | 0.005 | 0.099 | 0.263 | 0.690 | 1.970 | 1.440 | 1.300 |
| 840 | 0.042 | - | 0.423 | 0.218 | 0.676 | 1.710 | 2.690 | 0.009 | 0.105 | 0.293 | 0.716 | 2.660 | 1.490 | 1.340 |
| 960 | 0.043 | 0.096 | 0.444 | 0.234 | 0.710 | 1.750 | 2.690 | - | 0.111 | 0.320 | 0.741 | 2.130 | 1.530 | 1.370 |
| 1200 | 0.054 | 0.107 | 0.466 | 0.265 | 0.731 | 1.810 | 2.660 | - | 0.124 | 0.334 | 0.782 | 2.220 | 1.570 | 1.430 |
| 1500 | 0.064 | 0.126 | 0.495 | 0.312 | 0.755 | 1.860 | 2.620 | - | 0.139 | 0.363 | 0.819 | 2.280 | 1.660 | 1.460 |
| 1800 | 0.085 | 0.129 | 0.546 | 0.336 | 0.775 | 1.900 | 2.570 | - | 0.148 | 0.402 | 0.857 | 2.310 | 1.690 | 1.490 |
| 2100 | 0.098 | 0.134 | 0.603 | 0.355 | 0.775 | 1.910 | 2.550 | - | 0.164 | 0.436 | 0.898 | 2.300 | 1.720 | 1.510 |
| 2400 | 0.100 | 0.140 | 0.524 | 0.371 | 0.775 | 1.920 | 7.520 | - | 0.190 | 0.463 | 0.937 | 2.290 | 1.730 | 1.520 |
| 2700 | 0.106 | 0.159 | 0.640 | - | 0.775 | 1.920 | - | - | 0.207 | 0.488 | 0.976 | - | 1.720 | - |
| 3000 | 0.110 | 0.171 | 0.666 | 0.415 | 0.775 | 1.910 | 2.490 | - | 0.215 | 0.517 | 0.999 | 2.270 | 1.720 | 1.540 |
| 3600 | 0.121 | 0.176 | 0.694 | 0.445 | 0.775 | 1.900 | 2.460 | - | 0.246 | 0.533 | 0.999 | 2.250 | 1.730 | 1.570 |
| 4200 | 0.130 | 0.205 | 0.706 | 0.477 | 0.775 | 1.880 | 2.450 | - | 0.257 | 0.536 | 0.999 | 2.220 | 1.750 | 1.570 |
| 4800 | 0.144 | 0.198 | 0.724 | 0.531 | - | 1.810 | 2.420 | - | 0.282 | 0.546 | 0.999 | 2.200 | 1.750 | - |
| 5400 | 0.164 | 0.189 | - | 0.527 | - | 1.790 | 2.400 | - | 0.255 | 0.565 | 0.999 | 2.160 | 1.730 | - |
| 6000 | 0.168 | 0.207 | - | 0.532 | - | - | - | - | 0.261 | - | - | - | 1.710 | - |

Specimen Surface
Area (cm²)  19.2454*  9.5786  9.6711  9.7576  9.6724  9.7034  9.7421  19.251*  3.5652  9.6956  9.7123  9.6366  9.6178  9.7072

*Double Specimens Used

## CONTINUOUS WEIGHT-GAIN OXIDATION TEST DATA FOR INCO 713C

Weight Gain/Area (mg/cm²)

| Time Min. | Inco 713C Heat #1 (601) | | | | | | Inco 713C Heat #2 (602) | | | | |
|---|---|---|---|---|---|---|---|---|---|---|---|
| | 1600°F (#58) | 1600°F (#61) | 1800°F (#45) | 2000°F (#38) | 2100°F (#39) | 2100°F (#52) | 1600°F (#56) | 1800°F (#17) | 2000°F (#40) | 2000°F (#55) | 2100°F (#37) |
| 3 | - | 0.021 | 0.052 | 0.070 | 0.130 | 0.150 | - | 0.003 | 0.090 | - | 0.090 |
| 5 | 0.005 | 0.031 | 0.071 | 0.080 | 0.170 | 0.300 | 0.006 | 0.007 | 0.110 | 0.026 | 0.120 |
| 10 | 0.005 | 0.047 | 0.083 | 0.110 | 0.230 | 0.390 | 0.012 | 0.014 | 0.150 | 0.049 | 0.150 |
| 15 | 0.005 | 0.062 | 0.088 | 0.130 | 0.270 | 0.390 | 0.016 | 0.022 | 0.170 | 0.066 | 0.160 |
| 20 | 0.005 | 0.071 | 0.091 | 0.150 | 0.290 | 0.490 | 0.018 | 0.026 | 0.190 | 0.081 | 0.190 |
| 30 | 0.008 | 0.092 | 0.100 | 0.190 | 0.330 | 0.700 | 0.023 | 0.041 | 0.220 | 0.110 | 0.220 |
| 40 | 0.008 | 0.106 | 0.105 | 0.210 | 0.370 | 0.760 | 0.025 | 0.051 | 0.240 | 0.140 | 0.230 |
| 60 | 0.009 | 0.121 | 0.115 | 0.260 | 0.430 | 0.830 | 0.029 | 0.068 | 0.270 | 0.184 | 0.270 |
| 80 | 0.009 | 0.133 | 0.123 | 0.290 | 0.480 | 0.880 | 0.033 | 0.081 | 0.300 | 0.247 | 0.290 |
| 100 | 0.010 | 0.144 | 0.129 | 0.310 | 0.530 | 0.930 | 0.035 | 0.091 | 0.310 | 0.293 | 0.310 |
| 120 | 0.011 | 0.148 | 0.133 | 0.310 | 0.560 | 0.980 | 0.040 | 0.100 | 0.320 | 0.335 | 0.330 |
| 180 | 0.013 | 0.150 | 0.144 | 0.330 | 0.660 | 1.110 | 0.051 | 0.120 | 0.340 | 0.365 | 0.550 |
| 240 | 0.015 | 0.156 | 0.145 | 0.340 | 0.710 | 1.200 | 0.062 | 0.130 | 0.350 | 0.380 | 0.410 |
| 300 | 0.022 | 0.164 | 0.150 | 0.340 | 0.810 | 1.310 | 0.069 | 0.140 | 0.355 | 0.390 | 0.430 |
| 360 | 0.026 | 0.172 | 0.152 | 0.340 | 0.870 | - | 0.076 | 0.160 | 0.360 | 0.399 | 0.450 |
| 420 | 0.029 | 0.179 | 0.154 | 0.340 | 0.930 | 1.540 | 0.080 | 0.170 | 0.370 | 0.408 | 0.470 |
| 480 | 0.031 | 0.185 | 0.158 | 0.340 | 0.990 | 1.650 | 0.084 | 0.180 | 0.370 | 0.415 | 0.490 |
| 540 | 0.035 | 0.194 | 0.161 | 0.340 | 1.050 | 1.760 | 0.089 | 0.190 | 0.380 | 0.423 | 0.500 |
| 600 | 0.037 | 0.202 | 0.163 | 0.340 | 1.110 | 1.850 | 0.091 | 0.200 | 0.390 | 0.433 | 0.520 |
| 720 | 0.038 | 0.216 | 0.170 | 0.340 | 1.220 | 2.000 | 0.095 | 0.210 | 0.410 | 0.446 | 0.550 |
| 840 | 0.043 | 0.228 | 0.172 | 0.340 | 1.330 | 2.150 | 0.097 | 0.220 | 0.430 | 0.457 | 0.590 |
| 960 | 0.045 | 0.244 | 0.173 | 0.340 | 1.440 | 2.250 | 0.097 | 0.230 | 0.440 | 0.465 | 0.610 |
| 1200 | 0.051 | 0.266 | 0.178 | 0.340 | 1.610 | 2.420 | 0.100 | 0.240 | 0.460 | 0.478 | 0.620 |
| 1500 | 0.067 | 0.267 | 0.180 | 0.340 | 1.770 | 2.540 | 0.113 | 0.250 | 0.470 | 0.480 | 0.640 |
| 1800 | 0.076 | 0.268 | 0.180 | 0.340 | 1.920 | 2.590 | 0.123 | 0.260 | 0.490 | 0.492 | 0.660 |
| 2100 | 0.077 | 0.276 | 0.180 | 0.340 | 1.960 | 2.620 | 0.121 | 0.280 | 0.530 | - | 0.670 |
| 2400 | 0.077 | 0.282 | 0.180 | 0.340 | - | 2.630 | 0.110 | 0.300 | 0.570 | - | 0.690 |
| 2700 | - | 0.300 | - | - | - | - | - | - | - | - | - |
| 3000 | 0.109 | 0.318 | 0.192 | 0.380 | - | 2.630 | 0.111 | 0.310 | 0.660 | 0.577 | 0.940 |
| 3600 | 0.132 | 0.333 | 0.200 | 0.460 | - | 2.640 | 0.123 | 0.340 | 0.730 | 0.552 | 1.230 |
| 4200 | 0.149 | 0.359 | 0.200 | 0.460 | - | - | 0.137 | 0.360 | 0.760 | 0.546 | 1.460 |
| 4800 | 0.171 | - | 0.200 | - | - | - | 0.147 | 0.370 | 0.810 | - | 1.670 |
| 5400 | 0.181 | - | 0.211 | - | - | - | 0.157 | 0.370 | 0.820 | - | 1.820 |
| 6000 | 0.184 | 0.407 | - | - | - | - | - | - | - | - | - |
| Specimen Surface Area (cm²) | 9.7650 | 9.7465 | 9.9227 | 9.7653 | 9.7666 | 9.7382 | 9.7292 | 9.7845 | 9.8221 | 9.7859 | 9.7472 |

APPENDIX V-A

## MATRIX COMPOSITION OF THE ALLOYS

| Alloy | Type[a] Analysis | a/o Element | | | | | | | | | | | |
|---|---|---|---|---|---|---|---|---|---|---|---|---|---|
| | | Ni | Cr | Co | Mo | Fe | W | Al | Ti | Mn | Cb | Zr | Si |
| René Y | Total | 45.22 | 24.49 | 2.05 | 5.56 | 19.35 | 0.20 | - | - | 1.06 | - | - | 1.64 |
| | Matrix | 45.57 | 24.93 | 2.07 | 5.01 | 19.50 | 0.18 | - | - | 1.08 | - | - | 1.61 |
| IN-100 | Total | 55.77 | 10.28 | 13.53 | 1.59 | 0.14 | - | 11.68 | 4.98 | 0.02 | - | 0.05 | 0.12 |
| | Matrix | 19.66 | 27.75 | 43.76 | 4.58 | 0.44 | - | - | - | 0.06 | - | 0.15 | 0.37 |
| SM-200 | Total | 60.58 | 10.60 | 10.09 | - | 0.98 | 3.57 | 9.71 | 2.56 | 0.01 | 0.79 | 0.02 | 0.27 |
| | Matrix | 47.44 | 19.84 | 22.21 | - | 2.16 | 7.57 | - | - | 0.01 | - | 0.04 | 0.60 |
| U-700 | Total | 54.75 | 15.80 | 13.80 | 2.35 | 0.10 | - | 8.30 | 4.14 | 0.01 | - | 0.02 | 0.10 |
| | Matrix | 35.53 | 30.26 | 29.08 | 4.64 | 0.21 | - | - | - | 0.02 | - | 0.05 | 0.21 |
| Inco 713C | Total | 65.53 | 14.43 | 0.61 | 3.18 | 0.63 | - | 11.84 | 1.28 | 0.03 | 1.60 | 0.02 | 0.16 |
| | Matrix | 54.78 | 33.53 | 1.58 | 7.91 | 1.64 | - | - | - | 0.08 | - | 0.06 | 0.41 |
| René 41 | Total | 54.46 | 21.83 | 10.30 | 5.72 | 0.21 | - | 3.06 | 3.68 | 0.06 | - | - | 0.14 |
| | Matrix | 46.92 | 30.63 | 14.73 | 7.12 | 0.30 | - | - | - | 0.09 | - | - | 0.21 |

(a) Total refers to total chemical analysis; matrix analysis refers to a Phaccmp derived analysis of matrix when considering partitioning of elements in γ' and carbides

184

STATIC OXIDATION WEIGHT-GAIN DATA (mg/cm²)

| Spec No. | Alloy | 1600°F | | | 1800°F | | | 2000°F | | |
|---|---|---|---|---|---|---|---|---|---|---|
| | | 100 Hrs | 400 Hrs | 1000 Hrs | 100 Hrs | 400 Hrs | 1000 Hrs | 100 Hrs | 400 Hrs | 1000 Hrs |
| 1 | IN-100 Ht #1 | 1.76 | 2.94 | 3.25* (3.34) | 1.76* (1.79) | 1.65* (1.90) | 0.92* (1.91) | -0.24* (1.85) | -0.28* (2.97) | -0.48* (4.88) |
| 2 | (67V3261) | 1.77 | 2.87 | 2.97* (3.06) | 1.57* (1.66) | 2.00* (2.06) | 0.96* (2.05) | -0.26* (1.74) | 0.35* (2.85) | -0.41* (4.41) |
| | Average | 1.77 | 2.91 | 3.11* (3.20) | 1.67* (1.73) | 1.83* (1.98) | 0.94* (1.98) | -0.25* (1.80) | 0.03* (2.91) | -0.03* (4.64) |
| 3 | IN-100 Ht #2 | 1.91 | 2.25 | 3.46* (3.46) | 1.94* (2.04) | 2.15* (2.34) | 1.63* (2.29) | 0.14* (1.87) | -0.49* (3.57) | -0.02* (5.13) |
| 4 | (VT582/583) | 1.81 | 2.41 | 3.51* (3.05) | 1.81* (1.97) | 2.02* (2.25) | 1.82* (3.07) | 0.08* (1.89) | -0.21* (2.98) | +0.40* (5.21) |
| | Average | 1.86 | 2.33 | 3.24* (3.27) | 1.88* (2.01) | 2.08* (2.30) | 1.73* (2.68) | 0.11* (1.88) | -0.35* (3.27) | +0.19* (5.17) |
| 5 | Inco 713C Ht #1 | 0.32 | 0.97 | 0.28 | 0.80 | *(0.59) | *(0.89) | 0.21* (0.45) | -0.55* (1.34) | -0.96* (1.72) |
| 6 | (601) | 0.36 | 0.72 | 0.52 | 0.94 | *(0.69) | *(1.16) | 0.32* (0.58) | -1.13* (1.07) | -0.89* (1.14) |
| | Average | 0.34 | 0.85 | 0.40 | 0.87 | *(0.64) | *(1.03) | 0.27* (0.52) | -0.84* (1.20) | -0.92* (1.43) |
| 7 | Inco 713C Ht #2 | 0.51 | 0.75 | 0.51 | 1.18 | *(0.89) | *(0.70) | 0.48* (0.96) | -1.65* (1.29) | -0.99* (1.69) |
| 8 | (602) | 0.72 | 0.78 | 0.23 | 0.95 | *(0.52) | *(0.70) | 1.24* (1.40) | -1.86* (1.17) | -1.26* (2.42) |
| | Average | 0.61 | 0.77 | 0.37 | 1.06 | *(0.71) | *(0.70) | 0.86* (1.18) | -1.76* (1.23) | -1.12* (2.06) |
| 9 | René 41 Ht #1** | 1.06 | 1.81 | 3.37 | 2.37 | -0.08* (3.89) | 0.08* (7.45) | 4.06* (5.09) | -5.77* (8.51) | -11.65* (12.27) |
| 10 | (TV-394) | 0.84 | 1.73 | 3.08 | 2.35 | 0.25* (3.96) | -0.06* (7.83) | 4.08* (4.83) | -6.23* (9.63) | -10.27* (11.96) |
| | Average | 0.95 | 1.77 | 3.23 | 2.36 | 0.09* (3.93) | 0.01* (7.64) | 4.07* (4.96) | -6.00* (9.07) | -10.96* (12.12) |
| 11 | U-7CO Ht #1** | 0.48 | 0.80 | 0.87 | 0.56 | *(0.76) | *(0.75) | 1.43* (1.64) | 1.54* (5.82) | 1.92* (6.57) |
| 12 | (6-4084) | 0.21 | 0.88 | 1.07 | 0.38 | *(0.57) | *(0.69) | 1.45* (1.69) | 1.21* (3.85) | 1.82* (6.05) |
| | Average | 0.35 | 0.84 | 0.97 | 0.47 | *(0.67) | *(0.71) | 1.45* (1.67) | .37* (4.83) | 1.87* (6.31) |
| 13 | René Y Ht #1 | 0.26 | 0.85 | 0.92 | 0.61 | 1.12 | 1.25 | 0.94 | 1.63 | 2.53 |
| 14 | (HS 64-711) | 0.42 | 0.74 | 0.78 | 0.68 | 1.13 | 1.30 | 0.95 | 1.56 | 2.92 |
| | Average | 0.34 | 0.80 | 0.85 | 0.65 | 1.13 | 1.28 | 0.95 | 1.59 | 2.72 |
| 15 | René Y Ht #2 | 0.41 | 0.87 | 1.20 | 1.00 | 1.84 | 2.08 | 0.99 | 1.51 | 2.88 |
| 16 | (HS 65-590) | 0.34 | 1.21 | 1.50 | 0.91 | 1.87 | 2.37 | 1.08 | 1.52 | 2.51 |
| | Average | 0.38 | 1.04 | 1.35 | 0.96 | 1.86 | 2.22 | 1.04 | 1.52 | 2.69 |
| 17 | SM-200 Ht #1 | 0.42 | 0.68 | 0.57 | 0.82 | *(0.91) | *(0.72) | -0.49* (1.53) | -3.71* (2.66) | -3.39* (3.11) |
| 18 | (3/4V2804) | 0.30 | 0.72 | 0.57 | 0.76 | *(1.84) | *(0.70) | -0.15* (1.65) | -3.14* (1.79) | -3.45* (3.11) |
| | Average | 0.36 | 0.70 | 0.57 | 0.79 | *(1.37) | *(0.71) | -0.32* (1.59) | -3.42* (2.22) | -3.42* (3.11) |
| 19 | SM-200 Ht #2 | 0.31 | 1.35 | 0.42 | 0.83 | *(2.01) | *(1.00) | -1.43* (2.11) | -3.51* (1.88) | -2.11* (1.21) |
| 20 | (3/4V2865) | 0.34 | 0.61 | 0.46 | 0.82 | *(1.00) | *(1.03) | -0.85* (1.74) | -3.49* (2.39) | -1.93* (1.67) |
| | Average | 0.33 | 0.98 | 0.44 | 0.83 | *(1.50) | (1.01) | -1.14* (1.92) | -3.50* (2.13) | -2.02* (1.44) |

*Denotes spalling of oxide during cooling - value in parenthesis is net weight gain of specimen plus spalled products.

**Being used for standards.

185

## FLAME TUNNEL OXIDATION WEIGHT CHANGE DATA – $(mg/cm^2)$

| Alloy | Spec No. | 400 Hrs/1600°F | | | | Spec No. | 400 Hrs/2000°F | | | |
|---|---|---|---|---|---|---|---|---|---|---|
| | | 100 Hrs | 200 Hrs | 300 Hrs | 400 Hrs | | 100 Hrs | 200 Hrs | 300 Hrs | 400 Hrs |
| René Y Ht #1 | 1 | -0.07 | -0.14 | -0.11 | -0.24 | 1 | +0.17 | -0.42 | -1.06 | -0.51 |
| (64-711) | 2 | -0.05 | -0.14 | -0.09 | -0.30 | 2 | +0.11 | -0.46 | -1.53 | -0.94 |
| Average* | | -0.06 | -0.14 | -0.10 | -0.27 | | +0.14 | -0.44 | -1.29 | -0.73 |
| Totals** | | | (-0.20) | (-0.30) | (-0.57) | | | (-0.30) | (-1.59) | (-2.34) |
| IN-100 Ht #1 | 3 | +0.06 | +0.12 | +0.01 | -0.04 | 3 | -1.86 | -1.06 | -1.03 | -0.95 |
| (67V3261) | 4 | +0.08 | +0.16 | +0.01 | +0.20 | 4 | -1.32 | -0.78 | -0.51 | -0.81 |
| Average* | | +0.07 | +0.14 | +0.01 | +0.08 | | -1.59 | -0.92 | -0.77 | -0.88 |
| Totals** | | | (+0.21) | (+0.22) | (+0.30) | | | (-2.51) | (-3.28) | (-4.16) |
| SM-200 Ht #1 | 5 | +0.27 | +0.06 | +0.68 | -0.06 | 5 | -1.63 | -1.65 | -1.45 | -1.97 |
| (34V2804) | 6 | +0.25 | +0.08 | +0.70 | -0.04 | 6 | -1.37 | -1.55 | -2.09 | -1.49 |
| Average* | | +0.26 | +0.07 | +0.69 | -0.05 | | -1.50 | -1.50+ | -1.77 | -1.73 |
| Totals** | | | (+0.33) | (+1.02) | (+0.97) | | | (-3.00) | (-4.77) | (-6.50) |
| U-700 Ht #1 | 7 | +0.85 | +0.06 | +0.34 | -0.09 | 7 | -0.51 | -0.31 | -0.63 | -1.67 |
| (6-4084) | 8 | +0.81 | +0.04 | +0.38 | -0.13 | 8 | -0.91 | -0.55 | -0.63 | -0.93 |
| Average* | | +0.83 | +0.05 | +0.36 | -0.11 | | -0.71 | -0.43 | -0.63 | -1.30 |
| Totals** | | | (+0.92) | (+1.28) | (+1.17) | | | (-1.14) | (-1.77) | (-3.07) |
| Inco 713C Ht #1 | 9 | +0.16 | -0.03 | +0.45 | -0.11 | 9 | -0.78 | -1.64 | -3.44 | -2.72 |
| (601) | 10 | +0.28 | -0.05 | +0.61 | -0.13 | 10 | -1.18 | -2.22 | -3.68 | -2.66 |
| Average* | | +0.22 | -0.04 | +0.53 | -0.12 | | -0.98 | -1.93 | -3.56 | -2.69 |
| Totals** | | | (+0.18) | (+0.71) | (+0.59) | | | (-2.91) | (-6.47) | (-9.16) |
| René 41 Ht #1 | 11 | +0.53 | -0.14 | +0.29 | -0.27 | 11 | -1.75 | -4.01 | -14.00 | -30.46 |
| (TV-394) | 12 | +0.51 | -0.34 | +0.11 | -0.15 | 12 | -1.09 | -4.17 | -18.94 | -14.34 |
| Average* | | +0.52 | -0.24 | +0.20 | -0.21 | | -1.42 | -4.09 | -16.47 | -22.40 |
| Totals** | | | (+0.28) | (+0.48) | (+0.27) | | | (-5.51) | (-21.98) | (-44.38) |

*Incremental weight change

**Accumulative weight change

## FLAME TUNNEL OXIDATION WEIGHT CHANGE DATA DURING 1000 HRS/1600°F EXPOSURE (mg/cm²)

| Alloy | Spec No. | 100 Hrs | 200 Hrs | 300 Hrs | 400 Hrs | 500 Hrs | 600 Hrs | 700 Hrs | 800 Hrs | 900 Hrs | 1000 Hrs |
|---|---|---|---|---|---|---|---|---|---|---|---|
| René V Ht #1 | 1 | -0.15 | -0.27 | -0.22 | -0.31 | -0.21 | -0.17 | -0.10 | -0.02 | -0.13 | -0.04 |
| (64-711) | 2 | -0.15 | -0.31 | -0.22 | -0.34 | -0.19 | -0.13 | -0.12 | -0.04 | -0.03 | -0.09 |
| Average* | | -0.15 | -0.29 | -0.22 | -0.33 | -0.20 | -0.15 | -0.11 | -0.03 | -0.08 | -0.07 |
| Total** | | | (-0.44) | (-0.66) | (-0.69) | (-0.89) | (-1.04) | (-1.15) | (-1.18) | (-1.26) | (-1.33) |
| IN-100 Ht #1 | 3 | +0.33 | +0.68 | +0.43 | +0.23 | +0.45 | +0.14 | +0.14 | +0.10 | +0.07 | +0.22 |
| (67VS261) | 4 | +0.35 | +0.44 | +0.27 | +0.19 | +0.41 | +0.20 | +0.10 | +0.12 | +0.07 | +0.14 |
| Average* | | +0.34 | +0.56 | +0.35 | +0.21 | +0.43 | +0.34 | +0.12 | +0.11 | +0.07 | +0.18 |
| Total** | | | (+0.90) | (+1.25) | (+1.46) | (+1.89) | (+2.23) | (+2.35) | (+2.46) | (+2.53) | (+2.71) |
| SM-200 Ht #1 | 5 | -0.15 | +0.01 | +0.02 | +0.27 | +0.40 | +0.08 | +0.07 | +0.11 | +0.02 | +0.02 |
| (34V2804) | 6 | -0.17 | +0.03 | +0.02 | +0.27 | +0.40 | +0.02 | +0.05 | +0.01 | +0.07 | +0.08 |
| Average* | | +0.16 | +0.02 | +0.02 | +0.27 | +0.40 | +0.05 | +0.06 | +0.07 | +0.05 | +0.05 |
| Total** | | | (+0.18) | (+0.20) | (+0.47) | (+0.87) | (+0.92) | (+0.98) | (+1.04) | (+1.09) | (+1.14) |
| U-700 Ht #1 | 7 | +0.20 | +0.41 | +0.11 | +0.21 | +0.45 | +0.09 | +0.03 | +0.10 | +0.06 | +0.01 |
| (6-4084) | 8 | +0.20 | +0.45 | +0.13 | +0.21 | +0.41 | +0.07 | +0.29 | +0.08 | +0.08 | +0.01 |
| Average* | | +0.20 | +0.43 | +0.12 | +0.21 | +0.43 | +0.08 | +0.16 | +0.09 | +0.07 | +0.01 |
| Total** | | | (+0.63) | (+0.75) | (+0.96) | (+1.39) | (+1.47) | (+1.63) | (+1.72) | (+1.79) | (+1.80) |
| Inco 713C Ht #1 | 9 | +0.12 | -0.07 | -0.05 | -0.33 | +0.31 | +0.05 | -0.04 | +0.02 | +0.01 | +0.07 |
| (6C1) | 10 | +0.12 | -0.09 | -0.05 | -0.33 | +0.35 | -0.03 | -0.02 | -0.02 | +0.01 | +0.03 |
| Average* | | +0.12 | -0.08 | -0.05 | -0.33 | +0.33 | +0.01 | -0.03 | +0.02 | +0.01 | +0.05 |
| Total** | | | (+0.04) | (-0.01) | (-0.34) | (-0.01) | (0.00) | (-0.03) | (-0.01) | (0.00) | (+0.05) |
| René 41 Ht #1 | 11 | +0.32 | +0.02 | +0.09 | +0.23 | +0.39 | +0.03 | +0.05 | +0.14 | -0.01 | +0.10 |
| (TV-394) | 12 | +0.30 | +0.14 | +0.07 | +0.25 | +0.45 | +0.11 | -0.01 | +0.06 | +0.03 | -0.12 |
| Average* | | +0.31 | +0.08 | +0.08 | +0.24 | +0.42 | +0.07 | +0.02 | +0.10 | +0.01 | -0.01 |
| Total** | | | (+0.39) | (+0.47) | (+0.71) | (+1.13) | (+1.20) | (+1.22) | (+1.32) | (+1.33) | (+1.32) |

*Incremental weight change

**Accumulative weight change

## FLAME TUNNEL OXIDATION WEIGHT CHANGE DATA DURING 1000 HRS./2000°F EXPOSURE (mg/cm²)

| Alloy | Spec No. | 100 Hrs | 200 Hrs | 300 Hrs | 400 Hrs | 500 Hrs | 600 Hrs | 700 Hrs | 800 Hrs | 900 Hrs | 1000 Hrs |
|---|---|---|---|---|---|---|---|---|---|---|---|
| René Y Ht #1 | 1 | +0.02 | -1.14 | -1.48 | -0.93 | -0.96 | -0.88 | -0.75 | -0.65 | -0.78 | -3.62 |
| (64-711) | 2 | +0.02 | -1.10 | -1.23 | -1.05 | -1.05 | -1.06 | -0.76 | -0.87 | -3.99 | -4.22 |
| Average* | | +0.02 | -1.12 | -1.35 | -0.99 | -1.00 | -0.97 | -0.75 | -0.76 | -2.39 | -3.92 |
| Totals** | | | (-1.10) | (-2.45) | (-3.44) | (-4.44) | (-5.41) | (-6.16) | (-6.92) | (-9.31) | (-13.23) |
| IN-100 Ht #1 | 3 | -3.18 | -0.51 | -0.94 | -0.53 | -1.99 | -3.94 | -4.88 | -5.76 | -9.46 | -17.65 |
| (67V2261) | 4 | -3.00 | -0.41 | -0.78 | -1.05 | -1.56 | -2.32 | -4.49 | -8.68 | -10.95 | -19.67 |
| Average* | | -3.09 | -0.46 | -0.86 | -0.79 | -1.77 | -3.13 | -4.68 | -7.22 | -9.71 | -18.66 |
| Totals** | | | (-3.55) | ( 4.41) | (-5.20) | (-6.97) | (-10.10) | (-14.78) | (-22.00) | (-31.71) | (-50.37) |
| SM-200 Ht #1 | 5 | -6.03 | -1.35 | -1.99 | -3.71 | -1.99 | -3.58 | -5.42 | -8.83 | -13.07 | -17.79 |
| (34V2804) | 6 | -6.31 | -2.30 | -2.20 | -3.87 | -2.67 | -4.79 | -6.58 | -11.55 | -14.33 | -17.25 |
| Average* | | -6.17 | -1.97 | -2.09 | -3.79 | -2.33 | -4.18 | -6.00 | -10.19 | -13.70 | -17.52 |
| Totals** | | | (-8.14) | (-10.13) | (-13.92) | (-16.25) | (-20.43) | (-26.43) | (-36.62) | (-50.32) | (-67.84) |
| U-700 Ht #1 | 7 | -0.41 | -2.00 | -2.26 | -3.50 | -1.08 | -1.09 | -2.05 | -3.05 | -8.36 | -14.69 |
| (E-4084) | 8 | -0.69 | -1.83 | -2.28 | -3.42 | -0.83 | -1.57 | -2.03 | -3.04 | -11.22 | -15.35 |
| Average* | | -0.55 | -1.91 | -2.27 | -3.46 | -0.95 | -1.53 | -2.04 | -3.04 | -9.99 | -15.02 |
| Totals** | | | (-2.46) | (-4.73) | (-8.19) | (-9.14) | (-10.67) | (-12.71) | (-15.75) | (-25.74) | (-40.76) |
| Inco 713C Ht #1 | 9 | -3.16 | -3.10 | -4.80 | -7.45 | -4.66 | -4.17 | -3.87 | -3.51 | -2.88 | -2.88 |
| (601) | 10 | -2.47 | -2.99 | -4.44 | -7.17 | -4.48 | -4.57 | -3.93 | -3.00 | -2.76 | -4.07 |
| Average* | | -2.81 | -3.04 | -4.62 | -7.31 | -4.57 | -4.37 | -3.90 | -3.25 | -2.82 | -3.48 |
| Totals** | | | (-5.85) | (-10.47) | (-17.81) | (-22.38) | (-26.75) | (-30.65) | (-33.90) | (-36.72) | (-40.20) |
| René 41 Ht #1 | 11 | -0.25 | -8.43 | -13.27 | -31.31 | -25.99 | -32.63 | -20.90 | -28.71 | -13.31 | -21.94 |
| (TV-394) | 12 | +0.12 | -7.03 | -16.39 | -34.38 | -29.06 | -34.43 | -22.12 | -28.21 | -13.18 | -17.81 |
| Average* | | -0.12 | -7.73 | -14.83 | -32.84 | -27.52 | -33.53 | -21.51 | -28.46 | -13.25 | -19.88 |
| Totals** | | | (-7.85) | (-22.68) | (-55.52) | (-83.04) | (-116.57) | (-138.08) | (-166.54) | (-179.79) | (-199.67) |

*Incremental weight change

**Accumulative weight change

## TABLE X-A

**CONTINUOUS WEIGHT-GAIN OXIDATION TEST DATA AT 1800°F IN GRIT BLAST CONDITION**

Weight Gain/Area (mg/cm$^2$)

| Time Min. | Inco 713C (#38) | U-700* (#37) | IN-100 (#35) | IN-100 (#36) |
|---|---|---|---|---|
| 1 | 0.003 | 0.005 | – | 0.010 |
| 3 | 0.010 | 0.011 | 0.010 | 0.020 |
| 5 | 0.017 | 0.021 | 0.021 | 0.030 |
| 10 | 0.031 | 0.037 | 0.036 | 0.050 |
| 15 | 0.046 | – | 0.051 | 0.060 |
| 20 | 0.053 | 0.069 | 0.067 | 0.070 |
| 30 | 0.072 | 0.080 | 0.092 | 0.100 |
| 40 | 0.087 | 0.102 | 0.118 | 0.120 |
| 60 | 0.111 | 0.128 | 0.164 | 0.160 |
| 80 | 0.128 | 0.160 | 0.205 | 0.200 |
| 100 | 0.144 | 0.182 | 0.247 | 0.230 |
| 120 | 0.154 | 0.192 | 0.277 | 0.260 |
| 150 | 0.164 | 0.214 | 0.318 | 0.300 |
| 180 | 0.175 | 0.235 | 0.360 | 0.340 |
| 240 | 0.190 | 0.273 | 0.431 | 0.420 |
| 300 | 0.200 | 0.326 | 0.503 | 0.500 |
| 360 | 0.211 | 0.374 | 0.555 | 0.560 |
| 420 | 0.216 | 0.412 | 0.601 | 0.610 |
| 480 | 0.221 | 0.444 | 0.657 | 0.640 |
| 540 | 0.231 | 0.460 | 0.699 | 0.700 |
| 600 | 0.252 | 0.486 | 0.740 | 0.730 |
| 720 | 0.252 | 0.518 | 0.822 | 0.800 |
| 840 | 0.262 | 0.551 | 0.904 | 0.840 |
| 960 | 0.272 | 0.567 | 0.976 | 0.890 |
| 1200 | 0.303 | 0.583 | 1.217 | 0.970 |
| 1500 | 0.334 | 0.631 | 1.541 | 1.040 |
| 1800 | 0.365 | 0.663 | 1.746 | 1.100 |
| 2400 | 0.421 | 0.706 | 2.085 | 1.210 |
| 3000 | 0.452 | 0.748 | 2.466 | 1.320 |
| 3600 | 0.436 | 0.786 | 2.835 | 1.430 |
| 4200 | 0.411 | 0.828 | 3.082 | 1.630 |
| 4800 | 0.334 | 0.866 | 3.339 | 1.890 |
| 5400 | 0.349 | 0.898 | 3.688 | 2.040 |

| Specimen Surface Area (cm$^2$) | 9.7380 | 9.3510 | 9.7340 | 9.7270 |

*Astroloy Sheet

# REFERENCES

1.  Wlodek, S. T., "The Oxidation of Ni-2% ThO$_2$" R62FPD140, General Electric Company, Evendale, Ohio, May 4, 1962.

2.  Wlodek, S. T., "The Oxidation of René 41 and Udimet 700", Trans. AIME (1964), <u>230</u>, p. 1078.

3.  Wlodek, S. T., "The Oxidation of Hastelloy Alloy X", Trans. AIME (1964), <u>230</u>, p. 177.

4.  Sannier, J., Dominget, R., & Darras, R., "Air Oxidation of Two Heat Resistant Alloys; Nicral D and Hastelloy X", J. Nucl. Mater., (1959), <u>3</u>, p. 213.

5.  Radavich, J. F., "High Temperature Oxidation of Gas-Turbine Alloys", in High Temperature Materials, R. F. Hehemann and G. M. Ault, eds., p. 520, John Wiley & Sons, New York, 1959.

6.  Malamand, F. & Vidal, G., "The Effect of Oxidation on the Surface Chemical Composition of Superalloys", Rech. Aeron., (1957), No. 56, p. 47.

7.  Preece, A., & Lucas, G., "The High Temperature Oxidation of Some Cobalt-Base and Nickel-Base Alloys", J. Inst. Metals (1952-53), <u>81</u>, p. 219.

8.  Poulignier, J., Buckle, C., & Malamand, F., "Oxidation of Precipitation Hardened Ni-Cr-Co-Mo Alloys Under the Effect of Surface Work Hardening", Rech. Aeron., (1961), No. 85, p. 15.

9.  Poulignier, J., "The Effect of Abrasion on the High-Temperature Oxidation of Nickel-Base Superalloys", Corrosion Anti-Corrosion, (1962), <u>10</u>, p. 221.

# REFERENCES

(Continued)

10. Buckle, C., Malamand, F., & Poulignier, J., "On a Particular Case of Oxidation in Precipitation Strengthened Ni-Cr-Co-Mo Superalloys, Compt. Rend., (1961), 252, p. 3042.

11. Lehmann, C. R., & Poynter, V. M., General Electric Company, FPD, Evendale, Ohio, Private Communication.

12  A. U. Seybolt, "Oxidation of Metals" General Electric Company, Research & Development Center, Report No. 62-RL-3151M, November, 1962.

13. Tedmon, C. S., Jr., "The Effect of Oxide Volatilization on the Oxidation Kinetics of Cr and Fe-Cr Alloys", General Electric Company, Research & Development Center, Report No. 66-C-094, April 1966.

14. Lewis, H., "The Kinetics of the Oxidation Process in the Nickel-Chromium-Base Alloys", International Nickel, Ltd., Presented for Publication.

15. L. R. Woodyatt, H. J. Beattie, & C. T. Sims:  Trans. Met. Soc. AIME, 1966, Vol. 236, No. 4, pp 519-527.

16  Rapp, R. A., "Kinetics Microstructures & Mechanism of Internal Oxidation - Its Effect and Prevention in High Temperature Alloy Oxidation", Corrosion (1965) 21, pp. 382-401.

17. Evans, U. R., "The Corrosion and Oxidation of Metals"; Scientific Principles and Practical Applications, St. Martin's Press, Inc., New York, 1960.

18. Hagel, W. C., Trans. ASM 56, p. 583 (1963).

19. Gulbransen, E. A., & K. F. Andrew, "Oxidation Studies on the Nickel Chromium and Nickel-Aluminum Heater Alloys", J. Electrochem. Soc. (1959), 106, 941.

## DOCUMENT CONTROL DATA - R&D

*(Security classification of title, body of abstract and indexing annotation must be entered when the overall report is classified)*

| 1. ORIGINATING ACTIVITY (Corporate author) | 2a. REPORT SECURITY CLASSIFICATION |
|---|---|
| General Electric Company  Engineering Department  Cincinnati, Ohio 45215 | Unclassified |
| | 2b. GROUP  N/A |

**3. REPORT TITLE**

Nickel-Base Superalloy Oxidation

**4. DESCRIPTIVE NOTES (Type of report and inclusive dates)**

Technical Report   1 July 1965 - 31 January 1967

**5. AUTHOR(S) (Last name, first name, initial)**

Wasielewski, Gerald E.

| 6. REPORT DATE | 7a. TOTAL NO. OF PAGES | 7b. NO. OF REFS |
|---|---|---|
| January 1967 | 191 | 19 |

| 8a. CONTRACT OR GRANT NO.  AF 33(615)-2861 | 9a. ORIGINATOR'S REPORT NUMBER(S) |
|---|---|
| b. PROJECT NO.  7321 | AFML-TR-67-30 |
| c.  Task No. 732102 | 9b. OTHER REPORT NO(S) (Any other numbers that may be assigned this report) |
| d. | |

**10. AVAILABILITY/LIMITATION NOTICES:** This document is subject to special export controls and each transmittal to foreign governments or foreign nationals may be made only with prior approval of the Materials & Ceramics Division (MAAM) Air Force Materials Laboratory, Wright-Patterson AFB, Ohio 45433.

| 11. SUPPLEMENTARY NOTES | 12. SPONSORING MILITARY ACTIVITY |
|---|---|
| | Air Force Materials Laboratory  Research and Technology Division  Wright-Patterson AFB, Ohio 45433 |

**13. ABSTRACT:** A program to determine the phenomenological oxidation behavior of five commercial nickel-base alloys (IN-100, SM-200, Inco 713C, René 41, and U-700) and one experimental alloy (René Y) is described to assure the intelligent application of these alloys and aid in the development of alloys with improved surface stability.

The oxidation characteristics were established as a function of alloy composition, surface preparation, and environmental variables such as time (5 min to 1000 hrs), temperature (1400 to 2100°F), and air flow rate (to 75 ft/sec). The extent of scale and subscale reactions were measured, the reaction products identified and correlated with morphology, and the accompanying kinetics of their formation studied.

The oxidation behavior of these alloys is complex due to the interplay between heterogeneous oxide growth, oxide interaction, oxide volatilization, and spalling. However, the general oxidation behavior is controlled by the competition between scaling and internal oxidation reactions which could be estimated by thermodynamics. Increased air flow, thermal cycling, and surface deformation generally decreased the oxidation resistance of the alloys. All the commercial alloys would be limited to service temperatures below 1800°F due to excessive spalling, oxide vaporization, or intergranular oxidation. René Y displayed potential application at temperatures in excess of 2000°F due to the lanthanum induced formation of a protective $MnCr_2O_4$ spinel oxide.

Higher Al/Cr ratios (lower Cr) and minor additions of "rare earths" and Mn were suggested and demonstrated as an effective means of improving the surface stability of nickel-base alloys.

**DD FORM 1473** (1 JAN 64)

193

Security Classification

| 14. KEY WORDS | LINK A | | LINK B | | LINK C | |
|---|---|---|---|---|---|---|
| | ROLE | WT | ROLE | WT | ROLE | WT |
| | | | | | | |
| | | | | | | |
| | | | | | | |
| | | | | | | |
| | | | | | | |
| | | | | | | |
| | | | | | | |

## INSTRUCTIONS

1. ORIGINATING ACTIVITY: Enter the name and address of the contractor, subcontractor, grantee, Department of Defense activity or other organization (corporate author) issuing the report.

2a. REPORT SECURITY CLASSIFICATION: Enter the overall security classification of the report. Indicate whether "Restricted Data" is included. Marking is to be in accordance with appropriate security regulations.

2b. GROUP: Automatic downgrading is specified in DoD Directive 5200.10 and Armed Forces Industrial Manual. Enter the group number. Also, when applicable, show that optional markings have been used for Group 3 and Group 4 as authorized.

3. REPORT TITLE: Enter the complete report title in all capital letters. Titles in all cases should be unclassified. If a meaningful title cannot be selected without classification, show title classification in all capitals in parenthesis immediately following the title.

4. DESCRIPTIVE NOTES: If appropriate, enter the type of report, e.g., interim, progress, summary, annual, or final. Give the inclusive dates when a specific reporting period is covered.

5. AUTHOR(S): Enter the name(s) of author(s) as shown on or in the report. Enter last name, first name, middle initial. If military, show rank and branch of service. The name of the principal author is an absolute minimum requirement.

6. REPORT DATE: Enter the date of the report as day, month, year, or month, year. If more than one date appears on the report, use date of publication.

7a. TOTAL NUMBER OF PAGES: The total page count should follow normal pagination procedures, i.e., enter the number of pages containing information.

7b. NUMBER OF REFERENCES: Enter the total number of references cited in the report.

8a. CONTRACT OR GRANT NUMBER: If appropriate, enter the applicable number of the contract or grant under which the report was written.

8b, &c, & 8d. PROJECT NUMBER: Enter the appropriate military department identification, such as project number, subproject number, system numbers, task number, etc.

9a. ORIGINATOR'S REPORT NUMBER(S): Enter the official report number by which the document will be identified and controlled by the originating activity. This number must be unique to this report.

9b. OTHER REPORT NUMBER(S): If the report has been assigned any other report numbers (either by the originator or by the sponsor), also enter this number(s).

10. AVAILABILITY/LIMITATION NOTICES: Enter any limitations on further dissemination of the report, other than those imposed by security classification, using standard statements such as:

(1) "Qualified requesters may obtain copies of this report from DDC."

(2) "Foreign announcement and dissemination of this report by DDC is not authorized."

(3) "U. S. Government agencies may obtain copies of this report directly from DDC. Other qualified DDC users shall request through

_____ ."

(4) "U. S. military agencies may obtain copies of this report directly from DDC. Other qualified users shall request through

_____ ."

(5) "All distribution of this report is controlled. Qualified DDC users shall request through

_____ ."

If the report has been furnished to the Office of Technical Services, Department of Commerce, for sale to the public, indicate this fact and enter the price, if known.

11. SUPPLEMENTARY NOTES: Use for additional explanatory notes.

12. SPONSORING MILITARY ACTIVITY: Enter the name of the departmental project office or laboratory sponsoring (paying for) the research and development. Include address.

13. ABSTRACT: Enter an abstract giving a brief and factual summary of the document indicative of the report, even though it may also appear elsewhere in the body of the technical report. If additional space is required, a continuation sheet shall be attached.

It is highly desirable that the abstract of classified reports be unclassified. Each paragraph of the abstract shall end with an indication of the military security classification of the information in the paragraph, represented as (TS), (S), (C), or (U).

There is no limitation on the length of the abstract. However, the suggested length is from 150 to 225 words.

14. KEY WORDS: Key words are technically meaningful terms or short phrases that characterize a report and may be used as index entries for cataloging the report. Key words must be selected so that no security classification is required. Identifiers, such as equipment model designation, trade name, military project code name, geographic location, may be used as key words but will be followed by an indication of technical context. The assignment of links, rules, and weights is optional.

Security Classification